The crystallography of three flavor quark matter

by

Rishi Sharma

Submitted to the Department of Physics
in partial fulfillment of the requirements for the degree of

Doctor of Philosophy in Physics

at the

MASSACHUSETTS INSTITUTE OF TECHNOLOGY

May 2007

Author ... .
Department of Physics
May 30, 2007

Certified by. .....
Krishna Rajagopal
Professor
Thesis Supervisor

Accepted by .....
Thomas J. Greytak
Associate Department Head for Education, Professor

The crystallography of three flavor quark matter

by

Rishi Sharma

Submitted to the Department of Physics
on May 30, 2007, in partial fulfillment of the
requirements for the degree of
Doctor of Philosophy in Physics

Abstract

The nature of cold three-flavor quark matter at the large (but not asymptotic) densities relevant to neutron star phenomenology is not resolved. The gapless CFL phase, which was previously believed to have the lowest free energy, was recently shown to be unstable in the sense that some phase must have lower free energy. The nature of the instability motivates the hypothesis that the stable phase is a crystalline color superconductor. In this thesis, we present the calculation of the free energies of three-flavor crystalline color superconductors for realistic crystal structures in the Ginzburg-Landau approximation. All previous work on this subject neglected the strange quarks; we include them, with qualitative consequences. We calculate free energies for many crystal structures, and find two (based upon cubic symmetry) that have lower free energy than the gapless CFL phase over the lower density half of the relevant parameter space. They are therefore good candidates for the phase quark matter exists in, if it is present in the cores of neutron stars. We investigate the implications of the existence of a crystalline color superconducting core on the phenomenology of glitches in neutron stars. The key ingredient in the standard explanation of the origin of glitches is the presence of a rigid lattice in a superfluid medium which provides sites where vortices in the superfluid can be pinned, a situation that exists in the inner crust of the neutron stars. By deriving the effective action of the phonons in the crystalline phases, we determine that these are very rigid, with a shear modulus 20 to 1000 times larger than that of neutron star crusts. They are at the same time superfluid and a rough estimate of the pinning force on vortices gives answers comparable to that for pinning in the inner crust. This raises the possibility that (some) glitches could originate in quark matter cores of neutron stars.

Thesis Supervisor: Krishna Rajagopal
Title: Professor

Acknowledgments

First and foremost, I would like to thank Krishna for being a great teacher and advisor. His support and encouragement through these years have been amazing. One particular episode stands out in my mind, when on the eve of my first job interview he was happy to read through and comment on my presentation, at about eleven in the night. Needless to say I learnt a lot of physics from him. But I learnt much more, *how* to do physics, and enough lessons for life that would make another thesis in itself.

I would like to thank my family for their love and unwavering support. My parents, for their strength in difficult times, and my sister who has been the responsible and protecting one despite her being the younger sibling.

I would also like to thank my friends. Ajay, for being a great apartment mate. I'll always remember Mauro for our conversations ranging from Italian grammar to String theory. Qudsia and Guido, for advice and fun discussions. Onur, Murali, Sreekar and Vinay, for introducing me to life beyond the boundaries of the MIT campus. They and others have helped pull me through the ebbs of graduate school and been there to enjoy the highs with.

I would like to thank Massimo Mannarelli for discussions, fruitful collaboration and friendship. Rob Pisarski, Michael Forbes, Mark Alford, Kenji Fukushima, Elena Gubankova and others for discussions.

I also acknowldge Jeffrey Bowers, whose thesis and notes were invaluable for me.

Contents

List of Figures

List of Tables

Chapter 1

Introduction

1.1 Overview

In this thesis we will discuss the nature of cold three flavor quark matter at large, but not asymptotically large densities.

Driven by the strong and attractive color interaction, cold dense quark matter exists as a color superconductor. While it is well established that quark matter at asymptotically large densities exists in the Color Flavor Locked phase, the answer for the nature of the phase at intermediate densities is not yet settled. The strange quark mass and conditions of neutrality and weak equilibrium tend to separate the Fermi surfaces of the quarks, which in turn puts stress on the Color Flavor Locked phase. Crystalline superconductivity allows pairing between quarks living on separated Fermi surfaces and is therefore an attractive possibility in this regime. We explore this possibility in detail in this thesis.

One of the two central results presented here is the identification of two crystalline color superconducting structures whose free energies — calculated in the Ginzburg-Landau approximation — are smaller than those of known homogeneous phases in the regime of interest for neutron star phenomenology. Secondly, we show that these phases are very rigid, as evinced by their large shear modulus. This is interesting because they are at the same time superfluid. This result may have bearing on the phenomenon of glitches observed in rotating neutron stars.

Our aim in Chapter 1 is to expain, without going into technical details, the two results stated above and to present the broader body of knowledge in which this piece of work fits in. To this end, we begin with a discussion of the phase diagram of Quantum Chromodynamics.

1.2 The phase diagram of QCD

Over the last couple of decades, Quantum Chromodynamics (QCD) [1] has been firmly established as the fundamental theory of strong interactions. It has also become clear that the theory has a very rich phase diagram (see [2] for reviews). From experiments and theoretical calculations we know the properties of phases of QCD in certain regimes. These various phases differ markedly in their symmetry, the dominant degrees of freedom, etc.

In vacuum, QCD exhibits color confinement. The low energy excitation spectrum features only color singlet particles and resonances. Chiral symmetry (which is an approximate symmetry of nature) is spontaneously broken. The calculation of the properties of the QCD vacuum starting from its fundamental action is a challenge because it is a strongly interacting field theory, and therefore usual perturbative techniques fail. Lattice QCD has risen to the challenge and we can now calculate the masses and other properties of several low mass baryons and mesons to a fair accuracy [3, 4] .

Since QCD is asymptotically free [1], we expect that quarks and gluons become deconfined [5] and weak coupling methods become applicable in regimes where the typical momentum exchange between particles is much larger than Λ_{QCD}. For example, at temperatures much larger than Λ_{QCD}, we expect that quarks and gluons will be deconfined and QCD matter will exist as a weakly coupled plasma [5, 6]. Another example is quark matter at asymptotically large densities [9]. The small separation between the quarks implies a large magnitude of the typical momentum exchange and hence a small gauge coupling. We know from calculations that at low temperature, asymptotically dense quark matter exists in the Color Flavor Locked (CFL), color

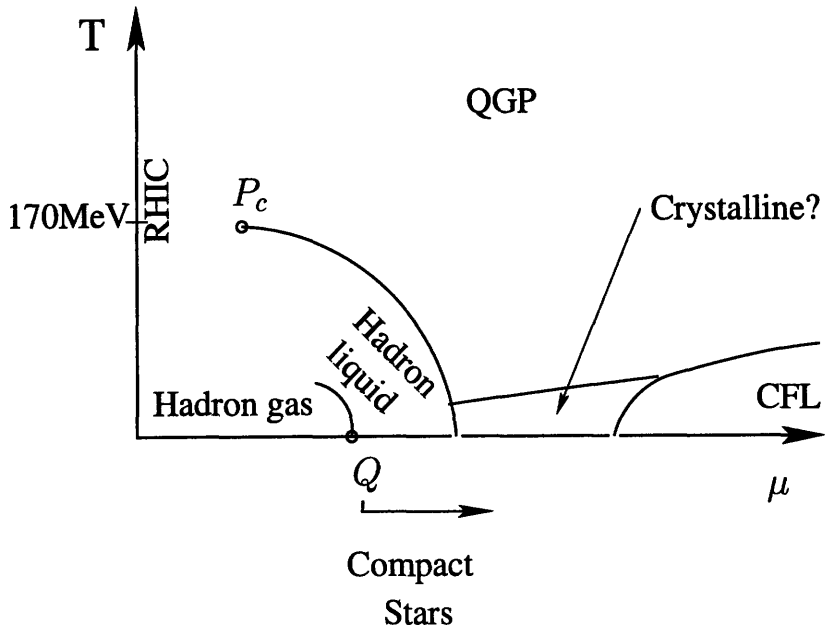

Figure 1-1: A schematic phase diagram of QCD.

superconducting phase, and understand the properties of this phase well from first principles.

A relevant question to ask is how these different phases connect to each other as we vary the thermodynamic variables μ, the quark number chemical potential[1], and temperature T. Results from experiments, lattice QCD simulations and theoretical models have helped paint a schematic picture for the phase diagram of QCD, shown in Figure 1-1.

Moving along the "y" axis, or the temperature axis, corresponds to increasing the temperature at zero quark number chemical potential. Lattice QCD simulations [7] provide us with first principle, theoretical results along this line. It seems likely that the transition from the confined phase to the deconfined Quark Gluon Plasma (QGP) is a crossover, and occurs at about 170MeV. Heavy ion collisions at the Relativistic Heavy Ion Collider (RHIC) [10] (and in future, at the LHC) probe experimentally the interesting region above the estimated crossover temperature.

[1] μ can be thought of as the average of the three chemical potentials associated with the number of u, d and s quarks, respectively. This is related to the baryon number chemical potential μ_B by the relation $3\mu = \mu_B$

As we move to the right of the temperature axis close to the crossover, the transition to deconfined matter is believed to become stronger and eventually turn into a first order phase transition, beginning from the critical point P_c. (In recent work, authors of [11] suggest evidence for an alternative scenario where the transition from confined matter to the QGP phase remains a crossover at high baryon densities, and there is no critical point.) The location of P_c is uncertain. The reason is that lattice QCD calculations at non-zero chemical potential suffer from the sign problem, and while progress has been made in understanding the diagram close to the temperature axis, the uncertainties increase as μ/T becomes large. Model calculations suggest that the first order transition curve meets the "x" axis at some high density [13, 14]. This is the region where (for now) we do not have the benefit of lattice calculations.

Now let us start from the origin and move along the "x" axis. At zero temperature on the left of the point marked Q is vacuum. At a small but non-zero temperature we have a gas of hadrons. As we move towards the right on the μ axis from the origin, the curve starting at Q marks the first order transition from a gas of hadrons to a hadron liquid. Nuclei are droplets of the hadron liquid phase. This first order transition has been explored by low energy hadron collisions [12] and by theoretical models. Off the μ axis, at non-zero temperatures, the transition occurs at smaller chemical potentials and eventually the first order line ends at a critical point that sits at a temperature of about 10MeV.

As we continue to move towards the right, our handle on the parameters of the theory becomes weaker. At densities several times nuclear density, the overlap between nucleons becomes very large and quarks should become deconfined [13, 14, 15, 16, 17, 18, 19]. The transition from hadronic matter to deconfined quark matter is expected to be first order. But the precise location of this transition point is uncertain not only because of uncertainties in the parameters of hadronic matter, but also because of uncertainties in the phase of deconfined quark matter on the immediate right of this transition. On the other hand, such densities may be present in the cores of neutron stars.

The philosophy we will follow in the thesis is to assume that cores of neutron stars

contain deconfined quark matter, and try to calculate observable consequences of this assumption for their phenomenology.

The fundamental insight about the properties of deconfined quark matter at low temperature is derived from the work of Bardeen, Cooper and Schrieffer (BCS), who showed that if the interaction between fermions living at the Fermi surface is attractive, then the Fermi surface is unstable to the formation of Cooper pairs [20]. The interaction between quarks is attractive for states of two quarks that are antisymmetric in color indices, and hence quarks form Cooper pairs. The ground state is characterized by a non-zero expectation value of the diquark operator. This spontaneously breaks the $SU(3)$ color symmetry, and (at least some of) the gluons attain a mass by the Meissner effect. Cold dense quark matter is necessarily a color superconductor [9].

This general conclusion however does not tell us the pattern of pairing. That requires finding the pairing ansatz which has the lowest free energy. At asymptotically high densities, i.e. skipping to the extreme right of the μ axis, the problem simplifies because the strange quark mass can be neglected and the u, d and s quarks can be treated as massless. It is well accepted that in this regime cold quark matter exists in the CFL phase [21, 22, 23, 24]. This phase features a highly symmetric pattern of pairing where quarks of all the species which differ in their color and flavor are paired with each other with the same strength. Gauge symmetry is broken such that eight gauge fields get a Meissner mass, and all the fermionic quasiparticle excitations are gapped. We will discuss the CFL phase further in Section 1.3.

But as we decrease the chemical potential, the effect of the strange quark mass becomes more and more important [25, 26]. In neutral unpaired quark matter the strange quark mass has the effect of splitting the u, d and s Fermi surfaces and tends to disrupt the cross-species BCS pairing that characterizes the CFL phase. If we imagine beginning at asymptotically high densities and reducing the density, and suppose that CFL pairing is disrupted by the heaviness of the strange quark before color superconducting quark matter is superseded by baryonic matter, the CFL phase must be replaced by some phase of quark matter in which there is less, and less symmetric,

pairing [17, 25, 30, 31, 32, 33]. Several candidate phases have been proposed which have lower free energies than the CFL phase and unpaired quark matter in some range of intermediate densities which interpolate between nuclear matter and CFL matter. We will discuss some of these possibilities in Sections 1.4.3,1.4.4.

We will argue in this thesis that — at least in a window of densities that might be found at the cores of neutron stars — the ground state of three flavor quark matter is the crystalline color superconducting phase [33, 34, 38, 42, 43, 44]. It is color superconducting because the diquark condensate is non-zero in this phase. The crystalline in the name signifies that the diquark condensate varies periodically in space.

If we begin with a color superconductor at $T = 0$ and raise the temperature, eventually it becomes entropically favorable to break the Cooper pairs thermally. The critical temperature, T_c, depends on the strength of the pairing and therefore on μ [13, 47, 48]. For temperatures larger than T_c, all symmetries are restored, and we transit into a phase where the quarks and gluons remain deconfined, the QGP.

The typical pairing energy between quarks is of the order of 10s of MeV, much larger than the few 10s of KeV temperatures found in neutron stars [49, 53]. Therefore we will restrict our attention to $T = 0$ throughout the thesis.

1.3 The color flavor locked phase

At asymptotically large densities, meaning $M_s/\mu \to 0$, the u, d and s quarks can all be treated as massless. (Keeping the regime of physical interest in mind, we will ignore the heavier quarks. For $N_f > 3$, see [54].) Also, the requirement that bulk matter should be electrically and color neutral and in weak equilibrium is satisfied for $M_s/\mu \to 0$ by taking the quark number chemical potentials of all the 9 quark species (three flavor and three colors) to be equal to μ.

Ignoring the small weak interaction, the classical action is symmetric under handed flavor rotations of the quarks, $SU(3)_L \times SU(3)_R$. It also posesses the $SU(3)$ color gauge symmetry, and a $U(1)$ vector symmetry. A linear combination of the flavor

and $U(1)$ vector symmetry is of course gauged to give electromagnetism, but we will ignore this for the moment. Finally, the $U(1)_A$ symmetry is anomalous and will be ignored in the discussion.

In the absence of color interactions, the ground state will consist of 9 species of fermions, filling momentum eigenstates up to a common Fermi energy $p_F = \mu$. Since the low momentum quark states are Fermi blocked, the typical momentum exchange between quarks is of the order of the Fermi momentum which is large, meaning that the gauge coupling g is weak, and only quarks close to the Fermi surface will be affected by the interactions. There is one subtlety in the argument above because the cross-section for forward scattering in fact has a logarithmic divergence $\sim \int d\theta/\theta$ [56, 47, 55]. As we will see in a moment, in the ground state, quarks of opposite momentum form a BCS condensate with a gap parameter Δ_0. For theories where fermions attract via a point interaction, the gap parameter goes as $\exp(-\#/g^2)$. The qualitative effect of this extra logarithm in QCD where the interaction is mediated by gluons, is that the gap goes as $\exp(-\#/g)$: it is enhanced. The pattern of symmetry breaking however remains the same, and we discuss this next.

Driven by the color interaction that is attractive in the color antisymmetric channel, the quarks form Cooper pairs [20]. The diquark operator in the ground state has a non-zero expectation value of the form [9],

$$\langle \psi(x)_{si\alpha} \psi(x)_{tj\beta} \rangle \propto \Delta_0 (C\gamma^5)_{st} \sum_I \epsilon_{I\alpha\beta} \epsilon_{Iij} \ , \tag{1.1}$$

or equivalently in the two component Weyl notation,

$$\langle \psi_L(x)_{ai\alpha} \psi_L(x)_{bj\beta} \rangle = \langle \psi_R(x)_{ai\alpha} \psi_R(x)_{bj\beta} \rangle \propto \Delta_0 \epsilon_{ab} \sum_I \epsilon_{I\alpha\beta} \epsilon_{Iij} \ , \tag{1.2}$$

where i, j are the flavor indices that run over 1, 2 and 3, corresponding to u, d and s respectively. α, β are color indices that also run over 1, 2 and 3, corresponding to r (red), g (green) and b (blue) respectively. s, t are four component Dirac spinor indices and C is the charge conjugation matrix, while a and b are indices in the two

component Weyl space. Δ_0 is the order parameter that defines the strength of the pairing when M_s is taken to be zero. It can be thought of as the typical binding energy of the Cooper pairs.

As mentioned, at truly asymptotic densities, Δ_0 can be computed from first principle QCD calculations, treating the coupling between gluons and quarks as weak. At the leading order, the dominant quark quark interaction can be taken to be that given by a single gluon exchange [47, 55, 56]. The calculation is still necessarily a non-perturbative calculation because the spontaneous breaking of gauge symmetry can not appear at any order in weak coupling. (Recall from above that Δ_0 goes as exponential of a quantity proportional to $-1/g$, which can never be obtained from an expansion in g.) But the weak coupling approximation is only reliable for $\mu \gg 10^8$MeV [57] (which turns out to correspond to $g \sim 0.8$), much larger than the $\mu \sim 500$MeV chemical potentials we are interested in. An extrapolation of the asymptotic results down to $\mu \sim 500$MeV gives values of Δ_0 ranging from 10 to 100MeV. This is an extrapolation of a calculation to a regime where it is not valid, but it can give us some understanding about the scale of Δ_0. An alternative approach is to model the QCD interaction with a phenomenological interaction term. The free parameters of the model are chosen to give reasonable vacuum physics [19, 14, 21, 22, 13, 58, 59, 60]. For example, one can add to the free theory of quarks, a NJL four Fermi interaction term which has the quantum numbers of single gluon exchange. This has two parameters, a momentum cutoff Λ and the NJL coupling G. If they are chosen to give a reasonable value for the vacuum chiral condensate and then use these to calculate the gap parameter, we get similar values of Δ_0. In the thesis, we will use the NJL model to calculate the properties like the free energy of the color superconducting phases. While this will not give us sufficient control to compare the favorability of these phases with nuclear matter, it will allow us to compare different candidate superconducting phases with each other. In the absence of more rigorous calculations of Δ_0, we will treat it as an unknown parameter which sets the energy scale of the pairing between quarks, expecting it have a value between 10 to 100MeV. When we need to get a feel for the energy scales, we will often use $\Delta_0 = 25$MeV as a rough guideline.

We can understand the features of the ansatz (1.1) that make it a favorable choice, as follows.

The condensate (1.1) is antisymmetric in color indices. This is reasonable because the color interaction is attractive in the color antisymmetric channel and this is what drives the condensation in the first place. The presence of C on the right hand side ensures that the condensate is antisymmetric in spinor indices, which implies that it is invariant under rotations. This can be thought of as the generalization of spin singlet pairing to this relativistic situation. This rotational symmetry allows us to cover the Fermi surface uniformly by pairing, giving the maximum benefit. (Other possibilities have been investigated [9, 61, 14, 21, 33] and found to be less favorable.) Since ψ is a fermionic field, the condensate then *has* to be antisymmetric in flavor indices, as can be seen to be true. This means in particular, quarks of different flavors pair with each other. Finally, consistent with the paradigm of BCS pairing, the condensate is independent of the position space coordinate, which means quarks of opposite momentum pair with each other. This is the most efficient way to pair the entire area of the Fermi surface for s-wave interactions.

The symmetry breaking pattern of the condensate is quite beautiful. It breaks the $SU(3)$ gauge symmetry completely, meaning that all the 8 gauge bosons attain non-zero Meissner masses, but has the remarkable property that it leaves a global $SU(3)_{L+R+color}$ unbroken. Because the I index is summed from 1 to 3 (Eq. 1.1), the CFL condensate can be seen to be invariant under a rotation in color space and a simultaneous vector flavor rotation in opposite direction. In other words, color and flavor rotations are "locked" and hence the name color flavor locked phase. The gluons are connected to each other by this locked symmetry, implying that they all have the same mass.

So far we have ignored $U(1)$ electromagnetism. The gauge boson for this symmetry, the photon A_μ, couples to the generator of electromagnetic gauge transformations, Q, which is independent of color and is a diagonal matrix in flavor space,

$$Q = \mathrm{diag}(\frac{2}{3}, -\frac{1}{3}, -\frac{1}{3}) \,. \tag{1.3}$$

Consider now the generator of color gauge transformations T_8, corresponding to the gauge field A_μ^8, which is independent of flavor and is diagonal in color space,

$$T_8 = \mathrm{diag}(-\frac{1}{\sqrt{3}}, \frac{1}{2\sqrt{3}}, \frac{1}{2\sqrt{3}}) \,. \tag{1.4}$$

One can very easily check that the combination $1_c \otimes Q + (2/\sqrt{3})T_8 \otimes 1_f$, called the $\tilde{Q}$ charge, gives zero when acting on the condensate (1.1) and thus the condensate is neutral under $\tilde{Q}$. Therefore a linear combination of gauge fields A_μ and A_μ^8, which corresponds to $U(1)$ gauge transformations generated by the $\tilde{Q}$ charge, is unbroken. This gauge field is therefore massless, and the orthogonal component turns out to be massive. This situation is familiar from the symmetry breaking pattern in the Weinberg-Salam model of electroweak symmetry breaking where a linear combination of $U(1)$ hypercharge and isospin gauge fields gives the massless photon while another gives the massive Z_μ boson. Here though, the electromagnetic coupling constant e is about a factor of 10 smaller than the strong coupling constant g and the gauge field corresponding to $U(1)_{\tilde{Q}}$ consists mostly of the photon, with a small admixture of A_μ^8.

The 9 quarks give rise to 9 quasiparticles which lie in two irreducible representations of the $SU(3)_{L+R+color}$, namely the octet, which features a gap Δ_0 and the singlet with gap $2\Delta_0$.

The only "laboratories" where dense quark may exist in nature, are the cores of neutron stars, where the chemical potential μ can not be much larger than 500MeV. The strange quark mass M_s in this medium, can be expected to lie somewhere between its current mass of about 100MeV and the vacuum constituent mass of order 500MeV. Clearly then, it is not a good approximation to take the strange quark as massless. Taking into account M_s has the effect of disrupting the highly symmetric CFL pattern of condensation, as we now discuss.

1.4 Effect of the strange quark mass

1.4.1 Neutral unpaired quark matter

Let us simplify the situation, for a moment, by turning off the interaction between quarks. Then as discussed before, quarks will fill momentum eigenstates up to maximum momenta which have energy equal to the chemical potential. But when we include M_s, in a crucial departure from the situation at asymptotic densities, the Fermi momentum of the strange quark will be smaller than the massless u and d quarks.

When we take into account electromagnetic interactions, the smaller strange quark Fermi momentum means that there are not enough $-e/3$ charged d and s quarks to neutralize the $2e/3$ charged u quarks [25, 26, 27, 28, 29]. To restore electrical neutrality we introduce to the Lagrangian a Lagrange multiplier μ_e that is a gauge chemical potential which couples to the electric charge. This modifies the chemical potentials "seen" by the three flavors of quarks, as follows,

$$\begin{aligned} \mu_u &= \mu - \frac{2}{3}\mu_e \\ \mu_d &= \mu + \frac{1}{3}\mu_e \\ \mu_s &= \mu + \frac{1}{3}\mu_e \ . \end{aligned} \tag{1.5}$$

By looking at detailed balance for the equations,

$$\begin{aligned} d &\rightarrow u + e + \bar{\nu}_e \\ s &\rightarrow u + e + \bar{\nu}_e \ , \end{aligned} \tag{1.6}$$

and noting that neutrinos can freely escape from the system, we conclude that the chemical potentials given by Eq. (1.5) satisfy conditions of weak equilibrium with μ_e as the chemical potentials for the electrons.

The free energy of this system of unpaired fermions is given by,

$$\begin{aligned}\Omega_{\rm N} = 3\times 2\Big[&\int \frac{d^3\mathbf{p}}{(2\pi)^3}(|\mathbf{p}|-\mu_u)\theta(|\mathbf{p}|-\mu_u)+\int \frac{d^3\mathbf{p}}{(2\pi)^3}(|\mathbf{p}|-\mu_d)\theta(|\mathbf{p}|-\mu_d)\\ &+\int \frac{d^3\mathbf{p}}{(2\pi)^3}(\sqrt{\mathbf{p}^2+M_s^2}-\mu_s)\theta(\sqrt{\mathbf{p}^2+M_s^2}-\mu_s)\Big]\\ &+2\int \frac{d^3\mathbf{p}}{(2\pi)^3}(|\mathbf{p}|-\mu_e)\theta(|\mathbf{p}|-\mu_e)\\ =-\frac{3}{12\pi^2}\Big[&(\mu_u)^4+(\mu_d)^4-(\mu_s^4)\Big((\frac{5M_s^2}{2\mu_s^2}-1)\sqrt{1-\frac{M_s^2}{\mu_s^2}}-\frac{3M_s^4}{2\mu_s^4}\cosh^{-1}(\frac{\mu_s}{M_s})\Big)\Big]\\ &-\frac{1}{12\pi^2}(\mu_e^4)\,,\end{aligned} \tag{1.7}$$

with μ_u, μ_d and μ_s given by Eq. (1.5). The term in the square brackets is the contribution of the quarks and the contribution $\propto \mu_e^4$ comes from the electrons. There is a prefactor of 3 for the quark contribution because of the three colors (the chemical potentials for the species depend on flavor but not color) and the factor of 2 comes from the spin degeneracy. The N in the subscript represents that this is the contribution from "normal", or unpaired quark matter. Electrical neutrality is enforced by requiring $\partial\Omega/\partial\mu_e = 0$.

We will consider the situation where M_s is small compared to μ and work only till the lowest order in M_s^2/μ^2. The motivation for this comes from understanding the scales of the quantities involved. The largest scale in the problem is the chemical potential μ which sets the overall size of the Fermi surface. We are working in the weak coupling approximation, where the dynamics are dictated by quarks living close to the Fermi surface. Thus, when we consider pairing in the next Section, we will quote results which are correct to the lowest order in Δ_0/μ, which is justified by estimates which show that $\Delta_0 \sim$ 10s of MeV and $\mu \sim 350 - 500$MeV in the region of interest. Similarly, M_s affects the sizes of the Fermi momenta by quantities of the order of M_s^2/μ and we will be interested in situations where Δ_0 is comparable to M_s^2/μ, meaning that M_s^2/μ^2 is comparable to Δ_0/μ. Hence we work to the lowest order in M_s^2/μ^2. (Corrections to this approximation has been studied for the gapless-

CFL phase, that we will discuss below, in Ref. [133] and for two flavor crystalline color superconductor in Ref. [38].)

For neutral unpaired quark matter, to lowest order in M_s^2/μ^2 we find for μ_e,

$$\mu_e = \frac{M_s^2}{4\mu} , \tag{1.8}$$

with corrections of order M_s^4/μ^3. As a check we note that $\mu_e > 0$, which will indeed tend to increase the number of d and s quarks, and reduce the number of u quarks. Since μ_e is proportional to M_s^2/μ the contribution of the electrons to the free energy (and to neutrality!), is very small, and we will ignore it from now on.

To the lowest order in $(M_s/\mu)^2$, the effect of the M_s on the strange Fermi surface can be taken into account by treating the strange quark as massless, but with a chemical potential that is reduced by $M_s^2/(2\mu)$.

$$p_F^s = \sqrt{(\mu+\mu_e)^2 - M_s^2} = \mu + \mu_e - \frac{M_s^2}{2\mu} + \mathcal{O}(M_s^4/\mu^3) . \tag{1.9}$$

Finally, let us note that the system is color neutral because there are equal number of quarks of each color. In general, as we shall see below will be the case when we consider pairing between quarks, we need to introduce gauge chemical potentials also for color charges, in order to ensure color neutrality. This entails introducing Lagrange multipliers μ_3 and μ_8 respectively for the two commuting generators T_3 and $T_8 \times 2/\sqrt{3}$, which generate the Cartan subalgebra of $SU(3)$ color. (T_3 and T_8 are taken to be the standard Gell-Mann matrices with norm 1/2 and the factor of $2/\sqrt{3}$ gives the conventional choice for the normalization of μ_8.) For non-zero μ_3 and μ_8, chemical potentials for different colors of quarks of the same flavor will be different. One can calculate the free energy in the presence of these potentials, and impose color neutrality by demanding $\partial\Omega/\partial\mu_3 = \partial\Omega/\partial\mu_8 = 0$ and thereby easily verify that μ_3 and μ_8 are zero for color neutral unpaired quark matter.

We can summarize the discussion as follows. To lowest order in M_s^2/μ^2, the three

quarks can all be treated as massless, with Fermi momenta given by,

$$\begin{aligned} p_F^u &= \mu - \frac{2}{3}\mu_e \\ p_F^d &= \mu + \frac{1}{3}\mu_e = p_F^u + 2\delta\mu_3 \\ p_F^s &= \mu + \frac{1}{3}\mu_e - \frac{M_s^2}{\mu} = p_F^u - 2\delta\mu_2 \qquad (1.10) \\ &\text{with } p_F^e = \mu_e \\ \text{and consequently, } \delta\mu_3 &= \delta\mu_2 = \frac{M_s^2}{8\mu} . \end{aligned}$$

Pictorially, (see Figure 1-2) one can imagine three concentric Fermi surfaces. The smallest being the s Fermi surface, encompassed by the u Fermi surface whose radius is larger by an amount $M_s^2/4\mu$, which in turn is encompassed by the d Fermi surface which is larger than the u by the same amount. We are interested in how the phases are affected as we vary the chemical potential of the system, and the parameter M_s^2/μ — which dictates the splitting between the Fermi surfaces — is the main driver of these changes. At asymptotic densities $M_s^2/\mu \to 0$ and the Fermi surfaces overlap. As we go to lower densities, the splitting between the Fermi surfaces increases.

So far we have ignored pairing between quarks. Let us now see what effect this has on the pairing.

1.4.2 Stress on pairing and color flavor unlocking

The splitting of the Fermi surfaces of quarks of different flavor in neutral, unpaired quark matter causes stress on the cross species, BCS pairing, that symbolizes the CFL phase. Pairing is strongest between quarks living at the Fermi surface, but if we try to pair, say, a d quark with momentum $\mathbf{p}$ on the d Fermi surface, with a u quark with momentum $-\mathbf{p}$, then the u quark will not lie on the u Fermi surface if the Fermi surfaces of quarks of different flavors are split [30, 31, 33] (Figure 1-2).

The situation where the Fermi surfaces of the species of fermions that want to pair together are split in the absence of pairing, arises in other contexts. For example, such conditions have been created experimentally in systems of ultracold gases of

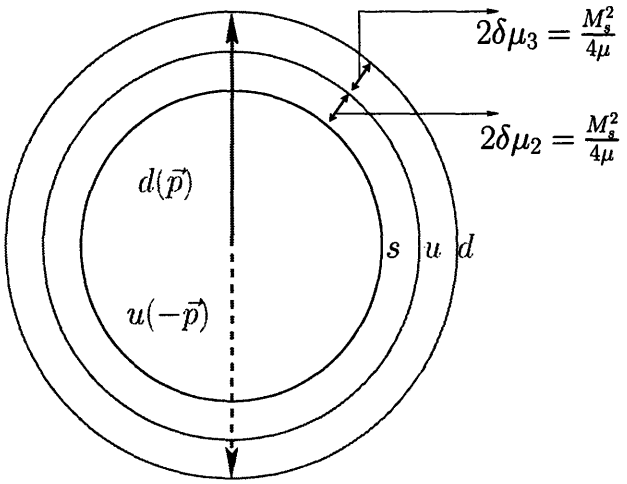

Figure 1-2: (Color Online): The u (red online), d (green online) and s (blue online) Fermi surfaces in neutral unpaired quark matter. To lowest order in M_s^2/μ^2, the separation between the $s-u$ and the $u-d$ Fermi surfaces is the same and is equal to $M_s^2/(4\mu)$. Separation of Fermi surfaces causes stress on cross-species BCS pairing. For example, a $d(\mathbf{p})$ quark on the d Fermi surface, can not find a partner $u(-\mathbf{p})$ quark on the u Fermi surface.

fermions [74]. These gases are trapped in a suitable magnetic trap, and the interaction between the fermions can be tuned. In traps of ^{6}Li ions, magnetic fields can be tuned to be close to a Feshbach resonance such that the ^{6}Li atoms in two different hyperfine states feel an attractive $s-$wave interaction. The strength of the attraction can be adjusted to be strong but not strong enough to force the formation of bound "molecules" of ^{6}Li atoms. When the number density (in the trap) of these two species is the same, atoms of the two species form Cooper pairs. By controlling the number density of the different species to be unequal [75], a stress in pairing can be created as discussed in the previous paragraph.

One way to form BCS-like pairing between Fermi surfaces that are split in the absence of pairing, is to allow the Fermi momenta of the species of fermions that pair to deviate from their values given by the chemical potentials and equalize. This exacts a free energy cost proportional to $\mu^2\delta\mu^2$ because we need to create particles or holes that fill up a shell of thickness of order $\delta\mu$. But there is a competing gain proportional to $\mu^2\Delta^2$ from BCS pairing, which can be understood as follows. Forming

a Cooper pair lowers the Free energy of the system by Δ, and there are of order $\mu^2\Delta$ pairs formed because electrons in a shell of thickess Δ and radius μ pair together. For massless particles, the most favorable value to equalize the Fermi momenta turns out to be the average of the chemical potentials of the species that pair together.

The values of the gauge chemical potentials that ensured neutrality for unpaired quark matter may no longer ensure neutrality after pairing. This is because of two reasons. Firstly, the location of the Fermi momenta specify the number of particles of a particular species that are present in the system. On choosing the Fermi momenta to be different from the chemical potential for that particular species, the relation between particle number and chemical potentials is modified and therefore the values of chemical potentials that ensure neutrality may change. Furthermore, BCS pairing changes the relation beween Fermi momentum and particle number for any species that participates in pairing. This is because the quasiparticles in a paired system are not just the fermions but linear combinations of fermions and holes. One needs to reevaluate the net number of particles after pairing. This gives a further modification of the chemical potentials.

Taking an ansatz of the form Eq. (1.1), we see that the free energy is given by [33]

$$\Omega_{\rm CFL} - \Omega_{\rm N} \approx -\frac{3}{\pi^2}\mu^2\Delta_0^2 + \frac{3}{\pi^2}\mu^2\Big(\frac{M_s^2}{4\mu}\Big)^2 . \tag{1.11}$$

where the first term (1.11) comes from pairing and the second comes from the rearrangement of Fermi surfaces.

We see that the CFL phase is less favorable than unpaired quark matter when $M_s^2/\mu > 4\Delta_0$. This can be intuitively understood because as we move to lower denstities, meaning increase the splitting between the Fermi surfaces, the gain in free energy due to pairing ceases to be more favorable than the free energy cost associated with allowing the Fermi momenta to be different from the chemical potential.

Finally we note that the gauge chemical potentials are given by [33]

$$\mu_e = \mu_3 = 0, \quad \mu_8 = -\frac{M_s^2}{2\mu} . \tag{1.12}$$

1.4.3 Gapless color flavor locked phase

It turns out that the CFL pairing has to break down at densities even larger than those given by $M_s^2/(4\mu) > \Delta$. Let us consider the largest difference between the effective chemical potentials of quarks that pair, with $\mu_e = \mu_3 = 0$, $\mu_8 = -M_s^2/(2\mu)$. This occurs between the $db - sg$ quarks (for more details see [62, 63]), and is given by

$$\mu_{db}^{\text{eff}} - \mu_{sg}^{\text{eff}} = \frac{M_s^2}{2\mu} - \mu_8 = \frac{M_s^2}{\mu} \,. \tag{1.13}$$

Instead of keeping the pairing between all the quark species equal (to Δ_0) as in the CFL phase, it is favorable to break (actually weaken) the $db-sg$ pairing as soon as the difference between the two chemical potentials becomes equal to the energy required to break the $db - sg$ pair. Namely, when $\mu_{db} - \mu_{sg} > 2\Delta_0$, giving, $M_s^2/\mu > 2\Delta_0$.

This motivates us to consider a pairing ansatz of form,

$$\langle \psi_{si\alpha}(x)\psi_{tj\beta}(x)\rangle \propto (C\gamma^5)_{st} \sum_I \Delta_I \epsilon_{I\alpha\beta}\epsilon_{Iij} \,. \tag{1.14}$$

While Eq. (1.14) retains the color, flavor and spin antisymmetry of CFL pairing, the ansatz allows the strength of the pairing to be different for pairing between different species. From the discussion above, we would expect Δ_1 — which measures the strength of the pairing between $db - sg$ quarks — to be the smallest, an expectation that is borne out by the calculation. Note that if the Δ_I in Eq. (1.14) are not equal, the condensate no longer has a remaining $SU(3)_{L+R+color}$ symmetry that was present in the CFL phase.

For $M_s^2/(2\mu) > \Delta$, the phase defined by the ansatz (1.14), has a lower free energy than the CFL phase. It features regions of momentum space where the quarks are not involved in pairing, and quarks living at the boundaries of these "blocking regions" form quasiparticles that can be excited without giving extra energy to the system. That is, they have gapless excitations [62, 63]. This phase is called the gapless Color Flavor Locked (gCFL) phase.

The variation on BCS pairing — in which the same species of fermions that

pair feature gapless quasiparticles — has also been proposed in an atomic physics context [69]. In all these contexts, however, the gapless paired state turns out in general to suffer from a "magnetic instability": it can lower its energy by the formation of counter-propagating currents [70, 71, 72].

In the atomic physics context, the resolution of the instability is phase separation, into macroscopic regions of two phases in one of which standard BCS pairing occurs and in the other of which no pairing occurs [73, 75, 76]. In three-flavor quark matter, where the instability of the gCFL phase has been established in Refs. [71, 72], phase coexistence would require coexisting components with opposite color charges, in addition to opposite electric charges, making it very unlikely that a phase separated solution can have lower energy than the gCFL phase [63, 83].

It seems likely, therefore, that a ground state with counter-propagating currents is required. This could take the form of a crystalline color superconductor [34, 35, 36, 37, 38, 39, 40, 41, 42, 43, 44, 99, 45, 46], as we will discuss at length below.

The gCFL phase is an important benchmark to compare the free energy of phases in the intermediate density regime because the true ground state should have a free energy less than that of the gCFL phase. We shall aim to find (and find) crystalline phases which have a free energy less than the gCFL phase for a wide range of densities.

We first briefly survey other possibilities that have been proposed as the ground states of quark matter in the intermediate density regime.

1.4.4 Other possibilities

A much studied candidate phase studied in the literature is the 2SC (two flavor superconducting) phase. It is less symmetric than the CFL phase but still only involves conventional BCS pairing. The initial motivation to look at two flavor pairing was to let the massless u and d [64, 14, 19] quarks pair with each other, leaving the massive s quarks unpaired. The pairing ansatz considered is,

$$\langle \psi_{si\alpha}(x)\psi_{tj\beta}(x)\rangle \propto (C\gamma^5)_{st}\Delta_3\epsilon_{3ij}\epsilon_{3\alpha\beta}\ . \tag{1.15}$$

However, we know from our our discussion of neutrality that the strange quark mass tends to separate the u and d quarks Fermi surfaces as well. (See [33, 65, 66] for the effect of neutrality on the 2SC phase.) In fact, a systematic search of all possible patterns of pairing shows that such stress on pairing is unavoidable if we demand condensates that are antisymmetric in color and spin [67]. When neutrality is taken into account, the 2SC phase, like the gCFL phase, is known to feature gapless modes, giving rise to the gapless 2SC phase [68]. This phase, like the gCFL phase, suffers from the "chromomagnetic instability", where some of the gauge fields get an imaginary Meissner mass.

It is also known that the CFL phase is likely to be augmented by kaon condensation [84, 85]. Condensation of kons reduces the free energy of the CFL phase. For M_s^2/μ close to 2Δ, this kaon condensed phase is unstable to formation of a phase in which a CFL kaon condensate carries a current in one direction balanced by a counter-propagating current in the opposite direction carried by gapless quark quasiparticles [86, 87]. This meson supercurrent phase has been shown to have a lower free energy than the gCFL phase near $M_s^2/\mu = 2\Delta$, and could be the resolution of the instability in the gCFL phase, in particular near $M_s^2/\mu = 2\Delta$.

During our discussion so far, we have restricted our attention to condensates that are antisymmetric in color and Dirac indices. As we discussed, antisymmetry in color was motivated by the fact that the interaction between quarks is attractive in that channel, and antisymmetry in Dirac indices by the desire to have a rotationally invariant condensate. But in light of the fact that the Fermi surfaces of different flavors are split in neutral unpaired quark matter, we could imagine relaxing these conditions, considering symmetry in either Dirac or color indices [89], thereby allowing symmetry in flavor indices which permits pairing quarks of the same flavor. However, studies show that these spin-1 or color symmetric phases are less favorable than gCFL matter.

In this thesis we will concentrate on the possibility that the ground state of quark matter in at least part of the intermediate density regime is crystalline color superconducting matter, which we discuss next.

1.5 Crystalline color superconductivity

As we discussed in Section 1.4.3, the gCFL phase has an instability towards the formation of counter propagating currents. Crystalline superconducting phases have counter propagating currents and seem to be free from magnetic instability [99], which is consistent with the result we will see in Chapter 2, that many of them have free energies that are lower than that of the (unstable) gCFL phase for wide ranges of parameter values.

The central idea of crystalline pairing that makes it an attractive candidate phase when the Fermi surfaces of Fermions that pair are split, is that it allows fermions living on split Fermi surfaces to pair with each other. It does so by allowing Cooper pairs with nonzero total momenta $2\mathbf{q}^a$, with $\mathbf{q}^a$ taken from some set of momentum vectors $\{\mathbf{q}\}$. We will take the magnitude of these momenta to be equal and of the order of the splitting between Fermi surfaces. We shall see the motivation for this choice in a moment. Their directions must be determined to give a favorable structure. In position space, this corresponds to condensates that vary in space

$$\Delta(x) \propto \Delta \sum_{\mathbf{q}^a \in \{\mathbf{q}\}} \exp(2i\mathbf{q}^a \cdot \mathbf{x}). \tag{1.16}$$

The $\mathbf{q}^a$s are therefore reciprocal vectors which define the crystal structure of the condensate which is modulated periodically in space and therefore spontaneously breaks space translation invariance.

The intuitive argument why these are expected to be favorable when the Fermi surfaces are split is that since they allow us to pair quarks without shifting the values of the Fermi momenta, they avoid the Free energy cost associated with moving the Fermi surfaces from their preferred positions given by the chemical potentials.

Furthermore, this also implies that the number of particles of any species deviates from the values given by the chemical potentials only because of pairing. Thus the values obtained for the gauge chemical potentials by imposing neutrality in a crystalline superconducting state differ from the values in unpaired quark matter only

because of pairing, which further implies that the difference is small for small pairing. We will work in the approximation that the pairing is weak, and approximate the values of the gauge chemical potentials to be the same as in unpaired quark matter, namely $\mu_e = M_s^2/(4\mu)$, $\mu_3 = \mu_8 = 0$ so that the position of the u, d and s Fermi surfaces are given by Eq. (1.10).

Crystalline superconductivity features a non BCS kind of pairing, first proposed in the the context of electronic superconductivity by Larkin, Ovchinnikov, Fulde and Ferrel (LOFF) [90], where Zeeman splitting could give rise to a separation between the Fermi surfaces of the fermions that pair: namely the spin up and spin down electrons. Observing them in these systems has been a challenge because the simplest way to create a Zeeman split, by applying a uniform magnetic field to the sample, also induces surface currents in the superconducing sample, which try to keep out the magnetic field. (The is the Meissner effect at work.)

Applying a magnetic flux to a superconducting sample greater than some critical flux H_c destroys superconductivity (or induces magnetic vortices) in the sample, but that is not because of the splitting of the u and d Fermi surfaces. Rather it is because of the much larger coupling between the orbital component of the electron angular momentum to the magnetic field which induces large surface currents. In their study, LOFF were attempting to theoretically model a situation where a Zeeman splitting could be created by the presence of magnetic impurities in a superconducting sample.

A possible example where the Fermi surfaces of the up and down spin electrons can be split by applying an external magnetic field without inducing large currents is a class of superconductors called "heavy fermion superconductors" where the effective mass of the electrons is very large. There have been reports of discovery of the LOFF phase in UPd_2Al_3 which is such a material [91, 92]. (For a recent review see [93]) More recently, studies done on $CeCoIn_5$ [94] suggest a transition to a LOFF phase.

Another possibility is to apply a large magnetic field in the plane of a quasi two dimensional [96] or one dimensional [97] sample, so that there is "no room" for induced currents to exist. Studies in layered organic superconductors have shown indications for a possible crystalline state.

The complications that are present in electronic systems, where an external magnetic field is used to create a split in the Fermi surfaces, are not there in the quark matter scenario that we are interested in, where this situation is created naturally because of the effect of the strange quark mass along with requirements of neutrality and weak equilibrium.

We begin by discussing crystalline color superconducting phases in the simple situation where we ignore the s quarks from consideration and consider pairing only between the u and d quarks. This will lay the ground and provide valuable intuition for the physical situation we are interested in, namely crystalline superconductivity in three flavor quark matter.

1.5.1 Two flavor crystalline pairing

Consider two Fermi surfaces, representing u and d quarks, split by an amount $2\delta\mu$, as shown in Figure 1-3. As we discussed above, we will consider condensates of form

$$\langle u_{s\alpha}(x) d_{t\beta}(x) \rangle \propto \Delta (C\gamma^5)_{st} \epsilon_{3\alpha\beta} \sum_{\mathbf{q}^a \in \{\mathbf{q}\}} \exp(2i\mathbf{q}^a \cdot \mathbf{x}) \; . \tag{1.17}$$

The set of momentum vectors $\{\mathbf{q}\}$ defines the modulation of the crystalline condensate in position space. The color and flavor structure of the condensate is reminiscent of the 2SC phase, and follows from considerations of color and spin antisymmetry.

To motivate the ansatz, Eq. (1.17), we look in detail at a special case when there is only one fixed momentum vector $\mathbf{q}$ in the set $\{\mathbf{q}\}$. The direction of $\mathbf{q}$ is chosen spontaneously and we take it to be parallel to the z axis here, while its magnitude is chosen to minimize the free energy. The condensate, then, varies in position space as a single plane wave

$$\langle u(x) d(x) \rangle \propto \Delta \exp(2i\mathbf{q} \cdot \mathbf{x}) \; , \tag{1.18}$$

where we have stripped the right-hand-side of the flavor and spin indices which only

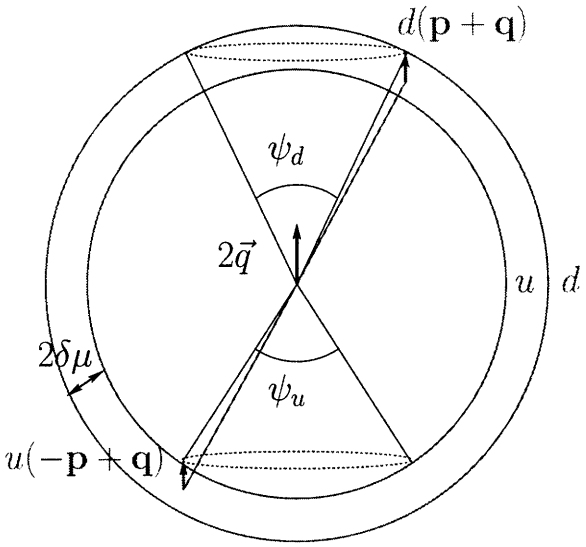

Figure 1-3: (Color Online): The diagram shows the pairing rings on the u (red online) and d (green online) Fermi surfaces. By allowing cooper pairs with momentum $2\mathbf{q}$, we can pair quarks along the rings. The pairing rings have opening angles ψ_u and ψ_d as shown. In weak coupling, with $|\mathbf{q}|$, $\delta\mu \ll \mu$, $\psi_u \approx \psi_d \approx 2\arccos(\delta\mu/|\mathbf{q}|)$.

give four copies of the same problem. Rewriting Eq. (1.18) in Fourier space, we get

$$\langle u(-\mathbf{p}+\mathbf{q})d(\mathbf{p}+\mathbf{q})\rangle \propto \Delta\,. \tag{1.19}$$

This means that Cooper pairs have a net momentum $2\mathbf{q}$.

Concentrating on the quarks living right at the Fermi surface, if the magnitude of $\mathbf{q}$ is taken to be exactly equal to $\delta\mu$, then Eq. (1.19) would allow pairing between a d quark on the north pole of the d Fermi surface with a u quark on the south pole of the u Fermi surface. With $|\mathbf{q}|$ larger than $\delta\mu$ we can pair quarks along rings on the Fermi surfaces, as shown in Figure 1-3.

Considering now also quarks off the Fermi surface, we can understand which quarks are involved in pairing, as follows. First let $\Delta \to 0$. Then u quarks with momentum $-\mathbf{p}+\mathbf{q}$ pair with d quarks with momentum $\mathbf{p}+\mathbf{q}$ when both the states are either both "Fermi occupied" or both "Fermi empty". In momentum space, the occupied states of $u(-\mathbf{p}+\mathbf{q})$ form a sphere which is shifted towards the $+z$ axis by

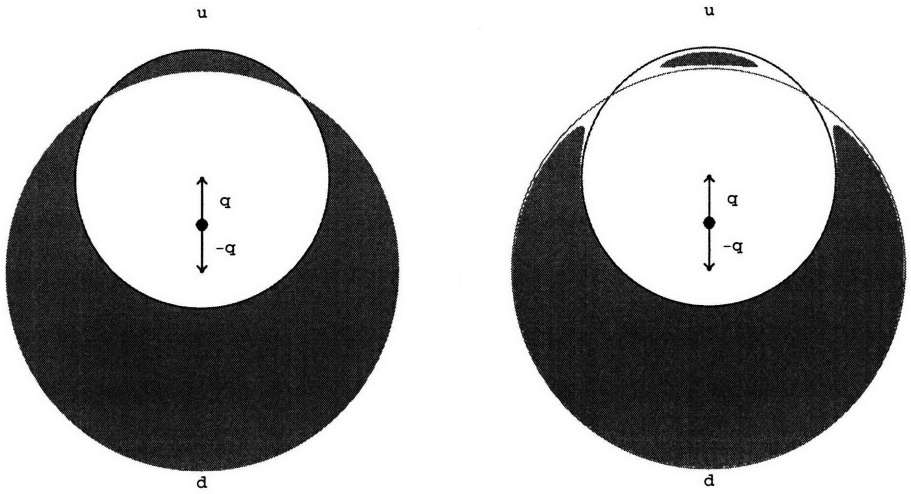

Figure 1-4: (Color online) Left panel: The larger circle (green online) represents the d quark Fermi surface, shifted down by $\mathbf{q}$, and the small circle (red online) represents the u quark Fermi surface, reflected about the centre and shifted up by $\mathbf{q}$. The shaded regions represent the "blocking regions", consisting of quarks that do not participate in pairing. Rest of the quarks may pair. This figure represents the situation in $\Delta \to 0$. Right panel: Represents the same diagram for non-zero Δ. The "pairing region" spills over into the "blocking region" and the pairing rings on the Fermi surface expand into bands. The diagram is from [34]. The volume of the upper blocking region is different from that of the lower blocking region, and hence the gapless modes carry a net current which cancels the current carried by the condensate Eq. (1.18). The total current in the crystalline phase with the condensate in Eq. (1.18), is zero.

$|\mathbf{q}|$. Similarly the occupied states of $d(\mathbf{p}+\mathbf{q})$ form a sphere shifted towards the $-z$ axis by $|\mathbf{q}|$ as shown in Figure 1-4. The intersection of the two spheres represent the two pairing rings on the u and d Fermi surfaces (though note that the u ring lies on the opposite side to that shown in Figure 1-3 because the u sphere is flipped before shifting). The shaded regions are where the Fermi occupancy of the u and d quarks is opposite and are the "blocking regions". The rest of momentum space represents the regions where quarks may pair, the "pairing regions". Now, for nonzero Δ, the pairing regions "spill over" into the blocking regions (Figure 1-4), the penetration depends upon the magnitude of Δ. For Figure 1-3 this implies that the pairing rings thicken into pairing bands of width Δ. The boundaries of the blocking regions feature gapless excitations as was also the case in the gCFL phase.

We are working in the weak coupling limit with $|\mathbf{q}|, \delta\mu,\ \Delta \ll \mu$. In this limit the opening angle of the ring is determined by the ratio of $\delta\mu$ and $|\mathbf{q}|$. As we shall describe below, the most favorable value of $|\mathbf{q}|$, in a Ginzburg-Landau approximation, is

$$|\mathbf{q}| = \eta\delta\mu\ . \tag{1.20}$$

with $\eta = 1.1997...$ In weak coupling, the opening angles of both the u and d rings are approximately equal and are given by $\psi = 2\arccos(\delta\mu/|\mathbf{q}|) \approx 67.1°$.

As we discussed before, a superconductor can respond to the splitting of Fermi surfaces by changing the Fermi momentum and forming a phase featuring BCS-like pairing. In the case of two flavor pairing the free energy of this BCS-like phase, called the 2SC phase, is given by

$$\Omega_{2SC} - \Omega_N \approx \frac{2\mu^2}{\pi^2}\delta\mu^2 - \frac{\mu^2}{\pi^2}\Delta_{2SC}^2\ , \tag{1.21}$$

where Δ_{2SC} is the value of the gap parameter with $\delta\mu = 0$. This is related to Δ_0, the gap parameter at zero splitting in the CFL phase, by the relation $\Delta_{2SC} = 2^{1/3}\Delta_0$ [8]. $\Delta_0 = 25$MeV gives $\Delta_{2SC} = 31.5$MeV.

For

$$\delta\mu > \frac{\Delta_{2SC}}{\sqrt{2}}\ , \tag{1.22}$$

the normal phase is more favorable than the paired phase, and as we increase $\delta\mu$ from 0, there is a first order transition from the 2SC phase to unpaired matter at $\delta\mu_c = \Delta_{2SC}/\sqrt{2}$. This point is called the Clogston point. (All this is very reminiscent of our discussion of CFL matter at non-zero M_s.)

We compare the free energies of the 2SC phase and the single plane wave "crystalline" phase (1.18) as a function of $\delta\mu$ in Figure 1-5.

From the free energy diagram we conclude that a single plane wave condensate is not favored over the 2SC phase for a large range of parameter space. But intuition suggests that since a single plane wave condensate allows pairing along rings on the Fermi surfaces, we can cover a larger area on the Fermi surfaces by considering pairing

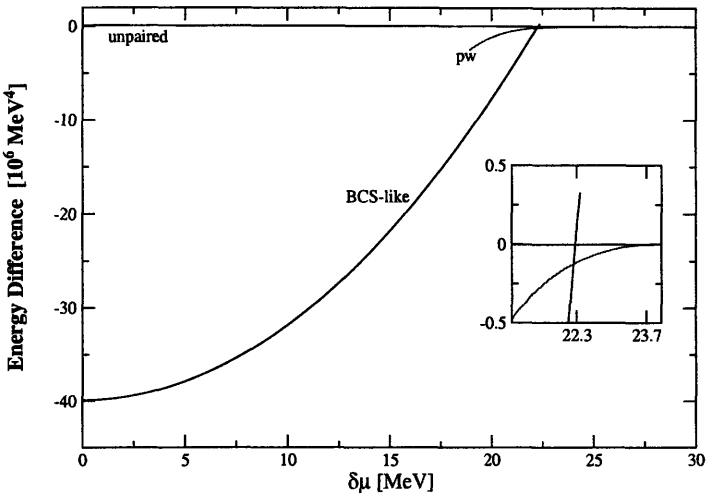

Figure 1-5: Comparison of the free energy of the single plane wave condensate with the BCS-like (2SC) phase. The plot has been made with $\Delta_{2SC} = 31.5$MeV and $\mu = 500$MeV. The zero of the free energy corresponds to the unpaired phase. We see that the 2SC phase becomes unfavorable compared to the unpaired phase at the Clogston point $\delta\mu_c = \Delta_{2SC}/\sqrt{2} = 22.3$MeV. But the single plane wave "crystalline" phase — labelled by "pw" in the figure — has lower free energy already at a slightly smaller $\delta\mu$ and is the preferred phase from that point to $\delta\mu_* \approx 0.754\Delta_{2SC} = 23.75$MeV. The transition from this simple "crystalline" phase to unpaired quark matter is a second order transition, as can be judged by the fact that the "pw" curve merges with the "unpaired" curve smoothly.

along multiple plane waves as in Eq. (1.17). Our aim, then, is to try to find a set of momentum vectors $\{\mathbf{q}\}$ so that the free energy of the superconductor is as small as possible.

The calculation of the free energy for crystalline phases with more than one plane wave has been studied in detail only in the Ginzburg-Landau approximation which is an expansion of the free energy of a phase in a power series of the order parameter. The expression for the Free energy should be consistent with all the symmetries of the Lagrangian, whether broken or unbroken. The coefficients in the expansion can be determined from the microscopic theory that describes the system, and depend upon the parameters of the theory. The value taken by the order parameter is one that minimizes the free energy.

We will now see the rather abstract description of the previous paragraph in

practice below, which will make it clearer. For a crystalline phase with condensate Eq. (1.17), the Ginzburg-Landau expansion of the free energy in Δ has the form,

$$\Omega_{\text{crystalline}}(\Delta) = \frac{2\mu^2}{\pi^2}\left[P\alpha|\Delta|^2 + \frac{\beta}{2}|\Delta|^4 + \frac{\gamma}{3}|\Delta|^6\right] + \mathcal{O}(\Delta^8) \tag{1.23}$$

Here, P is the number of planewaves in the set $\{\mathbf{q}\}$, and we have subtracted the free energy associated with neutral unpaired quark matter. Only terms proportional to $|\Delta|^2$ can appear in the free energy because the Lagrangian is invariant under independent global phase rotation of the u and d quark fields, which means that the the free energy should be invariant under phase rotations of Δ. The values of the Ginzburg-Landau coefficients, $P\alpha$, β and γ depend on the crystal structure, and the search for the most favorable crystal structure(s) entails the calculation of these coefficients for many crystal structures and finding one(s) which have the lowest free energy. As mentioned, α, β and γ can be calculated from the microscopic theory, which we take to be quarks interacting via the NJL model, which mocks up the QCD color interaction.

To see how this is done, we will need to introduce some notation. We write the condensate as

$$\langle u(x)d(x)\rangle \propto \sum_{\mathbf{q}^a\in\{\mathbf{q}\}} \Delta(\mathbf{q}^a)e^{2i\mathbf{q}^a\cdot\mathbf{x}}\,. \tag{1.24}$$

In Eq. (1.24), we have introduced a dependence of Δ on $\mathbf{q}^a$. At the last step, we will let Δ to be the same of all $\mathbf{q}$ as in Eq. (1.17), but in the intermediate steps, this dependence will allow us to keep track of which $\mathbf{q}^a$ go with which $\Delta(\mathbf{q}^a)$.

Formally, the free energy is the potential obtained by integrating all the quarks out of the system. The Ginzburg-Landau expansion of the free energy, correct to some order in $\Delta(\mathbf{q}^a)$ can be written down by treating $\Delta(\mathbf{q}^a)$ as an interaction vertex and summing all Feynman diagrams that arise, up to that order. Since the quarks are completely integrated out they will only appear in the propagators of loop integrals. This leaves us with a power series in $\Delta(\mathbf{q}^a)$ and $\Delta^*(\mathbf{q}^a)$, as desired. The dependence on momenta $\{\mathbf{q}\}$ comes in because $\Delta(\mathbf{q}^a)$ injects a momentum $-2\mathbf{q}^a$ into the loop

and each $\Delta^*(\mathbf{q}^a)$ injects $2\mathbf{q}^a$. The free energy has the form

$$\begin{aligned}\Omega_{\text{crystalline}}(\{\Delta(\mathbf{q}^a)\}) \propto\ & \mathcal{I}(\mathbf{q}^a,\mathbf{q}^b)\Delta(\mathbf{q}^a)\Delta^*(\mathbf{q}^b)\delta_{\mathbf{q}^a-\mathbf{q}^b} \\ & + \mathcal{J}(\mathbf{q}^a,\mathbf{q}^b,\mathbf{q}^c,\mathbf{q}^d)\Delta(\mathbf{q}^a)\Delta^*(\mathbf{q}^b)\Delta(\mathbf{q}^c)\Delta^*(\mathbf{q}^d)\delta_{\mathbf{q}^a-\mathbf{q}^b+\mathbf{q}^c-\mathbf{q}^d} \\ & + \mathcal{K}(\mathbf{q}^a,\mathbf{q}^b,\mathbf{q}^c,\mathbf{q}^d,\mathbf{q}^e,\mathbf{q}^f)\Delta(\mathbf{q}^a)\Delta^*(\mathbf{q}^b)\Delta(\mathbf{q}^c)\Delta^*(\mathbf{q}^d)\Delta(\mathbf{q}^e)\Delta^*(\mathbf{q}^f)\delta_{\substack{\mathbf{q}^a-\mathbf{q}^b+\mathbf{q}^c-\mathbf{q}^d \\ +\mathbf{q}^e-\mathbf{q}^f}} + \dots .\end{aligned} \tag{1.25}$$

In Eq. (1.25), $\mathcal{I}(\mathbf{q}^a,\mathbf{q}^b) = \pi^2/(2\mu^2 G) + \Pi(\mathbf{q}^a,\mathbf{q}^b)$, where G is the strength of the NJL coupling constant and $\Pi(\mathbf{q}^a,\mathbf{q}^b)$ is a loop integral with two momentum insertions $-2\mathbf{q}^a$ and $2\mathbf{q}^b$. $\mathcal{J}(\mathbf{q}^a,\mathbf{q}^b,\mathbf{q}^c,\mathbf{q}^d)$ is a loop integral with 4 momentum insertions $-2\mathbf{q}^a$, $2\mathbf{q}^b$, $-2\mathbf{q}^c$ and $2\mathbf{q}^d$ and similarly $\mathcal{K}(\mathbf{q}^a,\mathbf{q}^b,\mathbf{q}^c,\mathbf{q}^d,\mathbf{q}^e,\mathbf{q}^f)$ is loop integral with 6 momentum insertions. The Kronecker δ functions of $\mathbf{q}^a$s constrain the net momentum added to the loop to be zero. This is true because of momentum conservation: although translational symmetry is spontaneously broken by the ansatz Eq. (1.17), it is a symmetry of the Lagrangian and hence also the free energy.

The quadratic coefficient $\mathcal{I}(\mathbf{q}^a,\mathbf{q}^b)$ is the simplest. Because of the Kronecker delta imposing $\mathbf{q}^a = \mathbf{q}^b$, it is only a function of $\mathbf{q}^a$ and is not affected by the relative orientation of the $\mathbf{q}^a$s. ($\mathcal{I},\mathcal{J},\mathcal{K}..$ are also functions of the parameters of the theory, $\delta\mu$, $\Delta_{2\text{SC}}$, but we are not writing the explicit dependence on these for clarity.) Furthermore because of rotational symmetry it depends only on the magnitude of the $\mathbf{q}^a$. On the face of it $\mathcal{I}(\mathbf{q}^a,\mathbf{q}^a)$ depends on G, but that dependence combines with the dependence on the momentum cutoff Λ that is needed to regulate the loop integral Π, to give a final answer that is a function of $\Delta_{2\text{SC}}$ only and not of G and Λ individually. We give this function below.

$$\mathcal{I}(\mathbf{q}^a,\mathbf{q}^a) = \alpha(|\mathbf{q}^a|,\delta\mu) = -1 + \frac{\delta\mu}{2|\mathbf{q}^a|}\log\Big(\frac{|\mathbf{q}^a|+\delta\mu}{|\mathbf{q}^a|-\delta\mu}\Big) - \log\Big(\frac{\Delta_{2\text{SC}}^2}{4(|\mathbf{q}^a|^2-\delta\mu^2)}\Big)\ . \tag{1.26}$$

Our aim is to choose the magnitudes and the directions of $\mathbf{q}^a$ to obtain as small a free energy as possible. We simplify the problem by choosing the magnitudes of $\mathbf{q}^a$ to ensure that the quadratic term is as small as possible. This is an approximation

because in principle we should find the $|\mathbf{q}^a|$ to minimize the full $\Omega_{\text{crystalline}}$, but may be a reasonable approximation when Δ is small so that the quadratic term is dominant. Minimizing $\alpha(|\mathbf{q}^a|, \delta\mu)$ with respect to $|\mathbf{q}^a|$ fixes the magnitude of all the momentum vectors to be equal $|\mathbf{q}^a| = \eta\delta\mu$ for all a, where η satisfies the equation,

$$-1 + \frac{1}{2\eta}\log\left(\frac{\eta+1}{\eta-1}\right) . \tag{1.27}$$

Numerically $\eta = 1.1997...$ With this value of η, α simplifies to,

$$\alpha(\delta\mu) = -\frac{1}{2}\log\left(\frac{\Delta_{2\text{SC}}^2}{4\delta\mu^2(\eta^2-1)}\right) \tag{1.28}$$

Now taking $\Delta(\mathbf{q}^a) = \Delta$ for all a in Eq. (1.25), we get back the Ginzburg-Landau expansion Eq. (1.23) with α defined as in Eq. (1.28) and β and γ given by,

$$\beta = \sum_{\mathbf{q}^a,\mathbf{q}^b,\mathbf{q}^c,\mathbf{q}^d} \mathcal{J}(\mathbf{q}^a,\mathbf{q}^b,\mathbf{q}^c,\mathbf{q}^d)\delta_{\mathbf{q}^a-\mathbf{q}^b+\mathbf{q}^c-\mathbf{q}^d} \tag{1.29}$$

$$\gamma = \sum_{\substack{\mathbf{q}^a,\mathbf{q}^b,\mathbf{q}^c,\mathbf{q}^d \\ ,\mathbf{q}^e,\mathbf{q}^f}} \mathcal{K}(\mathbf{q}^a,\mathbf{q}^b,\mathbf{q}^c,\mathbf{q}^d,\mathbf{q}^e\mathbf{q}^f)\delta_{\substack{\mathbf{q}^a-\mathbf{q}^b+\mathbf{q}^c-\mathbf{q}^d \\ +\mathbf{q}^e-\mathbf{q}^f}} \tag{1.30}$$

β and γ do depend on the directions of the momentum vectors and to have as small a free energy as possible, we would like to choose these directions of $\{\hat{\mathbf{q}}^a\}$ so that β and γ are as small as possible.

It is useful to understand how the coefficients behave as a function of $\delta\mu$. As can be seen from Eq. (1.28), α is negative for $\delta\mu < \delta\mu_*$ with $\delta\mu_*$ given by,

$$\delta\mu_* = \frac{\Delta_{2\text{SC}}}{2\sqrt{\eta^2-1}} \approx 0.754\Delta_{2\text{SC}} \tag{1.31}$$

and changes sign at $\delta\mu_*$. β and γ do not change sign as a function of $\delta\mu$, only their magnitude becomes smaller as $\delta\mu$ increases [39]. The fact that α becomes positive at $\delta\mu_*$ is of course not a coincidence. If β and γ are positive, this implies that the value of Δ at which $\Omega_{crystalline}$ given in Eq. (1.23) is minimum is non-zero for $\delta\mu < \delta\mu_*$ and zero for $\delta\mu \geq \delta\mu_*$. There is a second order phase transition at $\delta\mu_*$ from the paired

phase to the unpaired phase as we increase $\delta\mu$ from below $\delta\mu_*$ to above $\delta\mu_*$. Indeed, for a single plane wave β and γ are positive as we would expect from Figure 1-5. For a structure which shows a second order transition, the value of Δ at the minimum of Ω is close to zero near the phase transition point, and a Ginzburg-Landau calculation is quantitatively accurate near $\delta\mu_*$.

For structures that have β negative and γ positive, the transition from the pairing phase to the unpaired phase as we increase $\delta\mu$, occurs at a $\delta\mu > \delta\mu_*$, and is a first order transition. The Ginzburg-Landau expansion can not be quantitatively accurate for such structures, but it can still tell us about qualitative features that make crystal structures favorable.

From an analysis of several crystal structures in [39], the authors distilled two principles that help restricting the myriad possibilities of crystalline condensates.

- If two momentum vectors $\mathbf{q}^a$ and $\mathbf{q}^b$ from the set $\{\mathbf{q}\}$ are at an angle less than 67.1°, then β and γ are large and positive and the crystalline structure is unfavorable. It is possible to understand this intuitively as follows. For each $\mathbf{q}^a$, there is a corresponding pairing ring on the u (also d) Fermi surface, which has an opening angle 67.1°. If two momentum vectors make an angle close to, or smaller than, 67.1°, the pairing rings intersect each other and the structure is unfavorable. When the two pairing rings intersect, the two pairing rings are "competing" to pair the quarks that lie on their intersection.

- From Eqs. (1.29) and (1.30), we see that β and γ are sums of integrals, where the sums are taken to be over momentum vectors taken such that the net momentum added to the loop is zero. Highly symmetric crystal structures, which have many sets of momentum vectors $\mathbf{q}$ such that the momentum conservation condition can be satisfied, are favorable.

The most favorable set of momentum vectors features 8 momentum vectors in $\{\mathbf{q}\}$ [39]. These point towards the vertices of a regular cube, forming a BCC reciprocal

lattice. In position space, the condensate varies like a FCC crystal structure,

$$\begin{aligned}\Delta(x) =& 2\Delta\Big[\cos\big(\frac{2\pi}{a}(x+y+z)\big)+\cos\big(\frac{2\pi}{a}(x-y+z)\big)\\ &+\cos\big(\frac{2\pi}{a}(x+y-z)\big)+\cos\big(\frac{2\pi}{a}(-x+y+z)\big)\Big]\,.\end{aligned} \tag{1.32}$$

Here, a is the size of the cubic lattice and is given by

$$a=\frac{\sqrt{3}}{|\mathbf{q}|}\approx\frac{4.536}{\delta\mu}\,. \tag{1.33}$$

For $\delta\mu=\Delta_{2SC}/\sqrt{2}$ and taking a typical estimate for $\Delta_{2SC}=30$MeV, we get a about 42fm.

For this structure both β and γ are negative and the free energy is unbounded from below if we stop the expansion to the sextic order. For the complete three flavor case that we discuss now, when we include the strange quark, we find that for the most favorable structures we find, the Δ^4 coefficients are negative but the Δ^6 coefficients are positive. This implies that the free energy as a function of Δ is bounded from below and we can minimize it and find the value of Δ (this is solving the gap equation) and Ω at the minimum. The transition to unpaired state from the paired state is first order, and hence the calculation is not quantitatively reliable, but this allows us to get an understanding of the magnitude of the free energy and Δ.

1.5.2 Three flavor crystalline pairing

The natural generalization of the two flavor ansatz to the case where the s quark is included, is

$$\langle\psi_{si\alpha}(x)d_{tj\beta}(x)\rangle\propto\Delta(C\gamma^5)_{st}\sum_I\epsilon_{Iij}\epsilon_{I\alpha\beta}\sum_{\mathbf{q}_I^a\in\{\mathbf{q}_I\}}\exp(2i\mathbf{q}_I^a\cdot\mathbf{x})\,. \tag{1.34}$$

This features three condensates Δ_1, Δ_2 and Δ_3 corresponding to $s-d$, $u-s$ and $u-d$ pairing respectively. (We have suppressed the color indices which can be found

from the color epsilon symbols in Eq. (1.34).) To each condensate I corresponds a set of momentum vectors $\{\mathbf{q}_I\}$ which dictates how it is modulated in space, specifying a set of three crystal structures.

A simpler condensate of this form was first proposed by [44] who considered the case where the three sets of momentum vectors contain one momentum vector each, i.e. each condensate varies in space as a planewave. We generalized this in [46], allowing for more complicated crystal structures. Chapter 2 is based on Ref. [46]. Here we review the main ideas and the central results from the chapter.

As was done in the two-flavor context by [39], we want to calculate and compare the free energy expressions for several crystal structures, and find the ones that are most favorable. Here the situation is more complicated because there are three crystal structures. We can simplify the situation somewhat by making an approximation, $\Delta_1 = 0$ [44, 45]. It is reasonable to expect that because the d and s Fermi surfaces are twice as far apart from each other as each is from the intervening u Fermi surface, the pairing between d and s quarks is smaller compared to the $u-d$ and $u-s$ pairing.

This means that we consider crystal structures in which there are two condensates

$$\begin{aligned} \langle ud \rangle &\sim \Delta_3 \sum_{\mathbf{q}_3^a \in \{\mathbf{q}_3\}} \exp\left(2i\mathbf{q}_3^a \cdot \mathbf{r}\right) \\ \langle us \rangle &\sim \Delta_2 \sum_{\mathbf{q}_2^a \in \{\mathbf{q}_2\}} \exp\left(2i\mathbf{q}_2^a \cdot \mathbf{r}\right) \ . \end{aligned} \tag{1.35}$$

The search for favorable structures can be thought of as involving two steps. Choosing candidate condensates for $u-d$ pairing and for $s-u$ pairing, and then trying to orient them so as to get as favorable a structure as possible.

In Chapter 2 we calculate the free energies of the crystal structures in a Ginzburg-Landau approximation. The expression for the free energy with the ansatz of (1.35)

has the form

$$\Omega_{\text{crystalline}}(\Delta_2,\Delta_3)=\frac{2\mu^2}{\pi^2}\Bigg[P_2\alpha_2|\Delta_2|^2+P_3\alpha_3|\Delta_3|^2+\frac{1}{2}\Big(\beta_2|\Delta_2|^4+\beta_3|\Delta_3|^4+\beta_{32}|\Delta_2|^2|\Delta_3|^2\Big)$$
$$+\frac{1}{3}\Big(\gamma_2|\Delta_2|^6+\gamma_3|\Delta_3|^6+\gamma_{322}|\Delta_3|^2|\Delta_2|^4+\gamma_{233}|\Delta_3|^4|\Delta_2|^2\Big)\Bigg]\,. \tag{1.36}$$

This form again follows from the desired symmetry under individual phase rotations of the Δ_2 and Δ_3 condensates.

We can see from the expression Eq. (1.36) that if we set Δ_2 to zero, treating only $\langle ud\rangle$ pairing, we get back to the two-flavor Ginzburg-Landau analysis of Ref. [39]. This means that α_3, β_3 and γ_3 in Eq. (1.36) are exactly the same coefficients that appear in the two flavor calculation and can be taken from [39]. The same conclusion can be reached for α_2, β_2 and γ_2 by taking $\Delta_3=0$. Not only does this reduce our work, but is important because it gives us a direction in our search for favorable crystal structures. First of all since α_2 and α_3 have no "mixed" terms, determining the magnitude of vectors in $\{\mathbf{q}_2\}$ and $\{\mathbf{q}_3\}$ by minimizing the quadratic coefficient fixes the magnitudes of all the momentum vectors, $|\mathbf{q}_2^a|=\eta\delta\mu_2$ for all $\mathbf{q}_2^a\in\{\mathbf{q}_2\}$ and $|\mathbf{q}_3^a|=\eta\delta\mu_3$ for all $\mathbf{q}_3^a\in\{\mathbf{q}_3\}$, with $\eta=1.1997..$ as in the two-flavor case. Secondly, if these two-flavor coeffecients are large and positive, meaning that the structures formed by $\{\mathbf{q}_2\}$ and $\{\mathbf{q}_3\}$ seen individually are unfavorable two-flavor structures, then $\Omega_{\text{crystalline}}$ receives large positive contributions from β_2, β_3, γ_2 and γ_3, and the combined structure is unlikely to be favorable unless there are some special cancellations from the interactions of these condensates (no such cancellations are seen, see Chapter 2).

The "mixed" coefficients, β_{23} and γ_{233} are new terms that encode the interaction between the two condensates. From calculations of β_{23}, γ_{233} a crucial general conclusion emerges that the free energy of a candidate three-flavor crystal structure becomes less favorable the closer any $\mathbf{q}_2^a$ comes to the antipodes of any $\mathbf{q}_3^b$. This can be understood using an argument similar to the one used when we discussed two-

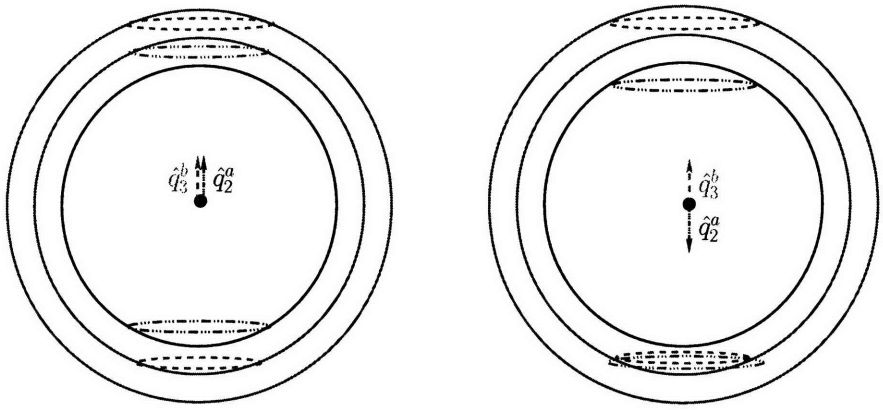

Figure 1-6: This figure shows pairing rings for momentum vectors $\mathbf{q}_2^a$ and $\mathbf{q}_3^b$. On the left $\mathbf{q}_2^a$ is parallel to $\mathbf{q}_3^b$ and the pairing rings on the u Fermi surface, common to the $u-d$ and $u-s$ pairing, are as far apart as they can be. On the right, $\mathbf{q}_2^a$ and $\mathbf{q}_3^b$ are at the antipodes of each other and the pairing rings overlap on the u Fermi surface.

flavor crystalline pairing, namely structures are unfavorable when different pairing rings compete for the same quarks by intersecting. Pairing rings corresponding to two momentum vectors in the same set, say $\{\mathbf{q}_3\}$, intersect when the two vectors say $\mathbf{q}_3^a$ and $\mathbf{q}_3^b$ are closer to each other than 67.1°. In the three flavor case, pairing rings associated with momentum vector $\mathbf{q}_2^a$ corresponding to $u-d$ pairing, and $\mathbf{q}_3^b$ corresponding to $u-s$ pairing can intersect on the common u Fermi surface if the angle between the two vectors is larger than $180-67.1°$, i.e., when $\mathbf{q}_2^a$ and $\mathbf{q}_3^b$ are close to the antipodes of each other (see Figure 1-6). As we will discuss in Chapter 2, structures become more unfavorable the closer any $\mathbf{q}_2^a$ comes to the antipodes of any $\mathbf{q}_3^b$ and in Chapter 3 we will see this to be valid for simple "crystalline" condensates containing two plane waves, even beyond the Ginzburg-Landau approximation.

The first observation begs us to consider the most favorable two-flavor crystal structure we saw in the last Section, eight $\mathbf{q}^a$s pointing towards the vertices of the cube, for $\{\mathbf{q}_2\}$ and $\{\mathbf{q}_3\}$. But we need to be careful to orient the two crystals so as to keep all the vectors $\mathbf{q}_3^a$ as "far" from the antipodes of all the vectors $\mathbf{q}_2^b$, as possible. The best orientation we found was one where the cube corresponding to the $\{\mathbf{q}_2\}$ is obtained by the rotation of the cube corresponding to $\{\mathbf{q}_3\}$ by 45 degrees about an axis passing through its center, and the center of a face (see Figure 4-1 in Chapter 4).

We call this structure 2Cube45z and it turns out to be one of the two most favorable structures we find.

The other structure that turns out to be very robust has four vectors each in $\{\mathbf{q}_3\}$ and $\{\mathbf{q}_2\}$. With a fewer number of vectors than in the cube, we are no longer choosing the most favorable two-flavor structures for $\{\mathbf{q}_2\}$ and $\{\mathbf{q}_3\}$ (see Figure 4-1 in Chapter 4). But with fewer vectors, we can do a better job of keeping the vectors in one set away from the antipodes of the vectors in the other set. The structure, "CubeX", has four $\mathbf{q}_3^a$'s and four $\mathbf{q}_2^a$'s which *together* point at the eight corners of a cube in momentum space and can be argued to be likely to be favorable (see Chapter 2).

As we mentioned at the end of the previous Section is the case for CubeX and 2Cube45z, $\Omega_{\text{crystalline}}(\Delta, \Delta)$ is positive for large Δ for all the crystal structures that we investigate because the Δ^6 term is always positive. Hence we can use our sextic Ginzburg-Landau expansion to evaluate Δ and Ω at the minimum of $\Omega(\Delta, \Delta)$ for all the three-flavor structures that we analyze. We show in Figure 1-7 the free energies for 2Cube45z and CubeX, and how they compare with the homogeneous pairing phases.

We find that the 2Cube45z and the CubeX structures have large condensation energies, easily 1/3 to 1/2 of that in the CFL phase with $M_s = 0$, which is $3\Delta_0^2\mu^2/\pi^2$. This is remarkable, given the only quarks that pair are those lying on (admittedly many) rings on the Fermi surfaces, whereas in the CFL phase with $M_s = 0$ pairing occurs over the entire u, d and s Fermi surfaces.

The gCFL phase has a lower free energy than the CFL phase and unpaired quark matter for M_s^2/μ between $2\Delta_0$ and $5.7\Delta_0$, but as mentioned in Section 1.4.3, it is unstable. We find that three-flavor crystalline color superconducting quark matter has a lower free energy than both gCFL quark matter and unpaired quark matter within a wide regime of density. For

$$2.9\Delta_0 < \frac{M_s^2}{\mu} < 10.4\Delta_0 \tag{1.37}$$

the crystalline phase with one or other of the two crystal structures that we argue are

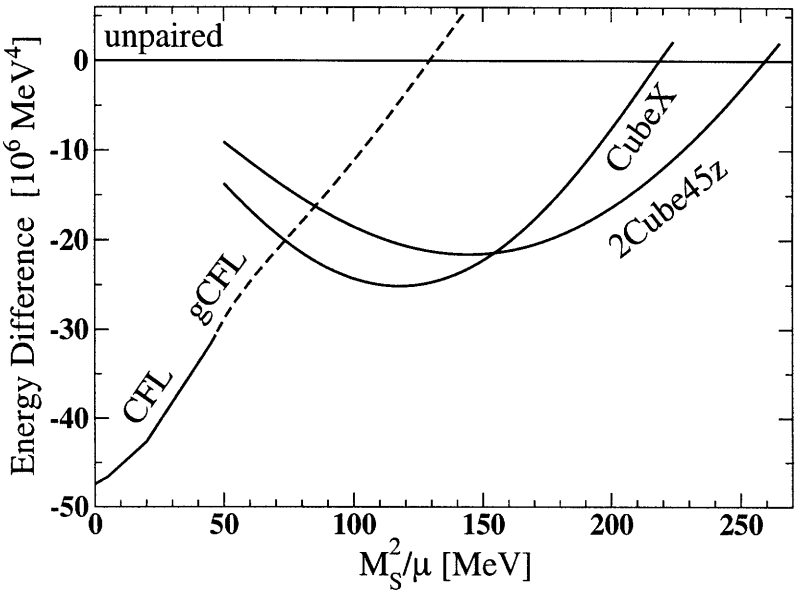

Figure 1-7: Plot of the free energies of the crystalline phases 2Cube45z and CubeX, and comparison with the homogeneous phases CFL and the gCFL. The zero is taken to be the free energy of neutral unpaired quark matter. The "x" axis is M_s^2/μ which is proportional to the splitting of the Fermi surfaces. At the very left, $M_s^2/\mu = 0$, which corresponds to asymptotically high densities. The CFL phase is the favored phase in this regime. As we move towards the right, there is a stress on the CFL pairing. The gCFL phase has a lower free energy than the CFL phase for $M_s^2/\mu > 2\Delta_0$, but is unstable. In making the diagram, we have taken Δ_0, the gap parameter in the CFL phase with $M_s = 0$, to be 25MeV, and μ to be 500MeV. We see that the two crystalline phases are favored over homogeneous pairing phases over a large range of parameters.

most favorable has lower free energy (greater condensation energy) than CFL quark matter, gCFL quark matter, and unpaired quark matter. This window in parameter space is in no sense narrow.

If we take representative values of M_S and Δ_0, $M_s = 250$MeV and $\Delta_0 = 25$MeV, then Eq. (1.37) translates into a window of μ,

$$847\text{MeV} > \mu > 240\text{MeV} \, . \tag{1.38}$$

In reality both M_s and Δ_0 are functions of μ, and taking this into account modifies the window in μ given by Eq. (1.38). See Ref. [131] for an analysis in which both

$M_s(\mu)$ and $\Delta_0(\mu)$ are calculated self-consistently in an NJL model, confirming that the window in μ corresponding to (1.37) is broad indeed. Even though it may not be quantitatively reliable, the breadth of the regime (1.38), corresponding to the remarkable robustness of the two most favorable crystalline phases which can be understood on qualitative grounds, makes it plausible that quark matter at densities accessible in neutron stars, say with $\mu \sim 350-500$ MeV, will be in a crystalline phase. (Unless Δ_0 is closer to 100 than it is to 10, in which case quark matter at accessible densities will be in the CFL phase.)

We can also see from Figure 1-7 that unless the Ginzburg-Landau approximation is underestimating the condensation energy of the crystalline phase by about a factor of two, there is a fraction of the "gCFL window" (with $2\Delta_0 < M_s^2/\mu < 2.9\Delta_0$, in the Ginzburg-Landau approximation) in which no crystalline phase has lower free energy than the gCFL phase. This is thus the most likely regime in which to find the current-carrying meson condensates of Refs. [86, 87].

However there is a caveat. The Ginzburg-Landau approximation is an expansion in small Δ and is valid if $\Delta \ll \delta\mu$, where $\delta\mu \sim M_s^2/(8\mu)$ and Δ is the gap parameter of the crystalline color superconducting phase which minimizes the free energy. We can see from Figure 1-8 that the most favored crystal structures can have $\Delta/\delta\mu$ as large as $\sim 1/2$, meaning that we are pushing the approximation hard and so should not trust it quantitatively.

In Chapter 3 [45], we analyze a particularly simple one parameter family of "crystal" structures in three-flavor quark matter. We consider the case when $\{\mathbf{q}_2\}$ contains a single vector $\mathbf{q}_2$ and similarly $\{\mathbf{q}_3\}$ contains a single vector $\mathbf{q}_3$. From rotational invariance, the free energy of the "crystal" structure can depend only on the magnitudes of $\mathbf{q}_2$ and $\mathbf{q}_3$, and the angle between them, which we call ϕ. We can calculate the free energies of this family of condensates in the Ginzburg-Landau approximation by calculating $\beta_{2,3,23}$ and $\gamma_{2,3,233,322}$. But it turns out that we can do the calculation without making an expansion in Δ for this family of condensates, which allows us to check the "goodness" of the approximation in this simple setting.

The transition from these two-planewave structures to unpaired quark matter is

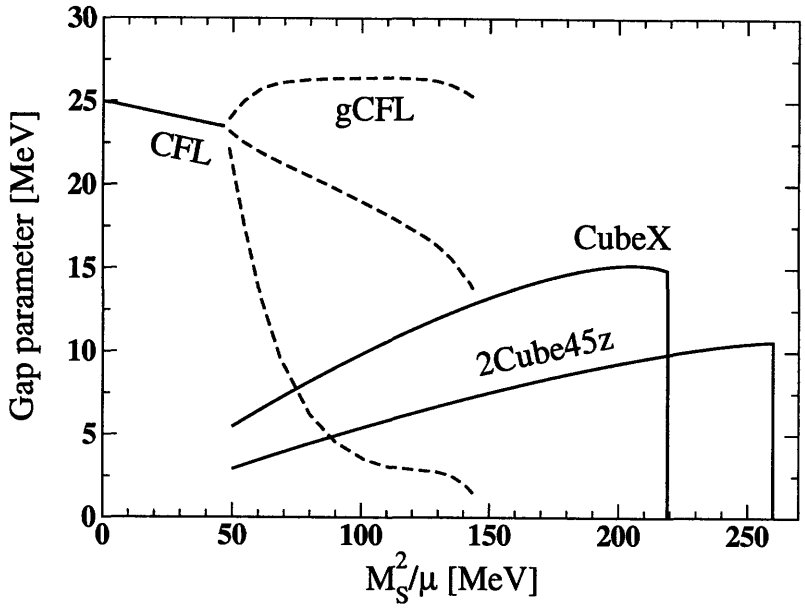

Figure 1-8: Plot of the gap parameter of the crystalline phases 2Cube45z and CubeX, and comparison with the homogeneous phases CFL and the gCFL. We can see that Δ_0 is equal to 25MeV, and we take μ to be 500MeV as for the free energy plot. The value of the gap parameters we obtain for these crystalline condensates is very large, up to $\Delta_0/2$.

second order. We find that the approximation works best close to the second order point where Δ tends to zero, which is no surprise. We also find that, at least for the simple crystal structures, when it breaks down it always underestimates the gap Δ and the condensation energy, and is in this sense conservative. Furthermore, we find that the Ginzburg-Landau approximation correctly determines which crystal structure among the one parameter family has the largest gap and lowest free energy. We shall see, however, that the range of validity of the Ginzburg-Landau approximation does depend on the crystal structure.

In general, a Ginzburg-Landau expansion is likely to be dubious precisely in the cases of interest: if a crystalline phase exists with a free energy lower than that of the gCFL phase, such a phase will be characterized by robust pairing meaning that Δ will not be much smaller than Δ_0. This means that to rigorously show the favorability of crystalline superconductivity over gCFL matter, we need to do a beyond Ginzburg-

Landau calculation. Recently progress has been made towards the calculation of the free energy of crystalline superconductors without using the Ginzburg-Landau approximation [77, 78, 79, 80] in condensed matter systems. We are investigating the application of their techniques to the quark matter context.

But the robustness of these phases (Figure 1-7) and the wide window where they are favorable in (1.37), as well as the evidence from Chapter 3 that at least in some cases the Ginzburg-Landau approximation is conservative, motivates us to look at the implication of their existence in the cores of neutron stars, for their phenomenology.

1.6 What neutron stars can tell us about color superconductivity

The only place in nature where we expect to find cold dense quark matter is at the cores of neutron stars [49, 51, 52]. These are extremely dense objects, carrying a mass of around $1 - 2M_{\odot}$, bound by gravitational interaction in an approximately spherical region of radius about 10km. Most of this mass is baryonic and hence these compact objects are valuable testing grounds for theories about dense baryonic matter.

For example, measurements of the mass and radii of neutron stars can tell us about the Equation of State (EoS), i.e. the relation between the pressure and the energy density of dense matter [53]. The interior of a neutron star is under hydrostatic equilibrium under the attractive force of gravity and a balancing pressure in the matter. (We ignore, for the sake of discussion, effects due to rotation, magnetic forces etc.) The relation that mathematically expresses this equilibrium is known as the Tolman-Oppenheimer-Volkoff (TOV) equation and can be solved for a given EoS to give the structure of the neutron star. The relation between the mass and the radius of neutron stars can then be compared with experimental observations. Masses have been measured for about 40 neutron stars [51], but the observation of their radii is much more difficult.

At zero temperature the pressure of the system is just the negative of the free

energy density. In a color superconducting phase this is determined largely by the free energy of unpaired quark matter, which goes as μ^4. Pairing is a Fermi surface phenomenon and its contribution is much less, proportional to $\mu^2\Delta^2$. Hence the first guess would be that color superconductivity will not have a major effect on the EoS of quark matter. But the situation is more subtle than that because the contribution to the free energy from the "bag" constant may cancel the contribution from unpaired quark matter and the pairing contribution can be important [53]. By studying the structure of hybrid stars, model neutron stars with a quark matter core, authors of Ref. [50] found that for certain choice of parameters these hybrid stars could have the same mass-radius relation as a star without any deconfined quark matter. Their results suggest that this would be a difficult way to learn whether cores of neutron stars have quark matter cores or not.

Another possible example of how observing the structure of neutron stars can elucidate features in the phase diagram of dense QCD, is the observation of gravitational radiation from the inspiral of a neutron star in a binary system. Baryon density (and correspondingly the baryon number chemical potential) increases as we descend into a neutron star. The presence of a sharp phase transition in the phase diagram — possibly between hadronic and quark matter — lying at a chemical potential somewhere between its value close to the surface and the value at the core, should show up as a sudden change in the density profile of the star. This may be picked up in the pattern of gravitational waves emitted during the inspiral which may show features at two different times, corresponding to the merger of the outer layer and the inner core respectively.

Such observations may help us indirectly to conclude if deconfined quark matter is present in neutron stars. But color superconductivity has a more direct consequence on the cooling and transport properties of neutron stars, than its structure. This is because superconductivity dramatically changes the low energy spectrum of the quasiparticles in the system, which determines these properties. One aspect that has been explored in literature is the cooling of neutron stars. Neutron stars lose a large percent of the gravitational energy they gain after the supernova explosion in the form

of neutrinos, and within seconds their temperature drops to a few 100s of KeV. This is followed by a period of more gradual cooling [108] via indirect neutrino emission, which lasts for about a million years. The two microscopic properties that determine rate of cooling are neutrino emisivity and the specific heat. If they are kinematically allowed, the fastest way to create neutrinos that can carry away energy are the direct URCA processes, which give a fast neutrino emissivity $\varepsilon_\nu \sim T^6$ [105]. Direct URCA processes are kinematically suppressed in ordinary nuclear matter consisting only of protons and neutrons, and neutrino emission occurs via indirect URCA processes giving a smaller emissivity, $\varepsilon_\nu \sim T^8$. But other effects in dense nuclear matter, like the presence of hyperons, can allow direct URCA processes. Direct URCA processes are also allowed for unpaired quark matter. CFL pairing introduces a gap in the quasiparticle excitation spectrum and thus the direct URCA processes are suppressed. But phases that feature some gapless excitations of quarks, allow direct URCA processes and therefore cool at a fast rate.

The first steps toward calculating the cooling rate for neutron stars carrying three flavor crystalline quark matter were taken in Ref. [104]. Because the crystalline phases leave some quarks at their respective Fermi surfaces unpaired, it seems likely that their neutrino emissivity and heat capacity will be only quantitatively smaller than those of unpaired quark matter [105], not parametrically suppressed. This suggests that neutron stars with crystalline quark matter cores will cool by the direct URCA reactions, i.e. more rapidly than in standard cooling scenarios [106]. However, as we mentioned above, many other possible core compositions can open phase space for direct URCA reactions, making it unlikely that this will lead to a distinctive phenomenology [107].

There is one property that all homogeneous phases of matter proposed as candidates for the composition of neutron star cores have in common. They are fluid which means that they can not respond elastically to a shearing force. One of the main results that we will show in Chapter 4 is that crystalline phases are rigid solids, making them unique phases of dense QCD. This may lead to distinct phenomenology.

In Chapter 4, we study the elastic properties of the CubeX and the 2Cube45z

crystalline phases of three-flavor quark matter. We will evaluate the shear moduli of these two structures by computing, in the Ginzburg-Landau approximation, the effective Lagrangian for the phonon modes which emerge due to the spontaneous breaking of translation invariance by the crystalline condensates. (See Ref. [101, 102] for analyses of phonons in 2-flavor crystalline color superconducting phases.) The shear modulus is related to the coefficients of the spatial derivative terms that appear in the phonon effective Lagrangian. When these two crystalline phases are subject to shear stresses, they behave like rigid solids with shear moduli between 20 and 1000 times larger than those characteristic of conventional neutron star crusts.

At the same time the crystalline color superconducting phases are superfluids: their condensates all spontaneously break the $U(1)_B$ symmetry corresponding to quark number. (We shall always write the condensates as real. The choice of overall phase breaks $U(1)_B$, and long wavelength gradients in this phase correspond to supercurrents.)

The possibility that quark matter could occur in a solid phase has been raised previously by Xu [134]. He and his collaborators have explored some astrophysical consequences of a speculation that the quarks themselves could somehow be arranged in a crystalline lattice. The crystalline color superconducting phase is very different in character: being a superfluid, the quarks are certainly not frozen in place. Instead, what forms a crystalline pattern is the magnitude of the pairing condensate. Although it was clear prior to the present work that in this phase translational invariance is broken just as in a crystal, given that this phase is at the same time a superfluid it was not clear (at least to us) whether it was rigid. Here, we demonstrate by explicit calculation that this phase, which as we have discussed is plausibly the only form of quark matter that arises at densities reached within neutron star cores, is rigid indeed. Its shear modulus is parametrically of order $\Delta^2\mu^2$, which could have been guessed on dimensional grounds. The shear modulus is in no way suppressed relative to this natural scale, even though the crystalline color superconducting phase is superfluid.

As we shall discuss further in Chapter 4, that the crystalline phases are rigid as well as superfluid, may have significance for a particular aspect of neutron star

phenomenology. Namely (as suggested in reference [39]), pulsar glitches may originate in a rigid crystalline superconducting core. A spinning neutron star observed as a pulsar gradually spins down as it loses rotational energy to electromagnetic radiation. But, every once in a while the angular velocity at the crust of the star is observed to increase suddenly in a dramatic event called a glitch. The standard explanation [109, 110, 111, 112, 113, 114, 115, 116, 117, 118, 119, 120, 121] for their occurrence requires the presence of a superfluid in some region of the star which also features a rigid array of spatial inhomogeneities which can pin the rotational vortices in the rotating superfluid. In the standard explanation of pulsar glitches, these conditions are met in the inner crust of a neutron star which features a crystalline array of positively charged nuclei bathed in a neutron superfluid (and a neutralizing fluid of electrons). The angular momentum of the rotating superfluid is proportional to the density of vortices, meaning that as the star as a whole slows the vortices "want" to move apart. As they are pinned to a rigid structure, they cannot. Hence, this superfluid component of the star is spinning faster than the rest of the star. After sufficient time, when the "tension" in the vortices in some region reaches a critical point, there is a sudden "avalanche" in which vortices unpin and rearrange, reducing the angular momentum of the superfluid. The rest of the star, including in particular the surface whose angular velocity is observed, speeds up. We see that this mechanism requires superfluidity coexisting with a structure that is rigid enough that it does not easily deform when vortices pinned to it seek to move, and an adequate pinning force which pins vortices to the rigid structure in the first place.

In Chapter 4 we will see that the crystalline phases are rigid. Furthermore, it is reasonable to expect that the superfluid vortices that will result when crystalline color superconducting phases are rotated will have lower free energy if they are centered along intersections of nodal planes of the crystal structure, i.e. along lines along which the condensate already vanishes even in the absence of a rotational vortex. By virtue of being simultaneously superfluids and rigid solids, then, the crystalline phases of quark matter provide all the necessary conditions to be the locus in which (some) pulsar glitches originate. In Chapter 4, we also provide a crude estimate of

the pinning force and find that it is comparable to the corresponding value for a neutron star crust. Together, our calculation of the shear modulus and estimate of the pinning force make the core glitch scenario worthy of quantitative investigation. The central questions that remain to be addressed are the explicit construction of vortices in the crystalline phase and the calculation of their pinning force, as well as the timescale over which sudden changes in the angular momentum of the core are communicated to the (observed) surface, presumably either via the common electron fluid or via magnetic stresses.

Finally, the advent of gravity wave detectors opens a new possibility for unique signatures of the presence of rigid matter within neutron stars, independent of transient phenomena like glitches [135]. LIGO has already set limits on the steady-state gravity wave emission from 78 nearby pulsars [136], and these limits will become more stringent. Owen's work [135] shows that if an entire neutron star were solid, with a shear modulus as large as that we find for crystalline color superconducting quark matter, it could in principle support a quadrupole moment large enough such that the resulting gravity waves would already have been detected. This suggests that as the observational upper limits improve, the size of a putative rigid crystalline color superconducting quark matter core could be constrained. However, Owen's estimates for a star that is rigid in its entirety cannot be applied straightforwardly to the case where there is a rigid core surrounded by a fluid "mantle". Oblateness about the rotational z-axis is not enough to generate gravity waves; the quadrupole moment must be mis-aligned, such that the moment of inertia tensor satisfies $I_{xx} \neq I_{yy}$. It is hard to imagine how this could come about for a rigid quark matter core, whose shape will equilibrate to follow an equipotential surface via converting core material into mantle material or vice versa as needed at different locations along the core/mantle interface. Nevertheless, this line of enquiry warrants careful investigation.

Chapter 2

The crystallography of color superconducting quark matter.

2.1 Overview

In this chapter, we analyze and compare candidate crystal structures for the crystalline color superconducting phase in three-flavor quark matter. We determine the gap parameter Δ and free energy $\Omega(\Delta)$ for many possible crystal structures within a Ginzburg-Landau approximation, evaluating $\Omega(\Delta)$ to order Δ^6. In contrast to the two-flavor case, we find a positive Δ^6 term and hence an $\Omega(\Delta)$ that is bounded from below for all the structures that we analyze. This means that we are able to evaluate Δ and Ω as a function of the splitting between Fermi surfaces for all the structures we consider. We find two structures with particularly robust values of Δ and the condensation energy, within a factor of two of those for the CFL phase which is known to characterize QCD at asymptotically large densities. The robustness of these phases results in their being favored over wide ranges of density. However, it also implies that the Ginzburg-Landau approximation is not quantitatively reliable. We develop qualitative insights into what makes a crystal structure favorable, and use these to winnow the possibilities. The two structures that we find to be most favorable are both built from condensates with cubic symmetry.

2.2 Outline

The chapter is organized as follows. In Section 2.3, we shall specify the model we use and the simplifying assumptions we make, valid for $\Delta \ll \Delta_0$. One simplifying assumption that we make is that Δ_2 and Δ_3 are equal in magnitude, an assumption which is related to how electric neutrality is maintained. In Appendix A , we use our results to confirm the validity of this assumption. In Section 2.4 we introduce the Ginzburg-Landau expansion of the free energy, deferring the derivation of the expressions for the Ginzburg-Landau coefficients to Section 2.5 and their evaluation to Section 2.6. We give our results in Section 2.7, which suggest that cold quark matter at densities that may be present in the cores of neutron stars, may exist in the crystalline color superconducting phase. We therefore look ahead at possible implications on neutron star phenomenology in Section 2.8.

2.3 Model, simplifications and ansatz

2.3.1 Neutral unpaired three-flavor quark matter

We shall analyze quark matter containing massless u and d quarks and s quarks with an effective mass M_s. (Although the strange quark mass can be determined self-consistently by solving for an $\langle \bar{s}s \rangle$ condensate [65, 128, 129, 130, 131], we shall leave this to future work and treat M_s as a parameter.) The Lagrangian density describing this system in the absence of interactions is given by

$$\mathcal{L}_0 = \bar{\psi}_{i\alpha} \left(i \partial\!\!\!/ {}^{\alpha\beta}_{ij} - M^{\alpha\beta}_{ij} + \mu^{\alpha\beta}_{ij} \gamma_0 \right) \psi_{\beta j} \ , \tag{2.1}$$

where $i, j = 1, 2, 3$ are flavor indices and $\alpha, \beta = 1, 2, 3$ are color indices and we have suppressed the Dirac indices, where $M^{\alpha\beta}_{ij} = \delta^{\alpha\beta} \, \mathrm{diag}(0, 0, M_s)_{ij}$ is the mass matrix, where $\partial^{\alpha\beta}_{ij} = \partial \delta^{\alpha\beta} \delta_{ij}$ and where the quark chemical potential matrix is given by

$$\mu^{\alpha\beta}_{ij} = (\mu \delta_{ij} - \mu_e Q_{ij}) \delta^{\alpha\beta} + \delta_{ij} \left(\mu_3 T^{\alpha\beta}_3 + \frac{2}{\sqrt{3}} \mu_8 T^{\alpha\beta}_8 \right) , \tag{2.2}$$

with $Q = \mathrm{diag}(2/3, -1/3, -1/3)_{ij}$ the quark electric-charge matrix and T_3 and T_8 the Gell-Mann matrices in color space. We shall quote results at quark number chemical potential $\mu = 500$ MeV throughout.

In QCD, μ_e, μ_3 and μ_8 are the zeroth components of electromagnetic and color gauge fields, and the gauge field dynamics ensure that they take on values such that the matter is neutral [33, 88], satisfying

$$\frac{\partial \Omega}{\partial \mu_e} = \frac{\partial \Omega}{\partial \mu_3} = \frac{\partial \Omega}{\partial \mu_8} = 0 \ , \tag{2.3}$$

with Ω the free energy density of the system. In the NJL model that we shall employ, in which quarks interact via four-fermion interactions and there are no gauge fields, we introduce μ_e, μ_3 and μ_8 by hand, and choose them to satisfy the neutrality constraints (2.3). As we discussed in Chapter 1, the requirement of weak equilibrium is satisfied with μ_e as the chemical potential for electrons in the system.

We found in Chapter 1, Section 1.4.1, that to the lowest order in $M_s^2\mu^2$, in neutral unpaired quark matter, the u, d and s quarks can all be treated as massless with chemical potentials,

$$\begin{aligned} \mu_d &= \mu_u + 2\delta\mu_3 \\ \mu_u &= p_F^u \\ \mu_s &= \mu_u - 2\delta\mu_2 \end{aligned} \tag{2.4}$$

with

$$\delta\mu_3 = \delta\mu_2 = \frac{M_s^2}{8\mu} \equiv \delta\mu \ . \tag{2.5}$$

The choice of subscripts indicates that $2\delta\mu_2$ is the splitting between the Fermi surfaces for quarks 1 and 3 and $2\delta\mu_3$ is that between the Fermi surfaces for quarks 1 and 2, identifying u, d, s with $1, 2, 3$. (The prefactor 2 in the equations defining the $\delta\mu$'s is chosen to agree with the notation used in the analysis of crystalline color superconductivity in a two flavor model [34], in which the two Fermi surfaces were denoted by

$\mu \pm \delta\mu$ meaning that they were separated by $2\delta\mu$.)

The equality of $\delta\mu_2$ and $\delta\mu_3$ is only valid to leading order in M_s^2; at the next order, $\mu_e = M_s^2/(4\mu) - M_s^4/(48\mu^3)$ and $\delta\mu_3 = \mu_e/2$ while $\delta\mu_2 = \delta\mu_3 + M_s^4/(16\mu^3)$. In Section 2.6, we will utilize the fact that $\delta\mu_2$ and $\delta\mu_3$ are close to equal, but not precisely equal. The consequences of the fact that the splitting between the u and s Fermi surfaces is slightly larger than the splitting between the u and d Fermi surfaces were explored in Ref. [130].

2.3.2 Crystalline color superconductivity in neutral three-flavor quark matter

As we discussed in Chapter 1 we consider a condensate of the form

$$\langle \psi_{i\alpha}(x) C\gamma_5 \psi_{j\beta}(x) \rangle \propto \sum_{I=1}^{3} \sum_{\mathbf{q}_I^a \in \{\mathbf{q}_I\}} \Delta_I e^{2i\mathbf{q}_I^a \cdot \mathbf{r}} \epsilon_{I\alpha\beta} \epsilon_{Iij} \ , \tag{2.6}$$

where $\mathbf{q}_1^a$, $\mathbf{q}_2^a$ and $\mathbf{q}_3^a$ and Δ_1, Δ_2 and Δ_3 are the wave vectors and gap parameters describing pairing between the (d,s), (u,s) and (u,d) quarks respectively, whose Fermi momenta are split by $2\delta\mu_1$, $2\delta\mu_2$ and $2\delta\mu_3$ respectively. From (2.4), we see that $\delta\mu_2 = \delta\mu_3 = \delta\mu_1/2 = M_s^2/(8\mu)$. For each I, $\{\mathbf{q}_I\}$ is a set of momentum vectors that define the periodic spatial modulation of the crystalline condensate describing pairing between the quarks whose flavor is not I, and whose color is not I. Our goal in this paper is to compare condensates with different choices of $\{\mathbf{q}_I\}$s, that is with different crystal structures. To shorten expressions, we will henceforth write

$$\sum_{\mathbf{q}_I^a} \equiv \sum_{\mathbf{q}_I^a \in \{\mathbf{q}_I\}} \ . \tag{2.7}$$

We will calculate the free energy of phases with condensate Eq. (2.6) in the weak coupling (namely $\Delta_0, \delta\mu \ll \mu$) and Ginzburg-Landau (namely $\Delta \ll \Delta_0, \delta\mu$) approximations througout.

The analysis of neutrality in three-flavor quark matter in a crystalline color su-

perconducting phase is very simple in the Ginzburg-Landau limit in which $\Delta \ll \delta\mu$: because the construction of this phase does *not* involve rearranging any Fermi momenta prior to pairing, and because the assumption $\Delta \ll \delta\mu$ implies that the pairing does not significantly change any number densities, neutrality is achieved with the same chemical potentials $\mu_e = M_s^2/(4\mu)$ and $\mu_3 = \mu_8 = 0$ as in unpaired quark matter, and with Fermi momenta given in Eq. (2.4) as in unpaired quark matter. This result is correct only in the Ginzburg-Landau limit.

In the derivation of the Ginzburg-Landau approximation in Section 2.5, we shall make no further assumptions. However, in Sections 2.6 and 2.7 when we evaluate the Ginzburg-Landau coefficients and give our results, we shall make the further simplifying assumption that $\Delta_1 = 0$. Given that $\delta\mu_1$ is twice $\delta\mu_2$ or $\delta\mu_3$, it seems reasonable that $\Delta_1 \ll \Delta_2, \Delta_3$. We leave a quantitative investigation of condensates with $\Delta_1 \neq 0$ to future work.

2.3.3 NJL Model, and Mean-Field Approximation

We shall work throughout in a Nambu–Jona-Lasinio (NJL) model in which the QCD interaction between quarks is replaced by a point-like four-quark interaction, with the quantum numbers of single-gluon exchange, analyzed in mean field theory. This is not a controlled approximation. However, it suffices for our purposes: because this model has attraction in the same channels as in QCD, its high density phase is the CFL phase; and, the Fermi surface splitting effects whose qualitative consequences we wish to study can all be built into the model. This makes the NJL model valuable for making the comparisons that are our goal. Note that we shall assume throughout that $\Delta_0 \ll \mu$. This weak coupling assumption means that the pairing is dominated by modes near the Fermi surfaces. Quantitatively, this means that results for the gaps and condensation energies of candidate crystalline phases are independent of the cutoff in the NJL model when expressed in terms of the CFL gap Δ_0: if the cutoff is changed with the NJL coupling constant adjusted so that Δ_0 stays fixed, the gaps and condensation energies for the candidate crystalline phases also stay fixed.

The NJL interaction term added to the Lagrangian (2.1) is

$$\mathcal{L}_{\text{interaction}} = -\frac{3}{8}G(\bar{\psi}\Gamma^{A\nu}\psi)(\bar{\psi}\Gamma_{A\nu}\psi) \ , \tag{2.8}$$

where we have suppressed the color and flavor indices that we showed explicitly in (2.1), and have continued to suppress the Dirac indices. The full expression for $\Gamma^{A\nu}$ is $(\Gamma^{A\nu})_{\alpha i,\beta j} = \gamma^{\nu}(T^A)_{\alpha\beta}\delta_{ij}$, where the T^A are the color Gell-Mann matrices. The NJL coupling constant G has dimension -2, meaning that an ultraviolet cutoff Λ must be introduced as a second parameter in order to fully specify the interaction. Defining Λ as the restriction that momentum integrals be restricted to a shell around the Fermi surface, $\mu - \Lambda < |\mathbf{p}| < \mu + \Lambda$, the CFL gap parameter can then be evaluated: [9, 39]

$$\Delta_0 = 2^{\frac{2}{3}}\Lambda \exp\left[-\frac{\pi^2}{2\mu^2 G}\right] \ . \tag{2.9}$$

We shall see in subsequent Sections that in the limit in which which $\Delta \ll \Delta_0, \delta\mu \ll \mu$, all our results can be expressed in terms of Δ_0; neither G nor Λ shall appear. This reflects the fact that in this limit the physics of interest is dominated by quarks near the Fermi surfaces, not near Λ, and so once Δ_0 is used as the parameter describing the strength of the attraction between quarks, Λ is no longer visible; the cutoff Λ only appears in the relation between Δ_0 and G, not in any comparison among different possible paired phases. In our numerical evaluations in Section 2.7, we shall take $\mu = 500$ MeV, $\Lambda = 100$ MeV, and adjust G to be such that Δ_0 is 25 MeV.

In the mean-field approximation, the interaction Lagrangian (2.8) takes on the form

$$\mathcal{L}_{\text{interaction}} = \frac{1}{2}\bar{\psi}\Delta(x)\bar{\psi}^T + \frac{1}{2}\psi^T\bar{\Delta}(x)\psi, \tag{2.10}$$

where $\Delta(x)$ is related to the diquark condensate by the relations

$$\begin{aligned}\Delta(x) &= \frac{3}{4}G\Gamma^{A\nu}\langle\psi\psi^T\rangle(\Gamma_{A\nu})^T \\ \bar{\Delta}(x) &= \frac{3}{4}G(\Gamma^{A\nu})^T\langle\bar{\psi}^T\bar{\psi}\rangle\Gamma_{A\nu} \\ &= \gamma^0\Delta^\dagger(x)\gamma^0 \ .\end{aligned} \tag{2.11}$$

The ansatz (2.6) can now be made precise: we take

$$\Delta(x) = \Delta_{CF}(x) \otimes C\gamma^5 \ , \tag{2.12}$$

with

$$\Delta_{CF}(x)_{\alpha i,\beta j} = \sum_{I=1}^{3} \sum_{\mathbf{q}_I^a} \Delta(\mathbf{q}_I^a) e^{2i\mathbf{q}_I^a \cdot \mathbf{r}} \epsilon_{I\alpha\beta} \epsilon_{Iij} \ . \tag{2.13}$$

We have introduced notation that allows for the possibility of gap parameters $\Delta(\mathbf{q}_I^a)$ with different magnitudes for different I *and for different* a. In fact, we shall only consider circumstances in which $\Delta(\mathbf{q}_I^a) = \Delta_I$, as in (2.6). However, it will be very convenient in subsequent Sections to keep track of which Δ_I in a complicated equation "goes with" which $\mathbf{q}_I^a$, making this notation useful.

The full Lagrangian, given by the sum of (2.1) and (2.10), is then quadratic and can be written very simply upon introducing the two component Nambu-Gorkov spinor

$$\chi = \begin{pmatrix} \psi \\ \bar{\psi}^T \end{pmatrix} \text{ and hence } \bar{\chi} = \begin{pmatrix} \bar{\psi} & \psi^T \end{pmatrix} \ , \tag{2.14}$$

in terms of which

$$\mathcal{L} = \frac{1}{2} \bar{\chi} \begin{pmatrix} i\partial\!\!\!/ + \mu\!\!\!/ & \Delta(x) \\ \bar{\Delta}(x) & (i\partial\!\!\!/ - \mu\!\!\!/)^T \end{pmatrix} \chi \ . \tag{2.15}$$

Here, $\mu\!\!\!/ \equiv \mu\gamma_0$ and μ is the matrix (2.2), which we have argued simplifies to

$$\mu = \delta^{\alpha\beta} \otimes \text{diag}\,(\mu_u, \mu_d, \mu_s) \tag{2.16}$$

with the flavor chemical potentials given simply by (2.4). In subsequent Sections, we shall also often use the notation $\mu\!\!\!/_i \equiv \mu_i \gamma_0$, with $i = 1, 2, 3$ corresponding to u, d, s respectively.

The propagator corresponding to the Lagrangian (2.15) is given by

$$\begin{aligned}\langle\chi(x)\bar{\chi}(x')\rangle &= \begin{pmatrix} \langle\psi(x)\bar{\psi}(x')\rangle & \langle\psi(x)\psi^T(x')\rangle \\ \langle\bar{\psi}^T(x)\bar{\psi}(x')\rangle & \langle\bar{\psi}^T(x)\psi^T(x')\rangle \end{pmatrix} \\ &= \begin{pmatrix} iG(x,x') & iF(x,x') \\ i\bar{F}(x,x') & i\bar{G}(x,x') \end{pmatrix},\end{aligned} \tag{2.17}$$

where G and $\bar{G}$ are the "normal" components of the propagator and F and $\bar{F}$ are the "anomalous" components. They satisfy the coupled differential equations

$$\begin{aligned}&\begin{pmatrix} i\partial\!\!\!/ + \mu\!\!\!/ & \Delta(x) \\ \bar{\Delta}(x) & (i\partial\!\!\!/ - \mu\!\!\!/)^T \end{pmatrix}\begin{pmatrix} G(x,x') & F(x,x') \\ \bar{F}(x,x') & \bar{G}(x,x') \end{pmatrix} \\ &\qquad = \begin{pmatrix} 1 & 0 \\ 0 & 1 \end{pmatrix}\delta^{(4)}(x-x') \,.\end{aligned} \tag{2.18}$$

We can now rewrite (2.11) as

$$\begin{aligned}\Delta(x) &= \frac{3i}{4}G\Gamma^{A\nu}F(x,x)(\Gamma_{A\nu})^T \\ \bar{\Delta}(x) &= \frac{3i}{4}G(\Gamma^{A\nu})^T\bar{F}(x,x)\Gamma_{A\nu} \,,\end{aligned} \tag{2.19}$$

either one of which is the self-consistency equation, or gap equation, that we must solve. Without further approximation, (2.19) is not tractable. It yields an infinite set of coupled gap equations, one for each $\Delta(\mathbf{q}_I^a)$, because without further approximation it is not consistent to choose finite sets $\{\mathbf{q}_I\}$. When several plane waves are present in the condensate, they induce an infinite tower of higher momentum condensates [39]. The reason why the Ginzburg-Landau approximation, to which we now turn, is such a simplification is that it eliminates these higher harmonics.

2.4 Ginzburg-Landau Approximation: Introduction

The form of the Ginzburg-Landau expansion of the free energy can be derived using only general arguments. This, combined with results for two-flavor crystalline color superconductivity from Ref. [39], will allow us to draw some partial conclusions in this Section.

We shall only consider crystal structures in which all the vectors $\mathbf{q}_I^a$ in the crystal structure $\{\mathbf{q}_I\}$ are "equivalent". By this we mean that a rigid rotation of the crystal structure can be found which maps any $\mathbf{q}_I^a$ to any other $\mathbf{q}_I^b$ leaving the set $\{\mathbf{q}_I\}$ invariant. For such crystal structures, $\Delta(\mathbf{q}_I^a) = \Delta_I$, meaning that the free energy is a function only of Δ_1, Δ_2 and Δ_3. As explained in Section 2.3.2, the chemical potentials that maintain neutrality in three-flavor crystalline color superconducting quark matter are the same as those in neutral unpaired three-flavor quark matter. Therefore,

$$\Omega_{\text{crystalline}} = \Omega_{\text{unpaired}} + \Omega(\Delta_1, \Delta_2, \Delta_3) \ , \tag{2.20}$$

with Ω_{unpaired} given in Chapter 1 (1.7) with $\mu_e = M_s^2/(4\mu)$, and with $\Omega(0,0,0) = 0$. Our task is to evaluate the condensation energy $\Omega(\Delta_1, \Delta_2, \Delta_3)$. Since our Lagrangian is baryon number conserving and contains no weak interactions, it is invariant under a global $U(1)$ symmetry for each flavor. This means that Ω must be invariant under $\Delta_I \to e^{i\phi_I}\Delta_I$ for each I, meaning that each of the three Δ_I's can only appear in the combination $\Delta_I^*\Delta_I$. (Of course, the ground state can and does break these $U(1)$ symmetries spontaneously; what we need in the argument we are making here is only that they are not explicitly broken in the Lagrangian.) We conclude that if we expand

$\Omega(\Delta_1, \Delta_2, \Delta_3)$ in powers of the Δ_I's up to sextic order, it must take the form

$$\begin{aligned}\Omega(\{\Delta_I\}) =& \frac{2\mu^2}{\pi^2}\left[\sum_I P_I \alpha_I \, \Delta_I^* \Delta_I \right. \\ &+ \frac{1}{2}\left(\sum_I \beta_I (\Delta_I^* \Delta_I)^2 + \sum_{I>J} \beta_{IJ} \, \Delta_I^* \Delta_I \Delta_J^* \Delta_J \right) \\ &\left. + \frac{1}{3}\left(\sum_I \gamma_I (\Delta_I^* \Delta_I)^3 + \sum_{I \neq J} \gamma_{IJJ} \, \Delta_I^* \Delta_I \Delta_J^* \Delta_J \Delta_J^* \Delta_J + \gamma_{123} \, \Delta_1^* \Delta_1 \Delta_2^* \Delta_2 \Delta_3^* \Delta_3 \right)\right] ,\end{aligned} \tag{2.21}$$

where we have made various notational choices for later convenience. The overall prefactor of $2\mu^2/\pi^2$ is the density of states at the Fermi surface of unpaired quark matter with $M_s = 0$; it will prove convenient that we have defined all the coefficients in the Ginzburg-Landau expansion of the free energy relative to this. We have defined $P_I = \dim\{\mathbf{q}_I\}$, the number of plane waves in the crystal structure for the condensate describing pairing between quarks whose flavor and color are not I. Writing the prefactor P_I multiplying the quadratic term and writing the factors of $\frac{1}{2}$ and $\frac{1}{3}$ multiplying the quartic and sextic terms ensures that the α_I, β_I and γ_I coefficients are defined the same way as in Ref. [39]. The form of the Ginzburg-Landau expansion (2.21) is model independent, whereas the expressions for the coefficients α_I, β_I, β_{IJ}, γ_I, γ_{IJJ} and γ_{123} for a given ansatz for the crystal structure are model-dependent. In Section 2.5 we shall derive the Ginzburg-Landau approximation to our model, yielding expressions for these coefficients which we then evaluate in Section 2.6.

We see in Eq. (2.21) that there are some coefficients — namely α_I, β_I and γ_I — which multiply polynomials involving only a single Δ_I. Suppose that we keep a single Δ_I nonzero, setting the other two to zero. This reduces the problem to one with two-flavor pairing only, and the Ginzburg-Landau coefficients for this problem have been calculated for many different crystal structures in Ref. [39]. We can then immediately use these coefficients, called α, β and γ in Ref. [39], to determine our

α_I, β_I and γ_I. Using α_I as an example, we conclude that

$$\begin{aligned}\alpha_I = \alpha(q_I, \delta\mu_I) = -1 + \frac{\delta\mu_I}{2q_I}\log\left(\frac{q_I + \delta\mu_I}{q_I - \delta\mu_I}\right) \\ - \frac{1}{2}\log\left(\frac{\Delta_{2SC}^2}{4(q_I^2 - \delta\mu_I^2)}\right) ,\end{aligned} \tag{2.22}$$

where $\delta\mu_I$ is the splitting between the Fermi surfaces of the quarks with the two flavors other than I and $q_I \equiv |\mathbf{q}_I^a|$ is the length of the $\mathbf{q}$-vectors in the set $\{\mathbf{q}_I\}$. (We shall see momentarily why all have the same length.) In (2.22), Δ_{2SC} is the gap parameter in the BCS state obtained with $\delta\mu_I = 0$ and Δ_I nonzero with the other two gap parameters set to zero. Assuming that $\Delta_0 \ll \mu$, this gap parameter for 2SC (2-flavor, 2-color) BCS pairing is given by [54, 9]

$$\Delta_{2SC} = 2^{\frac{1}{3}}\Delta_0 \, . \tag{2.23}$$

For a given $\delta\mu_I$ and Δ_0, α_I given in (2.22) is minimized when [90, 34, 39]

$$q_I = \eta\,\delta\mu_I \text{ with } \eta = 1.1997 \, . \tag{2.24}$$

In the Ginzburg-Landau approximation, in which the Δ_I are assumed to be small, we must first minimize the quadratic contribution to the free energy, before proceeding to investigate the consequences of the quartic and sextic contributions. Minimizing α_I fixes the length of all the $\mathbf{q}$-vectors in the set $\{\mathbf{q}_I\}$, thus eliminating the possibility of higher harmonics. It is helpful to imagine the (three) sets $\{\mathbf{q}_I\}$ as representing the vertices of (three) polyhedra in momentum space. By minimizing α_I, we have learned that each polyhedron $\{\mathbf{q}_I\}$ can be inscribed in a sphere of radius $\eta\delta\mu_I$. From the quadratic contribution to the free energy, we do not learn anything about what shape polyhedra are preferable. In fact, the quadratic analysis in isolation would indicate that if $\alpha_I < 0$ (which happens for $\delta\mu_I < 0.754\,\Delta_{2SC}$) then modes with arbitarily many different $\hat{\mathbf{q}}_I$'s should condense. It is the quartic and sextic coefficients that describe the interaction among the modes, and hence control what shape polyhedra are in fact

preferable.

The quartic and sextic coefficients β_I and γ_I can also be taken directly from the two-flavor results of Ref. [39]. They are given by $\bar{\beta}/\delta\mu_I^2$ and $\bar{\gamma}/\delta\mu_I^4$ where $\bar{\beta}$ and $\bar{\gamma}$ are dimensionless quantities depending only on the directions of the vectors in the set $\{\mathbf{q}_I\}$. They have been evaluated for many crystal structures in Ref. [39], resulting in two qualitative conclusions. Recall that, as reviewed in Chapter 1 , the presence of a condensate with some $\hat{\mathbf{q}}_I^a$ corresponds to pairing on a ring on each Fermi surface with opening angle 67.1°. The first qualitative conclusion is that any crystal structure in which there are two $\hat{\mathbf{q}}_I^a$'s whose pairing rings intersect has *very* large, positive, values of both β_I and γ_I, meaning that it is strongly disfavored. The second conclusion is that regular structures, those in which there are many ways of adding four or six $\hat{\mathbf{q}}_I^a$'s to form closed figures in momentum space, are favored. Consequently, according to Ref. [39] the favored crystal structure in the two-flavor case has 8 $\hat{\mathbf{q}}_I^a$'s pointing towards the corners of a cube. Choosing the polyhedron in momentum space to be a cube yields a face-centered cubic modulation of the condensate in position space.

Because the β_I and γ_I coefficients in our problem can be taken over directly from the two-flavor analysis, we can expect that it will be unfavorable for any of the three sets $\{\mathbf{q}_I\}$ to have more than eight vectors, or to have any vectors closer together than 67.1°. At this point we cannot exclude the possibility that the large positive β_I and γ_I indicating an unfavorable $\{\mathbf{q}_I\}$ could be offset by large negative values for the other coefficients which we cannot read off from the two-flavor analysis. However, what we shall instead find in Section 2.7 is that β_{IJ} and γ_{IIJ} are positive in all cases that we have investigated. This means that we know of no exceptions to the rule that if a particular $\{\mathbf{q}_I\}$ is unfavorable as a two-flavor crystal structure, then any three-flavor condensate in which this set of $\mathbf{q}$-vectors describes either the Δ_1, Δ_2 or Δ_3 crystal structure is also disfavored.

In Section 2.5 we shall use our microscopic model to derive expressions for all the coefficients in the Ginzburg-Landau expansion (2.21), including rederiving those which we have taken above from the two-flavor analysis of Ref. [39]. The coefficients that we cannot simply read off from a two-flavor analysis are those that multiply terms

involving more than one Δ_I and hence describe the interaction between the three different Δ_I's. Before evaluating the expressions for the coefficients in Section 2.6, we shall make the further simpifying assumption that $\Delta_1 = 0$, because the separation $\delta\mu_1$ between the d and s Fermi surfaces is twice as large as that between either and the intervening u Fermi surface. This simplifies (2.21) considerably, eliminating the γ_{123} term and all the β_{IJ} and γ_{IIJ} terms except β_{32}, γ_{223} and γ_{332}.

2.5 The Ginzburg-Landau approximation: Derivation

We now derive the Ginzburg-Landau approximation to the NJL model specified in Section 2.3.3 . We proceed by first making a Ginzburg-Landau approximation to the gap equation, and then formally integrate the gap equation in order to obtain the free energy, since the gap equation is the variation of the free energy with respect to the gap parameters.

The gap equation (2.19) with which we closed Section 2.3 is an infinite set of coupled equations, one for each $\Delta(\mathbf{q}_I^a)$, with each equation containing arbitrarily high powers of the Δ's. In order to make a Ginzburg-Landau expansion, order by order in powers of the Δ's, we first integrate (2.18), obtaining

$$\begin{aligned} G(x,x') &= G^{(0)}(x,x') - \int d^4z\, G^{(0)}(x,z)\Delta(z)\bar{F}(z,x') \\ \bar{F}(x,x') &= -\int d^4z\, \bar{G}^{(0)}(x,z)\bar{\Delta}(z)G(z,x') \end{aligned} \tag{2.25}$$

with $G^{(0)} = (i\partial\!\!\!/ + \mu\!\!\!/)^{-1}$ and $\bar{G}^{(0)} = ((i\partial\!\!\!/ - \mu\!\!\!/)^T)^{-1}$. We then expand these equations order by order in $\Delta(x)$ by iterating them. To fifth order, for $\bar{F}$ we find

$$\begin{aligned} \bar{F} = &- \bar{G}^{(0)}\bar{\Delta}G^{(0)} - \bar{G}^{(0)}\bar{\Delta}G^{(0)}\Delta\bar{G}^{(0)}\bar{\Delta}G^{(0)} \\ &- \bar{G}^{(0)}\bar{\Delta}G^{(0)}\Delta\bar{G}^{(0)}\bar{\Delta}G^{(0)}\Delta\bar{G}^{(0)}\bar{\Delta}G^{(0)} + \mathcal{O}(\Delta^7)\ , \end{aligned} \tag{2.26}$$

where we have suppressed space-time coordinates and integrals for simplicity. We

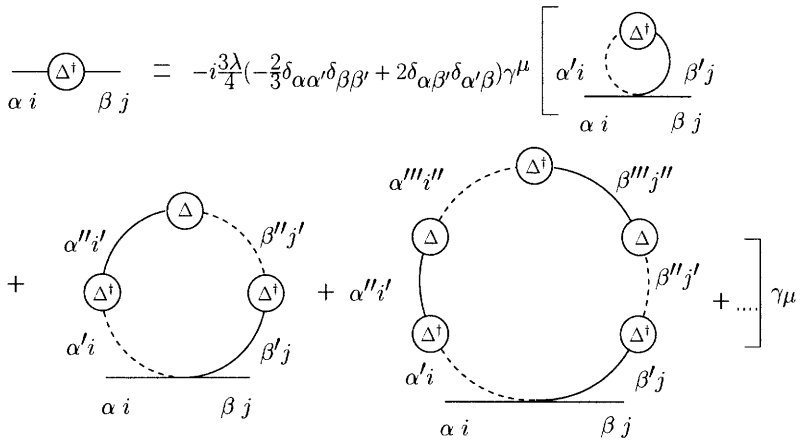

Figure 2-1: The gap equation. The labels α, β represent the external color indices and i, j represent the external flavor indices. All the other color-flavor indices are contracted. Δ_{CF} (and $\Delta^\dagger_{CF}$) are matrices of the form (2.13) and carry the same color and flavor indices as the neighbouring propagators. The dashed lines represent the propagator $(i\partial\!\!\!/ - \mu\gamma^0)^{-1}$ and the solid lines represent $(i\partial\!\!\!/ + \mu\gamma^0)^{-1}$. Evaluating the gap equation involves substituting (2.13) for Δ_{CF}, doing the contraction over the internal color-flavor indices, and evaluating the loop integrals in momentum space.

then substitute this expansion for $\bar{F}$ into the right-hand side of the gap equation for $\bar{\Delta}(x)$ in (2.19). After using the $C\gamma_5$ Dirac structure of our ansatz (2.12) and the identity $C(\gamma^\mu)^T C^{-1} = -\gamma^\mu$ to simplify the expression, we obtain the gap equation satisfied by $\Delta_{CF}(x)$, the part of our ansatz (2.12,2.13) that describes the color, flavor and spatial form of our condensate. To order Δ^5, we find

$$\begin{aligned}\Delta^\dagger_{CF} = \frac{-3iG}{4}(t^a)^T\gamma^\mu\Big[&\frac{1}{i\partial\!\!\!/ - \mu\gamma^0}\Delta^\dagger_{CF}\frac{1}{i\partial\!\!\!/ + \mu\gamma^0}\\ &+ \frac{1}{i\partial\!\!\!/ - \mu\gamma^0}\Delta^\dagger_{CF}\frac{1}{i\partial\!\!\!/ + \mu\gamma^0}\Delta_{CF}\frac{1}{i\partial\!\!\!/ - \mu\gamma^0}\Delta^\dagger_{CF}\frac{1}{i\partial\!\!\!/ + \mu\gamma^0}\\ &+ \frac{1}{i\partial\!\!\!/ - \mu\gamma^0}\Delta^\dagger_{CF}\frac{1}{i\partial\!\!\!/ + \mu\gamma^0}\Delta_{CF}\frac{1}{i\partial\!\!\!/ - \mu\gamma^0}\Delta^\dagger_{CF}\frac{1}{i\partial\!\!\!/ + \mu\gamma^0}\Delta_{CF}\frac{1}{i\partial\!\!\!/ - \mu\gamma^0}\Delta^\dagger_{CF}\frac{1}{i\partial\!\!\!/ + \mu\gamma^0}\Big]_{(x,x)}\gamma_\mu t^a\ ,\end{aligned} \tag{2.27}$$

where the differential operators act on everything to their right and where we have continued to simplify the notation by not writing the space-time, color and flavor arguments of the Δ_{CF}'s and by not writing the integrals. We then use the color Fierz

identity

$$(t^a)_{\alpha'\alpha}(t^a)_{\beta'\beta} = \left(-\frac{2}{3}\delta_{\alpha\alpha'}\delta_{\beta\beta'} + 2\delta_{\alpha'\beta}\delta_{\alpha\beta'}\right) \tag{2.28}$$

to rewrite (2.27) as shown diagrammatically in Fig. 2-1.

As written in (2.27) and shown in Fig. 2-1, what occurs on the left-hand side of the gap equation is the space-dependent condensate from (2.13),

$$\Delta^*_{CF}(x)_{\alpha i,\beta j} = \sum_I \epsilon_{I\alpha\beta}\epsilon_{Iij} \sum_{\mathbf{q}^a_I} \Delta^*(\mathbf{q}^a_I) e^{-2i\mathbf{q}^a_I\cdot\mathbf{r}} \ , \tag{2.29}$$

whereas we now wish to turn the gap equation into a set of coupled equations for the constants $\Delta(\mathbf{q}^a_I)$. Doing so requires simplification of the color-flavor structure of the right-hand side. Our ansatz for the color-flavor structure of the condensate, on the left-hand side, is antisymmetric in both color and flavor. However, direct evaluation of the right-hand side yields terms that are symmetric in color and flavor, in addition to the desired terms that are antisymmetric in both. This circumstance is familiar from the analysis of the CFL phase [21, 9], whose color-flavor structure we are after all employing. In the presence of a color and flavor antisymmetric condensate, a symmetric condensate must also be generated because doing so does not change any symmetries. The same argument applies here also. In the CFL phase, the symmetric condensate is both quantitatively and parametrically suppressed relative to the antisymmetric condensate, which is understandable based on the basic fact that the QCD interaction is attractive in the antisymmetric channel and repulsive in the symmetric channel. We therefore expect that here too if we were to include color and flavor symmetric condensates in our ansatz and solve for them, they would prove to be suppressed relative to the antisymmetric condensates, and furthermore expect that, as in the CFL phase, their inclusion would have negligible impact on the value of the dominant antisymmetric condensate. Hence, we drop the color and flavor symmetric terms occurring on the right-hand side of the gap equation. Upon so doing, the right-hand side of the gap equation, which we denote $R_{\alpha i,\beta j}$, has the

structure

$$R_{\alpha i,\beta j}(x) = \sum_I R_I(\mathbf{r})\epsilon_{I\alpha\beta}\epsilon_{Iij} \tag{2.30}$$

Because $\epsilon_{I\alpha\beta}\epsilon_{Iij}$ are linearly independent tensors for each value of I, in order for the gap equation to be satisfied for all values of α, β, i and j we must have

$$\sum_{\mathbf{q}_I^a} \Delta^*(\mathbf{q}_I^a) e^{-2i\mathbf{q}_I^a\cdot\mathbf{r}} = R_I(\mathbf{r}) \tag{2.31}$$

for all three values of I. This is a set of $\sum_I P_I$ coupled equations for the undetermined constants $\Delta(\mathbf{q}_I^a)$. (Recall that P_I is the number of vectors in the set $\{\mathbf{q}_I\}$.) After

transforming to momentum space, these gap equations can be written as follows:

$$\Delta^*(\mathbf{q}_I^a) = -\frac{2\mu^2 G}{\pi^2}\Bigg[\sum_{\mathbf{q}_I^b}\Delta^*(\mathbf{q}_I^b)\Pi_{jk}(\mathbf{q}_I^b,\mathbf{q}_I^a)\delta_{\mathbf{q}_I^b-\mathbf{q}_I^a}$$

$$+\sum_{\mathbf{q}_I^b\mathbf{q}_I^c\mathbf{q}_I^d}\Delta^*(\mathbf{q}_I^b)\Delta(\mathbf{q}_I^c)\Delta^*(\mathbf{q}_I^d)\,\mathcal{J}_{jkjk}(\mathbf{q}_I^b,\mathbf{q}_I^c,\mathbf{q}_I^d,\mathbf{q}_I^a)\delta_{\mathbf{q}_I^b-\mathbf{q}_I^c+\mathbf{q}_I^d-\mathbf{q}_I^a}$$

$$+\frac{1}{2}\sum_J\sum_{\mathbf{q}_J^b\mathbf{q}_J^c\mathbf{q}_I^d}\Delta^*(\mathbf{q}_J^b)\Delta(\mathbf{q}_J^c)\Delta^*(\mathbf{q}_I^d)\,\mathcal{J}_{kIkJ}(\mathbf{q}_J^b,\mathbf{q}_J^c,\mathbf{q}_I^d,\mathbf{q}_I^a)\delta_{\mathbf{q}_J^b-\mathbf{q}_J^c+\mathbf{q}_I^d-\mathbf{q}_I^a}$$

$$+\sum_{\mathbf{q}_I^b\mathbf{q}_I^c\mathbf{q}_I^d\mathbf{q}_I^e\mathbf{q}_I^f}\Delta^*(\mathbf{q}_I^b)\Delta(\mathbf{q}_I^c)\Delta^*(\mathbf{q}_I^d)\Delta(\mathbf{q}_I^e)\Delta^*(\mathbf{q}_I^f)\,\mathcal{K}_{jkjkjk}(\mathbf{q}_I^b,\mathbf{q}_I^c,\mathbf{q}_I^d,\mathbf{q}_I^e,\mathbf{q}_I^f,\mathbf{q}_I^a)\delta_{\mathbf{q}_I^b-\mathbf{q}_I^c+\mathbf{q}_I^d-\mathbf{q}_I^e+\mathbf{q}_I^f-\mathbf{q}_I^a}$$

$$+\sum_J\sum_{\mathbf{q}_J^b\mathbf{q}_J^c\mathbf{q}_I^d\mathbf{q}_I^e\mathbf{q}_I^f}\Delta^*(\mathbf{q}_J^b)\Delta(\mathbf{q}_J^c)\Delta^*(\mathbf{q}_I^d)\Delta(\mathbf{q}_I^e)\Delta^*(\mathbf{q}_I^f)\,\mathcal{K}_{kIkJkJ}(\mathbf{q}_J^b,\mathbf{q}_J^c,\mathbf{q}_I^d,\mathbf{q}_I^e,\mathbf{q}_I^f,\mathbf{q}_I^a)\delta_{\mathbf{q}_J^b-\mathbf{q}_J^c+\mathbf{q}_I^d-\mathbf{q}_I^e+\mathbf{q}_I^f-\mathbf{q}_I^a}$$

$$+\frac{1}{2}\sum_J\sum_{\mathbf{q}_J^b\mathbf{q}_J^c\mathbf{q}_J^d\mathbf{q}_J^e\mathbf{q}_I^f}\Delta^*(\mathbf{q}_J^b)\Delta(\mathbf{q}_J^c)\Delta^*(\mathbf{q}_J^d)\Delta(\mathbf{q}_J^e)\Delta^*(\mathbf{q}_I^f)\,\mathcal{K}_{kIkIkJ}(\mathbf{q}_J^b,\mathbf{q}_J^c,\mathbf{q}_J^d,\mathbf{q}_J^e,\mathbf{q}_I^f,\mathbf{q}_I^a)\delta_{\mathbf{q}_J^b-\mathbf{q}_J^c+\mathbf{q}_J^d-\mathbf{q}_J^e+\mathbf{q}_I^f-\mathbf{q}_I^a}$$

$$+\frac{1}{2}\sum_{J,K}\sum_{\substack{\mathbf{q}_I^b\mathbf{q}_J^c\mathbf{q}_K^d\\ \mathbf{q}_K^e\mathbf{q}_J^f}}\Delta^*(\mathbf{q}_I^b)\Delta(\mathbf{q}_J^c)\Delta^*(\mathbf{q}_K^d)\Delta(\mathbf{q}_K^e)\Delta^*(\mathbf{q}_J^f)\,\mathcal{K}_{JKIJIK}(\mathbf{q}_I^b,\mathbf{q}_J^c,\mathbf{q}_K^d,\mathbf{q}_K^e,\mathbf{q}_J^f,\mathbf{q}_I^a)\delta_{\mathbf{q}_I^b-\mathbf{q}_J^c+\mathbf{q}_K^d-\mathbf{q}_K^e+\mathbf{q}_J^f-\mathbf{q}_I^a}$$

$$+\frac{1}{4}\sum_{J,K}\sum_{\substack{\mathbf{q}_J^b\mathbf{q}_J^c\mathbf{q}_I^d\\ \mathbf{q}_K^e\mathbf{q}_K^f}}\Delta^*(\mathbf{q}_J^b)\Delta(\mathbf{q}_J^c)\Delta^*(\mathbf{q}_I^d)\Delta(\mathbf{q}_K^e)\Delta^*(\mathbf{q}_K^f)\,\mathcal{K}_{KIKJIJ}(\mathbf{q}_J^b,\mathbf{q}_J^c,\mathbf{q}_I^d,\mathbf{q}_K^e,\mathbf{q}_K^f,\mathbf{q}_I^a)\delta_{\mathbf{q}_J^b-\mathbf{q}_J^c+\mathbf{q}_I^d-\mathbf{q}_K^e+\mathbf{q}_K^f-\mathbf{q}_I^a}$$

$$+\frac{1}{4}\sum_{J,K}\sum_{\substack{\mathbf{q}_J^b\mathbf{q}_K^c\mathbf{q}_I^d\\ \mathbf{q}_J^e\mathbf{q}_K^f}}\Delta^*(\mathbf{q}_J^b)\Delta(\mathbf{q}_K^c)\Delta^*(\mathbf{q}_I^d)\Delta(\mathbf{q}_J^e)\Delta^*(\mathbf{q}_K^f)\,\mathcal{K}_{KIJKIJ}(\mathbf{q}_J^b,\mathbf{q}_K^c,\mathbf{q}_I^d,\mathbf{q}_J^e,\mathbf{q}_K^f,\mathbf{q}_I^a)\delta_{\mathbf{q}_J^b-\mathbf{q}_K^c+\mathbf{q}_I^d-\mathbf{q}_J^e+\mathbf{q}_K^f-\mathbf{q}_I^a}\Bigg], \tag{2.32}$$

where we have introduced a lot of notation that we now define and explain. First, recall from (2.7) that $\sum_{\mathbf{q}_I^b}$ means a sum over all the $\mathbf{q}_I^b$'s in the set $\{\mathbf{q}_I\}$. The δ's are therefore Kronecker δ's, indicating that only those $\mathbf{q}$-vectors that can be arranged to form a certain closed two-, four- or six-sided figure in momentum space are to be included in the sum. The sums over J are always understood to be sums over $J \neq I$, and the sums over K are always understood to be sums over $K \neq J$ and $K \neq I$. The remaining flavor subscripts in some terms which are not summed, denoted j or k, must always be chosen not equal to each other, not equal to I, and not equal to J if

J occurs. (This appears to leave an ambiguity related to the exchange of j and k in terms where both occur, but we shall see that the functions Π, $\mathcal{J}$ and $\mathcal{K}$ each have a cyclic symmetry that ensures that the two apparent choices of j and k are equivalent.) The functions Π, $\mathcal{J}$ and $\mathcal{K}$ are proportional to the various loop integrals that appear in the evaluation of the Feynman diagrams in the gap equation of Fig. 2-1. They are given by

$$\begin{aligned}
\Pi_{i,j}(\mathbf{k}_1,\mathbf{k}_2) &= -\frac{i\pi^2}{\bar{\mu}^2}\gamma^\mu \int \frac{d^4p}{(2\pi)^4}\frac{1}{(\not{p}-\not{\mu}_i)(\not{p}+2\not{k}_1+\not{\mu}_j)}\gamma_\mu \\
\mathcal{J}_{i,j,k,l}(\mathbf{k}_1,\mathbf{k}_2,\mathbf{k}_3,\mathbf{k}_4) &= -\frac{i\pi^2}{\mu^2}\gamma^\mu \int \frac{d^4p}{(2\pi)^4}\frac{1}{(\not{p}-\not{\mu}_i)(\not{p}+2\not{k}_1+\not{\mu}_j)} \\
&\quad \frac{1}{(\not{p}+2\not{k}_1-2\not{k}_2-\not{\mu}_k)(\not{p}+2\not{k}_1-2\not{k}_2+2\not{k}_3+\not{\mu}_l)}\gamma_\mu \\
\mathcal{K}_{i,j,k,l,m,n}(\mathbf{k}_1,\mathbf{k}_2,\mathbf{k}_3,\mathbf{k}_4,\mathbf{k}_5,\mathbf{k}_6) &= -\frac{i\pi^2}{\mu^2}\gamma^\mu \int \frac{d^4p}{(2\pi)^4}\frac{1}{(\not{p}-\not{\mu}_i)(\not{p}+2\not{k}_1+\not{\mu}_j)} \\
&\quad \frac{1}{(\not{p}+2\not{k}_1-2\not{k}_2+\not{\mu}_k)(\not{p}+2\not{k}_1-2\not{k}_2+2\not{k}_3+\not{\mu}_l)} \\
&\quad \frac{1}{(\not{p}+2\not{k}_1-2\not{k}_2+2\not{k}_3-2\not{k}_4-\not{\mu}_m)} \\
&\quad \frac{1}{(\not{p}+2\not{k}_1-2\not{k}_2+2\not{k}_3-2\not{k}_4+2\not{k}_5+\not{\mu}_n)}\gamma_\mu ,
\end{aligned} \tag{2.33}$$

where $\not{\mu}_i = \gamma^0\mu_i$ and $\not{k} = (0,\mathbf{k})_\mu\gamma^\mu = -\mathbf{k}\cdot\gamma$. The subscripts i, j etc. on the functions Π, $\mathcal{J}$ and $\mathcal{K}$ are flavor indices that give the flavor of the quark lines in the propagators going around the loops in Fig. 2-1. In each term in (2.32) the choice of flavor indices in Π, $\mathcal{J}$ or $\mathcal{K}$ is determined by the requirement that a given $\Delta(\mathbf{q}_I^a)$ must connect two propagators for quarks with flavors different from each other and I. For example, Δ_3 always connects a u and a d quark. The easiest way to see how this provides the explanation for the (perhaps initially peculiar looking) prescriptions for the $\mathcal{J}$ and $\mathcal{K}$ functions in each term in the gap equations (2.32) is to examine Fig. 2-2 below, which depicts examples of the contributions of Π, $\mathcal{J}$ and $\mathcal{K}$ to the free energy which we shall discuss next.

The gap equations that we have derived must be equivalent to the set of equations $\partial\Omega/\partial\Delta(\mathbf{q}_I^a) = 0$, because solutions to the gap equation are stationary points of the

free energy Ω. This means that integrating the gap equations determines Ω up to an overall multiplicative constant, which we can fix by requiring that we reproduce known results for the single-plane wave condensates, and up to an additive constant which we fix by the requirement that $\Omega_{\text{crystalline}} = \Omega_{\text{unpaired}}$ when all $\Delta(\mathbf{q}_I^a)$ are set to zero. We find

$$\begin{aligned}
\Omega\left(\{\Delta(\mathbf{q}_I^a)\}\right) = \frac{2\mu^2}{\pi^2} \sum_I \Bigg[& \sum_{\mathbf{q}_I^a \mathbf{q}_I^b} \Delta^*(\mathbf{q}_I^b)\Delta(\mathbf{q}_I^a) \left(\Pi_{jk}(\mathbf{q}_I^a, \mathbf{q}_I^b) + \frac{\pi^2}{2G\mu^2} \right) \delta_{\mathbf{q}_I^b - \mathbf{q}_I^a} \\
& + \frac{1}{2} \sum_{\mathbf{q}_I^b \mathbf{q}_I^c \mathbf{q}_I^d \mathbf{q}_I^a} \Delta^*(\mathbf{q}_I^b)\Delta(\mathbf{q}_I^c)\Delta^*(\mathbf{q}_I^d)\Delta(\mathbf{q}_I^a)\, \mathcal{J}_{jkjk}(\mathbf{q}_I^b, \mathbf{q}_I^c, \mathbf{q}_I^d, \mathbf{q}_I^a) \delta_{\mathbf{q}_I^b - \mathbf{q}_I^c + \mathbf{q}_I^d - \mathbf{q}_I^a} \\
& + \frac{1}{2} \sum_{J>I} \sum_{\mathbf{q}_J^b \mathbf{q}_J^c \mathbf{q}_I^d \mathbf{q}_I^a} \Delta^*(\mathbf{q}_J^b)\Delta(\mathbf{q}_J^c)\Delta^*(\mathbf{q}_I^d)\Delta(\mathbf{q}_I^a)\, \mathcal{J}_{kIkJ}(\mathbf{q}_J^b, \mathbf{q}_J^c, \mathbf{q}_I^d, \mathbf{q}_I^a) \delta_{\mathbf{q}_J^b - \mathbf{q}_J^c + \mathbf{q}_I^d - \mathbf{q}_I^a} \\
& + \frac{1}{3} \sum_{\substack{\mathbf{q}_I^b \mathbf{q}_I^c \mathbf{q}_I^d \mathbf{q}_I^e \\ \mathbf{q}_I^f \mathbf{q}_I^a}} \Delta^*(\mathbf{q}_I^b)\Delta(\mathbf{q}_I^c)\Delta^*(\mathbf{q}_I^d)\Delta(\mathbf{q}_I^e)\Delta^*(\mathbf{q}_I^f)\Delta(\mathbf{q}_I^a)\, \mathcal{K}_{jkjkjk}(\mathbf{q}_I^b, \mathbf{q}_I^c, \mathbf{q}_I^d, \mathbf{q}_I^e, \mathbf{q}_I^f, \mathbf{q}_I^a) \delta_{\substack{\mathbf{q}_I^b - \mathbf{q}_I^c + \mathbf{q}_I^d - \mathbf{q}_I^e \\ + \mathbf{q}_I^f - \mathbf{q}_I^a}} \\
& + \frac{1}{2} \sum_{J \neq I} \sum_{\substack{\mathbf{q}_J^b \mathbf{q}_J^c \mathbf{q}_I^d \mathbf{q}_I^e \\ \mathbf{q}_I^f \mathbf{q}_I^a}} \Delta^*(\mathbf{q}_J^b)\Delta(\mathbf{q}_J^c)\Delta^*(\mathbf{q}_I^d)\Delta(\mathbf{q}_I^e)\Delta^*(\mathbf{q}_I^f)\Delta(\mathbf{q}_I^a) \\
& \qquad \mathcal{K}_{kIkJkJ}(\mathbf{q}_J^b, \mathbf{q}_J^c, \mathbf{q}_I^d, \mathbf{q}_I^e, \mathbf{q}_I^f, \mathbf{q}_I^a) \delta_{\substack{\mathbf{q}_J^b - \mathbf{q}_J^c + \mathbf{q}_I^d - \mathbf{q}_I^e \\ + \mathbf{q}_I^f - \mathbf{q}_I^a}} \\
& + \frac{1}{4} \sum_{J \neq K \neq I \neq J} \sum_{\substack{\mathbf{q}_I^b \mathbf{q}_J^c \mathbf{q}_K^d \mathbf{q}_K^e \\ \mathbf{q}_J^f \mathbf{q}_I^a}} \Delta^*(\mathbf{q}_I^b)\Delta(\mathbf{q}_J^c)\Delta^*(\mathbf{q}_K^d)\Delta(\mathbf{q}_K^e)\Delta^*(\mathbf{q}_J^f)\Delta(\mathbf{q}_I^a) \\
& \qquad \mathcal{K}_{JKIJIK}(\mathbf{q}_I^b, \mathbf{q}_J^c, \mathbf{q}_K^d, \mathbf{q}_K^e, \mathbf{q}_J^f, \mathbf{q}_I^a) \delta_{\substack{\mathbf{q}_I^b - \mathbf{q}_J^c + \mathbf{q}_K^d - \mathbf{q}_K^e \\ + \mathbf{q}_J^f - \mathbf{q}_I^a}} \\
& + \frac{1}{12} \sum_{J \neq K \neq I \neq J} \sum_{\substack{\mathbf{q}_J^b \mathbf{q}_K^c \mathbf{q}_I^d \mathbf{q}_J^e \\ \mathbf{q}_K^f \mathbf{q}_I^a}} \Delta^*(\mathbf{q}_J^b)\Delta(\mathbf{q}_K^c)\Delta^*(\mathbf{q}_I^d)\Delta(\mathbf{q}_J^e)\Delta^*(\mathbf{q}_K^f)\Delta(\mathbf{q}_I^a) \\
& \qquad \mathcal{K}_{KIJKIJ}(\mathbf{q}_J^b, \mathbf{q}_K^c, \mathbf{q}_I^d, \mathbf{q}_J^e, \mathbf{q}_K^f, \mathbf{q}_I^a) \delta_{\substack{\mathbf{q}_J^b - \mathbf{q}_K^c + \mathbf{q}_I^d - \mathbf{q}_J^e \\ + \mathbf{q}_K^f - \mathbf{q}_I^a}} \Bigg] .
\end{aligned} \tag{2.34}$$

As in (2.32), in each term the flavor indices j and k (or just k) that are not summed over are understood to differ from each other and from the summed indices I (or I and J).

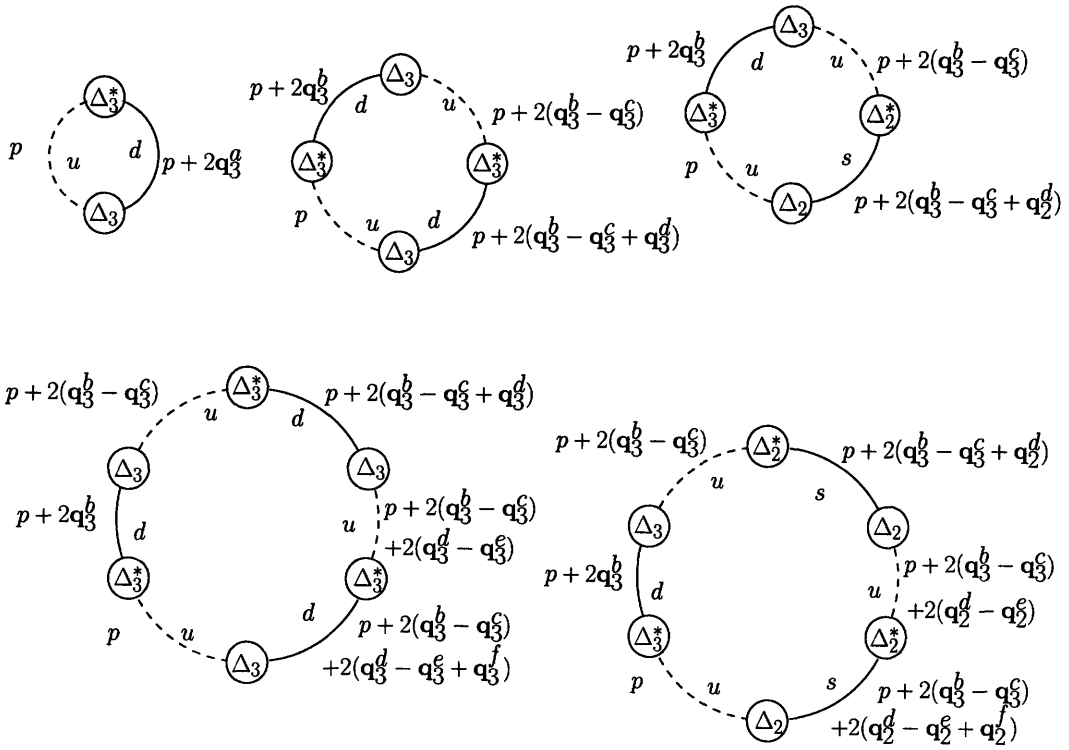

Figure 2-2: Examples of contributions to the free energy. The five diagrams depict a Π_{ud} contribution to $\alpha_3\Delta_3^*\Delta_3$, a $\mathcal{J}_{udud}$ contribution to $\beta_3(\Delta_3^*\Delta_3)^2$, a $\mathcal{J}_{udus}$ contribution to $\beta_{32}\Delta_3^*\Delta_3\Delta_2^*\Delta_2$, a $\mathcal{K}_{ududud}$ contribution to $\gamma_3(\Delta_3^*\Delta_3)^2$ and a $\mathcal{K}_{udusus}$ contribution to $\gamma_{322}\Delta_3^*\Delta_3(\Delta_2^*\Delta_2)^2$.

As we discussed in Section 2.4, we shall only consider crystal structures in which each of the three sets $\{\mathbf{q}_I\}$ are regular, in the sense that all the $\mathbf{q}_I^a$ in one set $\{\mathbf{q}_I\}$ are equivalent. This means that $\Delta(\mathbf{q}_I^a) = \Delta_I$, which simplifies the free energy (2.34) to the form (2.21) which we derived on general grounds in Section 2.4 and which we reproduce here

$$\Omega(\Delta_1,\Delta_2,\Delta_3) = \frac{2\mu^2}{\pi^2}\left[\sum_I P_I\alpha_I\Delta_I^*\Delta_I + \frac{1}{2}\left(\sum_I \beta_I(\Delta_I^*\Delta_I)^2 + \sum_{I>J}\beta_{IJ}\Delta_I^*\Delta_I\Delta_J^*\Delta_J\right)\right.$$
$$\left. + \frac{1}{3}\left(\gamma_I(\Delta_I^*\Delta_I)^3 + \sum_{I\neq J}\gamma_{IJJ}\Delta_I^*\Delta_I\Delta_J^*\Delta_J\Delta_J^*\Delta_J + \gamma_{123}\Delta_1^*\Delta_1\Delta_2^*\Delta_2\Delta_3^*\Delta_3\right)\right] \tag{2.35}$$

for continuity. Now, however, we have obtained explicit expressions for all of the

coefficients:

$$
\begin{aligned}
\alpha_I &= \Pi_{jk}(\mathbf{q}_I^a, \mathbf{q}_I^a) + \frac{\pi^2}{2G\mu^2} \\
\beta_I &= \sum_{\mathbf{q}_I^b \mathbf{q}_I^c \mathbf{q}_I^d \mathbf{q}_I^a} \mathcal{J}_{jkjk}(\mathbf{q}_I^b, \mathbf{q}_I^c, \mathbf{q}_I^d, \mathbf{q}_I^a) \delta_{\mathbf{q}_I^b - \mathbf{q}_I^c + \mathbf{q}_I^d - \mathbf{q}_I^a} \\
\beta_{JI} &= \sum_{\mathbf{q}_J^b \mathbf{q}_J^c \mathbf{q}_I^d \mathbf{q}_I^a} \mathcal{J}_{kIkJ}(\mathbf{q}_J^b, \mathbf{q}_J^c, \mathbf{q}_I^d, \mathbf{q}_I^a) \delta_{\mathbf{q}_J^b - \mathbf{q}_J^c + \mathbf{q}_I^d - \mathbf{q}_I^a} \\
\gamma_I &= \sum_{\substack{\mathbf{q}_I^b \mathbf{q}_I^c \mathbf{q}_I^d \\ \mathbf{q}_I^e \mathbf{q}_I^f \mathbf{q}_I^a}} \mathcal{K}_{jkjkjk}(\mathbf{q}_I^b, \mathbf{q}_I^c, \mathbf{q}_I^d, \mathbf{q}_I^e, \mathbf{q}_I^f \mathbf{q}_I^a) \delta_{\substack{\mathbf{q}_I^b - \mathbf{q}_I^c + \mathbf{q}_I^d - \mathbf{q}_I^e \\ + \mathbf{q}_I^f - \mathbf{q}_I^a}} \\
\gamma_{JII} &= \frac{3}{2} \sum_{\substack{\mathbf{q}_J^b \mathbf{q}_J^c \mathbf{q}_I^d \mathbf{q}_I^e \\ \mathbf{q}_I^f \mathbf{q}_I^a}} \mathcal{K}_{kIkJkJ}(\mathbf{q}_J^b, \mathbf{q}_J^c, \mathbf{q}_I^d, \mathbf{q}_I^e, \mathbf{q}_I^f, \mathbf{q}_I^a) \delta_{\substack{\mathbf{q}_J^b - \mathbf{q}_J^c + \mathbf{q}_I^d - \mathbf{q}_I^e \\ + \mathbf{q}_I^f - \mathbf{q}_I^a}} \\
\gamma_{123} &= \frac{3}{4} \sum_{I \neq J \neq K \neq I} \sum_{\substack{\mathbf{q}_I^b \mathbf{q}_J^c \mathbf{q}_K^d \mathbf{q}_K^e \\ \mathbf{q}_J^f \mathbf{q}_I^a}} \mathcal{K}_{JKIJIK}(\mathbf{q}_I^b, \mathbf{q}_J^c, \mathbf{q}_K^d, \mathbf{q}_K^e, \mathbf{q}_J^f, \mathbf{q}_I^a) \delta_{\substack{\mathbf{q}_I^b - \mathbf{q}_J^c + \mathbf{q}_K^d - \mathbf{q}_K^e \\ + \mathbf{q}_J^f - \mathbf{q}_I^a}} \\
&\quad + \frac{1}{4} \sum_{I \neq J \neq K \neq I} \sum_{\substack{\mathbf{q}_J^b \mathbf{q}_K^c \mathbf{q}_I^d \mathbf{q}_J^e \\ \mathbf{q}_K^f \mathbf{q}_I^a}} \mathcal{K}_{KIJKIJ}(\mathbf{q}_J^b, \mathbf{q}_K^c, \mathbf{q}_I^d, \mathbf{q}_J^e, \mathbf{q}_K^f, \mathbf{q}_I^a) \delta_{\substack{\mathbf{q}_J^b - \mathbf{q}_K^c + \mathbf{q}_I^d - \mathbf{q}_J^e \\ + \mathbf{q}_K^f - \mathbf{q}_I^a}} \, .
\end{aligned}
\tag{2.36}
$$

Here again, the unsummed indices j and k are chosen as described previously. Since the free energy (2.35) is invariant under phase rotations of the Δ_I we can henceforth take all the Δ_I real and positive. In Fig. 2-2, we give examples of contributions to the free energy. These examples should make clear the choice of flavor subscripts on the $\mathcal{J}$'s and $\mathcal{K}$'s in (2.36) and consequently in (2.32). They also illustrate the origin of the Kronecker δ's in so many of the expressions in this Section: each insertion of a $\Delta(\mathbf{q}_I^a)$ (or $\Delta^*(\mathbf{q}_I^a)$ adds (or subtracts) momentum $2\mathbf{q}_I^a$ to (from) the loop, meaning that the Kronecker δ's arise due to momentum conservation. The diagrams also illustrate that Π, $\mathcal{J}$ and $\mathcal{K}$ are invariant under simultaneous cyclic permutation of their flavor indices and momentum arguments, as this corresponds simply to rotating the corresponding diagrams.

We have succeeded in deriving expressions for the Ginzburg-Landau coefficients in our model; we shall turn to evaluating them in the next Section. Recall, however, that upon setting $\Delta_1 = 0$ and keeping in mind that we can obtain results for α_I, β_I

and γ_I from the two-flavor analyses in Ref. [39], all that we need to do is evaluate β_{32}, γ_{233} and γ_{322} for the crystal structures we wish to investigate. We shall largely focus on crystal structures for which $\{\hat{\mathbf{q}}_2\}$ and $\{\hat{\mathbf{q}}_3\}$ are "exchange symmetric", meaning that there is a sequence of rigid rotations and reflections which when applied to all the vectors in $\{\mathbf{q}_2\}$ and $\{\mathbf{q}_3\}$ together has the effect of exchanging $\{\hat{\mathbf{q}}_2\}$ and $\{\hat{\mathbf{q}}_3\}$. If we choose an exchange symmetric crystal structure, upon making the approximation that $\delta\mu_2 = \delta\mu_3$ and restricting our attention to solutions with $\Delta_2 = \Delta_3$ we have the further simplification that $\gamma_{322} = \gamma_{233}$. Once we learn how to evaluate the loop integrals $\mathcal{J}$ and $\mathcal{K}$ in the next Section, we will then in Section 2.7 evaluate β_{32} and γ_{322} for various crystal structures, enabling us to evaluate the magnitudes of their gaps and condensation energies.

2.6 Calculating Ginzburg-Landau coefficients

Calculating the Ginzburg-Landau coefficients (2.36) that specify $\Omega(\Delta_1, \Delta_2, \Delta_3)$ for a given crystal structure involves first evaluating the loop integrals Π, $\mathcal{J}$ and $\mathcal{K}$, defined in (2.33), and then summing those that contribute to a given Ginzburg-Landau coefficient. For example, we see from (2.36) that the Ginzburg-Landau coefficient β_{32} is given by summing $\mathcal{J}_{udus}(\mathbf{q}_3^b, \mathbf{q}_3^c, \mathbf{q}_2^d, \mathbf{q}_2^a)$ over all those vectors $\mathbf{q}_3^b$ and $\mathbf{q}_3^c$ in the set $\{\mathbf{q}_3\}$ and all those vectors $\mathbf{q}_2^d$ and $\mathbf{q}_2^a$ in the set $\{\mathbf{q}_2\}$ which satisfy $\mathbf{q}_3^b - \mathbf{q}_3^c + \mathbf{q}_2^d - \mathbf{q}_2^a = 0$, forming a closed four-sided figure in momentum space. Understanding how to evaluate the loop integrals Π, $\mathcal{J}$ and $\mathcal{K}$ requires some explanation, which is our goal in this Section. Performing the sum required to evaluate a given Ginzburg-Landau coefficient is then just bookkeeping, albeit nontrivial bookkeeping for complicated crystal structures.

We are working in a weak-coupling limit in which $\delta\mu$, $|\mathbf{q}| = q = \eta\delta\mu$, and $\Delta_{2\mathrm{SC}}$ are all much smaller than μ. This means that we can choose our cutoff Λ such that $\delta\mu, q, \Delta_{2\mathrm{SC}} \ll \Lambda \ll \mu$. Because $\Lambda \ll \mu$, the integration measure in the expressions

(2.33) for Π, $\mathcal{J}$ and $\mathcal{K}$ simplifies as follows:

$$-\frac{i\pi^2}{\mu^2}\int\frac{d^4p}{(2\pi)^4}\approx\int_{-\infty}^{+\infty}\frac{dp^0}{2\pi i}\int_{-\Lambda}^{\Lambda}\frac{ds}{2}\int\frac{d\hat{\mathbf{p}}}{4\pi}\,, \tag{2.37}$$

where $s\equiv|\vec{p}|-\mu$. We now see by power counting that Π is log-divergent as we take $\Lambda\gg\delta\mu,q,\Delta_{2\mathrm{SC}}$ whereas both $\mathcal{J}$ and $\mathcal{K}$ are Λ-independent in the large Λ limit. Thus, in evaluating $\mathcal{J}$ and $\mathcal{K}$, we can safely take $\Lambda\to\infty$ whereas we must keep Λ in the problem for a little longer in analyzing Π. Explicit evaluation of Π yields

$$\begin{aligned}\Pi_{ud}(\mathbf{q_3},\mathbf{q_3}) = &-1+\frac{\delta\mu_3}{2q_3}\log\left(\frac{q_3+\delta\mu_3}{q_3-\delta\mu_3}\right)\\ &-\frac{1}{2}\log\left(\frac{\Lambda^2}{q_3^2-\delta\mu_3^2}\right)\,.\end{aligned} \tag{2.38}$$

We can now use

$$\Delta_{2\mathrm{SC}}=2\Lambda e^{-\frac{\pi^2}{2G\mu^2}} \tag{2.39}$$

and the relation between α_3 and Π_{ud} given in (2.36) to evaluate α_3, obtaining the result (2.22). Notice that α_I depends on Λ and G only through $\Delta_{2\mathrm{SC}}$, and depends only on the ratios $q_I/\Delta_{2\mathrm{SC}}$ and $\delta\mu_I/\Delta_{2\mathrm{SC}}$. As discussed in Chapter 1 , α_I is negative for $\delta\mu_I/\Delta_{2\mathrm{SC}}<0.754$, and for a given value of this ratio for which $\alpha_I<0$, α_I is most negative for $q_I/\Delta_{2\mathrm{SC}}=\eta\,\delta\mu_I/\Delta_{2\mathrm{SC}}$ with $\eta=1.1997$. We therefore set $q_I=\eta\,\delta\mu_I$ henceforth and upon so doing obtain

$$\begin{aligned}\alpha(\delta\mu_I) &= -1+\frac{1}{2\eta}\log\left(\frac{\eta+1}{\eta-1}\right)\\ &\quad-\frac{1}{2}\log\left(\frac{\Delta_{2\mathrm{SC}}^2}{4\delta\mu_I^2(\eta^2-1)}\right)\\ &= -\frac{1}{2}\log\left(\frac{\Delta_{2\mathrm{SC}}^2}{4\delta\mu_I^2(\eta^2-1)}\right)\,,\end{aligned} \tag{2.40}$$

where in the last line we have used the definition of η derived from (2.22).

The evaluation of β_I and γ_I is described in Ref. [39]. From the integration measure (2.37) and the definitions of $\mathcal{J}$ and $\mathcal{K}$ (2.33) we see that β_I and γ_I have dimension -2

and -4, respectively. Since they are independent of Λ as long as $\Lambda \gg \delta\mu, q, \Delta_{2SC}$, and since G nowhere appears in their definition, there is no need to introduce Δ_{2SC}. This means that the only dimensionful quantity on which they can depend is $\delta\mu_I$ (since $q_I = \eta\delta\mu_I$ and since the propagators are independent of μ in the weak-coupling limit) and so we can write

$$\beta_I = \frac{\bar{\beta}_I}{\delta\mu_I^2} \text{ and } \gamma_I = \frac{\bar{\gamma}_I}{\delta\mu_I^4} , \tag{2.41}$$

where $\bar{\beta}_I$ and $\bar{\gamma}_I$ are dimensionless quantities that depend only on the shape of the polyhedron described by the set of vectors $\{\mathbf{q}_I\}$. The evaluation of the $\mathcal{J}$ and $\mathcal{K}$ loop integrals occurring in $\bar{\beta}$ and $\bar{\gamma}$ is described in Ref. [39], and results for many two-flavor crystal structures $\{\mathbf{q}_3\}$ are tabulated there. The evaluation is similar to but simpler than the evaluation of β_{32} and γ_{322}, to which we now turn.

β_{32} is the sum of $\mathcal{J}_{udus}(\mathbf{q}_3^b, \mathbf{q}_3^c, \mathbf{q}_2^d, \mathbf{q}_2^a)$, where the momentum vectors satisfy

$$\mathbf{q}_3^b - \mathbf{q}_3^c + \mathbf{q}_2^d - \mathbf{q}_2^a = 0 . \tag{2.42}$$

We now utilize the fact that $|\mathbf{q}_3^b| = |\mathbf{q}_3^c| = \eta\delta\mu_3$ and $|\mathbf{q}_2^d| = |\mathbf{q}_2^a| = \eta\delta\mu_2$ where $\delta\mu_3$ and $\delta\mu_2$ are similar in magnitude, but not precisely equal. (Recall from Section 2.3.1that both are given by $M_s^2/(8\mu)$ to this order, but that they differ at order M_s^4/μ^3.) Because $\delta\mu_2 \neq \delta\mu_3$, the condition (2.42) can only be satisfied if $\mathbf{q}_3^b = \mathbf{q}_3^c$, and $\mathbf{q}_2^d = \mathbf{q}_2^a$. We must therefore evaluate

$$\mathcal{J}_{udus}(\mathbf{q}_3^b, \mathbf{q}_3^b, \mathbf{q}_2^a, \mathbf{q}_2^a) = -\frac{i\pi^2}{\mu^2}\gamma^\mu \left[\int \frac{d^4p}{(2\pi)^4} \frac{1}{(\not{p} - \not{\mu}_u)(\not{p} + 2\not{q}_3^b + \not{\mu}_d)(\not{p} - \not{\mu}_u)(\not{p} + 2\not{q}_2^a + \not{\mu}_s)}\right] \gamma_\mu \tag{2.43}$$

We now expand the propagators in the weak-coupling limit, in which p^0, s, $|\mathbf{q}|$, $(\mu_d - \mu_u)$ and $(\mu_u - \mu_s)$ are all small compared to μ_u, as follows:

$$\begin{aligned} \frac{1}{\not{p} + 2\not{q} + \not{\mu}_i} &= \frac{(p^0 + \mu_i)\gamma^0 - (\mathbf{p} + 2\mathbf{q}) \cdot \gamma}{(p^0 + \mu_i - |\mathbf{p} + 2\mathbf{q}|)(p^0 + \mu_i + |\mathbf{p} + 2\mathbf{q}|)} \\ &\approx \frac{\mu_u\gamma^0 - \mathbf{p} \cdot \gamma}{(p^0 + \mu_u - (\mu_u - \mu_i) - |\mathbf{p}| - 2\mathbf{q} \cdot \hat{\mathbf{p}})(2\mu_u)} \\ &\approx \frac{1}{2}\left(\frac{\gamma^0 - \hat{\mathbf{p}} \cdot \gamma}{p^0 - s + (\mu_i - \mu_u) - 2\mathbf{q} \cdot \hat{\mathbf{p}}}\right) . \end{aligned} \tag{2.44}$$

Similarly,

$$\frac{1}{\not{p}+2\not{q}-\not{\mu}_i} \approx \frac{1}{2}\left(\frac{\gamma^0+\hat{\mathbf{p}}\cdot\gamma}{p^0+s-(\mu_i-\mu_u)+2\mathbf{q}\cdot\hat{\mathbf{p}}}\right) . \tag{2.45}$$

Eq. (2.43) then simplifies to

$$\mathcal{J}_{udus}(\mathbf{q}_3^b,\mathbf{q}_3^b,\mathbf{q}_2^a,\mathbf{q}_2^a) = \int \frac{d\hat{\mathbf{p}}}{4\pi}\int_{-\infty}^{+\infty}\frac{dp^0}{2\pi i}\int_{-\infty}^{+\infty} ds\left[\frac{1}{(p^0+s)^2(p^0-s-\hat{\mathbf{p}}\cdot 2\mathbf{q}_3^b+2\delta\mu_3)}\right.$$
$$\left.\frac{1}{(p^0-s-\hat{\mathbf{p}}\cdot 2\mathbf{q}_2^a-2\delta\mu_2)}\right] \tag{2.46}$$

where we have used $\delta\mu_3=\frac{1}{2}(\mu_d-\mu_u)$ and $\delta\mu_2=\frac{1}{2}(\mu_u-\mu_s)$.

To integrate (2.46), we Wick rotate p^0 to ip^4 and then do the s integral by contour integration. This gives two contibutions with different sign factors, sign(p^4) and sign$(-p^4)$, which are complex conjugates of each other. Combining the two, the integration over p^4 is of form $2\Re e\int_\epsilon^{+\infty} dp^4(...)$ where we have started the p^4 integration from the infinitesimal positive number ϵ instead of zero, thus defininig the principal value of the integral. The integration over p^4 can now be carried out safely to obtain

$$\begin{aligned}\mathcal{J}_{udus}(\mathbf{q}_3^b,\mathbf{q}_3^b,\mathbf{q}_2^a,\mathbf{q}_2^a) &= -\frac{1}{4}\int\frac{d\hat{\mathbf{p}}}{4\pi}\Re e\left[\frac{1}{(i\epsilon-\hat{\mathbf{p}}\cdot\mathbf{q}_3^b+\delta\mu_3)(i\epsilon-\hat{\mathbf{p}}\cdot\mathbf{q}_2^a-\delta\mu_2)}\right]\\ &= -\frac{1}{4\delta\mu_2\delta\mu_3}\int\frac{d\hat{\mathbf{p}}}{4\pi}\Re e\left[\frac{1}{(i\epsilon-\eta\hat{\mathbf{p}}\cdot\hat{\mathbf{q}}_3^b+1)(i\epsilon-\eta\hat{\mathbf{p}}\cdot\hat{\mathbf{q}}_2^a-1)}\right] ,\end{aligned} \tag{2.47}$$

where $\eta=\frac{|\mathbf{q}_3|}{\delta\mu_3}=\frac{|\mathbf{q}_2|}{\delta\mu_2}$. From rotational symmetry it follows that the value of (2.47) depends only on the angle between the momentum vectors $\hat{\mathbf{q}}_3^b$ and $\hat{\mathbf{q}}_2^a$, which we denote by ϕ. We therefore define the dimensionless quantities

$$\bar{J}_{32}(\phi) = \delta\mu_2\delta\mu_3\,\mathcal{J}_{udus}(\mathbf{q}_3^b,\mathbf{q}_3^b,\mathbf{q}_2^a,\mathbf{q}_2^a) \tag{2.48}$$

and, correspondingly,

$$\bar{\beta}_{32} = \delta\mu_2\delta\mu_3\beta_{32} . \tag{2.49}$$

$\bar{J}_{32}$ can be evaluated analytically by using Feynman parameters to simplify the integrand in (2.47). The result is

$$\bar{J}_{32}(\phi) = \frac{1}{4\,\eta\cos(\phi/2)}\left[\frac{1}{\sqrt{\eta^2\sin^2(\phi/2)-1}}\arctan\left(\frac{\sqrt{\eta^2\sin^2(\phi/2)-1}}{\eta\cos(\phi/2)}\right)\right] . \quad (2.50)$$

This completes the evaluation of the loop integral $\mathcal{J}$ needed to calculate β_{32} for any crystal structure. We summarize the calculation by noting that for a given crystal structure, β_{32} depends only on the shape of the polyhedra defined by $\{\mathbf{q}_2\}$ and $\{\mathbf{q}_3\}$ and on their relative orientation, depends on the Fermi surface splittings $\delta\mu_3$ and $\delta\mu_2$, and is obtained using (2.49) with

$$\bar{\beta}_{32} = \sum_{\mathbf{q}_3^b,\mathbf{q}_2^a} \bar{J}_{32}(\angle\hat{\mathbf{q}}_3^b\hat{\mathbf{q}}_2^a) , \quad (2.51)$$

where $\bar{J}_{32}(\phi)$ is given by (2.50).

We turn now to the evaluation of γ_{322}. From (2.36),

$$\gamma_{322} = \frac{3}{2}\sum_{\substack{\mathbf{q}_3^b,\mathbf{q}_3^c,\\ \mathbf{q}_2^d,\mathbf{q}_2^e,\mathbf{q}_2^f,\mathbf{q}_2^a}} \mathcal{K}_{udusus}(\mathbf{q}_3^b,\mathbf{q}_3^c,\mathbf{q}_2^d,\mathbf{q}_2^e,\mathbf{q}_2^f,\mathbf{q}_2^a) , \quad (2.52)$$

and we again use the fact that the $\mathbf{q}_3$'s and $\mathbf{q}_2$'s do not have precisely the same length to conclude that the momentum vectors must satisfy both

$$\mathbf{q}_3^b = \mathbf{q}_3^c \quad (2.53)$$

and

$$\mathbf{q}_2^d - \mathbf{q}_2^e + \mathbf{q}_2^f - \mathbf{q}_2^a = 0 . \quad (2.54)$$

In the following expressions, it is always understood that (2.54) is satisfied although we will not complicate equations by eliminating one of the $\mathbf{q}_2$'s in favor of the other three. We can see without calculation that, unlike $\mathcal{J}$, $\mathcal{K}$ will not reduce to depending only on a single angle between two momentum vectors. It will depend on the shape

made by the four $\mathbf{q}_2$ vectors satisfying (2.54), which can in fact be specified by two angles, as well as on the angles that specify the direction of $\mathbf{q}_3^b$ relative to the shape made by the four $\mathbf{q}_2$'s.

The expression for $\mathcal{K}$ is given in (2.33) and can also be read off from the bottom right Feynman diagram in Fig. 2-2. It is given by

$$\mathcal{K}_{udusus}(\mathbf{q}_3^b, \mathbf{q}_3^b, \mathbf{q}_2^d, \mathbf{q}_2^e, \mathbf{q}_2^f, \mathbf{q}_2^a) = -\frac{i\pi^2}{\mu^2} \times \gamma^\mu \int \frac{d^4p}{(2\pi)^4} \left[\frac{1}{(\not{p} - \not{\mu}_u)(\not{p} + 2\not{\mathbf{q}}_3^b + \not{\mu}_d)(\not{p} - \not{\mu}_u)} \right.$$
$$\left. \frac{1}{(\not{p} + 2\not{\mathbf{q}}_2^d + \not{\mu}_s)(\not{p} + 2(\not{\mathbf{q}}_2^d - \not{\mathbf{q}}_2^e) - \not{\mu}_u)(\not{p} + 2(\not{\mathbf{q}}_2^d - \not{\mathbf{q}}_2^e + \not{\mathbf{q}}_2^f) + \not{\mu}_s)} \right] \gamma_\mu \cdot \tag{2.55}$$

After simplifying the propagators using (2.44), we can rewrite equation (2.55) as

$$\mathcal{K}_{udusus}(\mathbf{q}_3^b, \mathbf{q}_3^b, \mathbf{q}_2^d, \mathbf{q}_2^e, \mathbf{q}_2^f, \mathbf{q}_2^a) = \int \frac{d\hat{\mathbf{p}}}{4\pi} \int_{-\infty}^{+\infty} \frac{dp^0}{2\pi i} \int_{-\infty}^{+\infty} ds \left[\frac{1}{(p^0 + s)^2} \right.$$
$$\frac{1}{(p^0 + s + \hat{\mathbf{p}} \cdot 2(\mathbf{q}_2^d - \mathbf{q}_2^e))(p^0 - s - \hat{\mathbf{p}} \cdot 2\mathbf{q}_3^b + 2\delta\mu_3)}$$
$$\left. \frac{1}{(p^0 - s - \hat{\mathbf{p}} \cdot 2\mathbf{q}_2^d - 2\delta\mu_2)(p^0 - s - \hat{\mathbf{p}} \cdot 2(\mathbf{q}_2^d - \mathbf{q}_2^e + \mathbf{q}_2^f) - 2\delta\mu_2)} \right] \tag{2.56}$$

Unlike in the evaluation of $\mathcal{J}_{udus}$, we are not able to do the s and p^0 integrals analytically without introducing Feynman parameters to simplify the integrand at this stage, before doing any of the integrals. We introduce one set of Feynman parameters, x_1, x_2, to collect denominators of the form $p^0 + s + ..$ and another set, y_1, y_2, y_3, to

collect the denominators of form $p^0 - s + ...$ This reduces the integral to

$$\mathcal{K}_{udusus}(\mathbf{q}_3^b, \mathbf{q}_3^b, \mathbf{q}_2^d, \mathbf{q}_2^e, \mathbf{q}_2^f, \mathbf{q}_2^a) = \int_0^1 \prod_{n=1}^{2} dx_n \, \delta\left(1 - \sum_{n=1}^{2} x_n\right) \int_0^1 \prod_{m=1}^{3} dy_m \, \delta\left(1 - \sum_{m=1}^{3} y_m\right)$$
$$\times \int \frac{d\hat{\mathbf{p}}}{4\pi} \int_{-\infty}^{+\infty} \frac{dp^0}{2\pi i} \int_{-\infty}^{+\infty} ds \left[\frac{4(1-x_2)}{(p^0 + s + 2x_2 \hat{\mathbf{p}} \cdot [\mathbf{q}_2^d - \mathbf{q}_2^e])^3}\right]$$
$$\left[\frac{1}{p^0 - s - 2\hat{\mathbf{p}} \cdot [y_1 \mathbf{q}_3^b + y_2 \mathbf{q}_2^d + y_3(\mathbf{q}_2^d - \mathbf{q}_2^e + \mathbf{q}_2^f)] + y_1 2\delta\mu_3 - y_2 2\delta\mu_2 - y_3 2\delta\mu_2}\right]^3 . \tag{2.57}$$

We now perform the p^0 and s integrations in (2.57), following steps analogous to the integration arising in the expression for $\mathcal{J}_{udus}$. i.e. Wick rotate p^0 to ip^4, do the s integral by contour integration, add the two complex conjugate contributions thus obtained to write the integration over p^4 as $2\Re e \int_\epsilon^{+\infty} dp^4(...)$ and then perform the integration over p^4. This gives us

$$\mathcal{K}_{udusus}(\mathbf{q}_3^b, \mathbf{q}_3^b, \mathbf{q}_2^d, \mathbf{q}_2^e, \mathbf{q}_2^f, \mathbf{q}_2^a) = -\frac{3}{8}\Re e \int_0^1 \prod_{n=1}^{2} dx_n \, \delta\left(1 - \sum_{n=1}^{2} x_n\right) \int_0^1 \prod_{m=1}^{3} dy_m \, \delta\left(1 - \sum_{m=1}^{3} y_m\right)$$
$$\times \int \frac{d\hat{\mathbf{p}}}{4\pi} \left[\frac{1-x_2}{i\epsilon + \hat{\mathbf{p}} \cdot [x_2(\mathbf{q}_2^d - \mathbf{q}_2^e) - (y_1 \mathbf{q}_3^b + y_2 \mathbf{q}_2^d + y_3(\mathbf{q}_2^d - \mathbf{q}_2^e + \mathbf{q}_2^f))] + y_1 \delta\mu_3 - y_2 \delta\mu_2 - y_3 \delta\mu_2}\right]^4 . \tag{2.58}$$

Finally, we do the $d\hat{\mathbf{p}}$ integral and obtain

$$\mathcal{K}_{udusus}(\mathbf{q}_3^b, \mathbf{q}_3^b, \mathbf{q}_2^d, \mathbf{q}_2^e, \mathbf{q}_2^f, \mathbf{q}_2^a) = \frac{1}{8}\Re e \int_0^1 \prod_{n=1}^{2} dx_n \, \delta\left(1 - \sum_{n=1}^{2} x_n\right)$$
$$\int_0^1 \prod_{m=1}^{3} dy_m \, \delta\left(1 - \sum_{m=1}^{3} y_m\right) (1 - x_2)$$
$$\times \frac{|x_2(\mathbf{q}_2^d - \mathbf{q}_2^e) - (y_1 \mathbf{q}_3^b + y_2 \mathbf{q}_2^d + y_3(\mathbf{q}_2^d - \mathbf{q}_2^e + \mathbf{q}_2^f))|^2 + 3[y_1 \delta\mu_3 - y_2 \delta\mu_2 - y_3 \delta\mu_2]^2}{\left[|x_2(\mathbf{q}_2^d - \mathbf{q}_2^e) - (y_1 \mathbf{q}_3^b + y_2 \mathbf{q}_2^d + y_3(\mathbf{q}_2^d - \mathbf{q}_2^e + \mathbf{q}_2^f))|^2 - [y_1 \delta\mu_3 - y_2 \delta\mu_2 - y_3 \delta\mu_2 + i\epsilon]^2\right]^3} . \tag{2.59}$$

Noting that we can replace $\mathbf{q}_2$ by $\eta \hat{\mathbf{q}}_2$ and $\mathbf{q}_3$ by $\eta \hat{\mathbf{q}}_3$, we conclude that, as expected, $\mathcal{K}_{udusus}$ depends only upon the shape of the polyhedra defined by $\{\mathbf{q}_2\}$ and $\{\mathbf{q}_3\}$

and on the Fermi surface splittings $\delta\mu_3$ and $\delta\mu_2$. We cannot simplify (2.59) further for general $\delta\mu_2$, $\delta\mu_3$. However, if we now set $\delta\mu_2 = \delta\mu_3 = \delta\mu$, which is corrected only at order M_s^4/μ^3, we can then factor out the dependence on the Fermi surface splitting, since the only dimensionful quantity in the integrand is then $\delta\mu$. Defining, for $\delta\mu_2 = \delta\mu_3 = \delta\mu$,

$$\mathcal{K}_{ududus}(\mathbf{q}_3^b, \mathbf{q}_3^b, \mathbf{q}_2^d, \mathbf{q}_2^e, \mathbf{q}_2^f, \mathbf{q}_2^a) = \frac{1}{\delta\mu^4}\bar{K}_{322}(\mathbf{q}_3^b, \mathbf{q}_3^b, \mathbf{q}_2^d, \mathbf{q}_2^e, \mathbf{q}_2^f, \mathbf{q}_2^a)\ , \tag{2.60}$$

and using $|\mathbf{q}_I| = \eta\delta\mu_I$, for all the momentum vectors, we find that $\bar{K}_{322}$ is given by

$$\begin{aligned}\bar{K}_{322}(\mathbf{q}_3^b, \mathbf{q}_3^b, \mathbf{q}_2^d, \mathbf{q}_2^e, \mathbf{q}_2^f, \mathbf{q}_2^a) =& \frac{1}{8}\int_0^1 dx_2(1-x_2)\int_0^1 dy_1 \int_0^{1-y_1} dy_2 \\ & \Re e \frac{\eta^2|\mathbf{a}(x_2,y_1,y_2)|^2 + 3(1-2y_1)^2}{[\eta^2|\mathbf{a}(x_2,y_1,y_2)|^2 - (1-2y_1)^2 + i\epsilon]^3}\ ,\end{aligned} \tag{2.61}$$

where

$$\mathbf{a} = x_2\left(\hat{\mathbf{q}}_2^d - \hat{\mathbf{q}}_2^e\right) - \left(y_1\hat{\mathbf{q}}_3^b + y_2\hat{\mathbf{q}}_2^d + (1-y_1-y_2)(\hat{\mathbf{q}}_2^d - \hat{\mathbf{q}}_2^e + \hat{\mathbf{q}}_2^f)\right)\ . \tag{2.62}$$

For general arguments we were not able to do the integrals that remain in (2.61) analytically and therefore evaluated it numerically. Since $\bar{K}_{322}(\mathbf{q}_3^b, \mathbf{q}_3^b, \mathbf{q}_2^d, \mathbf{q}_2^e, \mathbf{q}_2^f, \mathbf{q}_2^a)$ is the limit of the function $\bar{K}_{322}(\mathbf{q}_3^b, \mathbf{q}_3^b, \mathbf{q}_2^d, \mathbf{q}_2^e, \mathbf{q}_2^f, \mathbf{q}_2^a, \epsilon)$ as $\epsilon \to 0$, we numerically evaluated the integral appearing in (2.61) at four values of ϵ and extrapolated (using a cubic polynomial to fit the values) to $\epsilon = 0$. Finally

$$\bar{\gamma}_{322} = \gamma_{322}\delta\mu^4 \tag{2.63}$$

is found by summing $\bar{K}_{322}$ evaluated with all possible choices of momentum vectors $(\mathbf{q}_3^b, \mathbf{q}_3^b, \mathbf{q}_2^d, \mathbf{q}_2^e, \mathbf{q}_2^f, \mathbf{q}_2^a)$ satisfying (2.54) and multiplying this sum by 3/2.

2.7 Results

2.7.1 Generalities

We shall assume that $\Delta_1 = 0$ throughout this Section. As described previously, this simplification is motivated by the fact that Δ_1 describes the pairing of d and s quarks, whose Fermi surfaces are twice as far apart from each other as either is from that of the u quarks. We shall focus most of our attention on exchange symmetric crystal structures, as defined at the end of Section 2.5 , in which the polyhedra defined by $\{\hat{\mathbf{q}}_2\}$ and $\{\hat{\mathbf{q}}_3\}$ are related by a rigid rotation. In Section 2.7.4 we will discuss one example in which $\{\hat{\mathbf{q}}_2\}$ and $\{\hat{\mathbf{q}}_3\}$ are not exchange symmetric, and we have evaluated others. However, as none that we have investigated prove to be favorable, we shall make the notational simplifications that come with assuming that $\{\hat{\mathbf{q}}_2\}$ and $\{\hat{\mathbf{q}}_3\}$ are exchange symmetric, as this implies $\alpha_2 = \alpha_3 \equiv \alpha$, $P_2 = \dim\{\mathbf{q}_2\} = P_3 = \dim\{\mathbf{q}_3\} \equiv P$, $\beta_2 = \beta_3 \equiv \beta$ and $\gamma_{322} = \gamma_{233}$. The final simplification we employ is to make the approximation that $\delta\mu_2 = \delta\mu_3 \equiv \delta\mu = M_s^2/(8\mu)$. As described in Section 2.3.1, this approximation is corrected by terms of order M_s^4/μ^3. Upon making all these simplifying assumptions and approximations, the free energy (2.35) reduces to

$$\begin{aligned}\Omega(\Delta_2,\Delta_3) = \frac{2\mu^2}{\pi^2}\Bigg[& P\alpha(\delta\mu)\big(\Delta_2^2+\Delta_3^2\big) \\ & + \frac{1}{2}\frac{1}{\delta\mu^2}\big(\bar{\beta}(\Delta_2^4+\Delta_3^4)+\bar{\beta}_{32}\Delta_2^2\Delta_3^2\big) \\ & + \frac{1}{3}\frac{1}{\delta\mu^4}\big(\bar{\gamma}(\Delta_2^6+\Delta_3^6)+\bar{\gamma}_{322}(\Delta_2^2\Delta_3^4+\Delta_2^4\Delta_3^2)\big)\Bigg] ,\end{aligned} \tag{2.64}$$

where $\bar{\beta}$, $\bar{\gamma}$, $\bar{\beta}_{32}$ and $\bar{\gamma}_{322}$ are the dimensionless constants that we must calculate for each crystal structure as described in Section 2.7, and where the $\delta\mu$-dependence of α is given by Eq. (2.40).

In order to find the extrema of $\Omega(\Delta_2, \Delta_3)$ in (Δ_2, Δ_3)-space, it is convenient to write (Δ_2, Δ_3) as $\sqrt{2}(\Delta_r \cos\theta, \Delta_r \sin\theta)$ in terms of which the free energy (2.64) is

given by

$$\begin{aligned}&\Omega(\Delta_r,\theta) = \\ &\frac{2\mu^2}{\pi^2}\left[2P\alpha(\delta\mu)\Delta_r^2+\frac{2}{\delta\mu^2}\bar{\beta}\Delta_r^4+\frac{8}{3\delta\mu^4}\bar{\gamma}\Delta_r^6\right. \\ &\left.+\left(\frac{\Delta_r^4}{2\delta\mu^2}(\bar{\beta}_{32}-2\bar{\beta})+\frac{2\Delta_r^6}{3\delta\mu^4}(\bar{\gamma}_{322}-3\bar{\gamma})\right)\sin^2 2\theta\right].\end{aligned} \tag{2.65}$$

Because $\sin^2(2\theta)$ has extrema only at $\theta = \pi/4$ and $\theta = 0, \pi/2$, we see that extrema of $\Omega(\Delta_2, \Delta_3)$ either have $\Delta_2 = \Delta_3 = \Delta$, or have one of Δ_2 and Δ_3 vanishing. The latter class of extrema are two-flavor crystalline phases. We are interested in the solutions with $\Delta_2 = \Delta_3 = \Delta$. The stability of these solutions relative to those with only one of the Δ's nonzero appears to be controlled by the sign of the factor that multiplies $\sin^2 2\theta$ in (2.65). However, we shall show in Appendix A that the three-flavor crystalline phases that we construct, with $\Delta_2 = \Delta_3 = \Delta$, are electrically neutral whereas the two-flavor solutions in which only one of the Δ's is nonzero are not. Setting $\Delta_2 = \Delta_3 = \Delta$, the free energy becomes

$$\Omega(\Delta) = \frac{2\mu^2}{\pi^2}\left[2P\alpha(\delta\mu)\Delta^2+\frac{\Delta^4}{2\delta\mu^2}\bar{\beta}_{\text{eff}}+\frac{\Delta^6}{3\delta\mu^4}\bar{\gamma}_{\text{eff}}\right] , \tag{2.66}$$

where we have defined

$$\begin{aligned}\bar{\beta}_{\text{eff}} &= 2\bar{\beta}+\bar{\beta}_{32} \\ \bar{\gamma}_{\text{eff}} &= 2\bar{\gamma}+2\bar{\gamma}_{322} \ .\end{aligned} \tag{2.67}$$

We have arrived at a familiar-looking sextic order Ginzburg-Landau free energy function, whose coefficients we will evaluate for specific crystal structures in Section 2.7.2 and 2.7.4. First, however, we review the physics described by this free energy depending on whether $\bar{\beta}_{\text{eff}}$ and $\bar{\gamma}_{\text{eff}}$ are positive or negative.

If $\bar{\beta}_{\text{eff}}$ and $\bar{\gamma}_{\text{eff}}$ are both positive, the free energy (2.66) describes a second order phase transition between the crystalline color superconducting phase and the normal phase at the $\delta\mu$ at which $\alpha(\delta\mu)$ changes sign. From (2.40), this critical point occurs

where $\delta\mu = 0.754\,\Delta_{2SC}$. In plotting our results, we will take the CFL gap to be $\Delta_0 = 25$ MeV, making $\Delta_{2SC} = 2^{1/3}\Delta_0 = 31.5$ MeV. Recalling that $\delta\mu = M_s^2/(8\mu)$, this puts the second order phase transition at

$$\left.\frac{M_s^2}{\mu}\right|_{\alpha=0} = 6.03\,\Delta_{2SC} = 7.60\,\Delta_0 = 190.0\text{ MeV}\ . \tag{2.68}$$

(The authors of Refs. [44, 45] neglected to notice that it is Δ_{2SC}, rather than the CFL gap Δ_0, that occurs in Eqs. (2.22) and (2.40) and therefore controls the $\delta\mu$ at which $\alpha = 0$. In analyzing the crystalline phase in isolation, this is immaterial since either Δ_0 or Δ_{2SC} could be taken as the parameter defining the strength of the interaction between quarks. However, in Section 2.7.5 we shall compare the free energies of the CFL, gCFL and crystalline phases, and in making this comparison it is important to take into account that $\Delta_{2SC} = 2^{1/3}\Delta_0$.) For values of M_s^2/μ that are smaller than (2.68) (that is, lower densities), $\alpha < 0$ and the free energy is minimized by a nonzero $\Delta = \Delta_{min}$ given by

$$\Delta_{min} = \delta\mu\sqrt{\frac{1}{2\bar{\gamma}_{eff}}\left(-\bar{\beta}_{eff} + \sqrt{\bar{\beta}_{eff}^2 - 8P\alpha(\delta\mu)\bar{\gamma}_{eff}}\right)}\ , \tag{2.69}$$

and thus describes a crystalline color superconducting phase.

If $\bar{\beta}_{eff} < 0$ and $\bar{\gamma}_{eff} > 0$, then the free energy (2.66) describes a first order phase transition between unpaired and crystalline quark matter occurring at

$$\alpha = \alpha_* = \frac{3\,\bar{\beta}_{eff}^2}{32\,P\bar{\gamma}_{eff}}\ . \tag{2.70}$$

At this positive value of α, the function $\Omega(\Delta)$ has a minimum at $\Delta = 0$ with $\Omega = 0$, initially rises quadratically with increasing Δ, and is then turned back downward by the negative quartic term before being turned back upwards again by the positive sextic term, yielding a second minimum at

$$\Delta = \delta\mu\sqrt{\frac{3\,|\bar{\beta}_{eff}|}{4\,\bar{\gamma}_{eff}}}\ , \tag{2.71}$$

also with $\Omega = 0$, which describes a crystalline color superconducting phase. For $\alpha < \alpha_*$, the crystalline phase is favored over unpaired quark matter. Eq. (2.40) must be used to determine the value of $\delta\mu$, and hence M_s^2/μ, at which $\alpha = \alpha_*$ and the first order phase transition occurs. If $\alpha_* \ll 1$, the transition occurs at a value of M_s^2/μ that is greater than (2.68) by a factor $(1 + \alpha_*)$. See Fig. 2-5 for an explicit example of plots of Ω versus Δ for various values of α for one of the crystal structures that we analyze in Section 2.7.4 which turns out to have a first order phase transition.

A necessary condition for the Ginzburg-Landau approximation to be quantitatively reliable is that the sextic term in the free energy is small in magnitude compared to the quartic, meaning that $\Delta^2 \ll \delta\mu^2|\bar{\beta}_{\rm eff}/\bar{\gamma}_{\rm eff}|$. If the transition between the unpaired and crystalline phases is second order, then this condition is satisfied close enough to the transition where $\Delta \to 0$. However, if $\bar{\beta}_{\rm eff} < 0$ and $\bar{\gamma}_{\rm eff} > 0$, making the transition first order, we see from (2.71) that at the first order transition itself Δ is large enough to make the quantitative application of the Ginzburg-Landau approximation marginal. This is a familiar result, coming about whenever a Ginzburg-Landau approximation predicts a first order phase transition because at the first order phase transition the quartic and sextic terms are balanced against each other. Even though it is quite a different problem, it is worth recalling the Ginzburg-Landau analysis of the crystallization of a solid from a liquid [28]. There too, a Ginzburg-Landau analysis predicts a first-order phase transition and thus predicts its own quantitative downfall. However, it remains important as a qualitative guide: it predicts a body-centered cubic crystal structure, and most elementary solids are body-centered cubic near their melting point. We shall find that our Ginzburg-Landau analysis predicts a first order phase transition; knowing that it is therefore at the edge of its quantitative reliability, we shall focus in Sections 2.7.5 and 2.8 on qualitative conclusions.

If $\bar{\gamma}_{\rm eff} < 0$, then the Ginzburg-Landau expansion of the free energy to sextic order in (2.66) is not bounded from below. The transition must be first order, with higher-than-sextic order terms making the free energy bounded. In this circumstance, all we learn from (2.66) is that the transition is first order; we cannot obtain an estimate of the transition point or of Δ at the first order transition. Even though $\bar{\gamma}$ is negative for

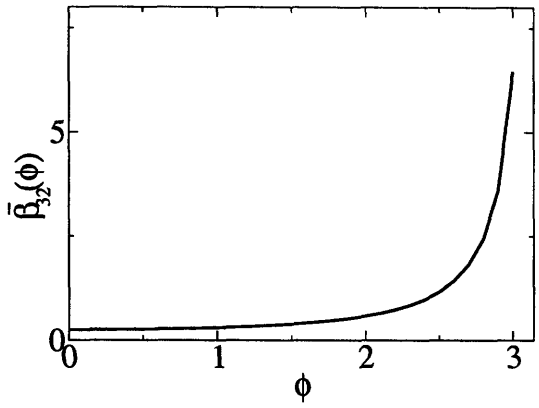

Figure 2-3: $\bar{\beta}_{32}(\phi) = \bar{J}_{32}(\phi)$ for the two plane wave "crystal" structure with condensate (2.72). ϕ is the angle between $\mathbf{q}_2$ and $\mathbf{q}_3$. For more complicated crystal structures, $\bar{\beta}_{32}$ is given by the sum in (2.51), meaning that it is a sum of $\bar{J}_{32}(\phi)$ evaluated at various values of ϕ corresponding to the various angles between a vector in $\{\mathbf{q}_2\}$ and a vector in $\{\mathbf{q}_3\}$.

many crystal structures [39], in all the three-flavor crystalline phases that we present in Section 2.7.4 we find that $\bar{\gamma}_{322}$ is positive and sufficiently large that $\bar{\gamma}_{\rm eff} = 2\bar{\gamma} + 2\bar{\gamma}_{322}$ is positive. We therefore need not discuss the $\bar{\gamma}_{\rm eff} < 0$ case any further.

2.7.2 Two plane wave structure

We begin with the simplest three-flavor "crystal" structure in which $\{\mathbf{q}_2\}$ and $\{\mathbf{q}_3\}$ each contain only a single vector, yielding a condensate

$$\Delta_{\alpha i,\beta j} = e^{2i\mathbf{q}_2\cdot\mathbf{r}}\Delta_2\epsilon_{2\alpha\beta}\epsilon_{2ij} + e^{2i\mathbf{q}_3\cdot\mathbf{r}}\Delta_3\epsilon_{3\alpha\beta}\epsilon_{3ij} \ , \tag{2.72}$$

in which the $\langle us\rangle$ and $\langle ud\rangle$ condensates are each plane waves. As explained in the previous subsection, we shall seek solutions with $\Delta_2 = \Delta_3 = \Delta$. We begin with such a simple ansatz because it will yield a qualitative lesson which will prove extremely helpful in winnowing the space of multiple plane wave crystal structures.

Let us now walk through the evaluation of all the coefficients in the free energy (2.66) for this two-plane wave structure. First, $P = 1$ (one vector in each of $\{\mathbf{q}_2\}$ and $\{\mathbf{q}_3\}$) and as always $\alpha(\delta\mu)$ is given by (2.40). Next, we obtain the results for $\bar{\beta}_2 = \bar{\beta}_3$

and $\bar{\gamma}_2 = \bar{\gamma}_3$ from the analysis of the single plane wave condensate in the two flavor model of Ref. [39]:

$$\begin{aligned} \bar{\beta}_2 &= \frac{1}{4}\frac{1}{\eta^2 - 1} = 0.569 \\ \bar{\gamma}_2 &= \frac{1}{32}\frac{\eta^2 + 3}{(\eta^2 - 1)^3} = 1.637 \,. \end{aligned} \tag{2.73}$$

We now turn to $\bar{\beta}_{32}$ and $\bar{\gamma}_{322}$ which describe the interaction between the $\langle us \rangle$ and $\langle ud \rangle$ condensates and which we have calculated in Section 2.6. In general, $\bar{\beta}_{32}$ is given by (2.51) but in this instance since $\{\mathbf{q}_2\}$ and $\{\mathbf{q}_3\}$ each contain only a single vector the sum in this equation reduces simply to

$$\bar{\beta}_{32} = \bar{J}_{32}(\phi) \tag{2.74}$$

where ϕ is the angle between $\mathbf{q}_2$ and $\mathbf{q}_3$ and where $\bar{J}_{32}(\phi)$ is given in Eq. (2.50). $\bar{\beta}_{32}$ is plotted as a function of ϕ in Fig. 2-3 [44, 45].

Turning to $\bar{\gamma}_{322}$, this is given by

$$\bar{\gamma}_{322} = \frac{3}{2}\bar{K}_{322}(\mathbf{q}_3, \mathbf{q}_3, \mathbf{q}_2, \mathbf{q}_2, \mathbf{q}_2, \mathbf{q}_2) \tag{2.75}$$

where $\bar{K}_{322}$ is given by Eq. (2.61). As occurred in the evaluation of β_{32}, the sum over $\mathbf{q}$-vectors in the general expression (2.36) has reduced to evaluating $\bar{K}_{322}$ just once, because $\{\mathbf{q}_2\}$ and $\{\mathbf{q}_3\}$ each contain only a single vector. For the special case where the last four arguments of $\bar{K}_{322}$ are the same, as in (2.75), $\bar{K}_{322}$ depends only on ϕ, the angle between $\mathbf{q}_2$ and $\mathbf{q}_3$, and the integrals in (2.61) can all be evaluated analytically, yielding

$$\begin{aligned} \bar{K}_{322}(\phi) =& \frac{1}{64\left(\eta\cos\frac{\phi}{2}\right)^3\left(\eta^2\sin^2\frac{\phi}{2} - 1\right)^{3/2}} \\ & \times \left[\eta^2 \arctan(b(\phi))\sin^2\frac{\phi}{2} + \frac{\left(\eta^2\sin^2\frac{\phi}{2} - 1\right)b(\phi)}{1 + b(\phi)^2} + \frac{b(\phi)\left(b(\phi)^2 - 1\right)}{\left(b(\phi)^2 + 1\right)^2}\right] , \end{aligned} \tag{2.76}$$

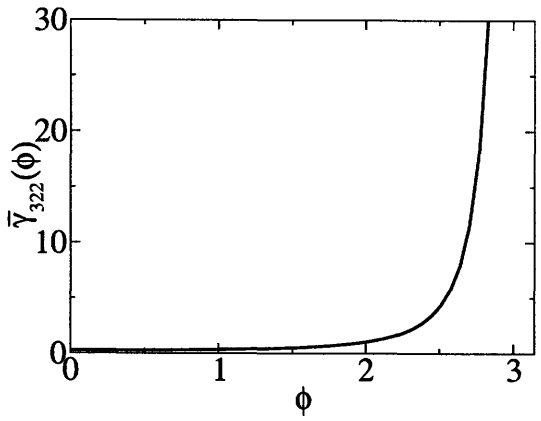

Figure 2-4: $\bar{\gamma}_{322}(\phi)$ for the two plane wave "crystal" structure with condensate (2.72). ϕ is the angle between $\mathbf{q}_2$ and $\mathbf{q}_3$. $\bar{\gamma}_{322}(0) = 0.243$ and $\bar{\gamma}_{322}(\phi)$ increases monotonically with ϕ.

where

$$b(\phi) = \frac{\sqrt{\eta^2 \sin^2 \frac{\phi}{2} - 1}}{\eta \cos \frac{\phi}{2}} \,. \tag{2.77}$$

$\bar{\gamma}_{322}$ is plotted as a function of ϕ in Fig. 2-4.

We note that for any angle ϕ, both $\bar{\beta}_{32}$ and $2\bar{\gamma}_{322}$ are positive quantities which when added to the positive $2\bar{\beta}$ and $2\bar{\gamma}$ give positive $\bar{\beta}_{\text{eff}}$ and $\bar{\gamma}_{\text{eff}}$, respectively. Hence, we see that upon making this two plane wave "crystal" structure ansatz we find a second order phase transition between the crystalline and unpaired phases, for all choices of the angle ϕ. We also note that both $\bar{\beta}_{32}(\phi)$ and $\bar{\gamma}_{322}(\phi)$ increase monotonically with ϕ, and diverge as $\phi \to \pi$. This tells us that within this two plane wave ansatz, the most favorable orientation is $\phi = 0$, namely $\mathbf{q}_2 \parallel \mathbf{q}_3$. Making this choice yields the smallest possible $\bar{\beta}_{\text{eff}}$ and $\bar{\gamma}_{\text{eff}}$ within this ansatz, and hence the largest possible Δ and condensation energy, again within this ansatz. The divergence at $\phi \to \pi$ tells us that choosing $\mathbf{q}_2$ and $\mathbf{q}_3$ precisely antiparallel exacts an infinite free energy price in the combined Ginzburg-Landau and weak-coupling limit in which $\Delta \ll \delta\mu, \Delta_0 \ll \mu$, meaning that in this limit if we chose $\phi = \pi$ we find $\Delta = 0$. Away from the Ginzburg-Landau limit, when the pairing rings on the Fermi surfaces widen into bands, choosing

$\phi = \pi$ exacts a finite price meaning that Δ is nonzero but smaller than that for any other choice of ϕ.

The high cost of choosing $\mathbf{q}_2$ and $\mathbf{q}_3$ precisely antiparallel can be understood qualitatively as arising from the fact that in this case the ring of states on the u-quark Fermi surface that "want to" pair with d-quarks coincides precisely with the ring that "wants to" pair with s-quarks (For example, if $\mathbf{q}_2$ and $\mathbf{q}_3$ point in the $-z$ and $+z$ directions, Δ_2 (Δ_3) describes pairing between s-quarks (d-quarks) within a ring in the northern hemisphere of the s- (d-)Fermi surface and u-quarks within a ring in the southern hemisphere of the u-Fermi surface. The rings on the u-Fermi surface coincide, as illustrated in Figure. 1-6 in Chapter 1.) In the most favorable case within the two-plane wave ansatz, where $\mathbf{q}_2 \parallel \mathbf{q}_3$, the two pairing rings on the u-quark Fermi surface are centered on antipodal points. (For example, if $\mathbf{q}_2$ and $\mathbf{q}_3$ both point in the $+z$ direction, Δ_2 (Δ_3) describes pairing of s-quarks (d-quarks) within a ring in the southern (northern) hemisphere of the s- (d-)Fermi surface and u-quarks within rings in the (northern) southern hemisphere of the u-Fermi surface.)

We will analyze the simple two plane wave ansatz (2.72) in the same NJL model that we employ upon making the weak-coupling approximation but without making a Ginzburg-Landau approximation in Chapter 3. We will find that all the qualitative lessons that we have learned from the Ginzburg-Landau approximation remain valid, including the favorability of the choice $\phi = 0$, but we learn further that in the two plane wave case the Ginzburg-Landau approximation always underestimates Δ. We will also see that the Δ at which the Ginzburg-Landau approximation breaks down shrinks as $\phi \to \pi$. We can understand this result as follows. The sextic term in the free energy (2.66) is small compared to the quartic term only if $\Delta^2 \ll \delta\mu^2\bar{\beta}_{\text{eff}}/\bar{\gamma}_{\text{eff}}$, making this a necessary condition for the quantitative validity of the Ginzburg-Landau approximation. As $\phi \to \pi$, $\bar{\gamma}_{\text{eff}}$ diverges more strongly than $\bar{\beta}_{\text{eff}}$: from (2.50) and (2.61)

we find that as $\phi \to \pi$,

$$\begin{aligned} \bar{\beta}_{\text{eff}} &\sim \bar{J}_{32} \sim \frac{\pi}{8\eta\sqrt{\eta^2-1}}\left(\frac{1}{\cos(\frac{\phi}{2})}\right) \\ \bar{\gamma}_{\text{eff}} &\sim \frac{3}{2}\bar{K}_{322} \sim \frac{3\pi}{256\eta(\sqrt{\eta^2-1})^3}\left(\frac{1}{\cos(\frac{\phi}{2})}\right)^3 . \end{aligned} \tag{2.78}$$

Therefore the Ginzburg-Landau calculation predicts that its own breakdown will occur at a Δ that decreases with increasing ϕ, as will find in Chapter 3 by explicit comparsion with a calculation that does not employ the Ginzburg-Landau approximation.

2.7.3 Implications for more plane waves: qualitative principles for favorable crystal structures

In this subsection we ask what lessons we can learn from the evaluation of the Ginzburg-Landau coefficients for the two plane wave "crystal" structure in Section 2.7.2 for crystal structures with more than one vector in $\{\mathbf{q}_2\}$ and $\{\mathbf{q}_3\}$.

First, we can conclude that $\bar{\beta}_{32}$ is positive for *any* choice of $\{\mathbf{q}_2\}$ and $\{\mathbf{q}_3\}$. The argument is simple: $\bar{\beta}_{32}$ is given in general by (2.51), a sum over $\bar{J}_{32}$ evaluated at a host of angles corresponding to all angles between a vector in $\{\mathbf{q}_2\}$ and $\{\mathbf{q}_3\}$. But, we see from Fig. 2-3 that $\bar{J}_{32}$ is positive at any angle.

Second, we *cannot* draw such a conclusion about γ_{322}. This coefficient is a sum over contributions of the form $\bar{K}_{322}(\mathbf{q}_3^b, \mathbf{q}_3^b, \mathbf{q}_2^d, \mathbf{q}_2^e, \mathbf{q}_2^f, \mathbf{q}_2^a)$ where the last four momentum vector arguments, selected from $\{\mathbf{q}_2\}$, must satisfy (2.54). The calculation in Section 2.7.2 whose result is plotted in Fig. 2-4 only demonstrates that those contributions in which the four $\mathbf{q}_3$ arguments are selected to all be the same vector are positive. For any crystal structure in which $\{\mathbf{q}_2\}$ contains two or more vectors, there are other contributions to $\bar{\gamma}_{322}$ that we have not evaluated in this Section which depend on one $\mathbf{q}_2$ vector and several $\mathbf{q}_3$ vectors, and thus on more than one angle. We know of instances where individual contributions $\bar{K}_{322}(\mathbf{q}_3^b, \mathbf{q}_3^b, \mathbf{q}_2^d, \mathbf{q}_2^e, \mathbf{q}_2^f, \mathbf{q}_2^a)$ in crystal

structures that we describe below *are* negative. However, we have found no crystal structure for which $\bar{\gamma}_{322}$ is negative.

The final lesson we learn is that crystal structures in which any of the vectors in $\{\mathbf{q}_2\}$ are close to antiparallel to any of the vectors in $\{\mathbf{q}_3\}$ are strongly disfavored. (The closer to antiparallel, the worse, with the free energy penalty for $\Delta \neq 0$ diverging for the precisely antiparallel case, driving Δ to zero.) If a vector in $\{\mathbf{q}_2\}$ is antiparallel (or close to antiparallel) to one in $\{\mathbf{q}_3\}$, this yields infinite (or merely large) positive contributions to $\bar{\beta}_{32}$ and to $\bar{\gamma}_{322}$ and hence to $\bar{\beta}_{\text{eff}}$ and $\bar{\gamma}_{\text{eff}}$. In the case of $\bar{\beta}_{32}$, these large positive contributions cannot be cancelled since all contributions are positive. In the case of $\bar{\gamma}_{322}$, negative contributions are possible but we know of no instances of divergent negative contributions to $\bar{\gamma}_{322}$ or indeed to any other coefficient in the Ginzburg-Landau expansion. The divergent positive contributions are associated with the tangential intersection (in the case of $\bar{\beta}$ and $\bar{\gamma}$ [39]) or coincidence (in the case of of $\bar{\beta}_{32}$ and $\bar{\gamma}_{322}$) of pairing rings on Fermi surfaces. We know of no configuration of rings that leads to an infinitely favorable (as opposed to unfavorable) free energy in the combined Ginzburg-Landau and weak-coupling limits. So, although we do not have a proof that the divergent positive contributions to $\bar{\gamma}_{322}$ arising as vectors in $\{\mathbf{q}_2\}$ and $\{\mathbf{q}_3\}$ approach one another's antipodes are uncancelled, we also see no physical argument for how this could conceivably arise. Certainly in all example crystal structures that we have considered, $\bar{\beta}_{32}$ and $\bar{\gamma}_{322}$ and hence $\bar{\beta}_{\text{eff}}$ and $\bar{\gamma}_{\text{eff}}$ diverge as vectors in $\{\mathbf{q}_2\}$ and $\{\mathbf{q}_3\}$ approach one another's antipodes.

We can now summarize the qualitative principles that we have arrived at for constructing favorable crystal structures for three-flavor crystalline color superconductivity. First, as described in Section 2.4 the sets $\{\mathbf{q}_2\}$ and $\{\mathbf{q}_3\}$ should each separately be chosen to yield crystal structures which, seen as separate two-flavor crystalline phases, are as favorable as possible. In Chapter 1 we have reviewed the results of Ref. [39] for how this should be done, and the conclusion that the most favored $\{\mathbf{q}_2\}$ or $\{\mathbf{q}_3\}$ in isolation consists of eight vectors pointing at the corners of a cube. Second, the new addition in the three-flavor case is the qualitative principle that $\{\mathbf{q}_2\}$ and $\{\mathbf{q}_3\}$ should be rotated with respect to each other in such a way as to

best keep vectors in one set away from the antipodes of vectors in the other set.

2.7.4 Multiple plane waves

In Table I we describe 11 different crystal structures that we have analyzed, and in Table II we give the coefficients that specify each Ginzburg-Landau free energy (2.64). The $\bar{\beta}$'s and $\bar{\gamma}$'s were calculated as described in Ref. [39]; $\bar{\beta}_{32}$'s and $\bar{\gamma}_{322}$'s were calculated as described in Section 2.6. We also give the combinations $\bar{\beta}_{\rm eff}$ and $\bar{\gamma}_{\rm eff}$ defined in (2.66) that specify the free energy as in (2.67). In those cases in which $\bar{\beta}_{\rm eff} < 0$, the phase transition between the crystalline phase and the unpaired phase is first order, occurring where $\alpha = \alpha_*$ with α_* given by (2.70). At the first order phase transition, unpaired quark matter with $\Delta = 0$ and crystalline quark matter with $\Delta(\alpha_*)$ given in (2.71) have the same free energy. We give both α_* and $\Delta(\alpha_*)$ in Table II.

The first row of the Tables describes the simple "crystal structure" analyzed in detail in Section 2.7.2, in which both $\{\mathbf{q}_2\}$ and $\{\mathbf{q}_3\}$ contain just a single vector, with $\mathbf{q}_2 \parallel \mathbf{q}_3$ as we have seen that this is the most favorable choice for the angle between $\mathbf{q}_2$ and $\mathbf{q}_3$. This condensate carries a baryon number current which means that the unpaired gapless fermions (in "blocking regions" in momentum space [34, 35]) must carry a current that is equal in magnitude but opposite in direction [34]. The analysis of this "crystal structure" in Sections 2.7.2 and 2.7.3 has proved instructive, giving us qualitative insight that we shall use to understand all the other crystal structures. However, in all rows in the Tables other than the first we have chosen crystal structures with condensates that carry no net current, meaning that the gapless fermions need carry no current. There is nothing in our mean-field analysis that precludes condensates carrying a net current, but we do not analyze them here primarily because it simplifies our task but also because we expect that, beyond mean-field theory, a phase containing gapless fermions carrying a net current is unlikely to be the favored ground state.

Let us next examine the last two rows of the Tables. Here, we consider two crystal structures in which $\{\mathbf{q}_2\}$ and $\{\mathbf{q}_3\}$ each contain eight vectors forming cubes.

Structure	Description	Largest Angle
2PW	$\{\mathbf{q}_2\}$ and $\{\mathbf{q}_3\}$ coincide; each contains one vector. (So, 2 plane waves with $\mathbf{q}_2 \parallel \mathbf{q}_3$.)	0°
SqX	$\{\mathbf{q}_2\}$ and $\{\mathbf{q}_3\}$ each contain two antiparallel vectors. The four vectors together form a square; those from $\{\mathbf{q}_2\}$ and those from $\{\mathbf{q}_3\}$ each form one stroke of an "X".	90°
Tetrahedron	$\{\mathbf{q}_2\}$ and $\{\mathbf{q}_3\}$ each contain two vectors. The four together form a tetrahedron.	109.5°
2Triangles	$\{\mathbf{q}_2\}$ and $\{\mathbf{q}_3\}$ coincide; each contains three vectors forming a triangle.	120°
Cube X See Eq. (2.83)	$\{\mathbf{q}_2\}$ and $\{\mathbf{q}_3\}$ each contain 4 vectors forming a rectangle. The 8 vectors together form a cube. The 2 rectangles intersect to look like an "X" if viewed end-on.	109.5°
2Tet	$\{\mathbf{q}_2\}$ and $\{\mathbf{q}_3\}$ coincide; each contains four vectors forming a tetrahedron.	109.5°
Twisted Cube	$\{\mathbf{q}_2\}$ and $\{\mathbf{q}_3\}$ each contain four vectors forming a square which could be one face of a cube. Instead, the eight vectors together form the polyhedron obtained by twisting the top face of a cube by 45° relative to its bottom face.	143.6°
2Octa90xy	$\{\mathbf{q}_2\}$ and $\{\mathbf{q}_3\}$ each contain 6 vectors forming an octahedron. The $\{\mathbf{q}_2\}$ vectors point along the positive and negative axes. The $\{\mathbf{q}_3\}$-octahedron is rotated relative to the $\{\mathbf{q}_2\}$-octahedron by 90° about the $(1,1,0)$-axis.	135°
2Octa45xyz	$\{\mathbf{q}_2\}$ and $\{\mathbf{q}_3\}$ each contain 6 vectors forming an octahedron. The $\{\mathbf{q}_2\}$ vectors point along the positive and negative axes. The $\{\mathbf{q}_3\}$-octahedron is rotated relative to the $\{\mathbf{q}_2\}$-octahedron by 45° about the $(1,1,1)$-axis.	143.6°
2Cube45z See Eq. (2.80)	$\{\mathbf{q}_2\}$ and $\{\mathbf{q}_3\}$ each contain 8 vectors forming a cube. The $\{\mathbf{q}_2\}$ vectors point along $(\pm 1, \pm 1, \pm 1)$. The $\{\mathbf{q}_3\}$-cube is rotated relative to that by 45° about the z-axis.	143.6°
2Cube45xy	$\{\mathbf{q}_2\}$ and $\{\mathbf{q}_3\}$ each contain 8 vectors forming a cube. The $\{\mathbf{q}_2\}$ vectors point along $(\pm 1, \pm 1, \pm 1)$. The $\{\mathbf{q}_3\}$-cube is rotated relative to that by 45° about the $(1,1,0)$-axis.	154.5°

Table 2.1: Descriptions of the crystal structures whose Ginzburg-Landau coefficients are given in Table II. The third column is the largest angle between any vector in $\{\mathbf{q}_2\}$ and any vector in $\{\mathbf{q}_3\}$. Other things being equal, we expect that the larger the largest angle, meaning the closer vector(s) in $\{\mathbf{q}_2\}$ get to vector(s) in $\{\mathbf{q}_3\}$, the bigger the $\bar{\beta}_{32}$ and $\bar{\gamma}_{322}$ and hence the bigger the $\bar{\beta}_{\text{eff}}$ and $\bar{\gamma}_{\text{eff}}$, and hence the less favorable the structure.

Structure	β	β_{32}	β_{eff}	$\bar{\gamma}$	$\bar{\gamma}_{322}$	$\bar{\gamma}_{\text{eff}}$	α_*	$\frac{\Delta(\alpha_*)}{\delta\mu}$
2PW	0.569	0.250	1.388	1.637	0.243	3.760	0	0
SqX	0.138	1.629	1.906	1.952	2.66	9.22	0	0
Tetrahedron	-0.196	2.146	1.755	1.450	7.21	17.29	0	0
2Triangles	-1.976	4.647	0.696	1.687	13.21	29.80	0	0
CubeX	-10.981	6.961	-15.001	-1.018	19.90	37.76	0.140	0.548
2Tet	-5.727	7.439	-4.015	4.350	30.35	69.40	0.0054	0.208
Twisted Cube	-16.271	12.445	-20.096	-37.085	315.5	556.8	0.0170	0.165
2Octa90xy	-31.466	18.665	-44.269	19.711	276.9	593.2	0.0516	0.237
2Octa45xyz	-31.466	19.651	-43.282	19.711	297.7	634.9	0.0461	0.226
2Cube45z	-110.757	36.413	-185.101	-459.24	1106.	1294.	0.310	0.328
2Cube45xy	-110.757	35.904	-185.609	-459.24	11358.	21798.	0.0185	0.0799

Table 2.2: Ginzburg-Landau coefficients for three-flavor crystalline color superconducting phases with various crystal structures, described in Table I. α_* is the α at which the transition from unpaired quark matter to a given crystalline phase occurs: $\alpha_* = 0$ if $\beta_{\text{eff}} > 0$ and the transition is second order; α_* is given by (2.70) if $\beta_{\text{eff}} < 0$ and the transition is first order. For a first order transition, $\Delta(\alpha_*)$, given in (2.71), is the magnitude of the gap at the transition.

Since the cube is the most favorable two-flavor crystal structure according to the analysis of Ref. [39], evident in the large negative $\bar{\beta}$ and $\bar{\gamma}$ for both these crystal structures in Table II, this should be a good starting point. We cannot have the two cubes coincident, as in that case there are vectors from $\{\mathbf{q}_2\}$ and vectors from $\{\mathbf{q}_3\}$ separated by a 180° angle, yielding infinite positive contributions to both $\bar{\beta}_{32}$ and $\bar{\gamma}_{322}$. So, we rotate the $\{\mathbf{q}_3\}$-cube relative to the $\{\mathbf{q}_2\}$ cube, in two different ways in the 2Cube45z and 2Cube45xy crystal structures described in Table I.

We explain explicitly in Appendix B why translating one cube relative to the other in position space by a fraction of a lattice spacing does not alleviate the problem: a relative rotation of the $\langle us \rangle$ and $\langle ud \rangle$ condensates is required. Qualitatively, this reflects the nature of the difficulty that occurs when a $\{\mathbf{q}_2\}$ vector is opposite to a $\{\mathbf{q}_3\}$ vector. It can be thought of as arising because the $\langle us \rangle$ and $\langle ud \rangle$ condensates both want to "use" those up quarks lying on the same ring on the up Fermi surface. It therefore makes sense that a relative rotation is required. Quantitatively, what we show in Appendix B is that Ω does not change if we translate the $\langle us \rangle$ condensate relative to the $\langle ud \rangle$ condensate.

We see in Table I that in the 2Cube45z structure, the largest angle between vectors in $\{\mathbf{q}_2\}$ and $\{\mathbf{q}_3\}$ is 143.6° whereas in the 2Cube45xy structure, that largest angle is 154.5° meaning that the rotation we have chosen does a less good job of keeping $\{\mathbf{q}_2\}$-vectors away from the antipodes of $\{\mathbf{q}_3\}$ vectors. Correspondingly, we see in Table II that 2Cube45xy has a much larger $\bar{\gamma}_{322}$ and hence $\bar{\gamma}_{\text{eff}}$, and hence has a first order phase transition occurring at a smaller α_* and with a smaller $\Delta(\alpha_*)$. This is an example confirming our general principle that, other things being equal, crystal structures in which $\{\mathbf{q}_3\}$ vectors come closer to $\{\mathbf{q}_2\}$ vectors will be disfavored. According to this principle, the 2Cube45z crystal structure should be particularly favorable as it employs the relative rotation between the two cubes that does the best possible job of keeping them apart.

We now turn to crystal structures with fewer than 16 plane waves. By having fewer than 8 plane waves in $\{\mathbf{q}_2\}$ and $\{\mathbf{q}_3\}$, we are no longer optimizing the two-flavor $\bar{\beta}$ and $\bar{\gamma}$. However, with fewer vectors it is possible to keep the $\{\mathbf{q}_2\}$- and

$\{\mathbf{q}_3\}$-vectors farther away from each other's antipodes. We list two crystal structures in which $\{\mathbf{q}_2\}$ and $\{\mathbf{q}_3\}$ have 6 waves forming octahedra. These are not particularly favorable two-flavor structures — $\bar{\gamma}$ is positive rather than being large and negative for the cube. 2Octa45xyz has the same largest angle between $\{\mathbf{q}_2\}$- and $\{\mathbf{q}_3\}$-vectors as 2Cube45z, but its significantly more positive $\bar{\beta}$ and $\bar{\gamma}$ make it significantly less favorable. Choosing the 2Octa90xy structure instead reduces the largest angle between $\{\mathbf{q}_2\}$- and $\{\mathbf{q}_3\}$-vectors from 143.6° to 135°, which improves $\bar{\beta}_{\text{eff}}$ and $\bar{\gamma}_{\text{eff}}$, but only slightly.

We investigate three crystal structures in which $\{\mathbf{q}_2\}$ and $\{\mathbf{q}_3\}$ each contain 4 vectors. Among these, the Twisted Cube is strongly disfavored by its significantly larger largest angle between $\{\mathbf{q}_2\}$- and $\{\mathbf{q}_3\}$-vectors. CubeX and 2Tet are both constructed by choosing $\{\mathbf{q}_2\}$ and $\{\mathbf{q}_3\}$ as subsets containing half the vectors from a cube. In the 2Tet structure, we choose the tetrahedra coincident since this does the best job of keeping vectors in $\{\mathbf{q}_2\}$ and $\{\mathbf{q}_3\}$ away from each other's antipodes. (Choosing the two tetrahedra so that their union forms a cube is the worst possible choice, as vectors in $\{\mathbf{q}_2\}$ and $\{\mathbf{q}_3\}$ are then antipodal.) In the CubeX structure, we choose the two rectangles such that their union forms a cube, as this does the best job of reducing the largest angle between vectors in $\{\mathbf{q}_2\}$ and $\{\mathbf{q}_3\}$; making the rectangles coincident would have been the worst possible choice. CubeX and 2Tet have the same largest angle, but they differ considerably in that the $\{\mathbf{q}_2\}$ and $\{\mathbf{q}_3\}$ rectangles that make up CubeX are more favorable two-flavor structures (lower $\bar{\beta}$ and $\bar{\gamma}$) than the tetrahedra that make up 2Tet. We see from Table II that the CubeX structure, with only 8 vectors in total, is particularly favorable: it is not possible to tell from Table II whether it is more or less favorable than 2Cube45z, since one has the larger α_* while the other has the larger $\Delta(\alpha^*)$. We shall evaluate their free energies below, and confirm that they are indeed comparable, and that these two structures have the lowest free energy of any in the Tables.

In the remaining rows of the Tables, we investigate one crystal structure in which $\{\mathbf{q}_2\}$ and $\{\mathbf{q}_3\}$ each contain 3 vectors, and two in which each contain 2 vectors. These structures all have positive $\bar{\beta}_{\text{eff}}$, and hence second order phase transitions, and so are

certainly not favored.

Inspecting the results in Table II shows that in all cases where we have investigated different three-flavor crystal structures built from the same $\{\mathbf{q}_2\}$ and $\{\mathbf{q}_3\}$, the one with the relative rotation between the two polyhedra that yields the smaller largest angle between vectors in $\{\mathbf{q}_2\}$ and $\{\mathbf{q}_3\}$ is favored. And, in all cases where we have investigated two crystal structures with same largest angle between vectors in $\{\mathbf{q}_2\}$ and $\{\mathbf{q}_3\}$, the one built from the more favorable two-flavor crystal structure is favored. We thus find no exceptions to the qualitative principles we described in Section 2.7.3. However, these qualitative principles certainly do not explain all the features of the results in Table II. For example, we have no qualitative understanding of why 2Cube45z and 2Cube45xy have such similar $\bar{\beta}_{32}$, whereas 2Cube45xy has a much larger $\bar{\gamma}_{322}$ as expected. For example, we have no qualitative understanding of why $\bar{\gamma}_{322}$ increases much more in going from 2Cube45xy to 2Cube45z than it does in going from 2Octa90xy to 2Octa45xyz. The calculations must be done; the qualitative principles are a good guide, but not a substitute.

The final crystal structure that we describe is one in which $\{\mathbf{q}_2\}$ is a cube while $\{\mathbf{q}_3\}$ is an octahedron, with the six $\{\mathbf{q}_3\}$-vectors pointing at the centers of the faces of the $\{\mathbf{q}_2\}$-cube. So, if the $\{\mathbf{q}_2\}$-vectors are taken to point along the $(\pm 1, \pm 1, \pm 1)$ directions then the $\{\mathbf{q}_3\}$ vectors point along the positive and negative axes. We chose to investigate this structure because it seems particularly symmetric and because it has an unusually small largest angle between vectors in $\{\mathbf{q}_2\}$ and $\{\mathbf{q}_3\}$ given the large number of vectors in total: 125.3°. Because $\{\mathbf{q}_2\}$ and $\{\mathbf{q}_3\}$ are not congruent, $\bar{\beta}_2 \neq \bar{\beta}_3$ and $\bar{\gamma}_2 \neq \bar{\gamma}_3$. All these coefficients can be found in Table II. We find $\bar{\beta}_{32} = 24.510$, $\bar{\gamma}_{322} = 419.9$ and $\bar{\gamma}_{233} = 4943$. Because $\{\hat{\mathbf{q}}_2\}$ and $\{\hat{q}_3\}$ are not exchange symmetric, the general argument that we gave in Section 2.7.1 for why extrema of $\Omega(\Delta_2, \Delta_3)$ — i.e. solutions to the gap equations — occur at $\Delta_2 = \Delta_3$ does not apply. However, we find that at the solution Δ_2 and Δ_3 differ by less than 20%. The large values of $\bar{\gamma}_{233}$ and $\bar{\gamma}_{322}$ make this crystal structure quite unfavorable — even though it has a (weak) first order phase transition, its free energy turns out to be comparable only to that of the 2PW structure, far above the free energy of the favored CubeX and 2Cube45z

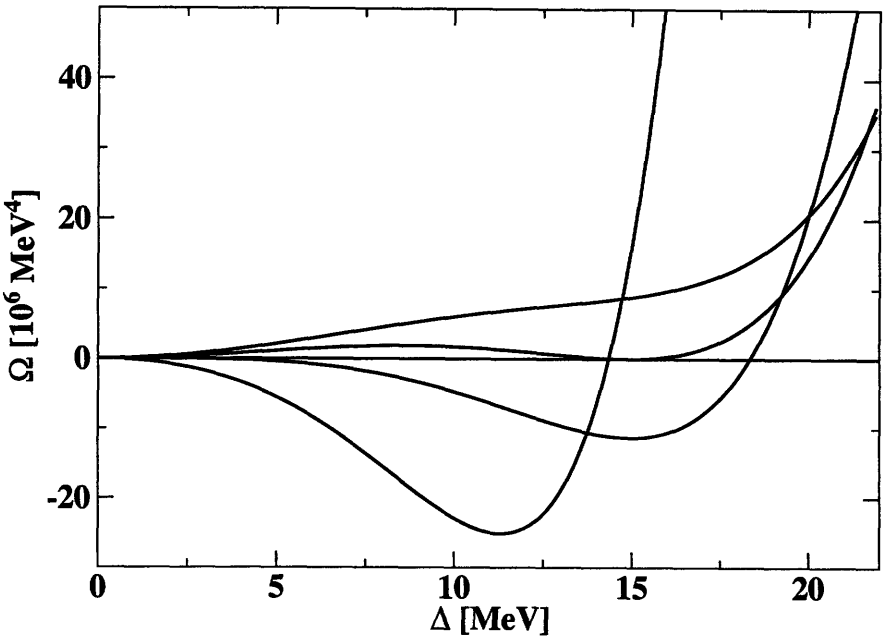

Figure 2-5: Free energy Ω vs. Δ for the CubeX crystal structure, described in Table II, at four values of M_s^2/μ. From top curve to bottom curve, as judged from the left half of the figure, the curves are $M_s^2/\mu = 240$, 218.61, 190, and 120 MeV, corresponding to $\alpha = 0.233$, 0.140, 0, -0.460. The first order phase transition occurs at $M_s^2/\mu = 218.61$ MeV. The values of Δ and Ω at the minima of curves like these are what we plot in Figs. 2-6 and 2-7.

structures. Furthermore, the arguments of Appendix A do not apply to a crystal structure like this, meaning that we do not expect this solution with $\Delta_2 \neq \Delta_3$ to be neutral. For this reason, and because it appears to be free-energetically unfavorable anyway, we will not investigate it further. We cannot say whether choosing $\{\mathbf{q}_2\}$ and $\{\mathbf{q}_3\}$ to not be exchange symmetric generically yields an unfavorable crystal structure, as we have not investigated many possibilities.

We have certainly not done an exhaustive search of three-flavor crystal structures. For example, we have only scratched the surface in investigating structures in which $\{\mathbf{q}_2\}$ and $\{\mathbf{q}_3\}$ are not exchange symmetric. We have investigated the structures that are the best that we can think of according to the qualitative principles described in Section 2.7.3. Readers should feel free to try others. (We are confident that in 2Cube45z we have found the most favorable structure obtained by rotating one

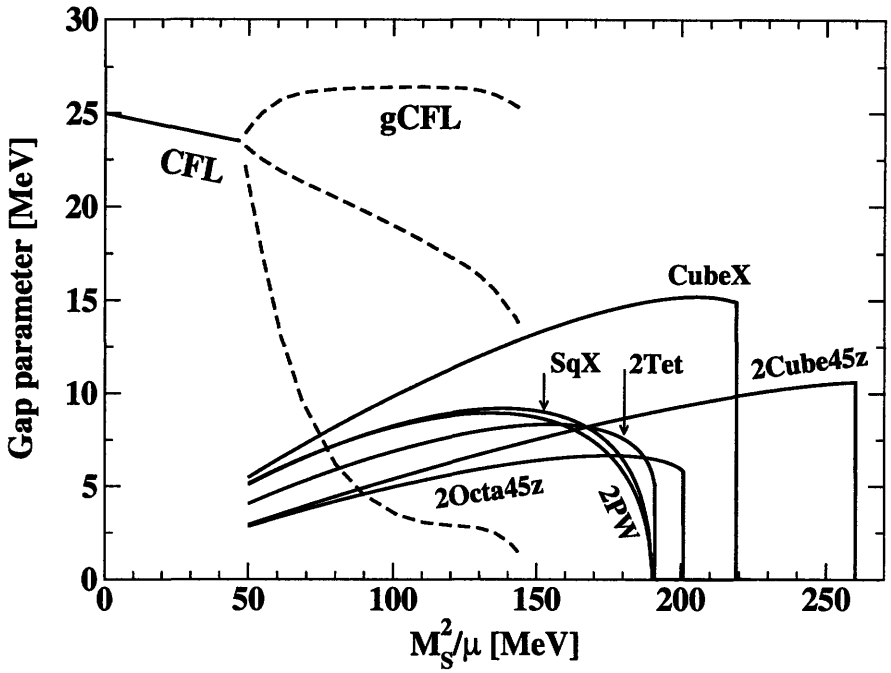

Figure 2-6: Gap parameter Δ versus M_s^2/μ for three-flavor crystalline color superconducting phases with various crystal structures. The crystal structures are described in Table II. For comparison, we also show the CFL gap parameter and the gCFL gap parameters Δ_1, Δ_2 and Δ_3 [62, 63]. Recall that the splitting between Fermi surfaces is proportional to M_s^2/μ, and that small (large) M_s^2/μ corresponds to high (low) density.

cube relative to another. We are not as confident that CubeX is the best possible structure with fewer than 8+8 vectors.) As we shall see in Section 2.7.5, however, the two most favorable structures that we have found, 2Cube45z and CubeX, are impressively robust and do a very good job of making the case that three-flavor crystalline color superconducting phases are the ground state of cold quark matter over a wide range of densities. If even better crystal structures can be found, this will only further strengthen this case.

2.7.5 Free energy comparisons

We can now evaluate and plot the gap parameter Δ and free energy $\Omega(\Delta)$ for all the crystal structures described in Table I, whose Ginzburg-Landau coefficients are given

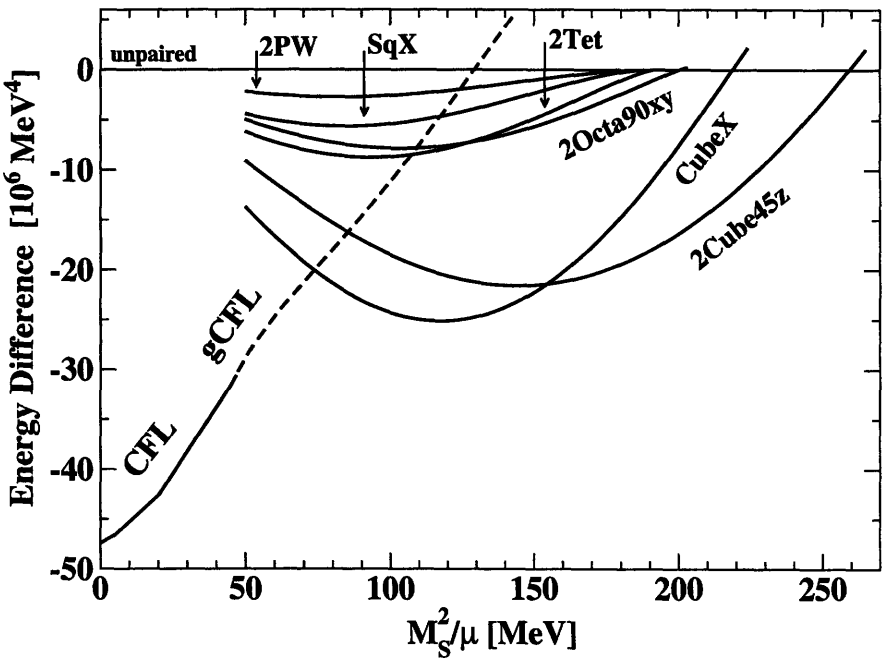

Figure 2-7: Free energy Ω versus M_s^2/μ for the three-flavor crystalline color superconducting phases with various crystal structures whose gap parameters are plotted in Fig. 2-6. The crystal structures are described in Table II. Recall that the gCFL phase is known to be unstable, meaning that in the regime where the gCFL phase free energy is plotted, the true ground state of three-flavor quark matter must be some phase whose free energy lies below the dashed line. We see that the three-flavor crystalline color superconducting quark matter phases with the most favorable crystal structures that we have found, namely 2Cube45z and CubeX described in (2.80) and (2.83), have sufficiently robust condensation energy (sufficiently negative Ω) that they are candidates to be the ground state of three-flavor quark matter over a wide swath of M_s^2/μ, meaning over a wide range of densities.

in Table II. For a given crystal structure, $\Omega(\Delta)$ is given by Eq. (2.66), with $\bar{\beta}_{\text{eff}}$ and $\bar{\gamma}_{\text{eff}}$ taken from Table II. The quadratic coefficient α is related to $\delta\mu$ by Eq. (2.40). Recall that we have made the approximation that $\delta\mu_2 = \delta\mu_3 = \delta\mu = M_s^2/(8\mu)$, valid up to corrections of order M_s^3/μ^4. At any value of M_s^2/μ, we can evaluate $\alpha(\delta\mu)$ and hence $\Omega(\Delta)$, determine Δ by minimizing Ω, and finally evaluate the free energy Ω at the minimum. In Fig. 2-5, we give an example of $\Omega(\Delta)$ for various M_s^2/μ for one crystal structure with a first order phase transition (CubeX), illustrating how the first order phase transition is found, and how the Δ solving the gap equations —

i.e. minimizing Ω — is found . We plot Δ and Ω at the minimum versus M_s^2/μ in Figs. 2-6 and 2-7 for some of the crystal structures in Tables I and II.

In Figs. 2-6 and 2-7, we show two examples of crystal structures for which the phase transition to the unpaired state is second order: 2PW and SqX. (See Table I for descriptions of these structures.) The second order phase transition occurs at $M_s^2/\mu = 7.60\Delta_0 = 190.0$ MeV, where $\alpha = 0$. (See Eq. (2.68).) We show four examples of crystal structures with first order phase transitions, occurring where $\alpha = \alpha_* > 0$ meaning at some $M_s^2/\mu > 190.0$ MeV. We show the two most favorable structures that we have found: CubeX and 2Cube45z. And, we show two examples (2Tet and 2Octa90xy) of structures with first order phase transitions that are more favorable than the structures with a second order transition, but less favorable than CubeX and 2Cube45z.

In Figs. 2-6 and 2-7, we have chosen the interaction strength between quarks such that the CFL gap parameter at $M_s = 0$ is $\Delta_0 = 25$ MeV. However, our results for both the gap parameters and the condensation energy for any of the crystalline phases can easily be scaled to any value of Δ_0. We saw in Section 2.6 that the quartic and sextic coefficients in the Ginzburg-Landau free energy do not depend on Δ_0. And, recall from Eq. (2.40) that Δ_0 enters α only through the combination $\Delta_{2SC}/\delta\mu$, where $\Delta_{2SC} = 2^{\frac{1}{3}}\Delta_0$ and $\delta\mu = M_s^2/(8\mu)$. This means that if we pick a $\Delta_0 \neq 25$ MeV, the curves describing the gap parameters for the crystalline phases in Fig. 2-6 are precisely unchanged if we rescale both the vertical and horizontal axes proportional to $\Delta_0/25$ MeV. In the case of Fig. 2-7, the vertical axis must be rescaled by $(\Delta_0/25\text{ MeV})^2$. Of course, the weak-coupling approximation $\Delta_0 \ll \mu$, which we have used for example in simplifying the propagators in (2.44), will break down if we scale Δ_0 to be too large. We cannot evaluate up to what Δ_0 we can scale our results reliably without doing a calculation that goes beyond the weak-coupling limit. However, such calculations have been done for the gCFL phase in Ref. [133], where it turns out that the gaps and condensation energies plotted Figs. 2-6 and 2-7 scale with Δ_0 and Δ_0^2 to good accuracy for $\Delta_0 \leq 40$ MeV with $\mu = 500$ MeV, but the scaling is significantly less accurate for $\Delta_0 = 100$ MeV. Of course, for Δ_0 as large as

100 MeV, any quark matter in a compact star is likely to be in the CFL phase. Less symmetrically paired quark matter, which our results suggest is in a crystalline color superconducting phase, will occur in compact stars only if Δ_0 is smaller, in the range where our results can be expected to scale well.

The qualitative behavior of Δ at smaller M_s^2/μ, well to the left of the unpaired/crystalline phase transitions in Fig. 2-6, can easily be understood. The quadratic, quartic and sextic coefficients in the free energy (2.66) are $\alpha(\delta\mu)$, $\beta_{\rm eff} = \bar{\beta}_{\rm eff}/\delta\mu^2$ and $\gamma_{\rm eff} = \bar{\gamma}_{\rm eff}/\delta\mu^4$. If α tended to a constant at small $\delta\mu$, then the solution $\Delta_{\rm min}$ that minimizes Ω would be proportional to $\delta\mu$. (See Eq. (2.69).) In fact, from (2.40) we see that $\alpha \propto \log\delta\mu$ at small $\delta\mu$, meaning that, according to (2.69), $\Delta_{\rm min}$ should vanish slightly more slowly than linear as $M_s^2/\mu \propto \delta\mu \to 0$, as in Fig. 2-6. And, since the Δ's vanish for $\delta\mu \to 0$, so do the condensation energies of Fig. 2-7.

Fig. 2-6 can be used to evaluate the validity of the Ginzburg-Landau approximation. The simplest criterion is to compare the Δ's for the crystalline phases to the CFL gap parameter Δ_0. This is the correct criterion in the vicinity of the 2nd order phase transition point, where $\delta\mu = M_s^2/(8\mu) \approx \Delta_0$. Well to the left, it is more appropriate to compare the Δ's for the crystalline phase to $\delta\mu = M_s^2/(8\mu)$. By either criterion, we see that all the crystal structures with first order phase transitions (including the two that are most favored) have Δ's that are large enough that the Ginzburg-Landau approximation is at the edge of its domain of validity, a result which we expected based on the general arguments in Section 2.7.1. Note that the Ginzburg-Landau approximation is controlled for those structures with second order phase transitions only near the second order phase transition, again a result that can be argued for on general grounds.

Fig. 2-7 makes manifest one of the central conclusions of our work. The three-flavor crystalline color superconducting phases with the two most favored crystal structures that we have found are robust by any measure. Their condensation energies reach about half that of the CFL phase at $M_s = 0$, remarkable given that in the CFL phase pairing occurs over the whole of all three Fermi surfaces. Correspondingly, these two crystal structures are favored over the wide range of M_s^2/μ seen in Fig. 2-7 and given

in Eq. (2.79).

Taken literally, Fig. 2-7 indicates that within the regime (2.79) of the phase diagram occupied by crystalline color superconducting quark matter, the 2Cube45z phase is favored at lower densities and the CubeX phase is favored at higher densities. Although, as detailed in Sections 2.7.3 and 2.7.4, we do have qualitative arguments why 2Cube45z and CubeX are favored over other phases, we have no qualitative argument why one should be favored over the other. And, we do not trust that the Ginzburg-Landau approximation is sufficiently quantitatively reliable to trust the conclusion that one phase is favored at higher densities while the other is favored at lower ones. We would rather leave the reader with the conclusion that these are the two most favorable phases we have found, that both are robust, that the crystalline color superconducting phase of three-flavor quark matter with one crystal structure or the other occupies a wide swath of the QCD phase diagram, and that their free energies are similar enough to each other that it will take a beyond-Ginzburg-Landau calculation to compare them reliably.

2.8 Conclusions, Implications, and Future Work

We have evaluated the gap parameter and free energy for three-flavor quark matter in crystalline color superconducting phases with varied crystal structures, within a Ginzburg-Landau approximation. Our central results are shown in Figs. 2-6 and 2-7. Descriptions of the crystal structures that we have investigated, together with the coefficients for the Ginzburg-Landau free energy (2.66) for each structure, are given in Tables I and II.

We have found two qualitative rules that guide our understanding of what crystal structures are favored in three-flavor crystalline quark matter. First, the $\langle ud \rangle$ and $\langle us \rangle$ condensates separately should be chosen to have favorable free energies, as evaluated in the two-flavor model of Ref. [39]. Second, the $\langle ud \rangle$ and $\langle us \rangle$ condensates should be rotated relative to each other in such a way as to maximize the angles between the wave vectors describing the crystal structure of the $\langle ud \rangle$ condensate and the antipodes

of the wave vectors describing the $\langle us \rangle$ condensate. This second qualitative rule can be understood as minimizing the "competition" between the two condensates for up quarks on the up Fermi surface as we discussed in Chapter 1.

Fig. 2-7 shows that over most of the range of M_s^2/μ where it was once considered a possibility, the gCFL phase can be replaced by a *much* more favorable three-flavor crystalline color superconducting phase. However, Fig. 2-7 also indicates that it is hard to find a crystal structure which yields a crystalline phase that has lower free energy than the gCFL phase at the lowest values of M_s^2/μ (highest densities) in the "gCFL window", closest to the CFL→gCFL transition. This narrow window where the gCFL curve remains the lowest curve in Fig. 2-7 is therefore the most likely place in the QCD phase diagram in which to find the gCFL phase augmented by current-carrying meson condensates described in Refs. [86, 87]. Except within this window, the crystalline color superconducting phases with either the CubeX or the 2Cube45z crystal structure provide an attractive resolution to the instability of the gCFL phase.

The three-flavor crystalline color superconducting phases with the CubeX and 2Cube45z crystal structures have condensation energies that can be as large as half that of the CFL phase. This robustness makes them the lowest free energy phase that we know of, and hence a candidate for the ground state of QCD, over a wide range of densities. To give a sense of the implications of the range of M_s^2/μ over which crystalline color superconductivity is favored, given by

$$2.9\Delta_0 < \frac{M_s^2}{\mu} < 10.4\Delta_0 \,, \tag{2.79}$$

and shown in Fig. 2-7, if we suppose that $\Delta_0 = 25$ MeV and $M_s = 250$ MeV, the window (2.79) translates to 240MeV $< \mu <$ 847MeV. With these choices of parameters, then, the lower part of this range of μ (higher part of the range of M_s^2/μ) is certainly superseded by nuclear matter. And, the high end of this range extends far beyond the $\mu \sim 500$ MeV characteristic of the quark matter at the densities expected at the very center of compact stars. Our result therefore suggests that if compact stars have quark matter cores, it is entirely reasonable to suppose that the *entire*

quark matter core could be in a crystalline color superconducting phase. Of course, if Δ_0 is larger, say $\sim$ 100 MeV, the entire quark matter core could be in the CFL phase. And, there are reasonable values of Δ_0 and M_s for which the outer layer of a possible quark matter core would be in a crystalline phase while the inner core would not. We do not know Δ_0 and M_s well enough to answer the question of what phases of quark matter occur in compact stars. However, our results add the possibility that as much as all of the quark matter in a compact star could be in a crystalline color superconducting phase to the menu of options that must ultimately be winnowed by confrontation with astrophysical observations.

We have identified two particularly favorable crystal structures, using the qualitative rules described above and by direct calculation. We do not believe that our Ginzburg-Landau approximation is sufficiently accurate to trust its determination of which of these two structures is more favorable. For this reason, we wish to leave the reader with a picture of both the 2Cube45z and CubeX crystal structures in position space. In the 2Cube45z phase, the color-flavor and position space dependence of the condensate, defined in (2.12) and (2.13), is given by

$$\begin{aligned}\Delta_{CF}(x)_{\alpha i,\beta j} =& \epsilon_{2\alpha\beta}\epsilon_{2ij}\, 2\Delta\left[\cos\frac{2\pi}{a}(x+y+z)+\cos\frac{2\pi}{a}(-x+y+z)\right.\\ &\left.+\cos\frac{2\pi}{a}(x-y+z)+\cos\frac{2\pi}{a}(-x-y+z)\right]\\ &+\epsilon_{3\alpha\beta}\epsilon_{3ij}\, 2\Delta\left[\cos\frac{2\pi}{a}\left(\sqrt{2}x+z\right)+\cos\frac{2\pi}{a}\left(\sqrt{2}y+z\right)\right.\\ &\left.+\cos\frac{2\pi}{a}\left(-\sqrt{2}y+z\right)+\cos\frac{2\pi}{a}\left(-\sqrt{2}x+z\right)\right],\end{aligned} \tag{2.80}$$

where α and β (i and j) are color (flavor) indices and where

$$a=\frac{\sqrt{3}\pi}{q}=\frac{4.536}{\delta\mu}=\frac{\mu}{1.764M_s^2} \tag{2.81}$$

is the lattice spacing of the face-centered cubic crystal structure. For example, with

$M_s^2/\mu = 100, 150, 200$ MeV the lattice spacing is $a = 72, 48, 36$ fm. Eq. (2.80) can equivalently be written as

$$\Delta_{CF}(x)_{\alpha i,\beta j} = \epsilon_{2\alpha\beta}\epsilon_{2ij}\Delta_2(\mathbf{r}) + \epsilon_{3\alpha\beta}\epsilon_{3ij}\Delta_3(\mathbf{r}) \ , \tag{2.82}$$

with (2.80) providing the expressions for $\Delta_2(\mathbf{r})$ and $\Delta_3(\mathbf{r})$. A three-dimensional contour plot that can be seen as depicting either $\Delta_2(\mathbf{r})$ or $\Delta_3(\mathbf{r})$ separately can be found in Ref. [39]. We have not found an informative way of depicting the entire condensate in a single contour plot. Note also that in (2.80) and below in our description of the CubeX phase, we make an arbitrary choice for the relative position of $\Delta_3(\mathbf{r})$ and $\Delta_2(\mathbf{r})$. We show in Appendix B that one can be translated relative to the other at no cost in free energy. Of course, as we have investigated in detail in Section 2.7, rotating one relative to the other changes the Ginzburg-Landau coefficients $\bar{\beta}_{32}$ and $\bar{\gamma}_{322}$ and hence the free energy.

In the CubeX phase, the color-flavor and position space dependence of the condensate is given by

$$\begin{aligned}\Delta_{CF}(x)_{\alpha i,\beta j} =& \epsilon_{2\alpha\beta}\epsilon_{2ij}\, 2\Delta\left[\cos\frac{2\pi}{a}(x+y+z) + \cos\frac{2\pi}{a}(-x-y+z)\right] \\ &+ \epsilon_{3\alpha\beta}\epsilon_{3ij}\, 2\Delta\left[\cos\frac{2\pi}{a}(-x+y+z) + \cos\frac{2\pi}{a}(x-y+z)\right] \ .\end{aligned} \tag{2.83}$$

We provide a depiction of this condensate in Fig. 2-8.

The gap parameter Δ is large enough in both the 2Cube45z and CubeX phases that the Ginzburg-Landau approximation that we have used to obtain our results is being pushed to the limits of its validity. Therefore, although we expect that the qualitative lessons that we have learned about the favorability of crystalline phases in three-flavor quark matter are valid, and expect that the relative favorability of the 2Cube45z and CubeX structures and the qualitative size of their Δ and condensation energy are trustworthy, we do not expect quantitative reliability of our results. There is therefore strong motivation to analyze crystalline color supercon-

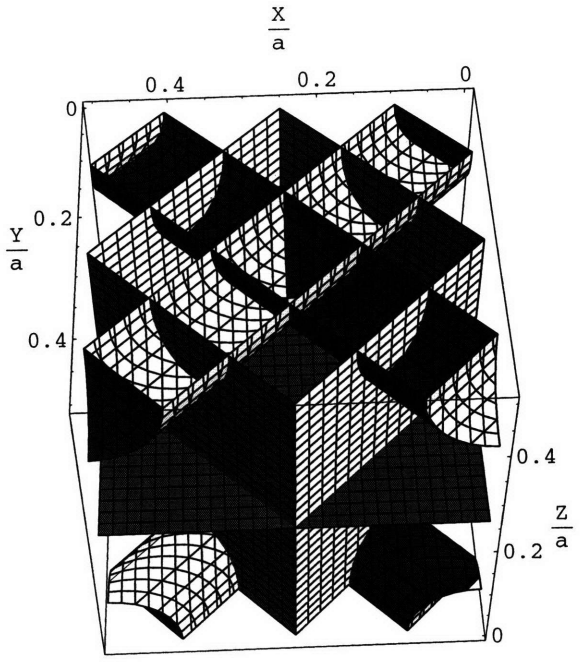

Figure 2-8: The CubeX crystal structure of Eq. (2.83). The figure extends from 0 to $a/2$ in the x, y and z directions. Both $\Delta_2(\mathbf{r})$ and $\Delta_3(\mathbf{r})$ vanish at the horizontal plane. $\Delta_2(\mathbf{r})$ vanishes on the darker vertical planes, and $\Delta_3(\mathbf{r})$ vanishes on the lighter vertical planes. On the upper (lower) dark cylinders and the lower (upper) two small corners of dark cylinders, $\Delta_2(\mathbf{r}) = +3.3\Delta$ ($\Delta_2(\mathbf{r}) = -3.3\Delta$). On the upper (lower) lighter cylinders and the lower (upper) two small corners of lighter cylinders, $\Delta_3(\mathbf{r}) = -3.3\Delta$ ($\Delta_3(\mathbf{r}) = +3.3\Delta$). Note that the largest value of $|\Delta_I(\mathbf{r})|$ is 4Δ, occurring along lines at the centers of the cylinders. The lattice spacing is a when one takes into account the signs of the condensates; if one looks only at $|\Delta_I(\mathbf{r})|$, the lattice spacing is $a/2$. a is given in (2.81). In (2.83) and hence in this figure, we have made a particular choice for the relative position of $\Delta_3(\mathbf{r})$ versus $\Delta_2(\mathbf{r})$. We show in Appendix B that one can be translated relative to the other with no cost in free energy.

ducting quark matter with these two crystal structures without making a Ginzburg-Landau approximation. This calculation can be performed for a family of simple "crystalline" condensates, and we discuss this in the next chapter (Chapter 3).

The specific heat of crystalline color superconducting quark matter is linear with T because of the presence of gapless quark excitations at the boundaries of the regions in momentum space where there are unpaired quarks [41]. Calculating the heat capacity of the CubeX and 2Cube45z structures should therefore yield only quantitative changes relative to that for unpaired quark matter, unlike in the gCFL case where the heat capacity is parametrically enhanced [108]. As a first guess the neu-

trino emissivity can be expected to go as $\sim T^6$, like it does in unpaired quark matter, because the surfaces of the "blocking regions" of crystalline superconductivity (see Figure. figure:shiftedspheres in Chapter 1) feature gapless modes. The detailed evaluation of the phase space for direct URCA neutrino emission from the CubeX and 2Cube45z phases will be a nontrivial calculation, given that thermally excited gapless quarks occurs on boundaries of nontrivial blocking regions [104]. (The direct URCA processes $u + e \to s + \nu$ and $s \to u + e + \bar{\nu}$ require s, u and e to all be within T of a place in momentum space where they are gapless and at the same time to have $\mathbf{p_u} + \mathbf{p_e} = \mathbf{p_s}$ to within T. Here, $T \sim$ keV is very small compared to all the scales relevant to the description of the crystalline phase itself.)

Beginning with Ref. [34], one of the motivations for the study of crystalline color superconducting quark matter has been the possibility that, if present within the core of a compact star, it could provide a region within which rotational vortices are pinned and hence a locus for the origin of (some) pulsar glitches. Or, the presence of crystalline quark matter within neutron stars could be ruled out if it predicts glitch phenomenology in qualitative disagreement with that observed.

There are two key microphysical properties of crystalline quark matter that must be estimated before glitch phenomenology can be addressed. The first is the pinning force. Estimating this will require analyzing how the CubeX and 2Cube45z respond when rotated. We expect vortices to form, and expect the vortices to be pinned at the intersections of the nodal planes at which condensates vanish. Analyzing the vortices in three-flavor crystalline phases will be nontrivial. One complication is that because baryon number current can be carried by gradients in the phase of either the $\langle us \rangle$ crystalline condensate or the $\langle ud \rangle$ condensate or both, and the most favorable vortex or vortices that form upon rotating the CubeX and 2Cube45z phases will have to be determined. Another complication arises because the vortex core size, $1/\Delta$, is only a factor of three to four smaller than the lattice spacing a. This means that the vortices cannot be thought of as pinned by an unchanged crystal; the vortices themselves will qualitatively deform the crystalline condensate in their vicinity.

The second microphysical quantity that is required is the shear modulus of the

crystal. After all, if vortices are well-pinned but the crystalline condensate can easily deform under shear stress, the vortices will be able to move regardless of the pinning force. Glitches occur if vortices are pinned and immobile while the spinning pulsar's angular velocity slows over years, with the glitch being triggered by the catastrophic unpinning and motion of long-immobile vortices. In order to immobilize vortices, and hence make glitches a possibility, both the pinning force and the shear modulus must be sufficient. The shear modulus can be related to the coefficients in the low energy effective theory that describes the phonon modes of the crystal [36, 101, 102]. This effective theory was analyzed, with its coefficients calculated, for the two-flavor crystalline color superconductor with face-centered cubic symmetry [102]. Extending this analysis to three-flavor crystalline color superconducting phases with the 2Cube45z and CubeX crystal structures is the subject matter of Chapter 4.

Chapter 3

Testing the Ginzburg Landau approximation in three flavor superconductivity

3.1 Overview

It is an open challenge to analyze the crystalline color superconducting phases that may arise in cold dense, but not asymptotically dense, three-flavor quark matter. At present the only approximation within which it seems possible to compare the free energies of the myriad possible crystal structures is the Ginzburg-Landau approximation, a calculation we discussed in detail in Chapter 2. In this chapter, we test this approximation on a particularly simple "crystal" structure in which there are only two condensates $\langle us \rangle \sim \Delta \exp(i\mathbf{q_2} \cdot \mathbf{r})$ and $\langle ud \rangle \sim \Delta \exp(i\mathbf{q_3} \cdot \mathbf{r})$ whose position-space dependence is that of two plane waves with wave vectors $\mathbf{q_2}$ and $\mathbf{q_3}$ at arbitrary angles. For this case, we are able to solve the mean-field gap equation without making a Ginzburg-Landau approximation. We find that the Ginzburg-Landau approximation works in the $\Delta \to 0$ limit as expected, find that it correctly predicts that Δ decreases with increasing angle between $\mathbf{q_2}$ and $\mathbf{q_3}$ meaning that the phase with $\mathbf{q_2} \parallel \mathbf{q_3}$ has the lowest free energy, and find that the Ginzburg-Landau approximation is conservative

in the sense that it underestimates Δ at all values of the angle between $\mathbf{q_2}$ and $\mathbf{q_3}$.

3.2 Outline

This chapter is organized as follows. In Section 3.3 we shall describe the one parameter family of three-flavor crystalline color superconductors that we analyze. In Section 3.4 we review the main results of our Ginzburg-Landau analysis that we carried out in Chapter 2 for these simple, three flavor "crystalline" condensates. In Section 3.5, we recast the High Density Effective Theory slightly, as needed for our purposes, and redo our analysis without the Ginzburg-Landau approximation. In Section 3.6 we show the numerical results of our analyses, make comparisons, and draw conclusions.

3.3 Model and Ansatz

The Lagrangian density describing the system of free quarks is given by

$$\mathcal{L}_0 = \bar{\psi}_{i\alpha} \left(i \partial\!\!\!/ {}^{\alpha\beta}_{ij} + \mu^{\alpha\beta}_{ij} \gamma_0 \right) \psi_{\beta j} \, . \tag{3.1}$$

We argued that for neutral crystalline color superconducting quark matter in the Ginzburg-Landau limit, the matrix μ takes the form,

$$\mu = \delta^{\alpha\beta} \otimes \mathrm{diag}\left(\mu_u, \mu_d, \mu_s\right) \, , \tag{3.2}$$

with, μ_u, μ_d and μ_s given by Eq. (2.4), with $\delta\mu_2 = \delta\mu_3 = M_s^2/(8\mu)$, and $\delta\mu_1 = (\mu_d - \mu_s)/2 = M_s^2/(4\mu) = 2\delta\mu$.

We will consider a condensate of the form,

$$\langle \psi_{\alpha i}(x) C\gamma_5 \psi_{\beta j}(x) \rangle \propto \sum_{I=1}^{3} \Delta_I \, e^{-2i\mathbf{q_I}\cdot\mathbf{r}} \epsilon_{I\alpha\beta} \epsilon_{Iij} \, , \tag{3.3}$$

where $\mathbf{q_1}$, $\mathbf{q_2}$ and $\mathbf{q_3}$ are the wave vectors and Δ_1, Δ_2 and Δ_3 are the gap parameters, describing pairing between the (d,s), (u,s) and (u,d) quarks respectively. The

condensate (3.3), first analyzed in Ref. [44], is the natural generalization of the condensate we discussed in Eq. (1.18) in Chapter 1, to the three-flavor setting, and the natural generalization of the CFL condensate (obtained by setting $\mathbf{q_1} = \mathbf{q_2} = \mathbf{q_3} = \mathbf{0}$) to the crystalline color superconductor setting.

As we argued in Chapter 1, we shall make the simplifying assumption that $\Delta_1 = 0$. Given that $\delta\mu_1$ is twice $\delta\mu_2$ or $\delta\mu_3$, it seems reasonable that $\Delta_1 \ll \Delta_2, \Delta_3$. We leave a quantitative investigation of the size of Δ_1 to future work, however. With Δ_1 set to zero, the symmetry of the problem is such that we expect and find solutions with $\Delta_2 = \Delta_3 \equiv \Delta$.

It should be noted, however, that these simplifications are rigorous only in the Ginzburg-Landau limit in which $\Delta \ll \delta\mu$. A full investigation of cases in which $\Delta \sim \delta\mu$ requires investigating the Ginzburg-Landau results $\mu_3 = \mu_8 = 0$, $\mu_e = M_s^2/(4\mu)$, $\Delta_1 = 0$, and $\Delta_2 = \Delta_3 = \Delta$ anew, as beyond the Ginzburg-Landau approximation these are all assumptions, not results. We will not pursue such a complete investigation here. However, we will be able to calculate the free energy of phases with condensate (3.3) without making an expansion in Δ that we used when we looked at the problem in Chapter 2 in Section 2.7.2. This will allow us to check how controlled the Ginzburg-Landau expansion is for condensates of form (3.3).

We will work in an NJL model in which the quarks interact via a point-like four fermion interaction, analyzed at the mean field level. Taking the condensate to have the form given in Eq. (3.3) with $\Delta_1 = 0$ the NJL interaction term can be written in mean field theory simply as

$$\mathcal{L}_\Delta = \sum_{I=2}^{3} \Delta_I^* \, e^{i2\mathbf{q}_\mathbf{I}\cdot\mathbf{r}} \, \epsilon_{I\alpha\beta}\, \epsilon_{Iij} \psi_{i\alpha}\, C\gamma_5\, \psi_{\beta j} \;+\; h.c.\,. \tag{3.4}$$

Note that since the direction of one of the two wave vectors is arbitrary, the quantities that have to be determined by minimizing the free-energy are Δ, the magnitude of the two wave vectors, and the angle ϕ between $\hat{\mathbf{q}}_\mathbf{2}$ and $\hat{\mathbf{q}}_\mathbf{3}$. As we discussed in Chapters 1 and 2 the magnitude of the wave vectors is given in the Ginzburg-Landau approximation by $|\mathbf{q_2}| = |\mathbf{q_3}| = \eta\delta\mu$ with $\eta = 1.1997$ as in the two-flavor model.

However, the angle ϕ between the wave vectors is a degree of freedom present here that has no analogue in the two-flavor model with condensate Eq. (1.18) in Chapter 1. Within the Ginzburg-Landau approximation we found the most favorable value of ϕ to be zero in Section 2.7.2. We check this result in Section 3.5.

We also saw in Section 2.7.2 that, $\Delta \to 0$ at $\delta\mu \to 0.754\Delta_{2SC}$, corresponding to $M_s^2/\mu = 6.032\Delta_{2SC}$. In the vicinity of this second order phase transition, the Ginzburg-Landau approximation is controlled, as in the two-flavor single planewave condensate we discussed in Section 1.5.1. Therefore, in Section 3.4 we will calculate the Ginzburg-Landau free energy only upto Δ^4.

3.4 Ginzburg-Landau analysis:a summary

The free energy of the crystalline color superconducting phase can be written as

$$\Omega = \frac{2\mu^2}{\pi^2}\left[\alpha(\Delta_2^2+\Delta_3^2)+\frac{\beta}{2}(\Delta_2^4+\Delta_3^4)+\frac{\beta_{23}}{2}\Delta_2^2\Delta_3^2\right]+\mathcal{O}(\Delta^6)\,, \tag{3.5}$$

where we have dropped the absolute value signs as henceforth we will assume that the $U(1)$ symmetries are broken such as to give real Δ's. The coefficients in the Ginzburg-Landau expansion (3.5) are given by the expressions

$$\begin{aligned}
\alpha &= \left(-1+\frac{\delta\mu}{2q}\ln\left|\frac{\delta\mu+q}{\delta\mu-q}\right|+\frac{1}{2}\ln\left|\frac{4(\delta\mu^2-q^2)}{\Delta_{2SC}^2}\right|\right)\,,\\
\beta &= \frac{1}{8}\Re e\int\frac{d\hat{\mathbf{p}}}{4\pi}\frac{-1}{(i\epsilon-\hat{\mathbf{p}}\cdot\mathbf{q}+\delta\mu)^2}=\frac{1}{\delta\mu^2}\frac{1}{4(\eta^2-1)}\,,\\
\beta_{23} &= \frac{1}{8}\Re e\int\frac{d\hat{\mathbf{p}}}{4\pi}\frac{-1}{(i\epsilon-\hat{\mathbf{p}}\cdot\mathbf{q}_2-\delta\mu)(i\epsilon-\hat{\mathbf{p}}\cdot\mathbf{q}_3+\delta\mu)}\,,\\
&= \frac{1}{\delta\mu^2}\bar{J}_{32}(\phi)
\end{aligned} \tag{3.6}$$

where $q \equiv |\mathbf{q}|$ and $\bar{J}_{32}$ is given in Eq. 2.50 and plotted as a function of ϕ in Figure 2-3.

We saw in Section 2.7.2, β is positive (and independent of ϕ) and β_{23} is positive for all ϕ. Hence there is a second order phase transition from unpaired quark matter to a phase with nonzero Δ_2 and Δ_3 at the largest value of $\delta\mu$ for which $\alpha = 0$ for

some value of q, irrespective of the value of ϕ. For larger $\delta\mu$, $\alpha > 0$ for all q and the unpaired phase is stable. The transition occurs at $\delta\mu = 0.754\Delta_{2SC}$, where modes with $q = \eta\delta\mu$ for $\eta = 1.1997$ become unstable to condensation, and Δ_2 and Δ_3 become nonzero. At lower values of $\delta\mu$, modes in a band of q have $\alpha < 0$ making them unstable, but the mode with $q = \eta\delta\mu$ is the one with the most negative α and we therefore assume that the condensate involves only the modes with $q_2 = q_3 = \eta\delta\mu$.

We now look for minima of the free energy with $\Delta_2 = \Delta_3 = \Delta$, where the free energy can then be written as

$$\Omega = \frac{2\mu^2}{\pi^2}\left[2\alpha\Delta^2 + \frac{1}{2}(2\beta + \beta_{23})\Delta^4\right] . \tag{3.7}$$

For values of $\delta\mu$ where α is negative, the solution is found at

$$\Delta^2 = \frac{2|\alpha|}{2\beta + \beta_{23}} \tag{3.8}$$

with

$$\Omega = -\frac{2\mu^2}{\pi^2}\frac{2\alpha^2}{(2\beta + \beta_{23})} . \tag{3.9}$$

The best choice of ϕ is the one that minimizes Ω, meaning the choice with the smallest β_{23}. From Fig. 2-3 we see that this corresponds to $\phi = 0$, with $\mathbf{q}_2 \parallel \mathbf{q}_3$. We shall provide plots of Δ and Ω versus M_s^2/μ for various values of ϕ in Section 3.6, where we shall compare these results to results obtained without making the Ginzburg-Landau approximation.

The free energy (3.5) can also be used to analyze the free energy of a two-flavor crystalline phase with a single-plane wave "crystal structure" in three flavor quark matter. Setting $\Delta_2 = 0$ and $\Delta_3 = \Delta$ (or equivalently setting $\Delta_3 = 0$ and $\Delta_2 = \Delta$) we find a solution with $\Delta^2 = |\alpha|/\beta$ and $\Omega = -\mu^2\alpha^2/(\pi^2\beta)$. Like the solution with $\Delta_2 = \Delta_3$, this solution is neutral in the Ginzburg-Landau limit. But as shown in the appendix, the solution with $\Delta_2 = \Delta_3$ is electrically neutral even if we relax the Ginzburg-Landau limit. When we make a comparison with the calculation done

without the Ginzburg-Landau expansion, we will restrict our attention to the the solution with $\Delta_2 = \Delta_3$. But ignoring this result for now, we explore for what values of ϕ the $\Delta_2 = \Delta_3$ solution has a lower free energy than that with $\Delta_2 = 0$. From (3.9) we see this happens of $(2\beta + \beta_{23}) < 4\beta$, meaning $\beta_{23} < 2\beta$. One can generalize to other solutions, and rule them out, by writing (Δ_2, Δ_3) as $\sqrt{2}(\Delta_r \sin\theta, \Delta_r \cos\theta)$ and then rewriting Eq. (3.5) as

$$\Omega = \frac{2\mu^2}{\pi^2}\left[2\alpha(\delta\mu)\Delta_r^2 + \frac{2}{\delta\mu^2}\bar{\beta}\Delta_r^4 + \frac{\Delta_r^4}{2\delta\mu^2}(\bar{\beta}_{32} - 2\bar{\beta})\sin^2 2\theta\right] \tag{3.10}$$

As long as $\alpha < 0$, there is a minimum with $\theta = \pi/4$ (namely $\Delta_2 = \Delta_3$) if $\beta_{23} < 2\beta$ and minima at $\theta = 0$ and $\theta = \pi/2$ if $\beta_{23} > 2\beta$. From Eqs. (2.50) and (3.6) we see that $\beta_{23} < 2\beta$ if $\bar{J}(\phi) < 1.138$, and from Fig. 2-3 we see that this occurs for $\phi < 2.485$ radians, or $\phi < 142.4°$.

The divergence of β_{23} at $\phi = \pi$ can be understood qualitatively. We see in Fig. 1-6 that there are two pairing rings on the up quark Fermi surface, because some up quarks pair with down quarks forming Cooper pairs with wave vector $2\mathbf{q_3}$ and other up quarks pair with strange quarks forming Cooper pairs with wave vector $2\mathbf{q_2}$. However, as shown in the right panel of Fig. 1-6, if $\phi = \pi$ the two pairing rings on the up quark Fermi surface are close to coincident. In the weak-coupling limit in which $\delta\mu/\mu \to 0$ (and $\Delta_{2SC} \to 0$ with $\delta\mu/\Delta_{2SC}$ fixed) these two rings become precisely coincident. We attribute the divergence in β_{23}, which indicates that antiparallel wave vectors pay an infinite free energy price and hence are forbidden, to the coincidence of these two pairing rings. Loosely speaking, it is as if these up quarks do not know whether to pair with their putative strange or down partners and so do neither. In contrast, if $\phi = 0$ as in the left panel of the Figure, the two pairing rings on the up Fermi surface are as far apart as they can be, and β_{23} and the free energy of the state are minimized. This qualitative understanding also highlights that it is only in the strict Ginzburg-Landau and weak coupling limits that the cost of choosing antiparallel wave vectors diverges. If $\Delta/\delta\mu$ is small but nonzero, the pairing regions are ribbons on the Fermi surfaces instead of lines. And, if $\delta\mu/\mu$ is small but not taken to zero (as of course is

the case in Fig. 1-6) then the two ribbons on the up Fermi surface will have slightly different diameter, as the Figure indicates. This means that we expect that if we do a calculation at small but nonzero $\Delta_{2SC} \sim \delta\mu$, and do not make a Ginzburg-Landau expansion, we should find some free energetic penalty for choosing $\phi = \pi$, but not a divergent one. We shall set up this calculation in Section 3.5 and see this expectation confirmed in Section 3.6.

3.5 NJL analysis without Ginzburg-Landau approximation

The two-flavor crystalline color superconducting phase with a single plane-wave "crystal" structure (1.18) has been analyzed in a variety of ways without making a Ginzburg-Landau approximation, going back to the work of Fulde and Ferrell [90]. In the QCD context, it was analyzed using a variational method in Ref. [34], using a diagrammatic method employing a modification of the Nambu-Gorkov formalism in Refs. [35, 38], and using the Nambu-Gorkov formalism simplified via the High Density Effective Theory in Ref. [36].

In the conventional Nambu-Gorkov formalism as applied to ordinary BCS pairing, one defines an eight-component Nambu-Gorkov spinor

$$\Psi(\mathbf{p}) = \begin{pmatrix} \psi(\mathbf{p}) \\ \bar{\psi}^T(-\mathbf{p}) \end{pmatrix} , \tag{3.11}$$

such that in this basis the pairing between fermions with momentum $\mathbf{p}$ and $-\mathbf{p}$ is described by an off-diagonal term in the fermion propagator. The condensate (1.18), however, describes pairing between u quarks with momentum $\mathbf{p}+\mathbf{q}$ and d quarks with momentum $-\mathbf{p}+\mathbf{q}$. This could be described via a propagator with terms in it that are off-diagonal in *momentum* space, rather than merely off-diagonal in "Nambu-Gorkov space". However, it is *much* easier to change to a basis in which the Nambu-Gorkov

spinor is written as [35]

$$\Psi(\mathbf{p}) = \begin{pmatrix} \psi_u(\mathbf{p}+\mathbf{q}) \\ \psi_d(\mathbf{p}-\mathbf{q}) \\ \bar{\psi}_u^T(-\mathbf{p}-\mathbf{q}) \\ \bar{\psi}_d^T(-\mathbf{p}+\mathbf{q}) \end{pmatrix} . \tag{3.12}$$

The pair condensate is then described by terms in the fermion propagator that are off-diagonal in Nambu-Gorkov space, occurring in the ψ_u-$\bar{\psi}_d^T$ and ψ_d-$\bar{\psi}_u^T$ entries. In this basis the fermions that pair have $\mathbf{p}$ and $-\mathbf{p}$, making the propagator diagonal in $\mathbf{p}$-space and the calculation tractable. One must always keep in mind that it is $\mathbf{p}+\mathbf{q}$ and $-\mathbf{p}+\mathbf{q}$ that are the momenta of the fermions that pair, not $\mathbf{p}$ and $-\mathbf{p}$. The variable $\mathbf{p}$ is an integration variable: in the gap equation or in the expression for the free energy, integrating over $\mathbf{p}$ sums the contributions of all the fermions although of course it turns out that only those lying near ribbons on the Fermi surfaces contribute significantly. Since $\mathbf{p}$ *is* an integration variable, we are free to change variables, for example rewriting the Nambu-Gorkov spinor as

$$\Psi(\mathbf{p}) = \begin{pmatrix} \psi_u(\mathbf{p}) \\ \psi_d(\mathbf{p}-2\mathbf{q}) \\ \bar{\psi}_u^T(-\mathbf{p}) \\ \bar{\psi}_d^T(-\mathbf{p}+2\mathbf{q}) \end{pmatrix} . \tag{3.13}$$

The form of the Nambu-Gorkov spinor (3.13) immediately suggests that we analyze our three-flavor crystalline phase with condensate (3.3) with Δ_1 set to zero by introducing the Nambu-Gorkov spinor

$$\Psi(\mathbf{p}) = \begin{pmatrix} \psi_u(\mathbf{p}) \\ \psi_d(\mathbf{p}-2\mathbf{q}_3) \\ \psi_s(\mathbf{p}-2\mathbf{q}_2) \\ \bar{\psi}_u^T(-\mathbf{p}) \\ \bar{\psi}_d^T(-\mathbf{p}+2\mathbf{q}_3) \\ \bar{\psi}_s^T(-\mathbf{p}+2\mathbf{q}_2) \end{pmatrix} . \tag{3.14}$$

Furthermore, it also indicates that it will not be possible to use this method of calculation if Δ_1 were kept nonzero, except for the special case in which $\mathbf{q}_1 = \mathbf{q}_2 - \mathbf{q}_3$. (That is, except in this special case which is far from sufficiently generic, it will not be possible to choose a Nambu-Gorkov basis such that one obtains a propagator that is diagonal in some momentum variable $\mathbf{p}$.) It is thus fortunate that, as explained in Section 3.3, it is reasonable on physical grounds to begin with $\Delta_1 = 0$, as we do throughout this paper. Finally, it seems unlikely that this method can be employed to analyze more complicated crystal structures analogous to the face-centered cubic structure that is favored in the two-flavor case [39]. Investigating such possibilities is feasible in the Ginzburg-Landau approximation, but the condensate that we are analyzing, with $\Delta_1 = 0$ and Δ_2 and Δ_3 each multiplying a single plane wave, is the most complex example that we currently know how to analyze without making the Ginzburg-Landau approximation.

We now implement the calculation in the basis (3.14) using the High Density Effective Theory formalism of Refs. [36, 100], valid in the weak-coupling limit in which $\Delta_{2\mathrm{SC}} \ll \mu$. We Fourier decompose the fermionic fields in the following nonstandard fashion:

$$\psi_{i\alpha}(x) = e^{-i\mathbf{k_i}\cdot\mathbf{x}} \int \frac{d\mathbf{n}}{4\pi} e^{-i\mu\mathbf{n}\cdot\mathbf{x}} \left(\psi_{i\alpha,\mathbf{n}}(x) + \psi^{-}_{i\alpha,\mathbf{n}}(x)\right) , \tag{3.15}$$

where $\mathbf{n}$ is a unit three-vector whose direction is integrated over, where $\mathbf{k_i}$ are three fixed vectors, one for each flavor, that we shall specify momentarily and where $\psi_{i\alpha,\mathbf{n}}(x)$ (resp. $\psi^{-}_{i\alpha,\mathbf{n}}(x)$) are positive (resp. negative) energy projections of the fermionic fields with flavor i and color α, as defined in Refs. [36, 100]. In the usual HDET approximation [100], the vectors $\mathbf{k}_i$ are zero and the field $\psi_{i\alpha,\mathbf{n}}(x)$ is used to describe quarks in a patch in momentum space in the vicinity of momentum $\mathbf{p} = \mu\mathbf{n}$. The introduction of the shift vectors means that now $\psi_{i\alpha,\mathbf{n}}(x)$ describes quarks with momenta in a patch in the vicinity of momentum $\mu\mathbf{n} + \mathbf{k}_i$, with $\mathbf{k}_i$ different for different flavors.

To reproduce (3.14), then, it appears that we should choose

$$\begin{aligned} \mathbf{k}_u &= 0 \\ \mathbf{k}_d &= 2\mathbf{q}_3 \\ \mathbf{k}_s &= 2\mathbf{q}_2 \,. \end{aligned} \tag{3.16}$$

We shall see this choice emerge in a different way below.

Substituting the expression (3.15) in Eqs. (2.1) and (3.4) and neglecting the contribution of antiparticles, the full Lagrangian reads

$$\begin{aligned} \mathcal{L} = \int \frac{d\mathbf{n}}{4\pi} \Bigg[& \psi^{\dagger}_{\mathbf{n},i\alpha} \left(iV \cdot \partial^{\alpha\beta}_{ij} + \delta\mu_i(\mathbf{n}) \delta^{\alpha\beta}\delta_{ij} \right) \psi_{\mathbf{n},\beta j} \\ & + \Big(\sum_{I=2}^{3} \Delta_I e^{i2\mathbf{q}_\mathbf{I}\cdot\mathbf{r}} \, \epsilon_{I\alpha\beta} \, \epsilon_{Iij} \psi_{\mathbf{n},i\alpha} \, C\gamma_5 \, \psi_{-\mathbf{n},\beta j} e^{-i(\mathbf{k}_\mathbf{i}+\mathbf{k}_\mathbf{j})\cdot\mathbf{r}} + h.c. \Big) \Bigg] , \end{aligned} \tag{3.17}$$

where $\delta\mu_i(\mathbf{n}) = P_i^F - \mu - \mathbf{k_i}\cdot\mathbf{n}$ and where the four vectors V^ν and $\bar{V}^\nu$ (the latter used only below) are defined by $V^\nu = (1, \mathbf{n})$ and $\bar{V}^\nu = (1, -\mathbf{n})$. We now see that we can get rid of the space dependence in the gap term by choosing the shift vectors $\mathbf{k_i}$ so that they satisfy

$$\begin{aligned} \mathbf{k_u} + \mathbf{k_d} &= 2\mathbf{q}_3 \\ \mathbf{k_u} + \mathbf{k_s} &= 2\mathbf{q}_2 \,. \end{aligned} \tag{3.18}$$

Because the $\mathbf{k}$'s were introduced arbitrarily in the decomposition (3.15), the calculation could in principle be done with any choice of $\mathbf{k}$'s. However, eliminating the space dependence in the gap term is an enormous simplification, equivalent to yielding a propagator that is diagonal in momentum space, and is what makes the calculation tractable. So, we shall always choose $\mathbf{k}$'s satisfying (3.18). According to (3.18), if we choose $\mathbf{k}_u = 0$, we recover (3.16). However, $\mathbf{k}_u$ can be chosen arbitrarily as long as $\mathbf{k}_d$ and $\mathbf{k}_s$ are then chosen to satisfy (3.18). This means that the choices of $\mathbf{k}$'s that get rid of the space dependence in the gap term are given by any combination related

to (3.16) by adding any vector to $\mathbf{k}_u$ and subtracting the same vector from $\mathbf{k}_d$ and $\mathbf{k}_s$. The geometric interpretation of two examples of choices of $\mathbf{k}$'s is described in Fig, 3-1. As this figure illustrates, the freedom to shift $\mathbf{k}_u$ while keeping $\mathbf{k}_u + \mathbf{k}_d$ and $\mathbf{k}_u + \mathbf{k}_s$ fixed corresponds to the freedom to shift integration variable, for example as we did in going from (3.12) to (3.13). In obtaining the results that we shall plot in Section V, we shall use the choice (3.16); however, we have checked numerically that different choices of $\mathbf{k}_u$ with $\mathbf{k}_d$ and $\mathbf{k}_s$ satisfying (3.18) yield the same results for the gap parameter and free energy. As Fig. 3-2 below indicates, these different choices yield quite different intermediate stages to the calculation so the fact that we find the expected agreement between them is a nontrivial check of our numerics.

We can now employ the Nambu-Gorkov basis defined in detail in Ref. [71] given by

$$\chi_A = \frac{1}{\sqrt{2}} \begin{pmatrix} \psi_{\mathbf{n}} \\ C\,\psi^*_{-\mathbf{n}} \end{pmatrix}_A , \tag{3.19}$$

where $A = 1 \ldots 9$ is a color-flavor index running over the nine quarks (three colors; three flavors) and where the $\psi_{\mathbf{n}}$ fields are defined via (3.15) with shift vectors chosen as in Eq. (3.16). In this basis, the full Lagrangian can be written in the compact form

$$\mathcal{L} = \sum_{\mathbf{n}} \chi^\dagger_A \; S^{-1}_{A,B}(\mathbf{n}) \; \chi_B \,, \tag{3.20}$$

with

$$S^{-1}_{A,B} = \begin{pmatrix} (V \cdot \ell + \delta\mu_A(\mathbf{n}))\,\delta_{AB} & -\Delta_{AB} \\ -\Delta_{AB} & (\bar{V} \cdot \ell - \delta\mu_A(-\mathbf{n}))\delta_{AB} \end{pmatrix} , \tag{3.21}$$

where $\ell_\nu = (\ell_0, \ell_\parallel \mathbf{n})$ is a four-vector. Here, $\ell_\parallel$ is the "radial" momentum component of ψ, parallel to $\mathbf{n}$. In HDET, the momentum of a fermion is written as $(\mu + \ell_\parallel)\mathbf{n}$, with the integration over momentum space separated into an angular integration over $\mathbf{n}$ and a radial integration over $-\delta < \ell_\parallel < \delta$. Here, the cutoff δ must be smaller than μ but must be much larger than Δ_{2SC}, $\delta\mu$ and Δ. In the results we plot in Section V, we shall take $\mu = 500$ MeV, $\delta = 300$ MeV and $\Delta_{2SC} = 25$ MeV.

From the Lagrangian (3.20), following a derivation analogous to that in Ref. [63],

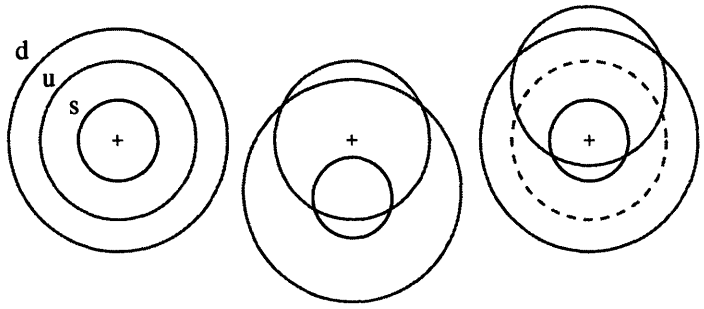

Figure 3-1: Sketches showing how different choices of the shift vectors $\mathbf{k_i}$ can be interpreted. The left panel shows unshifted d, u and s Fermi surfaces, in the absence of pairing. As in Fig. 1-6, we have exaggerated the magnitude of $\delta\mu/\mu$ for illustrative purposes. Now, suppose we have a condensate with $\mathbf{q_2} = \mathbf{q_3} \equiv \mathbf{q}$, with $\mathbf{q}$ a vector pointing upwards. In order to describe the $(\psi_{\mathbf{n},d}, \psi_{-\mathbf{n},u})$ and $(\psi_{\mathbf{n},s}, \psi_{-\mathbf{n},u})$ pairing, we shift the u, d and s Fermi surfaces by $-\mathbf{k}_u$, $-\mathbf{k}_d$ and $-\mathbf{k}_s$ respectively (since $\psi_{\mathbf{n},i}$ describes quarks in the vicinity of $\mu\mathbf{n} + \mathbf{k}_i$) and then reflect (i.e. take $\mathbf{n} \to -\mathbf{n}$) the u Fermi surface. The middle panel shows the outcome if we follow this procedure with shift vectors given by (3.16). The u Fermi surface is left unshifted (meaning its inversion is invisible in the Figure), and the d and s Fermi surfaces are shifted downwards by $2\mathbf{q}$. In the right panel, we instead choose $\mathbf{k}_u = 2\mathbf{q}$, which according to (3.18) then requires $\mathbf{k}_d = \mathbf{k}_s = 0$. The d and s Fermi surfaces are unshifted. The u Fermi surface has been shifted downwards by $2\mathbf{q}$ and then inverted, making it look as if it was shifted upwards. The location of the rings on the Fermi surfaces where pairing occurs are determined by the places where the circles cross. In both middle and right panels, the pairing rings on the d and s Fermi surface occur at their intersections with the u Fermi surfaces whereas the pairing rings on the u Fermi surface are antipodal to where these intersections appear in the Figure, since the u Fermi surface was inverted in constructing the Figure. Thus, both the right and middle panels of this figure correspond to the pairing sketched in the left panel of Fig. 1-6. The same calculation can be done by integrating over the momentum variable of either the middle or right panel; the difference between panels is just a change of integration variable. The origins of the momentum variables are indicated by the + in each panel. Note that if we had instead chosen to describe the $(\psi_{\mathbf{n},u}, \psi_{-\mathbf{n},d})$ and $(\psi_{\mathbf{n},u}, \psi_{-\mathbf{n},s})$ pairing, both the middle and right panels would look inverted relative to those given but this difference also corresponds to a change of integration variable, in this case $\mathbf{n} \leftrightarrow -\mathbf{n}$.

the thermodynamic potential per unit volume can be evaluated to be

$$\begin{aligned}\Omega &= -\frac{\mu^2}{4\pi^2}\sum_{a=1,18}\int_{-\delta}^{+\delta} d\ell_\parallel \int \frac{d\mathbf{n}}{4\pi}\,|E_a(\mathbf{n},\ell_\parallel)| \\ &\quad +\frac{2\Delta^2}{G}-\frac{\mu_e^4}{12\pi^2}\end{aligned} \tag{3.22}$$

where we have set $\Delta_2 = \Delta_3 = \Delta$ and where G is a coupling constant chosen in such a way that $\Delta_{2SC} = 25$ MeV in the CFL phase found at $\mu = 500$ MeV with $M_s = 0$. In this expression, the E_a are the energies of the quasiparticles in this phase. They are given by the 18 roots of $\det S^{-1} = 0$, seen as an equation for ℓ_0, with S^{-1} the Nambu-Gorkov inverse propagator given in (3.21). The quasiparticle energies are functions of $\ell_\parallel$ and $\mathbf{n}$, and also depend on the gap parameter Δ and the wave vectors $\mathbf{k_i}$. The doubling of degrees of freedom in the Nambu-Gorkov formalism means that the 18 roots come in pairs whose energies are related by $E_a(\mathbf{n},\ell_\parallel) = E_b(-\mathbf{n},\ell_\parallel)$. One set of nine roots describes $(\psi_{\mathbf{n},d},\psi_{-\mathbf{n},u})$ and $(\psi_{\mathbf{n},s},\psi_{-\mathbf{n},u})$ pairing, while the other set describes $(\psi_{\mathbf{n},u},\psi_{-\mathbf{n},d})$ and $(\psi_{\mathbf{n},u},\psi_{-\mathbf{n},s})$ pairing. Since $\mathbf{n}$ is integrated over, the free energy can be evaluated by doing the sum in (3.22) over either set of nine roots, instead of over all 18, and multiplying the sum by two.

In order to determine the lowest free energy state, we need to minimize the free energy Ω given in Eq. (3.22) with respect to the gap parameter Δ and with respect to ϕ, the angle between $\hat{\mathbf{q}}_2$ and $\hat{\mathbf{q}}_3$. One could also simultaneously minimize with respect to μ_e, μ_3 and μ_8. And, one could allow $\Delta_2 \neq \Delta_3$ and minimize with respect to the two gap parameters separately. However, in the results that we shall present in the next section we shall fix $\Delta_2 = \Delta_3 = \Delta$, $\mu_e = M_s^2/(4\mu)$ and $\mu_3 = \mu_8 = 0$, as is correct for small Δ and as we have done in the Ginzburg-Landau analysis of Section 3.4.

Before turning to comparing results obtained from the calculation presented in this section to those obtained with the Ginzburg-Landau approximation developed in Section 3.4, we close this section by calculating explicitly how the free energy Ω of Eq. (3.22) manifests the qualitative features described in Chapter 1 and sketched in Fig. 1-6, with pairing occurring along ribbons of the Fermi surfaces. The easiest way

to find the regions of momentum space in which pairing is important is to analyze the gap equation, obtained by varying Ω with respect to Δ. This takes the form

$$\Delta \propto \int_{-\delta}^{+\delta} d\ell_{\|} \int d\mathbf{n}\, f(\mathbf{n}, \ell_{\|}) \tag{3.23}$$

with

$$f(\mathbf{n}, \ell_{\|}) = \sum_{a=1}^{9} \frac{\partial E_a}{\partial \Delta} \mathrm{Sign}(E_a) \ . \tag{3.24}$$

(Either set of nine quasiparticle energies could be chosen, but to make the comparison with Fig. 3-1 we have used those describing $(\psi_{\mathbf{n},d}, \psi_{-\mathbf{n},u})$ and $(\psi_{\mathbf{n},s}, \psi_{-\mathbf{n},u})$ pairing.) In Fig. 3-2, we plot f, the integrand in the gap equation, as a function of $\ell_{\|}$ and $\cos\theta$ where θ is the polar angle specified by $\mathbf{n}$. (A plot of the integrand in the expression for Ω in Eq. (3.22) evaluated with Δ minus that evaluated with $\Delta = 0$ yields a very similar figure.) We have plotted $f(\cos\theta, \ell_{\|})$ for two different choices of the shift vectors $\mathbf{k}_i$, corresponding to the middle and right panels in Fig. 3-1. The differences between the two panels of Fig. 3-2 come entirely from the different choices of shift vectors; both panels correspond to the same condensate, with $\mathbf{q_2} \parallel \mathbf{q_3}$ as in the left panel of Fig. 1-6. And, we find excellent agreement when we integrate f depicted in either the left or the right panel of Fig. 3-2 to obtain the right-hand side of the gap equation (3.23), and similar agreement when we do the integral in Eq. (3.22) needed to evaluate the free energy Ω with either choice of shift vectors.

In both panels of Fig. 3-2, the bright white pairing regions near where the shifted and unshifted Fermi surfaces cross are clearly visible, as are the jet black blocking regions near the north and south poles of the Fermi surfaces at $\cos\theta = \pm 1$ where no pairing occurs. The pairing regions are centered at $\theta = 67.1°/2$ and $\theta = 180° - 67.1°/2$, corresponding to $\cos\theta = \pm 0.833$. The dark but not black regions between Fermi surfaces are places where either u-d or u-s pairing is blocked, but the other is allowed. Note that even though the formal pairing regions (regions where $f \neq 0$) extend far from the Fermi surfaces, the bright white regions where the maximal value of f is

attained are localized near where Fermi surfaces cross. So far, all as expected.

Even with a rather small value of Δ — in Fig. 3-2 $\Delta/\delta\mu = 0.056$ — the ribbons on the Fermi surfaces where pairing occurs do not look very narrow. In fact, if we increase Δ to the point at which $\Delta/\delta\mu = 0.19$, keeping all other parameters as in Fig. 3-2, the blocking regions at the north and south poles visible in Fig. 3-2 disappear entirely. The pairing "ribbons" become so wide that the ribbon centered at $\theta = 67.1°$ expands to encompass $\theta = 0$, becoming more of a hat for the Fermi surface than a ribbon on it. Furthermore, even in Fig. 3-2 where the pairing ribbons on the Fermi surfaces are somewhat narrow, in that there *are* blocking regions at the poles, these blocking regions are surrounded by regions of momentum space where pairing is quite significant. Just a little distance in $\ell_\parallel$ away from the Fermi surfaces, the angular extent of the regions where pairing is significant grows rapidly, becoming much wider than right at the Fermi surfaces themselves. These are all indications that even though the Ginzburg-Landau approximation is formally controlled by the parameter $\Delta/\delta\mu$, it may break down quantitatively at rather small values of $\Delta/\delta\mu$. After all, in the Ginzburg-Landau limit $\Delta/\delta\mu \to 0$ the pairing is dominated by infinitesimally narrow ribbons exactly where the shifted Fermi surfaces cross. Using this as a basis for approximation cannot yield even a qualitative description of the physics once $\Delta/\delta\mu \sim 0.2$, as even with this small a value of $\Delta/\delta\mu$ the regions where pairing is significant are no longer confined to narrow ribbons but have spread over considerable regions of the Fermi surfaces. Indeed, the extent of the bright white regions where pairing is significant in Fig. 3-2, in which $\Delta/\delta\mu = 0.056$, indicates that the Ginzburg-Landau approximation may cease to be quantitatively reliable at values of $\Delta/\delta\mu$ below 0.2.

3.6 Comparisons and conclusions

In Fig. 3-3 we compare our results for the gap parameter and the free energy in the crystalline color superconducting phase calculated in the Ginzburg-Landau approximation of Section 3.4 with those obtained without making this approximation

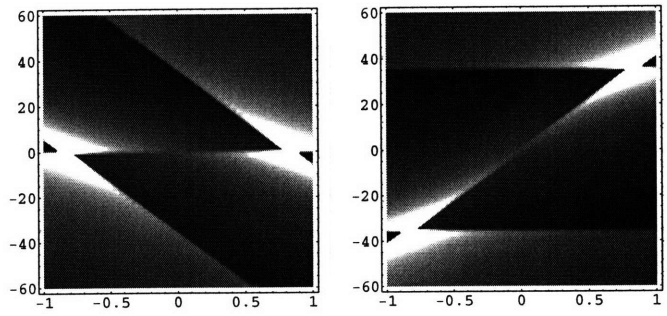

Figure 3-2: Gap equation integrand f, defined in Eq. (3.24), as a function of momentum. In each panel, the horizontal axis is $\cos\theta$ where θ is the polar angle specified by $\mathbf{n}$, the vertical axis is $\ell_\parallel$ in MeV, and the grey scale indicates the value of f: black corresponds to $f = 0$ and white to the largest values of f. In both panels, $\mu = 500$ MeV and $\delta\mu = 17.7$ MeV, which is $0.707\Delta_{2SC}$ for $\Delta_{2SC} = 25$ MeV, the interaction strength that we shall use in the next section. In both panels, $\mathbf{q}_2 = \mathbf{q}_3 \equiv \mathbf{q}$ with $q = 1.20\,\delta\mu = 21.2$ MeV and $\mathbf{q}$ pointing in the z-direction. And, in both panels $\Delta = 1$ MeV. In the left panel, $\mathbf{k}_u = 0$ and $\mathbf{k}_d = \mathbf{k}_s = 2\mathbf{q}$ as in the middle panel of Fig. 3-1. The unshifted u Fermi surface is centered in momentum space, meaning that it appears in the left panel as a horizontal line at $\ell_\parallel = 0$. The shifted d and s Fermi surfaces appear as diagonal lines, with the shifted d Fermi surface inside the u Fermi surface at the north pole ($\cos\theta = 1$) and the shifted s Fermi surface outside the u Fermi surface at the south pole. In the right panel, $\mathbf{k}_u = 2\mathbf{q}$ and $\mathbf{k}_d = \mathbf{k}_s = 0$ as in the right panel of Fig. 3-1. The unshifted d and s Fermi surfaces are centered in momentum space, meaning that they appear in the right panel as horizontal lines at $\ell_\parallel = \pm 2\delta\mu$. (Note that $\ell_\parallel$ is measured relative to where the unshifted u-Fermi surface would have been, shown as a dashed circle in the right panel of Fig. 3-1 that corresponds to $\ell_\parallel = 0$ in the right panel here.) The shifted u Fermi surface appears in the right panel here as a diagonal line, outside the d Fermi surface at the north pole and inside the s Fermi surface at the south pole. Pairing is most important in the bright white regions, centered where the shifted Fermi surfaces cross. The sketches provided in Fig. 1-6 and particularly in Fig. 3-1 serve to help visualize the "momentum-space geometry" and pairing regions depicted in the present figure.

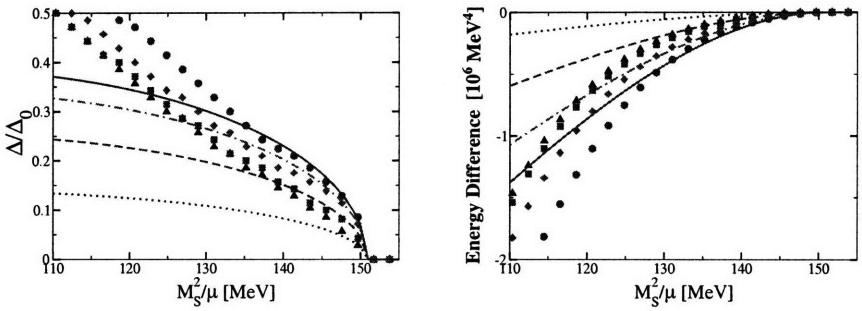

Figure 3-3: Plot of Δ/Δ_{2SC} (left panel) and of the free energy relative to neutral non interacting quark matter (right panel) as a function of M_s^2/μ for four values of the angle ϕ between $\mathbf{q_2}$ and $\mathbf{q_3}$. The various lines correspond to the calculations done in the Ginzburg-Landau approximation described in Section 3.4 whereas dots correspond to the NJL calculation of Section 3.5, done without making a Ginzburg-Landau approximation. The full lines (green online) and circles correspond to $\phi = 0$, the dashed-dotted lines (magenta online) and diamonds correspond to $\phi = 2\pi/3$, the dashed lines (red online) and squares correspond to $\phi = 7\pi/8$, the dotted lines (blue online) and triangles correspond to $\phi = 31\pi/32$.

in Section 3.5. We have done the calculations with $\mu = 500$ MeV and a coupling strength chosen so that Δ_{2SC}, the BCS gap in the CFL phase at $M_s = 0$, is 25 MeV. We vary M_s, but plot quantities versus M_s^2/μ because the most important effect of nonzero M_s is the splitting between the d, u and s Fermi momenta given in Eq. (2.4), controlled by $\delta\mu = M_s^2/(8\mu)$. We analyze the condensate (3.3) with $\Delta_2 = \Delta_3 \equiv \Delta$ and $q_2 = q_3 \equiv q$. At each value of M_s^2/μ, we choose $q = \eta\delta\mu = \eta M_s^2/(8\mu)$, where $\eta = 1.1997$. We fix $\mu_3 = \mu_8 = 0$ and $\mu_e = M_s^2/(4\mu)$, as appropriate for neutral three-flavor crystalline quark matter with $\Delta/\delta\mu \ll 1$, for which the Ginzburg-Landau approximation is valid. We leave investigating the extent to which these chemical potentials may shift at larger Δ to future work. We show our results for four values of the angle between $\mathbf{q_2}$ and $\mathbf{q_3}$: $\phi = 0$, $2\pi/3$, $7\pi/8$ and $31\pi/32$. The lines correspond to the Ginzburg-Landau analysis of Section 3.4, where we have plotted Δ and Ω of Eqs. (3.8) and (3.9), with the Gonzburg-Landau coefficients defined as in Eqs. (3.6) and (2-3) The points correspond to the NJL calculation of Section 3.5, where we have minimized Ω of Eq. (3.22) with respect to Δ.

We see in Fig. 3-3 that the NJL calculation has a second order transition at $M_s^2/\mu \sim 151$ MeV, corresponding to $\delta\mu \sim 0.754\Delta_{2SC}$, for all values of the angle ϕ. This result is in agreement with the Ginzburg-Landau calculation, in which the location of the phase transition depends only on α, which is independent of ϕ. We then see that near the phase transition, where Δ/Δ_{2SC} and hence $\Delta/\delta\mu$ are small, we find good agreement between the NJL calculation and the Ginzburg-Landau approximation, as expected. For all values of ϕ, as Δ/Δ_{2SC} increases as M_s^2/μ is decreased farther from the transition, we see that both Δ and $|\Omega|$ increase more rapidly with decreasing M_s^2/μ than predicted by the Ginzburg-Landau calculation. When the Ginzburg-Landau approximation breaks down, it does so conservatively, underpredicting both Δ and $|\Omega|$ for the entire one parameter family of "crystal structures" parameterized by ϕ. (This behavior also occurs in the two-flavor model with condensate (1.18) [39].) Furthermore, even where the Ginzburg-Landau approximation has broken down quantitatively, it correctly predicts the qualitative feature that at all values of M_s^2/μ the most favorable crystal structure is that with $\phi = 0$. As we saw in

the discussion of Fig. 1-6, this can be attributed at least qualitatively to the fact that for $\mathbf{q}_2 \parallel \mathbf{q}_3$ the two pairing ribbons on the u-Fermi surface are farthest apart. We see that the Ginzburg-Landau approximation is useful as a qualitative guide even where it has broken down quantitatively.

It is evident from Fig. 3-3 that the extent of the regime in which the Ginzburg-Landau approximation is quantitatively reliable is strongly ϕ-dependent. In the best case, which it turns out is $\phi = 0$, the results of the Ginzburg-Landau calculation are in good agreement with those of the full NJL calculation as long as $\Delta/\Delta_{2SC} \lesssim 0.25$, corresponding to $\Delta/\delta\mu \lesssim 0.35$. On the one hand, this looks like a somewhat small value of $\Delta/\delta\mu$. However, it is remarkable that the Ginzburg-Landau approximation works so well for this *large* a value of $\Delta/\delta\mu$: after all, we saw in the discussion of Fig. 3-2 in Section IV that for $\phi = 0$ even with $\Delta/\delta\mu$ only 0.19 the pairing "ribbons" that characterize the Ginzburg-Landau approximation have broadened into "pairing hats" encompassing the north and south poles of the Fermi surfaces. For larger ϕ, the Ginzburg-Landau approximation yields quantitatively reliable results only for much smaller Δ. For example, with $\phi = 31\pi/32$ we have zoomed in on the region near the second order phase transition and seen that the Ginzburg-Landau calculation does give results in quantitative agreement with the full NJL calculation, but only for $\Delta/\Delta_{2SC} \lesssim 0.04$, corresponding to $\Delta/\delta\mu \lesssim 0.05$. Why does the regime of quantitative validity of the Ginzburg-Landau approximation shrink with increasing ϕ? An explanation was suggested in Section 2.7.2, where we said that as $\phi \to \pi$, γ_{23} that appears in the sextic coefficient rises to infinity much faster than β_{23}, that appears in the quadratic coefficient. This suggests that the radius of convergence of the expansion in Δ shrinks as ϕ gets closer to π.

Thinking about the implication of this study for the more complex three flavor condensates we studied in Chapter 2 in the Ginzburg-Landau approximation, the results can be seen as either a glass half empty or a glass half full. On the one hand, we find that the approximation is quantitatively reliable only for values of $\Delta/\delta\mu$ that are small and for some crystal structures (those with $\mathbf{q}_2$ and $\mathbf{q}_3$ close to antiparallel) very small. This means that the more robust crystal structures with large gaps and

condensation energies, in particular for CubeX and 2Cube45z may not be described reliably within the Ginzburg-Landau approximation. On the other hand, we find that even when it breaks down quantitatively the Ginzburg-Landau approximation remains useful as a qualitative guide, correctly predicting that the favored "crystal" structure among our one parameter family of possibilities is that with $\mathbf{q}_2 \parallel \mathbf{q}_3$. In particular it is reassuring that, atleast for these simple condensates, one of the main rule of thumb we followed to winnow possible three flavor crystalline structures is true beyond the Ginzburg-Landau approximation. The sructures are more favorable the farther apart vectors in $\{\mathbf{q}_2\}$ are from the antipodes of $\{\mathbf{q}_3\}$. Finally, in all the cases where we have been able to test it, when the Ginzburg-Landau approximation breaks down it does so conservatively, underpredicting the magnitude of Δ and the favorability of the free energy.

To establish, using theoretical techniques, the existence of a window of densities where the crystalline color superconducting phase is the ground state of matter requires a calculation of the free energy of these complicated structures without making the Ginzburg-Landau approximation. An alternative possibility is to make a connection with observations of neutron stars, which can then test the existence of these phases in neutron star cores. One such application will form the center of our discussion in the next chapter.

Chapter 4

The rigidity of crystalline color superconducting quark matter

4.1 Overview

In this chapter we calculate the shear modulus of crystalline color superconducting quark matter, showing that this phase of dense, but not asymptotically dense, three-flavor quark matter responds to shear stress like a very rigid solid. To evaluate the shear modulus, we derive the low energy effective Lagrangian that describes the phonons that originate from the spontaneous breaking of translation invariance by the spatial modulation of the gap parameter Δ. These massless bosons describe space- and time-dependent fluctuations of the crystal structure and are analogous to the phonons in ordinary crystals. The coefficients of the spatial derivative terms of the phonon effective Lagrangian are related to the elastic moduli of the crystal; the coefficients that encode the linear response of the crystal to a shearing stress define the shear modulus. We analyze the two particular crystal structures which are energetically favored over a wide range of densities, in each case evaluating the phonon effective action and the shear modulus up to order Δ^2 in a Ginzburg-Landau expansion, finding shear moduli which are 20 to 1000 times larger than those of neutron star crusts. The crystalline color superconducting phase has long been known to be a superfluid — by picking a phase its order parameter breaks the quark-number

$U(1)_B$ symmetry spontaneously. Our results demonstrate that this superfluid phase of matter is at the same time a rigid solid. We close with a rough estimate of the pinning force on the rotational vortices which would be formed embedded within this rigid superfluid upon rotation. Our results raise the possibility that (some) pulsar glitches could originate within a quark matter core deep within a neutron star.

4.2 Outline

This chapter is organized as follows. For continuity we will rewrite the Lagrangian describing the quarks, in Section 4.3. We will also look back the CubeX and 2Cube45z condensates, which form the background crystal structures whose oscillations are the phonons. This will give us a chance write them in a coordinate system which turns out to be more convenient for the calculation than the one used in Chapter 2. In Section 4.4, we shall introduce in the Lagrangian, small displacements of a general diquark condensate which breaks translational symmetries. We will write a general expression for the effective action describing these displacement fields, by integrating out the fermions in the system. The final result for the phonon effective action is given in Eq. (4.66). We relate the coefficients of the terms in the effective action involving the spatial derivatives of the displacement fields to the shear modulus in Subsection 4.5.1 and then evaluate these coefficients for the CubeX and 2Cube45z crystals in Subsections 4.5.3 and 4.5.4 respectively. We end with a discussion of our results and their consequences in Section 4.6 .

We have moved two relevant consistency checks to the Appendices to maintain continuity. In Appendix C we show explicitly that the displacement fields are massless to all orders in the gap parameter, as they must be by Goldstone's theorem. In Appendix D we evaluate the effective action for a simple "crystalline" structure involving just two flavors of quarks and pairing with only a single wave vector $\mathbf{q}$. In this case, the calculation can be done without making an expansion in the gap parameter, Δ. We find that the results in the limit of small Δ are consistent with the Ginzburg-Landau calculation.

4.3 Setup

Here we quickly review aspects of three-flavor crystalline superconductivity that will be useful for our calculation below.

4.3.1 Lagrangian for three-flavor quark matter

The Lagrangian density describing the system of quarks is given by

$$\mathcal{L}_0 = \bar{\psi}_{i\alpha}\left(i\partial\!\!\!/^{\alpha\beta}_{ij} + \mu^{\alpha\beta}_{ij}\gamma_0\right)\psi_{\beta j} - \frac{3}{8}G\big(\bar{\psi}_{i\alpha}T^A_{\alpha\beta}\gamma^\nu\psi_{i\beta}\big)\big(\bar{\psi}_{j\gamma}T^A_{\gamma\delta}\gamma_\nu\psi_{j\delta}\big)\ , \tag{4.1}$$

where $\partial^{\alpha\beta}_{ij} = \partial\delta^{\alpha\beta}\delta_{ij}$ and the first term is the free part of the Lagrangian. The second term, proportional to G, is the NJL interaction term.

We argued in Chapters 1 and 2 that for crystalline color superconducting phases in the Ginzburg-Landau limit, μ simplifies to

$$\mu = \delta^{\alpha\beta} \otimes \mathrm{diag}\,(\mu_u, \mu_d, \mu_s)\ , \tag{4.2}$$

with,

$$\mu_d = \mu_u + 2\delta\mu_3, \quad \mu_u = p_F^u, \quad \mu_s = \mu_u - 2\delta\mu_2\ , \tag{4.3}$$

where μ_2 and μ_3 are given by,

$$\delta\mu_3 = \delta\mu_2 = \frac{M_s^2}{8\mu} \equiv \delta\mu\ . \tag{4.4}$$

In subsequent sections, we shall also often use the notation $\mu\!\!\!/_i \equiv \mu_i\gamma_0$, with $i = 1, 2, 3$ corresponding to u, d, s respectively.

Finally we remind the reader that μ_2 and μ_3 are equal only upto the leading order in M_s^2/μ^2 and differ by terms of order M_s^4/μ^3. We will use this fact in Appendix C.

4.3.2 The crystalline condensate

We consider condensates of form,

$$\langle \psi_{i\alpha}(x) C\gamma_5 \psi_{j\beta}(x) \rangle \propto \sum_{I=1}^{3} \sum_{\mathbf{q}_I^a \in \{\mathbf{q}_I\}} \Delta_I e^{2i\mathbf{q}_I^a \cdot \mathbf{r}} \epsilon_{I\alpha\beta} \epsilon_{Iij} \,. \tag{4.5}$$

As we discussed in Chapter 2, we will take $\Delta_1 = 0$ in our calculations. Making this and the Ginzburg-Landau approximations, we found two condensates in Chapter 2, CubeX and 2Cube45z, which have a smaller free energy than the gCFL phase, the CFL phase and unpaired quark matter, over a wide range of parameters. We describe these condensates in the next section.

4.3.3 The CubeX and 2Cube45z structures

The CubeX crystal structure is specified by two sets of unit vectors, $\{\hat{\mathbf{q}}_2\}$ and $\{\hat{\mathbf{q}}_3\}$ depicted in the left panel of Fig. 4-1. Taken together, the two sets of vectors point towards the eight vertices of a cube. The four vectors in $\{\hat{\mathbf{q}}_2\}$ all lie in a plane and point towards the vertices of a diagonal rectangle of the cube, while the four vectors $\{\hat{\mathbf{q}}_3\}$ form the complementary rectangle. We will use a coordinate system such that $\{\hat{\mathbf{q}}_2\}$ is given by $\{(1/\sqrt{3})(\pm\sqrt{2}, 0, \pm 1)\}$ (the four combinations of $\pm$ giving the four vectors in $\{\hat{\mathbf{q}}_2\}$) and $\{\hat{\mathbf{q}}_3\}$ is given by $\{(1/\sqrt{3})(0, \pm\sqrt{2}, \pm 1)\}$.

The 2Cube45z crystal structure is specified by two sets of unit vectors, $\{\hat{\mathbf{q}}_2\}$ and $\{\hat{\mathbf{q}}_3\}$ depicted in the right panel of Fig. 4-1. The two sets $\{\hat{\mathbf{q}}_2\}$ and $\{\hat{\mathbf{q}}_3\}$ *each* contains eight vectors that point towards the vertices of a cube. The cubes specified by $\{\hat{\mathbf{q}}_2\}$ and $\{\hat{\mathbf{q}}_3\}$ are rotated relative to each other by an angle 45° about one of their C_4 symmetry axis, passing through their common center. We will orient the coordinate axes such that $\{\hat{\mathbf{q}}_2\}$ is given by $\{(1/\sqrt{3})(\pm 1, \pm 1, \pm 1)\}$ and $\{\hat{\mathbf{q}}_3\}$ by $\{(1/\sqrt{3})(\pm\sqrt{2}, 0, \pm 1)\} \cup \{(1/\sqrt{3})(0, \pm\sqrt{2}, \pm 1)\}$, which corresponds to a relative rotation by 45° about the $\hat{z}$ axis.

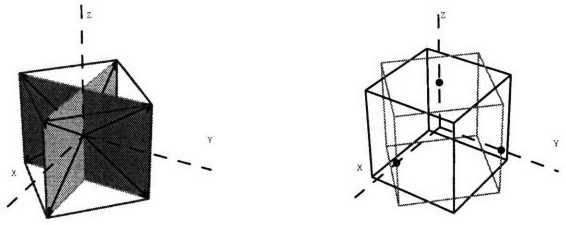

Figure 4-1: (Color online) Left panel: The momentum vectors forming the CubeX crystal structure. This structure consists of eight vectors that belong to two sets $\{\hat{\mathbf{q}}_2\}$ and $\{\hat{\mathbf{q}}_3\}$ which are shown as vectors which start from the origin. The four vectors in $\{\hat{\mathbf{q}}_2\}$ are given by $(1/\sqrt{3})(\pm\sqrt{2}, 0, \pm 1)$ and point toward the vertices of the light shaded rectangle (pink online) that lies in the $x-z$ plane. The four vectors in $\{\hat{\mathbf{q}}_3\}$ are given by $(1/\sqrt{3})(0, \pm\sqrt{2}, \pm 1)$ and point toward the vertices of the dark shaded rectangle (purple online) that lies in the $y-z$ plane. Taken together the two sets of vectors point towards the eight vertices of the light gray colored cube (only the edges are shown as light gray segments). Right panel: The end points of the vectors forming the 2Cube45z crystal structure. This structure consists of sixteen vectors that belong to two sets $\{\hat{\mathbf{q}}_2\}$ and $\{\hat{\mathbf{q}}_3\}$. The eight elements of the set $\{\hat{\mathbf{q}}_2\}$ point towards the vertices of the black cube (only the edges are shown), and are given by $(1/\sqrt{3})(\pm 1, \pm 1, \pm 1)$. The eight elements of the set $\{\hat{\mathbf{q}}_3\}$ point towards the vertices of the light gray cube, and are given by $\{(1/\sqrt{3})(\pm\sqrt{2}, 0, \pm 1)\} \cup \{(1/\sqrt{3})(0, \pm\sqrt{2}, \pm 1)\}$. The three dots denote the points where the axes meet the light gray cube, to clarify the orientation of the axes.

The lattice spacing for the face-centered cubic crystal structure is [39, 46]

$$a = \frac{\sqrt{3}\pi}{q} = \frac{4.536}{\delta\mu} = \frac{\mu}{1.764\, M_s^2} \,. \tag{4.6}$$

For example, with M_s^2/μ =100, 150, 200 MeV the lattice spacing is a =72, 48, 36 fm. The spacing between nodal planes is $a/2$.

4.4 The phonon effective action

In this Section, we present our calculation of the effective action for the phonons in crystalline color superconducting phases of quark matter. In Subection 4.4.1 we

describe the expression for the NJL interaction term in mean field theory. In Subsections 4.4.2 and 4.4.3 we introduce the phonon field and integrate the fermions out, yielding a formal expression for the phonon effective action. In Subsections 4.4.4 and 4.4.5 we introduce the Ginzburg-Landau approximation and evaluate the phonon effective action to order Δ^2.

4.4.1 NJL model in field approximation

In the mean field approximation, the interaction Lagrangian (4.1) takes on the form

$$\mathcal{L}_{\text{interaction}} = \frac{1}{2}\bar{\psi}\Delta(\mathbf{r})\bar{\psi}^T + \frac{1}{2}\psi^T\bar{\Delta}(\mathbf{r})\psi - \frac{3}{8}G\,\mathrm{tr}\big(\Gamma^T\langle\bar{\psi}^T\bar{\psi}\rangle\Gamma\big)\langle\psi\psi^T\rangle, \tag{4.7}$$

where, $\Gamma = T^a\gamma\mu$, tr represents the trace over color, flavor and Dirac indices, and where $\Delta(x)$ is related to the diquark condensate by the relations,

$$\begin{aligned}\Delta(x) &= \frac{3}{4}G\,\Gamma\langle\psi\psi^T\rangle\Gamma^T \\ \bar{\Delta}(x) &= \frac{3}{4}G\,\Gamma^T\langle\bar{\psi}^T\bar{\psi}\rangle\Gamma \\ &= \gamma^0\Delta^\dagger(x)\gamma^0\,.\end{aligned} \tag{4.8}$$

4.4.2 Introduction of the phonon field

We now consider the space- and time-dependent vibrations of the condensate, which will lead us to the effective Lagrangian for the phonon fields in the presence of a background condensate of the form (4.5). More precisely, we consider the condensate

$$\Delta(\mathbf{r}) = \Delta_{CF}(\mathbf{r}) \otimes C\gamma^5 \tag{4.9}$$

with

$$\Delta_{CF}(\mathbf{r})_{\alpha i,\beta j} = \sum_{I=1}^{3}\epsilon_{I\alpha\beta}\epsilon_{Iij}\Delta_I\sum_{\mathbf{q}_I^a}e^{2i\mathbf{q}_I^a\cdot\mathbf{r}}\,. \tag{4.10}$$

Sometimes we will write

$$\Delta_{CF}(\mathbf{r}) = \sum_{I=1}^{3} \epsilon_{I\alpha\beta}\epsilon_{Iij}\Delta_I(\mathbf{r}) \ , \tag{4.11}$$

with

$$\Delta_I(\mathbf{r}) \equiv \Delta_I \sum_{\mathbf{q}_I^a} e^{2i\mathbf{q}_I^a\cdot\mathbf{r}} \ . \tag{4.12}$$

Note that $I = 1, 2, 3$ correspond to $\langle ds\rangle$, $\langle us\rangle$ and $\langle ud\rangle$ condensates, respectively. When we evaluate the phonon effective Lagrangian for the CubeX and 2Cube45z crystals explicitly in Section 4.5, we will set $\Delta_1 = 0$ and I will then run over 2 and 3 only. The condensate (4.10) breaks translation invariance spontaneously and we therefore expect Goldstone bosons corresponding to the broken symmetries, namely phonons. Phonons are small position and time dependent displacements of the condensate and, since the three condensates in (4.11) can oscillate independently, we expect there to be three sets of displacement fields $\mathbf{u}_I(x)$. In the presence of the phonons, then,

$$\Delta_I(\mathbf{r}) \to \Delta_I^u(x) = \Delta_I(\mathbf{r} - \mathbf{u}_I(x)) \ , \tag{4.13}$$

and we will denote the corresponding quantities appearing on the left-hand sides of (4.11) and (4.9) as $\Delta_{CF}^u(x)$ and $\Delta^u(x)$ respectively, i.e.

$$\Delta_{CF}^u(x) = \sum_{I=1}^{3} \epsilon_{I\alpha\beta}\epsilon_{Iij}\Delta_I^u(x) \ , \tag{4.14}$$

and

$$\Delta^u(x) = \Delta_{CF}^u(x) \otimes C\gamma^5 \ . \tag{4.15}$$

(We apologize that we have denoted the displacement fields, and hence quantities like Δ^u, by the letter u which in other contexts, but not here, denotes up quarks.) In the mean field approximation, the full Lagrangian is quadratic in the fermion fields and can be written very simply upon introducing the two component Nambu Gorkov

spinor

$$\chi = \begin{pmatrix} \psi \\ \bar{\psi}^T \end{pmatrix} \text{ and hence } \bar{\chi} = \begin{pmatrix} \bar{\psi} & \psi^T \end{pmatrix} , \tag{4.16}$$

in terms of which

$$\mathcal{L} = \frac{1}{2}\bar{\chi}\begin{pmatrix} i\partial\!\!\!/ + \mu\!\!\!/ & \Delta^u(x) \\ \bar{\Delta}^u(x) & (i\partial\!\!\!/ - \mu\!\!\!/)^T \end{pmatrix}\chi + \frac{1}{16G}\mathrm{tr}\big((\bar{\Delta}^u)^T\Delta^u\big) . \tag{4.17}$$

The last term in Eq. (4.17) comes from the last term in Eq. (4.7), which simplifies to $(1/(16G))\mathrm{tr}((\bar{\Delta}^u)^T\Delta^u)$ for condensates given by Eqs. (4.14) and (4.15).

4.4.3 Integration over the χ fields

The spacing between vortices in the vortex array in a rotating superfluid neutron star is many microns, and we will be interested in shear stresses exerted over lengths of order or longer than this length scale. This means that we need the effective action for phonon excitations with wavelengths of this order or longer. This length scale is many many orders of magnitude longer than the microscopic length scales that characterize the crystalline phase. For example, the lattice spacing is many tens of fm. This means that we need the effective action for phonons whose wavelength can be treated as infinite and whose energy can be treated as zero, certainly many many orders of magnitude smaller than Δ.

The low energy quasiparticles in a crystalline color superconductor include the displacement fields $\mathbf{u}_I(x)$, which are massless because they are the Goldstone bosons of the broken translational symmetry. In addition, crystalline superconductors feature gapless fermionic modes, as we now explain. In the absence of pairing, quarks living at the Fermi surfaces can be excited without any cost in free energy; pairing in the crystalline phases yields gaps for quarks living in various ring-shaped bands around the Fermi surfaces, but leaves gapless fermionic modes at the boundaries of the pairing regions (loosely speaking, the remainder of the original Fermi surfaces other than the ring-shaped bands) [34, 35, 39, 46]. The low energy effective theory includes fermions

in the vicinity of the surfaces in momentum space that bound the pairing regions, in addition to the phonons that are our primary interest in this paper.

To find the low energy effective action which describes the phonons and the gapless fermionic excitations we need to integrate out those fermion fields which have an energy larger than some infrared cutoff $\Lambda_{\rm IR}$. For the application of interest to us, $\Lambda_{\rm IR}$ should be the energy of phonons with micron wavelengths. If we were interested in thermal properties, $\Lambda_{\rm IR}$ would be of order the temperature T. (Either of these energy scales is $\ll \Delta$, and by the end of this Subsection we will see that it is safe to set $\Lambda_{\rm IR} = 0$.) In order to formally implement this procedure, we define

$$\psi = \psi_> + \psi_< \quad \text{and hence,} \quad \bar{\psi} = \bar{\psi}_> + \bar{\psi}_< \,, \tag{4.18}$$

where $\psi_<$ and $\bar{\psi}_<$ contain modes with energy in $[0, \Lambda_{\rm IR}]$ and $\psi_>$ and $\bar{\psi}_>$ those with energy in $[\Lambda_{\rm IR}, \infty]$. Note that the boundary in momentum space between the $\psi_>$ and $\psi_<$ modes will be nontrivial surfaces that follow the boundaries of the pairing regions, where the gapless fermions are found. The corresponding decomposition for the Nambu Gorkov fields is,

$$\chi = \chi_> + \chi_< \quad \text{and hence} \quad \bar{\chi} = \bar{\chi}_> + \bar{\chi}_< \,, \tag{4.19}$$

where $\chi_>$, $\chi_<$, $\bar{\chi}_>$ and $\bar{\chi}_<$ are defined analogously to Eq. (4.16). Carrying out the functional integral over the $\chi_>$ and $\bar{\chi}_>$ fields will leave us with a low-energy effective action in terms of the $\mathbf{u}_I$, $\chi_<$ and $\bar{\chi}_<$ fields.

We begin with the path integral expression for the partition function,

$$Z[\mathbf{u}, \chi_<, \bar{\chi}_<] = \int \mathcal{D}[\chi_>]\mathcal{D}[\bar{\chi}_>] e^{i\int d^4x\, \mathcal{L}} \,, \tag{4.20}$$

where the action of the Lagrangian in Eq. (4.17) can be written in terms of the decomposed fields (4.19), as follows,

$$\int d^4x\, \mathcal{L} = \int d^4x \left[\frac{1}{16G} \mathrm{tr}\big((\bar{\Delta}^u)^T \Delta^u\big) + \bar{\chi}_> S^{-1} \chi_> + \bar{\chi}_< S^{-1} \chi_< \right] , \tag{4.21}$$

where the cross terms $\bar{\chi}_\rangle S^{-1}\chi_\langle$ and $\bar{\chi}_\langle S^{-1}\chi_\rangle$ do not appear because the integration over x^0 imposes energy conservation, and $\chi_\rangle$ and $\chi_\langle$ have support over different ranges of energy. The full inverse propagator, S^{-1}, in Eq. (4.21) is given by

$$S^{-1} = \begin{pmatrix} i\partial\!\!\!/ + \mu\!\!\!/ & \Delta^u(x) \\ \bar{\Delta}^u(x) & (i\partial\!\!\!/ - \mu\!\!\!/)^T \end{pmatrix} . \tag{4.22}$$

Since the Lagrangian is quadratic in the χ and $\bar{\chi}$ fields, the standard result for fermionic functional integrals gives

$$i\mathcal{S}[\mathbf{u}, \chi_\langle, \bar{\chi}_\langle] = \log(Z[\mathbf{u}, \chi_\langle, \bar{\chi}_\langle]) = i\int d^4x \left[\bar{\chi}_\langle S^{-1}\chi_\langle + \frac{1}{16G}\mathrm{tr}\big((\bar{\Delta}^u)^T\Delta^u\big)\right] + \frac{1}{2}\mathrm{Tr}_{\mathrm{ng}}\log\left(S^{-1}\right) , \tag{4.23}$$

where $\mathcal{S}[\mathbf{u}, \chi_\langle, \bar{\chi}_\langle]$ is the low energy effective action that we are after, at present still given at a rather formal level. Here, $\mathrm{Tr}_{\mathrm{ng}}$ symbolizes the trace over the Nambu-Gorkov index, the trace over color, flavor, Dirac indices and the trace over a set of functions on space-time, with energies lying in $[-\infty, -\Lambda_{\mathrm{IR}}] \cup [\Lambda_{\mathrm{IR}}, \infty]$. The factor $\frac{1}{2}$ appears before $\mathrm{Tr}_{\mathrm{ng}}$ because all the components of χ and $\bar{\chi}$ are not independent. The actual independent fields are ψ and $\bar{\psi}$. As promised, the effective action is a function of the low energy quark fields, which appear in $\bar{\chi}_\langle S^{-1}\chi_\langle$, and the phonon fields, which appear implicitly via the dependence of S^{-1} and Δ^u on $\mathbf{u}_I$.

We now concentrate on small displacements and hence drop all terms in the effective action of order $(\mathbf{u}_I)^3$ or higher. This is most simply done by looking at

$$\begin{aligned} \Delta^u_{CF}(x) &= \sum_{I=1}^{3} \epsilon_{I\alpha\beta}\epsilon_{Iij}\Delta_I \sum_{\mathbf{q}_I^a} e^{2i\mathbf{q}_I^a\cdot(\mathbf{r}-\mathbf{u}_I(x))}, \\ &= \sum_{I=1}^{3} \epsilon_{I\alpha\beta}\epsilon_{Iij}\Delta_I \sum_{\mathbf{q}_I^a} e^{2i\mathbf{q}_I^a\cdot\mathbf{r}} \left(1 - i\phi_I^a(x) - \frac{1}{2}\big(\phi_I^a(x)\big)^2\right) + \mathcal{O}\left(\phi(x)\right)^3 , \end{aligned} \tag{4.24}$$

where we have defined

$$2\mathbf{q}_I^a \cdot \mathbf{u}_I(x) = \phi_I^a(x) . \tag{4.25}$$

We will refer to both the $\mathbf{u}_I$ fields and ϕ_I^a fields as phonons, as we can write one in

terms of the other.

We now argue that as far as the calculation of the shear modulus is concerned, we can look only at the part of the effective action that describes the phonons. The remainder of the effective Lagrangian, where the low energy quark fields appear, can be written as

$$\bar{\chi}_\langle S^{-1} \chi_\langle = \mathcal{L}_f + \mathcal{L}_{f\phi} \tag{4.26}$$

with

$$\mathcal{L}_f = \bar{\chi}_\langle \begin{pmatrix} i\partial\!\!\!/ + \mu\!\!\!/ & \Delta(\mathbf{r}) \\ \bar{\Delta}(\mathbf{r}) & (i\partial\!\!\!/ - \mu\!\!\!/)^T \end{pmatrix} \chi_\langle \tag{4.27}$$

and

$$\mathcal{L}_{f\phi} = \bar{\chi}_\langle \begin{pmatrix} 0 & \Delta^u(x) - \Delta(\mathbf{r}) \\ \bar{\Delta}^u(x) - \bar{\Delta}(\mathbf{r}) & 0 \end{pmatrix} \chi_\langle \, . \tag{4.28}$$

We shall see in Section 4.5.1 that the shear modulus is related to the coefficient of

$$\frac{\partial \phi}{\partial x^u} \frac{\partial \phi}{\partial x^v} \tag{4.29}$$

in the Lagrangian, which makes it obvious that $\mathcal{L}_f$ does not contribute. The coefficient of (4.29) at the scale $\Lambda_{\rm IR}$ receives contributions from the $\chi_\rangle$ and $\bar{\chi}_\rangle$ fermions which have been integrated out. The phonons and low energy quarks (at an energy scale lower than $\Lambda_{\rm IR}$) interact via the $\mathcal{L}_{f\phi}$ term in the Lagrangian. Formally, then, one has to solve consistently for the phonon propagator and the quark propagator, which are coupled. However, the effect of the phonon-fermion interactions on the self consistent calculation of the gap parameter using $\mathcal{L}_f$ is small, because the quark loops come with an additional factor of μ^2, which is is much larger than $(\Lambda_{\rm IR})^2$, and hence the quark propagator can be considered to be unaffected by the phonons. The phonon propagator, and hence the shear modulus, will depend on the phonon-fermion interactions, meaning that the phonon propagator and consequently the coefficient of (4.29) will run as $\Lambda_{\rm IR}$ is reduced. However, as long as $\Lambda_{\rm IR}$ is much smaller than Δ, $|\mathbf{q}|$ and $\delta\mu$, the change in the value of the shear modulus from integrating out more fermions below the scale $\Lambda_{\rm IR}$ will be negligible compared to its value at $\Lambda_{\rm IR}$. This

means that we can take $\Lambda_{\rm IR} = 0$, integrating all of the fermions out from the system and obtaining an effective action for the phonons alone. This procedure is correct for the calculation of the shear modulus but would not be correct for, say, calculating the specific heat of the system, which is dominated by the gapless fermions not by the phonons. We have checked numerically that the difference between the shear modulus calculated with $\Lambda_{\rm IR} = 0$ and that with a small but nonzero $\Lambda_{\rm IR}$ is negligible.

Finally, therefore, the effective action we are interested in depends only on the phonon fields, and is given by

$$i\mathcal{S}[\mathbf{u}] = \log(Z[\mathbf{u}]) = i\int d^4x \left[\frac{1}{16G}\mathrm{tr}\big((\bar{\Delta}^u)^T\Delta^u\big)\right] + \frac{1}{2}\mathrm{Tr}_{\rm ng}\log\left(S^{-1}\right) \ , \qquad (4.30)$$

where now the $\mathrm{Tr}_{\rm ng}$ includes a trace over functions in space-time containing all energy modes.

For the single plane wave "crystal" structure in which only one of the Δ_I is nonzero and $\{\mathbf{q}_I\}$ contains only a single wave vector [90, 34], we can invert the Nambu-Gorkov inverse propagator in the absence of phonons without expanding in Δ, and can therefore obtain the effective action for the phonons up to second order in ϕ, to *all* orders in Δ. We shall do this exercise in Appendix D. For the realistic crystal structures, CubeX and 2Cube45z, however, we cannot invert the full inverse propagator and we therefore proceed by making a Ginzburg-Landau expansion in Δ.

4.4.4 Ginzburg-Landau expansion

In order to obtain the effective action for the phonon field we first separate the full inverse propagator, S^{-1}, defined in Eq. (4.22), into the free part, S_0^{-1} and a part containing the condensate, Σ, as follows: $S^{-1} = S_0^{-1} + \Sigma$, where

$$S_0^{-1} = \begin{pmatrix} i\partial\!\!\!/ + \mu\!\!\!/ & 0 \\ 0 & (i\partial\!\!\!/ - \mu\!\!\!/)^T \end{pmatrix} \qquad (4.31)$$

and

$$\Sigma = \begin{pmatrix} 0 & \Delta^u(\mathbf{r}) \\ \bar{\Delta}^u(\mathbf{r}) & 0 \end{pmatrix} . \tag{4.32}$$

Then, we can expand the term $\log(S^{-1})$ that appears on the right-hand side of Eq. (4.30) as

$$\mathrm{Tr}_{\mathrm{ng}}\big(\log(S_0^{-1}+\Sigma)\big) = \mathrm{Tr}_{\mathrm{ng}}\big(\log S_0^{-1}\big) + \mathrm{Tr}_{\mathrm{ng}}\big(S_0\Sigma\big) - \frac{1}{2}\mathrm{Tr}_{\mathrm{ng}}\big(S_0\Sigma\big)^2 + ... \tag{4.33}$$

where $\mathrm{Tr}_{\mathrm{ng}}\big(\log S_0^{-1}\big)$ is related to the free energy of unpaired (Normal) quark matter Ω_N by

$$\mathrm{Tr}_{\mathrm{ng}}\big(\log S_0^{-1}\big) = -i2\Omega_N \int d^4x = -i2VT\Omega_N \,, \tag{4.34}$$

with VT the space-time volume. Since

$$\big(S_0\Sigma\big) = \begin{pmatrix} 0 & (i\partial\!\!\!/ + \mu\gamma^0)^{-1}\Delta^u(x) \\ ((i\partial\!\!\!/ - \mu\gamma^0)^T)^{-1}\bar{\Delta}^u(x) & 0 \end{pmatrix} , \tag{4.35}$$

only even powers of $\big(S_0\Sigma\big)$ contribute to the trace over Nambu Gorkov indices and we can write,

$$\mathrm{Tr}_{\mathrm{ng}}\big(\log(S^{-1})\big) = -i2\Omega_N(VT) - \sum_{n=1}^{\infty}\frac{1}{n}\mathrm{Tr}\Big((i\partial\!\!\!/ + \mu\gamma^0)^{-1}\Delta^u(x)((i\partial\!\!\!/ - \mu\gamma^0)^T)^{-1}\bar{\Delta}^u(x)\Big)^n , \tag{4.36}$$

where, the Tr on the right hand side is over Dirac, color, flavor and space-time, and we have used the cyclic property of the trace to equate the two contributions obtained from the trace over the Nambu Gorkov index. Finally, substituting (4.36) back in (4.30) and simplifying the Dirac structure of the operators using the $C\gamma^5$ Dirac structure of the condensate and the properties of the charge conjugation matrix C, namely $C(\gamma^\mu)^T C^{-1} = -\gamma^\mu$ and $C^2 = -1$, we obtain

$$\begin{aligned} \mathcal{S}[\mathbf{u}] = &-\frac{1}{4G}\int d^4x\, \mathrm{tr}_{CF}\big((\Delta^u_{CF})^\dagger\Delta^u_{CF}\big) - \Omega_N(VT) \\ &- \frac{1}{2i}\sum_{n=1}^{\infty}\frac{1}{n}\mathrm{Tr}\Big((i\partial\!\!\!/ + \mu\gamma^0)^{-1}\Delta^u_{CF}(x)(i\partial\!\!\!/ - \mu\gamma^0)^{-1}\Delta^{u\dagger}_{CF}(x)\Big)^n , \end{aligned} \tag{4.37}$$

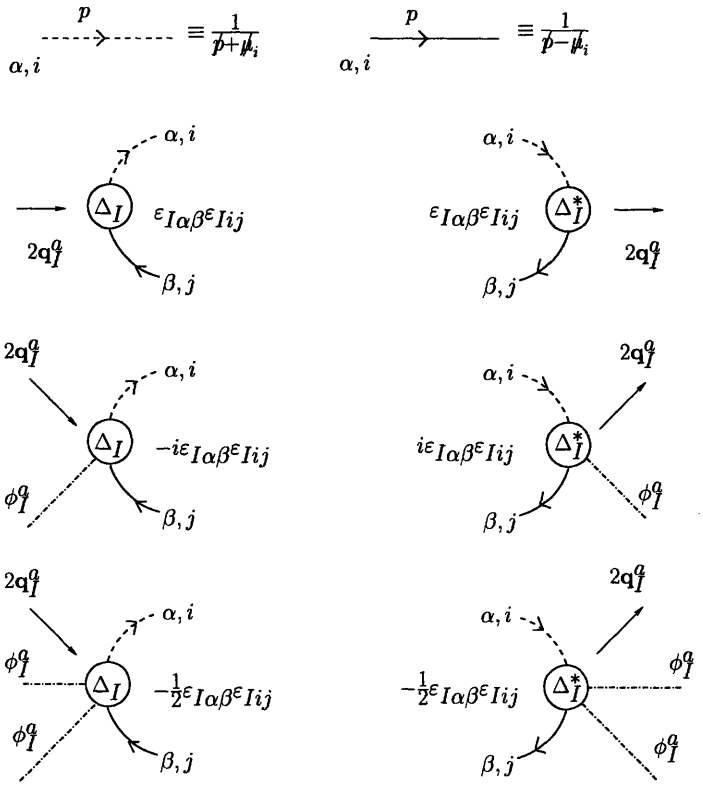

Figure 4-2: Propagators and interaction vertices for the Lagrangian up to order ϕ^2. The dashed lines represent propagating quarks, and the solid lines represent propagating quark holes. The dot-dash lines represent external phonons. The subscript on μ is the index of the flavor which is propagating, and determines the value of the chemical potential that appears in the propagator. The Δ_I vertex comes along with a momentum insertion $2\mathbf{q}_I^a$ and a vertex factor $\epsilon_{I\alpha\beta}\epsilon_{Iij}$. Similarly, Δ_I^* comes with a momentum insertion $-2\mathbf{q}_I^a$ and the same vertex factor.

where the trace tr_{CF} is over color and flavor indices and where $\Delta^{\mathbf{u}}_{CF}(x)$ depends on $\mathbf{u}_I(x)$ via Eqs. (4.24) and (4.25). Eq. (4.37) is the low energy effective action for the phonons, written as a Ginzburg-Landau expansion in Δ. We will calculate the leading contribution to $\mathcal{S}[\mathbf{u}]$, namely that proportional to Δ^2.

The first term on the right hand side of Eq. (4.37) does not have any derivatives acting on $\mathbf{u}_I$ and hence can only contribute to the mass of the phonon, which we know must be zero by Goldstone's theorem. In Appendix C, we show explicitly that the $\mathbf{u}_I$

dependence in $\int d^4x\, \mathrm{tr}_{CF}\big((\Delta^u_{CF})^\dagger \Delta^u_{CF}\big)$ cancels out, and its value is given simply by

$$\begin{aligned}\frac{1}{4G}\int d^4x\, \mathrm{tr}_{CF}\big((\Delta^u_{CF})^\dagger \Delta^u_{CF}\big) \\ = (VT)\frac{1}{G}\sum_I (\Delta_I \Delta_I^*) P_I \,,\end{aligned} \tag{4.38}$$

where P_I is the number of plane waves in $\{\mathbf{q}_I\}$.

We now proceed to evaluate the third term on the right hand side of Eq. (4.37) diagrammatically. We will expand the action $\mathcal{S}[\mathbf{u}]$ in Eq. (4.37) in powers of ϕ (or equivalently $\mathbf{u}_I$) up to second order in ϕ by using the Feynman rules described in Fig. 4-2.

The lowest order term is independent of ϕ. The sum of this term and of the term given in Eq. (4.38) has a simple interpretation. In the absence of phonons, and considering that the fermionic fields have been integrated out, the action in Eq. (4.37) turns out to be proportional to the free energy of the system. More specifically,

$$\mathcal{S}[\mathbf{u}=0] = -(VT)(\Omega_{\text{crystalline}} + \Omega_N) \,, \tag{4.39}$$

where $\Omega_{\text{crystalline}}$ is given as a Ginzburg-Landau series in Δ [46]. Since (4.39) is independent of ϕ it does not affect the equations of motion of the phonons and we will simply drop it from our calculation.

We now consider the term that is linear in ϕ. We will evaluate the leading term in the action proportional to Δ^2, which we will call $\mathcal{S}^{\phi\Delta^2}$ and which is represented diagrammatically in Fig. 4-3. Both terms shown in Fig. 4-3 are proportional to the trace of $\varepsilon_{I\alpha\beta}\varepsilon_{J\alpha\beta}\varepsilon_{Iij}\varepsilon_{Jij}$, which is nonzero only if $I = J$ and therefore only terms proportional to $\Delta_I^*\Delta_I$ are present. We could have anticipated this result from the symmetries of the problem. The Lagrangian conserves particle number for every flavor of quarks, which corresponds to symmetry under independent global phase rotations of quark fields of the three flavors, meaning independent phase rotations of the three Δ_I. The effective action should be invariant under these rotations and hence Δ_I can only occur in the combination $\Delta_I^*\Delta_I$. (Although the condensate spontaneously

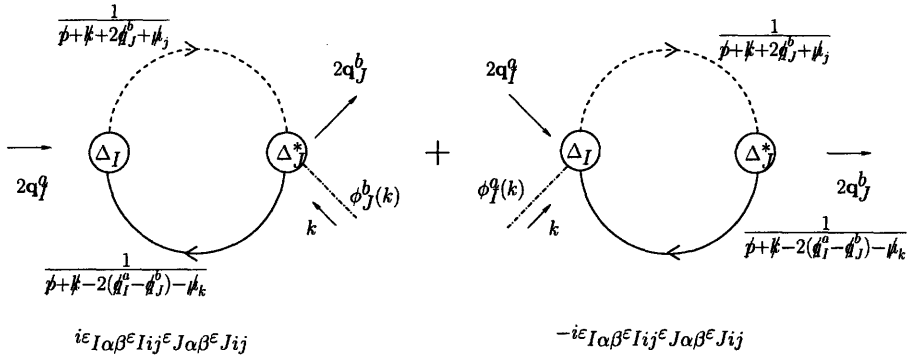

Figure 4-3: Diagrams that contribute to order $\phi\Delta^2$. The dashed lines represent propagating quarks, and the solid lines represent propagating quark holes. The interaction vertices have been defined in Fig. 4-2 and the color-flavor structure is also indicated. Note that the trace over the color-flavor epsilon tensors, $\varepsilon_{I\alpha\beta}\varepsilon_{J\alpha\beta}\varepsilon_{Iij}\varepsilon_{Iij}$ forces $I = J$ and momentum conservation implies $\mathbf{q}^a_I = \mathbf{q}^b_I$, as well as $k = 0$. The two contributions are then equal in magnitude and opposite in sign, and hence cancel.

breaks them, the requirement is that the Lagrangian has these symmetries.) Then, the sum of the diagrams in Fig. 4-3, which corresponds to the contribution to the action linear in the phonon field and second order in Δ, is given by

$$\begin{aligned}\mathcal{S}^{\phi\Delta^2} = \sum_I \Delta^*_I\Delta_I \sum_{\substack{j\neq k\\ \neq I}} \sum_{\mathbf{q}^a_I\mathbf{q}^b_I} \int \frac{d^4k}{(2\pi)^4} \int \frac{d^4p}{(2\pi)^4}(2\pi)^4\delta^{(4)}(2\mathbf{q}^a_I - 2\mathbf{q}^b_I + k) \\ \mathrm{tr}\left[\frac{\phi^a_I(k) - \phi^b_I(k)}{(\not p + 2\not q^b_I + \not k + \not\mu_j)(\not p - 2(\not q^a_I - \not q^b_I) + \not k - \not\mu_k)}\right],\end{aligned} \tag{4.40}$$

where k is the four momentum of the phonon field and the trace is over Dirac indices. The Dirac delta on the right-hand side ensures momentum conservation,

$$2\mathbf{q}^a_I - 2\mathbf{q}^b_I + k = 0\,, \tag{4.41}$$

meaning that the net momentum added to the loop is zero. But since we are looking at the low energy effective theory, we can take k much smaller than the momentum vectors $\mathbf{q}_I$ and therefore Eq. (4.41) can be satisfied only if $k = 0$ and $\mathbf{q}^a_I = \mathbf{q}^b_I$, which

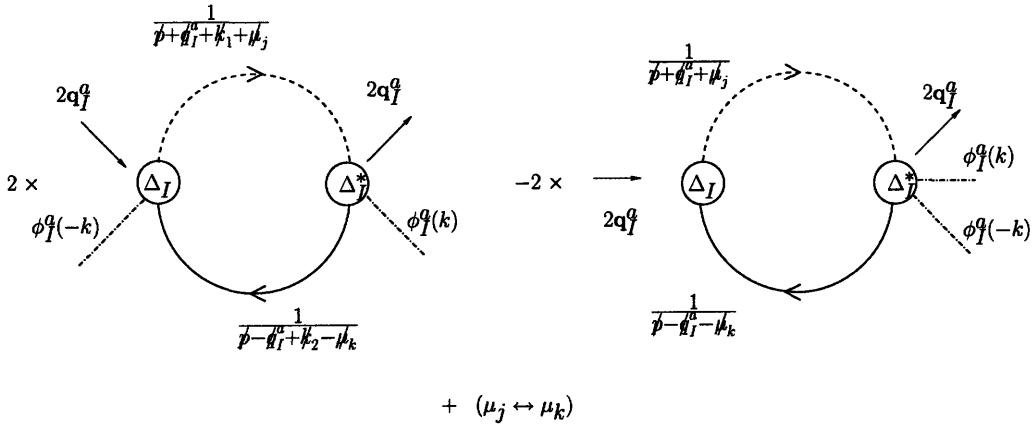

Figure 4-4: .
Diagrams that contribute to order $\phi^2\Delta^2$. In drawing the diagrams, we have used the fact that the trace of the color-flavor tensor forces $I = J$. We have also used the fact that momentum conservation requires that the net momenta added by the condensate and the phonons are separately zero. In the first diagram, momentum conservation at the Δ_I^* vertex imposes $k_2 - k_1 = k$.

means that $a = b$. Using this result, we find that (4.40) vanishes:

$$\mathcal{S}^{\phi\Delta^2} = 0\,. \tag{4.42}$$

That is, the term linear in ϕ is absent to order Δ^2. One can similarly argue that it is absent to all orders in Δ.

Now we consider the terms of order ϕ^2, which give the first nontrivial contribution to the phonon effective action. We will evaluate these terms to order Δ^2 and we will call the corresponding contribution to the action $\mathcal{S}^{\phi^2\Delta^2}$. The terms contributing to $\mathcal{S}^{\phi^2\Delta^2}$ arise from the diagrams given in Fig. 4-4, and give

$$\mathcal{S}^{\phi^2\Delta^2} = \sum_I \sum_{\mathbf{q}_I^a} \int \frac{d^4k}{(2\pi)^4} \phi_I^a(k)\phi_I^a(-k)\Delta_I^*\Delta_I \mathcal{P}_I^a(k)\,, \tag{4.43}$$

where $k = k_2 - k_1$ is the four momentum of the phonon and

$$\mathcal{P}_I^a(k) = i \sum_{\substack{j \neq k \\ \neq I}} \int \frac{d^4p}{(2\pi)^4} \mathrm{tr} \left[\frac{1}{(\not{p} + \not{q}_I^a + \not{k}_1 + \not{\mu}_j)(\not{p} - \not{q}_I^a + \not{k}_2 - \not{\mu}_k)} - \frac{1}{(\not{p} + \not{q}_I^a + \not{\mu}_j)(\not{p} - \not{q}_I^a - \not{\mu}_k)} \right], \tag{4.44}$$

where the trace is over Dirac indices. In the next Subsection we evaluate Eq. (4.44). The reader not interested in the details of our calculation will find in Eq. (4.65) the final expression for the effective action $\mathcal{S}^{\phi^2\Delta^2}$.

4.4.5 Evaluation of $\mathcal{S}^{\phi^2\Delta^2}$

We turn now to the evaluation of $\mathcal{P}_I^a(k)$ of Eq. (4.44) and hence, via (4.43), the leading nontrivial contribution to the phonon low energy effective action, $\mathcal{S}^{\phi^2\Delta^2}$.

To begin, if we set $k_1 = k_2 = 0$ in (4.44), implying that $k = 0$, we see that $\mathcal{P}_I^a(0) = 0$. In this way, we see explicitly that the phonons are massless to order Δ^2. As mentioned before, we are interested in the low energy, long wavelength phonons. We therefore expand $\mathcal{P}_I^a(k)$ in powers of k and drop terms of order k^3 and higher.

We are working in the limit in which $\delta\mu$, $q = |\mathbf{q}| = \eta\,\delta\mu$ and Δ are all much smaller than μ. ($\Delta \ll \mu$ follows from the weak coupling approximation and $\delta\mu \ll \mu$ follows from requiring $M_s^2 \ll \mu^2$. The Ginzburg-Landau approximation, which is the further requirement that $\Delta^2 \ll \delta\mu^2$, is not required in the derivation of the simplifications of Eq. (4.44) that follow.) This means that the integration measure in Eq. (4.44) can be approximated as follows:

$$i \int \frac{d^4p}{(2\pi)^4} \approx \frac{i\mu^2}{2\pi^2} \int_{-\infty}^{+\infty} \frac{dp^0}{2\pi} \int_{-\Lambda}^{\Lambda} ds \int \frac{d\hat{\mathbf{v}}}{4\pi}\,, \tag{4.45}$$

where $\hat{\mathbf{v}}$ is the unit velocity vector in the direction of the spatial momentum vector, $\hat{\mathbf{v}} = \mathbf{p}/|\mathbf{p}|$, and $\int d\hat{\mathbf{v}}$ represents the integral over solid angle covering the Fermi surface. The residual momentum s is defined by the relation $s \equiv |\mathbf{p}| - \bar{\mu}$, where $\bar{\mu}$ is an energy scale lying close to the quark Fermi surfaces. In evaluating $\mathcal{P}_I^a(k)$, we will take $\bar{\mu}$ to be

the arithmetic mean of μ_k and μ_j, for convenience, but since the two integrals on the right-hand side of Eq. (4.44) go as $\log(\Lambda)$ for large momenta, choosing any other value for $\bar{\mu}$ close to the Fermi surfaces changes the value of $\mathcal{P}_I^a(k)$ only by $\mathcal{O}(\delta\mu/\Lambda)$, which we will ignore. We introduce the two null vectors, $V^\mu = (1, \hat{\mathbf{v}})$ and $\tilde{V}^\mu = (1, -\hat{\mathbf{v}})$, as is done in the High Density Effective Theory (HDET) [100]. It is also useful to define four momenta $l^\mu \equiv (p^0, s\hat{\mathbf{v}}) = p^\mu - (0, \bar{\mu}\hat{\mathbf{v}})$, which can be thought of as residual momenta as measured from the Fermi surface. It is easy to verify that $V \cdot l = p^0 - s$ and $\tilde{V} \cdot l = p^0 + s$. In the weak coupling limit, for a generic four vector p' that is small compared to Λ, the propagators in Eq. (4.44) simplify as follows:

$$\begin{aligned}
\frac{1}{\not{p} + \not{p}' + \not{\mu}_j} &= \frac{(p^0 + (p')^0 + \mu_j)\gamma^0 - (\mathbf{p} + \mathbf{p}') \cdot \vec{\gamma}}{(p^0 + (p')^0 + \mu_j - |\mathbf{p} + \mathbf{p}'|)(p^0 + (p')^0 + \mu_j + |\mathbf{p} + \mathbf{p}'|)} \\
&\approx \frac{\bar{\mu}\gamma^0 - \mathbf{p} \cdot \vec{\gamma}}{(p^0 + (p')^0 + \bar{\mu} + (-\bar{\mu} + \mu_j) - |\mathbf{p}| - \mathbf{p}' \cdot \hat{\mathbf{v}})(2\bar{\bar{\mu}})} \\
&\approx \frac{1}{2}\left(\frac{\gamma^0 - \hat{\mathbf{v}} \cdot \vec{\gamma}}{p^0 + (p')^0 - s + (\mu_j - \bar{\mu}) - \mathbf{p}' \cdot \hat{\mathbf{v}}}\right) \\
&= \frac{1}{2}\left(\frac{V \cdot \gamma}{V \cdot (l + p') + (\mu_j - \bar{\mu})}\right)
\end{aligned} \tag{4.46}$$

and, similarly,

$$\begin{aligned}
\frac{1}{\not{p} + \not{p}' - \not{\mu}_k} &= \frac{(p^0 + (p')^0 - \mu_k)\gamma^0 - (\mathbf{p} + \mathbf{p}') \cdot \vec{\gamma}}{(p^0 + (p')^0 - \mu_k - |\mathbf{p} + \mathbf{p}'|)(p^0 + (p')^0 - \mu_k + |\mathbf{p} + \mathbf{p}'|)} \\
&\approx \frac{1}{2}\left(\frac{\gamma^0 + \hat{\mathbf{v}} \cdot \vec{\gamma}}{p^0 + (p')^0 + s - (\mu_k - \bar{\mu}) + \mathbf{p}' \cdot \hat{\mathbf{v}}}\right) \\
&= \frac{1}{2}\left(\frac{\tilde{V} \cdot \gamma}{\tilde{V} \cdot (l + p') - (\mu_k - \bar{\mu})}\right) .
\end{aligned} \tag{4.47}$$

Upon using these simplifications in Eq. (4.44), we obtain,

$$\begin{aligned}
\mathcal{P}_I^a(k) = \frac{\mu^2}{\pi^2}\Bigg[&\int_{-\infty}^{+\infty}\frac{dp^0}{2\pi i}\int_{-\Lambda}^{\Lambda} ds \int \frac{d\hat{\mathbf{v}}}{4\pi}\frac{1}{(V \cdot l - \hat{\mathbf{v}} \cdot \mathbf{q}_I^a + \delta\mu_I)(\tilde{V} \cdot l - \hat{\mathbf{v}} \cdot \mathbf{q}_I^a + \delta\mu_I)} \\
&- \int_{-\infty}^{+\infty}\frac{dp^0}{2\pi i}\int_{-\Lambda}^{\Lambda} ds \int \frac{d\hat{\mathbf{v}}}{4\pi}\frac{1}{(V \cdot (l + k_1) - \hat{\mathbf{v}} \cdot \mathbf{q}_I^a + \delta\mu_I)(\tilde{V} \cdot (l + k_2) - \hat{\mathbf{v}} \cdot \mathbf{q}_I^a + \delta\mu_I)}\Bigg] \\
&+ (\delta\mu_I \to -\delta\mu_I) .
\end{aligned} \tag{4.48}$$

By making the changes of variables $p^0 \to -p^0$, $s \to -s$, $\hat{\mathbf{v}} \to -\hat{\mathbf{v}}$ and $\delta\mu_I \to -\delta\mu_I$ it is easy to show that $\mathcal{P}_I^a(-k^0, \mathbf{k}) = \mathcal{P}_I^a(k^0, \mathbf{k})$. In addition, it is clear from Eq. (4.43) that only the part of $\mathcal{P}_I^a(k)$ that is even under $k \to -k$ contributes to $\mathcal{S}^{\phi^2\Delta^2}$. Hence, terms in the expansion of $\mathcal{P}_I^a(k)$ proportional to odd powers of k do not contribute to the effective action. Furthermore, at second order in k this implies that there cannot be terms proportional to $k_0\mathbf{k}\phi^2\Delta^2$ in the effective action. (Terms like $k_0^2\mathbf{k}^2\phi^2\Delta^2$ can of course appear, but are higher order in k.) This is useful because we can handle the spatial and time components of k independently, thereby simplifying the calculation of $\mathcal{P}_I^a(k)$.

In order to simplify the calculation we rewrite $\mathcal{P}_I^a(k)$ a little differently. Multiplying and dividing the integrand appearing in the second term in Eq. (4.48) (the integrand depending upon k_1 and k_2) by

$$\begin{aligned} &(\tilde{V}\cdot(l+k_1) - \hat{\mathbf{v}}\cdot\mathbf{q}_I^a + \delta\mu_I) \\ &\times (V\cdot(l+k_2) - \hat{\mathbf{v}}\cdot\mathbf{q}_I^a + \delta\mu_I) \end{aligned} \tag{4.49}$$

and collecting the term with numerator $\big(V\cdot k\big)\big(\tilde{V}\cdot k\big) = \big(V\cdot(k_2-k_1)\big)\big(\tilde{V}\cdot(k_2-k_1)\big)$, after some algebra we obtain

$$\begin{aligned} &\frac{2}{(V\cdot(l+k_1) - \hat{\mathbf{v}}\cdot\mathbf{q}_I^a + \delta\mu_I)(\tilde{V}\cdot(l+k_2) - \hat{\mathbf{v}}\cdot\mathbf{q}_I^a + \delta\mu_I)} \\ &\quad = -\frac{\big(V\cdot k\big)\big(\tilde{V}\cdot k\big)}{D(l+k_1)D(l+k_2)} + \frac{1}{D(l+k_1)} + \frac{1}{D(l+k_2)}\,, \end{aligned} \tag{4.50}$$

where

$$D(l) \equiv (\tilde{V}\cdot l + \delta\mu_I - \hat{\mathbf{v}}\cdot\mathbf{q}_I^a)(V\cdot l + \delta\mu_I - \hat{\mathbf{v}}\cdot\mathbf{q}_I^a)\,. \tag{4.51}$$

We can then write $\mathcal{P}_I^a(k)$ as $\mathcal{P}_I^a(k) = I_0 + I_1$ with

$$I_1 \equiv \frac{1}{2}\frac{\mu^2}{\pi^2}\int\frac{dp^0}{2\pi i}\int_{-\Lambda}^{\Lambda}ds\int\frac{d\hat{\mathbf{v}}}{4\pi}\frac{(V\cdot k)(\tilde{V}\cdot k)}{D(l+k_1)D(l+k_2)} + (\delta\mu_I \to -\delta\mu_I) \tag{4.52}$$

$$\begin{aligned} I_0 \equiv\ & \frac{\mu^2}{\pi^2}\int\frac{dp^0}{2\pi i}\int_{-\Lambda}^{\Lambda}ds\int\frac{d\hat{\mathbf{v}}}{4\pi}\frac{1}{D(l)} - \frac{1}{2}\frac{\mu^2}{\pi^2}\int\frac{dp^0}{2\pi i}\int_{-\Lambda}^{\Lambda}ds\int\frac{d\hat{\mathbf{v}}}{4\pi}\frac{1}{D(l+k_1)} \\ & -\frac{1}{2}\frac{\mu^2}{\pi^2}\int\frac{dp^0}{2\pi i}\int_{-\Lambda}^{\Lambda}ds\int\frac{d\hat{\mathbf{v}}}{4\pi}\frac{1}{D(l+k_2)} + (\delta\mu_I \to -\delta\mu_I)\,. \end{aligned} \tag{4.53}$$

The reason to separate $\mathcal{P}_I^a(k)$ as a sum of I_0 and I_1 will become clear in a moment, when we argue that $I_0 = 0$.

We now proceed to evaluate I_0 and I_1 separately. As we discussed, we can consider the spatial and the temporal parts of k independently, and we begin by taking $k = (0, \mathbf{k})$ with $\mathbf{k} = \mathbf{k}_2 - \mathbf{k}_1$. In this case I_0 can be expressed as a sum of three terms, each proportional (up to a prefactor $+\mu^2/\pi^2$ or $-\mu^2/(2\pi^2)$) to an integral of the form

$$\begin{aligned} \Pi(\mathbf{q}_I^a, \delta\mu_I, p') &= \int\frac{dp^0}{2\pi i}\int_{-\Lambda}^{\Lambda}ds\int\frac{d\hat{\mathbf{v}}}{4\pi}\frac{1}{D(l+p')} \\ &= \int\frac{dp^0}{2\pi i}\int_{-\Lambda}^{\Lambda}ds\int\frac{d\hat{\mathbf{v}}}{4\pi}\frac{1}{(p^0 - s - \hat{\mathbf{v}}\cdot\mathbf{p}' - \hat{\mathbf{v}}\cdot\mathbf{q}_I^a + \delta\mu_I)} \\ &\quad\times\frac{1}{(p^0 + s + \hat{\mathbf{v}}\cdot\mathbf{p}' - \hat{\mathbf{v}}\cdot\mathbf{q}_I^a + \delta\mu_I)}\,, \end{aligned} \tag{4.54}$$

where p' is in this case a purely spatial vector, $p' = (0, \mathbf{p}')$. This integral can be evaluated by following the steps outlined in Ref. [39]. We first perform a Wick rotation, $p^0 \to ip^4$, and then do the p^4 integration by the method of residues, followed by the ds and $d\hat{\mathbf{v}}$ integrals. For $\mathbf{p}' = 0$, the integral is calculated in Ref. [39] and is given by

$$\Pi(\mathbf{q}_I^a, \delta\mu_I, 0) = \left[-1 - \frac{1}{2}\log\left(\frac{\Lambda^2}{(\mathbf{q}_I^a)^2 - \delta\mu_I^2}\right) + \frac{\delta\mu_I}{2|\mathbf{q}_I^a|}\log\left(\frac{|\mathbf{q}_I^a| + \delta\mu_I}{|\mathbf{q}_I^a| - \delta\mu_I}\right)\right]\,. \tag{4.55}$$

By making the change of variables $s \to s - \hat{\mathbf{v}}\cdot\mathbf{p}'$ in Eq. (4.54), we see that the integrand appearing in the definition of $\Pi(\mathbf{q}_I^a, \delta\mu_I, p')$ in Eq. (4.54), can be written as the integral appearing in $\Pi(\mathbf{q}_I^a, \delta\mu_I, 0)$, but with the limits of s integration changed to $[-\Lambda - \hat{\mathbf{v}}\cdot\mathbf{p}', \Lambda - \hat{\mathbf{v}}\cdot\mathbf{p}']$. Since, Π goes as $\log(\Lambda)$, however, this change in limits changes the value of the integrand only by a quantity of order $\mathbf{k}/\Lambda$, which we ignore.

Thus,

$$I_0 = \frac{\mu^2}{\pi^2}\left[\Pi(\mathbf{q}_I^a, \delta\mu_I, 0) - \frac{1}{2}\Pi(\mathbf{q}_I^a, \delta\mu_I, 0) - \frac{1}{2}\Pi(\mathbf{q}_I^a, \delta\mu_I, 0)\right] + (\delta\mu_I \to -\delta\mu_I) = 0\,. \tag{4.56}$$

The integral I_1 can be evaluated using similar steps, namely Wick rotate $p^0 \to ip^4$, perform the p^4 integration by residues and then do the ds and $d\hat{\mathbf{v}}$ integrals. The final result is

$$I_1 = \frac{\mu^2}{\pi^2}\left[\Pi(\mathbf{q}_I^a, \delta\mu_I, 0) - \frac{1}{2}\Pi(\mathbf{q}_I^a - \frac{1}{2}\mathbf{k}, \delta\mu_I, 0) - \frac{1}{2}\Pi(\mathbf{q}_I^a + \frac{1}{2}\mathbf{k}, \delta\mu_I, 0)\right] + (\delta\mu_I \to -\delta\mu_I)\,. \tag{4.57}$$

We note that the final result depends only upon $\mathbf{k} = \mathbf{k}_2 - \mathbf{k}_1$. Expanding I_1 in $\mathbf{k}$, we find

$$\begin{aligned}\mathcal{P}_I^a(k) = &-\mathbf{k}_{||a}^2 \frac{\mu^2}{\pi^2}\left[\frac{1}{4(\mathbf{q}_I^{a2} - \delta\mu_I^2)} - \frac{1}{2(\mathbf{q}_I^a)^2}\left(1 + \frac{\delta\mu_I}{2|\mathbf{q}_I^a|}\log\left(\frac{|\mathbf{q}_I^a| - \delta\mu_I}{|\mathbf{q}_I^a| + \delta\mu_I}\right)\right)\right] \\ &- \mathbf{k}_{\perp a}^2 \frac{\mu^2}{\pi^2}\left[\frac{1}{4(\mathbf{q}_I^a)^2}\left(1 + \frac{\delta\mu_I}{2|\mathbf{q}_I^a|}\log\left(\frac{|\mathbf{q}_I^a| - \delta\mu_I}{|\mathbf{q}_I^a| + \delta\mu_I}\right)\right)\right] + \mathcal{O}(k^4)\,,\end{aligned} \tag{4.58}$$

where $\mathbf{k}_{||a}$ is the component of $\mathbf{k}$ which is parallel to $\mathbf{q}_I^a$, $\mathbf{k}_{||a} = \hat{\mathbf{q}}_I^a(\mathbf{k}\cdot\hat{\mathbf{q}}_I^a)$, and $\mathbf{k}_{\perp a}$ is the component perpendicular to $\mathbf{q}_I^a$, $\mathbf{k}_{\perp a} = \mathbf{k} - \mathbf{k}_{||a}$. In deriving Eq. (4.58) we did not assume any particular relations between $\mathbf{q}_I^a$ and $\delta\mu_I$, but now we choose the value of $|\mathbf{q}_I^a|$ given by Eq. (2.24) that minimizes the free energy. Substituting Eqs. (2.24) and (2.40) into Eq. (4.58) simplifies $\mathcal{P}_I^a(k)$ considerably, yielding

$$\mathcal{P}_I^a(k) = -\mathbf{k}_{||a}^2 \frac{\mu^2}{\pi^2}\left[\frac{1}{4\delta\mu_I^2(\eta^2 - 1)}\right] \quad \text{for } k = (0, \mathbf{k})\,, \tag{4.59}$$

where we have dropped the terms of order k^4.

The final expression for $\mathcal{P}_I^a(k)$ has the following features. First, the $\mathbf{k}_{\perp a}$ term has dropped out. This means that for a single plane wave condensate, phonons that propagate in the direction orthogonal to the plane wave that forms the condensate cost no energy up to order $(\mathbf{k}_{\perp a})^2\Delta^2\phi^2$. Second, we note that the coefficient in front of $(\mathbf{k}_{||a})^2$ is negative. This means that the crystal structure is stable with respect to small fluctuations in the direction of $\mathbf{q}_I^a$. (Recall that action goes like kinetic energy

minus potential energy; since here k is spatial, we have potential energy only meaning that decreasing the action corresponds to increasing the energy, hence stability.) This result is a direct consequence of the fact that we chose $|\mathbf{q}_I^a|$ to minimize α_I, meaning that any deviation from the most favorable modulation of the condensate in the direction of $\mathbf{q}_I^a$ increases the free energy of the system by an amount of order Δ^2.

We now evaluate I_0 and I_1 in the case where k is purely temporal, namely $k = (k^0, \mathbf{0})$ with $k^0 = k_2^0 - k_1^0$. With these k_1 and k_2, the value of I_1 turns out to be

$$\begin{aligned} I_1 = \frac{\mu^2}{\pi^2}\Bigg[& \frac{1}{2}\log\left(\frac{(\delta\mu_I - k_1^0 + (k^0/2))^2 - (\mathbf{q}_I^a)^2}{(\delta\mu_I - k_1^0)^2 - (\mathbf{q}_I^a)^2}\right) \\ & + (\delta\mu_I - k_1^0 + (k^0/2))\log\left(\frac{\delta\mu_I - k_1^0 + (k^0/2) + |\mathbf{q}_I^a|}{\delta\mu_I - k_1^0 + (k^0/2) - |\mathbf{q}_I^a|}\right) \\ & - (\delta\mu_I - k_1^0)\log\left(\frac{\delta\mu_I - k_1^0 + |\mathbf{q}_I^a|}{\delta\mu_I - k_1^0 - |\mathbf{q}_I^a|}\right) + \frac{1}{2}\log\left(\frac{(\delta\mu_I - k_2^0 - (k^0/2))^2 - (\mathbf{q}_I^a)^2}{(\delta\mu_I - k_2^0)^2 - (\mathbf{q}_I^a)^2}\right) \\ & + (\delta\mu_I - k_2^0 - (k^0/2))\log\left(\frac{\delta\mu_I - k_2^0 - (k^0/2) + |\mathbf{q}_I^a|}{\delta\mu_I - k_2^0 - (k^0/2) - |\mathbf{q}_I^a|}\right) \\ & - (\delta\mu_I - k_2^0)\log\left(\frac{\delta\mu_I - k_2^0 + |\mathbf{q}_I^a|}{\delta\mu_I - k_2^0 - |\mathbf{q}_I^a|}\right)\Bigg] + (\delta\mu_I \to -\delta\mu_I)\,. \end{aligned} \tag{4.60}$$

Although, it appears that Eq. (4.60) does not depend solely on $k_2^0 - k_1^0$, upon expanding in small k_1^0 and k_2^0, we find,

$$I_1 = (k^0)^2\frac{\mu^2}{\pi^2}\frac{1}{4((\mathbf{q}_I^a)^2 - \delta\mu_I^2)} + \mathcal{O}(k^4) \approx (k^0)^2\frac{\mu^2}{\pi^2}\frac{1}{4\delta\mu_I^2(\eta^2 - 1)}\,. \tag{4.61}$$

Turning now to I_0, this quantity is given by

$$I_0 = \frac{\mu^2}{\pi^2}\left[\Pi(\mathbf{q}_I^a, \delta\mu_I, 0) - \frac{1}{2}\Pi(\mathbf{q}_I^a, \delta\mu_I, k_1) - \frac{1}{2}\Pi(\mathbf{q}_I^a, \delta\mu_I, k_2)\right] \tag{4.62}$$

where $k_i = (k_i^0, \mathbf{0})$. When its third argument is a purely temporal four-vector, Π is

given by

$$\Pi(\mathbf{q}_I^a, \delta\mu_I, p') = \int \frac{dp^0}{2\pi i} \int_{-\Lambda}^{\Lambda} ds \int \frac{d\hat{\mathbf{v}}}{4\pi} \frac{1}{(p^0 + p'^0 - s - \hat{\mathbf{v}} \cdot \mathbf{q}_I^a + \delta\mu_I)} + \frac{1}{(p^0 + p'^0 + s - \hat{\mathbf{v}} \cdot \mathbf{q}_I^a + \delta\mu_I)} , \tag{4.63}$$

where $p' = (p'^0, \mathbf{0})$. It is apparent from Eq. (4.63) that by making the change of variables $p^0 \to p^0 + p'^0$ we obtain $\Pi(\mathbf{q}_I^a, \delta\mu_I, p'^0) = \Pi(\mathbf{q}_I^a, \delta\mu_I, 0)$, leading us to conclude from Eq. (4.62) that $I_0 = 0$. We advise the reader that in order to obtain the result $I_0 = 0$ by the approach that we have employed in a straightforward manner, it is important to shift p_0 before Wick rotating. (Note that if we calculate I_0 using dimensional regularization or by introducing a nonzero temperature and then taking the $T \to 0$ limit, we find $I_0 = 0$ in agreement with what we obtained by change of variables.) Finally, therefore, with $I_0 = 0$ we obtain

$$\mathcal{P}_I^a(k) = (k^0)^2 \frac{\mu^2}{\pi^2} \frac{1}{4\delta\mu_I^2(\eta^2 - 1)} \quad \text{for } k = (k^0, \mathbf{0}) . \tag{4.64}$$

We see that this comes with a positive sign, as is appropriate for a kinetic energy term.

Substituting the expressions given in Eqs. (4.59) and (4.64) back into the action (4.43), we obtain

$$\mathcal{S}^{\phi^2\Delta^2} = \sum_I \sum_{\mathbf{q}_I^a} \int \frac{d^4k}{(2\pi)^4} \phi_I^a(k)\phi_I^a(k) \left[k_0^2 - (\mathbf{k}_{||a})^2\right] \frac{\mu^2}{\pi^2} \frac{|\Delta_I|^2}{4\delta\mu_I^2(\eta^2 - 1)} , \tag{4.65}$$

where $\mathbf{k}_{||a} = \hat{\mathbf{q}}_I^a(\mathbf{k} \cdot \hat{\mathbf{q}}_I^a)$ and $\phi_I^a(k) = \mathbf{u}_I \cdot (2\mathbf{q}_I^a)$. Inverse Fourier transforming back to position space, and taking out a factor of half for future convenience, we obtain the effective action for the displacement fields:

$$\mathcal{S}[\mathbf{u}] = \frac{1}{2} \int d^4x \sum_I \frac{\mu^2}{\pi^2} \frac{2|\Delta_I|^2\eta^2}{(\eta^2 - 1)} \sum_{\mathbf{q}_I^a} \Big[\partial_0(\hat{\mathbf{q}}_I^a \cdot \mathbf{u}_I)\partial_0(\hat{\mathbf{q}}_I^a \cdot \mathbf{u}_I) - (\hat{\mathbf{q}}_I^a \cdot \vec{\partial})(\hat{\mathbf{q}}_I^a \cdot \mathbf{u}_I)(\hat{\mathbf{q}}_I^a \cdot \vec{\partial})(\hat{\mathbf{q}}_I^a \cdot \mathbf{u}_I)\Big] . \tag{4.66}$$

This is the low energy effective action for phonons in any crystalline color superconducting phase, valid to second order in derivatives, to second order in the gap parameters Δ_I's and to second order in the phonon fields u_I. This is the central technical result of our paper.

Because we are interested in long wavelength, small amplitude, phonon excitations, expanding to second order in derivatives and to second order in the u_I is satisfactory in every respect. Not so for the expansion to second order in the Δ_I. As we have discussed previously, the Ginzburg-Landau approximation is at the point of breaking down in the most favorable CubeX and 2Cube45z crystal structures. Before proceeding, we therefore ask what kind of corrections to (4.65) will arise at higher order in Δ. The first thing to note is that in the weak coupling limit μ appears only as an overall factor of μ^2 in front of the fermion loop integrals. After simplifying the fermionic propagators as in (4.46) and (4.47) and taking Λ to ∞, the only two independent dimensionful quantities that remain in the integrals are k and $\delta\mu_I$. (Recall that $|\mathbf{q}_I|$ is given by $\eta\delta\mu_I$ and so is not independent.) Since we found the action only up to terms which are second order in the derivatives and second order in Δ, to ensure the Lagrangian density has dimension four, only a dimensionless factor can multiply $\mu^2|\Delta_I|^2\partial^2\mathbf{u}_I^2$, as we can see is true in Eq. (4.66). Higher powers of Δ^2 will appear in Eq. (4.65) in combination with higher compensating powers of $\delta\mu^{-2}$. Consequently, there will be corrections to the coefficients of k_0^2 and $(\mathbf{k}_{\|a})^2$ in (4.65) suppressed by factors of $(\Delta^2/\delta\mu^2)$ relative to the leading order result that we have obtained. In addition, there will be new terms. There is no reason to expect that the coefficient of $(\mathbf{k}_{\perp a})^2$ will remain zero at $\mathcal{O}(\mu^2|\Delta_I|^4(\partial\mathbf{u}_I)^2/\delta\mu^2)$. Finally, we see that there are no terms in (4.65) that "mix" the different $\mathbf{u}_I(k)$. This follows from the color-flavor structure of the condensate as discussed above. At higher order, there will be terms proportional to $\mu^2|\Delta_I\Delta_J|^2\partial\mathbf{u}_I\partial\mathbf{u}_J/\delta\mu^2$, which do "mix" the different $\mathbf{u}_I$'s.

With the phonon effective action now in hand, in Section 4.5.2 we shall relate the coefficients of the terms in $\mathcal{S}(\mathbf{u})$ involving spatial derivatives acting on the displacement fields to the shear modulus of crystalline color superconducting quark matter with specified crystal structures.

4.5 Extracting the shear modulus

We see from Eq. (4.66) that the action of the phonon fields, $\mathcal{S}(\mathbf{u})$, is a sum of two terms: the kinetic energy, which has time derivatives acting on the fields $\mathbf{u}$, and the potential energy, which has spatial derivatives acting on $\mathbf{u}$. From the basic theory of elastic media [103], the potential energy is related to the elastic moduli that describe the energy cost of small deformations of the crystal. In this Section, we present this relation explicitly and calculate the shear modulus for the CubeX and 2Cube45z crystal structures.

4.5.1 Generalities

Let there be a set of displacement fields $\mathbf{u}_I$ propagating in a crystalline color superconducting material. (We will set the problem up in the general case where all the Δ_I are nonzero, meaning that I runs from 1 to 3.) The kinetic energy density for the displacement fields takes the form

$$\mathcal{K} = \frac{1}{2}\sum_{IJ}\sum_{mn}\rho_{IJ}^{mn}\,(\partial_0\mathbf{u}_I^m)(\partial_0\mathbf{u}_J^n)\,, \tag{4.67}$$

where $\mathbf{u}_I^m$, $\mathbf{u}_J^n$ are the space components of the vectors $\mathbf{u}_I$ and $\mathbf{u}_J$ respectively. (We will use the indices m, n, u and v to represent spatial indices in the following). As we are working only to order Δ^2, the only nonzero components of ρ_{IJ}^{mn} are those with $I = J$. We will choose the direction of the axes, x, y and z such that for every I and J, ρ_{IJ}^{mn} is diagonal in the m and n indices and we will denote the diagonal components of ρ_{IJ}^{mn} by ρ_I^m. We can then rewrite the kinetic energy density as

$$\mathcal{K} = \frac{1}{2}\sum_{I}\sum_{m}\rho_I^m(\partial_0\mathbf{u}_I^m)(\partial_0\mathbf{u}_I^m)\,. \tag{4.68}$$

At higher orders in Δ^2, we could need to choose a new linear combination of fields $\tilde{\mathbf{u}}_I^m = A_{IJ}^{mn}\mathbf{u}_J^n$ to render the kinetic energy diagonal in the IJ and mn indices.

The potential energy density to quadratic order in the displacement fields can be

written as

$$\mathcal{U} = \frac{1}{2} \sum_{IJ} \sum_{\substack{mn \\ uv}} \lambda_{IJ}^{munv} \frac{\partial \mathbf{u}_I^m}{\partial x^u} \frac{\partial \mathbf{u}_J^n}{\partial x^v} \,, \tag{4.69}$$

where λ_{IJ}^{munv} is the elastic modulus tensor. The components of the tensor $\partial \mathbf{u}_I^m / \partial x^n$ that are antisymmetric in the mn space indices are related to rigid rotations. The symmetric components of the tensor, namely the "strain tensor"

$$s_I^{mu} = \frac{1}{2} \Big(\frac{\partial \mathbf{u}_I^m}{\partial x^u} + \frac{\partial \mathbf{u}_I^u}{\partial x^m} \Big) \,, \tag{4.70}$$

tell us about deformations of the medium. In the previous Section we have shown that, to order Δ^2, there is no interaction between the displacement fields $\mathbf{u}_I$ and $\mathbf{u}_J$ with I different from J. Therefore λ_{IJ}^{munv} is diagonal in the I and J indices and, denoting the diagonal entries by λ_I^{munv}, we find

$$\mathcal{U} = \frac{1}{2} \sum_{I} \sum_{\substack{mn \\ uv}} \lambda_I^{munv} s_I^{mu} s_I^{nv} \,. \tag{4.71}$$

Next, we define the stress tensor acting on the crystal I as [103]

$$\sigma_I^{mu} = \frac{\partial \mathcal{U}}{\partial s_I^{mu}} \,, \tag{4.72}$$

which is symmetric in its spatial indices. For a potential $\mathcal{U}$ that is quadratic in the displacement fields and is given by (4.71), the stress tensor is

$$\sigma_I^{mu} = \lambda_I^{munv} s_I^{nv} \,. \tag{4.73}$$

The diagonal components of σ are proportional to the compression exerted on the system and are therefore related to the bulk modulus of the crystalline color superconducting quark matter. Since unpaired quark matter has a pressure $\sim \mu^4$, it gives a contribution to the bulk modulus that completely overwhelms the contribution from the condensation into a crystalline phase, which is of order $\mu^2 \Delta^2$. We shall therefore not calculate the bulk modulus. On the other hand, the response to shear stress arises

only because of the presence of the crystalline condensate.

The shear modulus can be defined as follows. Imagine exerting a static external stress σ_I having only an off-diagonal component, meaning $\sigma_I^{mu} \neq 0$ for a pair of space directions $m \neq u$, and all the other components of σ are zero. The system will respond with a strain s_I^{nv} satisfying (4.72). The shear modulus in the mu plane, ν_I^{mu}, is defined as half the ratio of the stress to the strain:

$$\nu_I^{mu} = \frac{\sigma_I^{mu}}{2s_I^{mu}} , \tag{4.74}$$

where the indices m and u are not summed. For a quadratic potential, with σ_I^{mn} given by (4.73), the shear modulus is

$$\nu_I^{mu} = \frac{\lambda_I^{munv} s_I^{nv}}{2s_I^{mu}} , \tag{4.75}$$

where n and v are summed but m and u are not. For all the crystal structures that we shall consider below, the only nonzero entries in λ^{munv} with $m \neq u$ are the λ^{mumu} entries, meaning that (4.73) simplifies even further to

$$\nu_I^{mu} = \frac{1}{2}\lambda_I^{mumu} , \tag{4.76}$$

again with m and u not summed.

Putting Eq. (4.68) and Eq. (4.71) together, the action for the displacement fields can be written as

$$\mathcal{S}[\mathbf{u}] = \int d^4x \, (\mathcal{K} - \mathcal{U}) = \frac{1}{2} \int d^4x \left(\sum_I \sum_m \rho_I^m (\partial_0 \mathbf{u}_I^m)(\partial_0 \mathbf{u}_I^m) - \sum_I \sum_{\substack{mn \\ uv}} \lambda_I^{munv} s_I^{mu} s_I^{nv} \right) . \tag{4.77}$$

The equations of motion obtained by extremizing the action $\mathcal{S}[\mathbf{u}]$ with respect to the displacement fields $\mathbf{u}$ are

$$\rho_I^m \frac{\partial^2 \mathbf{u}_I^m}{\partial t^2} = \lambda_I^{munv} \partial_u \partial_n u_I^v , \tag{4.78}$$

where I and m are not summed. The dispersion relations are found by solving

$$\mathrm{Det}\left[\rho_I^m k_0^2 \delta_{mn} - \lambda_I^{munv} k_u k_v\right] = 0 \tag{4.79}$$

for all I, where m is again not summed.

4.5.2 Elastic moduli of crystalline phases

In order to set up the extraction of the elastic moduli of crystalline phases, we need to rewrite the action (4.66) for a generic crystalline phase in a form which makes comparison to (4.77) straightforward. Writing the spatial indices in Eq. (4.66) explicitly, we obtain the low energy phonon effective action in the form

$$\begin{aligned} S[\mathbf{u}] = & \frac{1}{2}\int d^4x \sum_I \kappa_I \left[\left(\sum_{\mathbf{q}_I^a} (\hat{q}_I^a)^m (\hat{q}_I^a)^n \right) (\partial_0 \mathbf{u}_I^m)(\partial_0 \mathbf{u}_I^n) \right. \\ & \left. - \left(\sum_{\mathbf{q}_I^a} (\hat{q}_I^a)^m (\hat{q}_I^a)^u (\hat{q}_I^a)^n (\hat{q}_I^a)^v \right) (\partial_u \mathbf{u}_I^m)(\partial_v \mathbf{u}_I^n) \right] . \end{aligned} \tag{4.80}$$

where we have defined

$$\kappa_I \equiv \frac{2\mu^2 |\Delta_I|^2 \eta^2}{\pi^2(\eta^2 - 1)} . \tag{4.81}$$

For a given crystal structure, upon evaluating the sums in (4.80) and then using the definition (4.70) to compare (4.80) to (4.77), we can extract expressions for the λ tensor and thence for the shear moduli. The quantity κ is related to the elastic modulus for a condensate whose "crystal" structure is just a single plane wave, as discussed in Appendix D.

In the next two Subsections, we will calculate the shear modulus for the CubeX and 2Cube45z crystals. We will not discuss the expression for the kinetic energy density, $\mathcal{K}$, but it is easy (and necessary) to check that in each case below we have chosen our axes such that $\mathcal{K}$ only contains terms that are diagonal in the spatial indices m and n.

Note that henceforth we set $\Delta_1 = 0$ and $\Delta_2 = \Delta_3 = \Delta$, meaning that

$$\kappa_2 = \kappa_3 \equiv \kappa = \frac{2\mu^2|\Delta|^2\eta^2}{\pi^2(\eta^2-1)} \simeq 0.664\,\mu^2|\Delta^2|\,. \tag{4.82}$$

The shear moduli that we evaluate each take the form of a dimensionless constant times κ.

4.5.3 Shear modulus for the CubeX crystal

Orienting the axes as shown in the left panel of Fig. 1, we have $\{\hat{\mathbf{q}}_2\} = \{(1/\sqrt{3})(\pm\sqrt{2}, 0, \pm 1)\}$ and $\{\hat{\mathbf{q}}_3\} = \{(1/\sqrt{3})(0, \pm\sqrt{2}, \pm 1)\}$. Calculating the relevant sums and substituting in (4.80), we find that the potential energy is given by

$$\begin{aligned}\mathcal{U} =& \frac{4}{9}\kappa\Big(4(s_2^{xx})^2 + (s_2^{zz})^2\Big) + \frac{16}{9}\kappa(s_2^{xx}s_2^{zz}) + \frac{16}{9}\kappa\Big((s_2^{xz})^2 + (s_2^{zx})^2\Big) \\ &+ \frac{4}{9}\kappa\Big(4(s_3^{yy})^2 + (s_3^{zz})^2\Big) + \frac{16}{9}\kappa(s_3^{yy}s_3^{zz}) + \frac{16}{9}\kappa\Big((s_3^{yz})^2 + (s_3^{zy})^2\Big)\,.\end{aligned} \tag{4.83}$$

Recall that the only components of the stress tensor that are relevant to the calculation of the shear modulus are given by $\partial\mathcal{U}/\partial s_I^{mu}$ for $m \neq u$. These are

$$\sigma_2^{xz} = \sigma_2^{zx} = \frac{32}{9}\kappa\, s_2^{zx} \tag{4.84}$$

and

$$\sigma_3^{yz} = \sigma_3^{zy} = \frac{32}{9}\kappa\, s_3^{zy}\,, \tag{4.85}$$

from which we obtain

$$\nu_2^{xz} = \nu_2^{zx} = \frac{\sigma_3^{zx}}{2s_3^{zx}} = \frac{16}{9}\kappa \tag{4.86}$$

and

$$\nu_3^{yz} = \nu_3^{zy} = \frac{\sigma_3^{zy}}{2s_3^{zy}} = \frac{16}{9}\kappa\,. \tag{4.87}$$

We can display the result succinctly by writing two shear matrices ν_2 and ν_3, which have only off-diagonal entries and are symmetric in the spatial indices:

$$\nu_2 = \frac{16}{9}\kappa \begin{pmatrix} 0 & 0 & 1 \\ 0 & 0 & 0 \\ 1 & 0 & 0 \end{pmatrix}, \quad \nu_3 = \frac{16}{9}\kappa \begin{pmatrix} 0 & 0 & 0 \\ 0 & 0 & 1 \\ 0 & 1 & 0 \end{pmatrix}. \tag{4.88}$$

The zeroes in these matrices are easily understood. The Δ_2 crystal is translation invariant in the y-direction, because all the wave vectors in the set $\{\mathbf{q}_2\}$ lie in the xz-plane. This means that the xy- and yz-components of ν_2 are zero. The only nonzero shear modulus is that for shear in the xz-plane. Note also that the Δ_2 crystal has nonzero λ_3^{xxxx} and λ_3^{zzzz}, meaning that it has a nonzero Young's modulus for compression or stretching in the x- and z-directions confirming that, as the shear modulus indicates, it is rigid against deformations in the xz-plane. Similarly, the Δ_3 crystal is translation invariant in the x-direction, meaning that the only nonzero component of the shear modulus ν_3 is that for shear in the yz-plane.

The vortices in rotating crystalline color superconducting quark matter have currents of u, d and s quark-number flowing around them, meaning that the phase of both the Δ_2 and Δ_3 condensates winds once by 2π around a rotational vortex, and meaning that both Δ_2 and Δ_3 vanish at the core of the vortex. This in turn means that it will be free energetically favorable for the vortices to be pinned at places where the Δ_2 and Δ_3 condensates already vanish in the absence of a vortex. The Δ_2 crystal has two families of nodal planes where $\Delta_2(\mathbf{r})$ vanishes. One class of nodal planes are parallel to the xy-plane and are located at $z = ((2n+1)\pi\sqrt{3})/(4q)$, where n is an integer. The others are parallel to the yz-plane and are located at $x = ((2n+1)\pi\sqrt{6})/(4q)$. Similarly, the Δ_3 crystal has nodes along $z = ((2n+1)\pi\sqrt{3})/(4q)$ and $y = ((2n+1)\pi\sqrt{6})/(4q)$. So, we expect that the most favorable location of the vortices will be within the common nodal planes of the Δ_2 and Δ_3 condensates, namely, $z = ((2n+1)\pi\sqrt{3})/(4q)$. If these vortices are oriented in the x-direction, they will preferentially be located (i.e. will be pinned at) at $x = ((2n+1)\pi\sqrt{6})/(4q)$. And, if the vortices in an array of vortices oriented in the x-direction try to move apart (i.e. move in the yz-plane) as

the rotation slows, in order to move they will have to shear the Δ_2 crystal which has a nonzero ν_3^{yz}. Similiarly, if the vortices are oriented in the y-direction, they will preferentially be located (i.e. will be pinned at) at $y = ((2n+1)\pi\sqrt{6})/(4q)$. And, if the vortices in an array of vortices oriented in the y-direction try to move apart (i.e. move in the xz-plane), they will have to shear the Δ_3 crystal which has a nonzero ν_3^{xz}. Thus, the nonzero shear moduli that we have found in (4.88) are sufficient to ensure that vortices pinned within the CubeX phase are pinned to a rigid structure, with the relevant shear modulus having a magnitude $16\kappa/9$.

We note as an aside that further evidence for the rigidity of the CubeX crystal can be found by evaluating the phonon velocities and showing that at long wavelengths the velocity of transverse phonons (which are found in a rigid solid but not in a fluid) is comparable to that of the longitudinal phonons which are found in both fluids and solids. We will evaluate the velocities of the longitudinal phonons upon ignoring the existence of longitudinal oscillations in the gapless fermions, which have velocity $1/\sqrt{3}$ in the limit of weak coupling. For this reason, the longitudinal phonon velocity that we calculate should be seen only as a benchmark against which to compare the transverse phonon velocity. The true sound modes would be linear combinations of the longitudinal phonons and the fermionic sound waves, which must in reality be coupled. This complication does not arise for transverse phonons: the fluid of gapless fermions has no transverse sound waves; they can only arise as excitations of a rigid structure, like the crystalline condensate we analyze. Consider as an example the phonons of the Δ_2-crystal. From the dispersion relations (4.79) it is easy to show using $\rho_2^x = 8\kappa/3$, $\rho_2^y = 0$ and $\rho_2^z = 4\kappa/3$ that longitudinal phonons propagating in the x-direction have $v = \sqrt{2/3}$ while transverse phonons propagating in this direction have the same $v = \sqrt{2/3}$. For propagation in the z-direction, both modes turn out to have $v = \sqrt{1/3}$. For propagation in other directions, there are two phonon modes with differing velocities.

4.5.4 Shear modulus for the 2Cube45z crystal

Let us orient the coordinate axes such that $\{\hat{\mathbf{q}}_2\}$ contains the eight wave vectors $(1/\sqrt{3})(\pm 1, \pm 1, \pm 1)$ and $\{\hat{\mathbf{q}}_3\}$ contains $(1/\sqrt{3})(\pm\sqrt{2}, 0, \pm 1) \cup (1/\sqrt{3})(0, \pm\sqrt{2}, \pm 1)$. These wave vectors are shown in the right panel of Fig. 1. The potential energy is given by

$$\begin{aligned}\mathcal{U} =& \frac{8}{9}\kappa\Big((s_2^{xx})^2 + (s_2^{yy})^2 + (s_2^{zz})^2\Big) + \frac{16}{9}\kappa\Big((s_2^{xx})(s_2^{zz}) + (s_2^{yy})(s_2^{zz}) + (s_2^{xx})(s_2^{yy})\Big) \\ &+ \frac{16}{9}\kappa\Big((s_2^{xy})^2 + (s_2^{yx})^2 + (s_2^{yz})^2 + (s_2^{zy})^2 + (s_2^{xz})^2 + (s_2^{zx})^2\Big) \\ &+ \frac{8}{9}\kappa\Big(2(s_3^{xx})^2 + 2(s_3^{yy})^2 + (s_3^{zz})^2\Big) + \frac{16}{9}\kappa\Big((s_3^{yy})(s_3^{zz}) + (s_3^{xx})(s_3^{zz})\Big) \\ &+ \frac{16}{9}\kappa\Big((s_3^{xz})^2 + (s_3^{zx})^2 + (s_3^{yz})^2 + (s_3^{zy})^2\Big)\,,\end{aligned} \tag{4.89}$$

from which one can read off the nonzero entries of the λ_I^{munv} tensors for $I = 2$ and $I = 3$. In the case of Δ_2, where the axes are oriented perpendicular to the nodal planes of the crystal, the form of λ_2^{munv} for the cubic crystal are easily inferred from the symmetries of the cube [103]. There are in general only three independent nonzero entries in λ_2^{munv}, corresponding to the terms read from (4.89) with the form λ_2^{mmmm}, λ_2^{mmnn} and λ_2^{mumu}. The form of λ_2^{munv} read from (4.89) is therefore valid to all orders in Δ_2, although of course the values of the coefficients, including in particular the equality between the λ_2^{mmnn} and λ_2^{mumu} coefficients, will receive corrections at higher order. Finally, note that λ_3^{munv} read from (4.89) is obtained from λ_2^{munv} by rotating this tensor by 45° about the z-axis. Note that $\lambda_3^{xyxy} = \lambda_3^{yxyx}$ vanishes. This is a consequence (after the 45° rotation) of the equality of λ_2^{mmnn} and λ_2^{mumu} in the Δ_2 crystal, and is therefore not expected to persist at higher order in Δ_3.

As in the previous subsection, we extract the σ_I tensors and the matrices of shear moduli ν_I from the potential $\mathcal{U}$ of (4.89), obtaining in this case

$$\nu_2 = \frac{16}{9}\kappa \begin{pmatrix} 0 & 1 & 1 \\ 1 & 0 & 1 \\ 1 & 1 & 0 \end{pmatrix}, \quad \nu_3 = \frac{16}{9}\kappa \begin{pmatrix} 0 & 0 & 1 \\ 0 & 0 & 1 \\ 1 & 1 & 0 \end{pmatrix}. \tag{4.90}$$

As discussed above, there is no symmetry reason for $\nu_3^{xy} = 0$, so we expect that this component of the shear modulus is nonzero at order $\Delta^4/\delta\mu^2$. Note that if we were to rotate our coordinate axes by 45° about the z-axis, it would be ν_3 that has the zero entry while ν_2 would have all off-diagonal entries nonzero. (To confirm this, rotate the λ_I^{munv} tensors and re-extract the ν_I matrices, which are not tensors.)

The Δ crystal has nodes along $x = ((2n+1)\pi\sqrt{3})/(4q)$, $y = ((2n+1)\pi\sqrt{3})/(4q)$ and $z = ((2n+1)\pi\sqrt{3})/(4q)$. The Δ_3 crystal has nodes along $x \pm y = ((2n+1)\pi\sqrt{6})/(4q)$ and $z = ((2n+1)\pi\sqrt{3})/(4q)$. The nodes common to both lie along the $z = ((2n+1)\pi\sqrt{3})/(4q)$ planes. We therefore expect that the crystal will orient itself relative to the rotation axis such that rotation vortices lie within these planes. Depending on their orientation within the planes, they could be pinned where the perpendicular nodal planes of either the Δ_2 or the Δ_3 crystals intersect the $z = ((2n+1)\pi\sqrt{3})/(4q)$ planes.

We learn from our analysis that the crystals are weaker (smaller shear modulus) with respect to shear in certain planes. We saw this explicitly for ν_3^{xy}, which is zero to order Δ_3^2 and thus presumably weaker although nonzero when higher order terms are included. The same will apply to shear in any plane obtained from this one by a symmetry transformation of the crystal, and will apply to the analogous planes for the Δ_2 crystal. Note, however, that in the 2Cube45z structure the weak planes for the Δ_2 and Δ_3 crystals do not coincide. This means that if it so happens that motion of a rotational vortex in a certain direction is only impeded by the weaker shear modulus of the Δ_2 crystal, it will in fact be obstructed by the stronger shear modulus of the Δ_3 crystal, or vice versa. Thus, the relevant shear modulus in the analysis of vortex pinning and pulsar glitches is the stronger one, which we find to be $16\kappa/9$ to order Δ^2.

As in Section 4.5.3, we can find further evidence for the rigidity of the 2Cube45z crystal by evaluating the velocity of the transverse and longitudinal phonons. Considering the Δ_2-crystal as an example, from the dispersion relations (4.79) and $\rho_2^x = \rho_2^y = \rho_2^z = 8\kappa/3$ we find that for propagation in the x- or y- or z-direction the longitudinal phonon mode and the two transverse phonon modes all have $v = \sqrt{1/3}$.

For propagation in the $x \pm z$ directions, the longitudinal mode has $v = \sqrt{2/3}$ while one transverse mode has $v = \sqrt{1/3}$ and the other transverse mode, corresponding to transverse oscillations for which the restoring force would be given by the component of the shear modulus which vanishes at order Δ^2, turns out indeed to have $v = 0$. We see that the velocity of both the longitudinal and transverse phonons is anisotropic, as expected in a crystal, and see that they are comparable in magnitude, confirming that the nonzero components of the shear moduli are as large as the longitudinal elastic moduli, as expected for a very rigid body.

4.6 Conclusion

4.6.1 The rigidity of crystalline color superconducting quark matter

We have calculated the shear moduli of crystalline color superconducting quark matter with the CubeX and 2Cube45z crystal structures. Within the Ginzburg-Landau analysis of Ref. [46], one or other of these crystal structures is favored over unpaired quark matter and over spatially uniform paired phases like the CFL phase in the wide regime of densities given in Eq. (1.37). As we have explained in Sections 4.5.3 and 4.5.4, in both these structures the components of the shear moduli that make the crystals rigid with respect to vortices pinned within them take on the same value to order Δ^2, given by

$$\nu_{\rm CQM} = \frac{16}{9}\kappa \tag{4.91}$$

with κ defined by (4.82). Evaluating κ yields

$$\nu_{\rm CQM} = 2.47\,{\rm MeV/fm^3}\left(\frac{\Delta}{10\ {\rm MeV}}\right)^2\left(\frac{\mu}{400\ {\rm MeV}}\right)^2 \tag{4.92}$$

for the shear moduli of crystalline quark matter with these two crystal structures. If quark matter is found within neutron stars, it is reasonable to estimate that its quark

number chemical potential will lie in the range

$$350 \text{ MeV} < \mu < 500 \text{ MeV} . \tag{4.93}$$

The gap parameter Δ is less well known. According to the Ginzburg-Landau calculations of Ref. [46], Δ/Δ_0 is about 1/4 to 1/2, with Δ_0 the CFL gap parameter for $M_s = 0$. Here, Δ/Δ_0 for the CubeX crystal structure somewhat larger than that for the 2Cube45z structure and Δ/Δ_0 is a slowly increasing function of M_s^2/μ, meaning a slowly decreasing function of density [46]. It is reasonable to estimate that Δ_0 is between 10 and 100 MeV, but if Δ_0 is in the upper half of this range then quark matter at accessible densities is likely in the CFL phase, rather than in the crystalline phase. So, we suggest that in interpreting (4.92) it is reasonable to estimate that

$$5 \text{ MeV} \lesssim \Delta \lesssim 25 \text{ MeV} , \tag{4.94}$$

keeping in mind that a part of the uncertainty encompassed by this range comes from our lack of knowledge of Δ_0 and a part comes from the M_s^2/μ-dependence of Δ/Δ_0 described in Ref. [46]. The estimates (4.94) and (4.93) mean that our result (4.92) implies

$$0.47 \text{ MeV/fm}^3 < \nu_{\text{CQM}} < 24 \text{ MeV/fm}^3 . \tag{4.95}$$

We shall take this as an estimate of the magnitude of ν_{CQM}, although (4.92) is a better representation of our result for use in future work.

One qualitative way to appreciate how rigid the crystalline phases of quark matter are is to calculate the (anisotropic) velocities of long wavelength transverse and longitudinal phonons, as we have done for a few directions of propagation in the CubeX and 2Cube45z crystal structures in Sections 4.5.3 and 4.5.4 respectively. We find that the transverse modes, whose restoring forces are governed by the shear moduli, propagate with velocities that are comparable to the velocity of longitudinal phonons.

To appreciate more quantitatively how rigid the crystalline phases of quark matter prove to be, we compare the shear modulus that we have calculated to that for the

standard neutron star crust, which is a conventional crystal of positively charged ions immersed in a fluid of electrons (and, at sufficient depth, a fluid of neutrons). The shear modulus of this solid can be expressed as [122]

$$\nu_{\rm NM} = c\frac{n_i(Ze)^2}{a}\,, \tag{4.96}$$

where n_i is the number density of ions in the crust, Z is the atomic number of the positively charged ions, $a = (3/(4\pi n_i))^{1/3}$ is the average inter-ion spacing, $e^2 \simeq 4\pi/137$ and $c \sim 0.1 - 0.2$ is a dimensionless constant. Because the crust is electrically neutral, the number density of ions is related to n_e, the electron number density, by $n_i = n_e/Z$. And, n_e is given in terms of the mass and electric chemical potential μ_e of the electrons by

$$n_e = \frac{(\mu_e^2 - m_e^2)^{3/2}}{3\pi^2}\,, \tag{4.97}$$

where μ_e is estimated to be in the range $20 - 80$ MeV and $Z \sim 40 - 50$ [122]. Using these estimates, we find

$$0.092\ \text{keV/fm}^3 < \nu_{\rm NM} < 23\ \text{keV/fm}^3\ . \tag{4.98}$$

Comparing to (4.95), we see that crystalline quark matter is more rigid than the conventional neutron star crust by at least a factor of 20, and possibly by about three orders of magnitude.

We conclude that crystalline color superconducting quark matter is a very good solid indeed, which is remarkable since it is at the same time superfluid.

4.6.2 Toward pulsar glitch phenomenology

As discussed in the Introduction, the glitches that are observed to interrupt the gradual spin-down of spinning neutron stars are thought to arise from the sudden unpinning of an array of rotational vortices that had been pinned in place, at a fixed area density and hence a fixed angular momentum, while the other components of the star and in particular the observed surface had been gradually slowing down.

When the stressed vortices unpin and separate, the superfluid component loses angular momentum while the surface spins up. Can these phenomena originate within crystalline color superconducting quark matter in the core of a neutron star? This phase of matter is a superfluid while at the same time having a rigid spatial modulation of its superfluid condensate, as we have seen. Understanding whether this makes it a plausible locus for the origin of pulsar glitches requires addressing three questions: Is crystalline color superconducting quark matter rigid enough? Do vortices in this phase of matter get pinned? And, how rapidly can angular momentum be transferred from a crystalline quark matter core that has just glitched to the outer crust whose surface is observed?

Our calculation constitutes an affirmative answer to the first question. We have shown that both the CubeX and 2Cube45z crystal structures have shear moduli with magnitude (4.92) which are 20 to 1000 times greater than those of the conventional neutron star crust within which glitches have long been assumed to originate.

Next, do vortices in fact get pinned? With what pinning force? This is a much harder question to address quantitatively because doing so requires going beyond the long wavelength phonon effective action. The question is what is the difference in the energy per unit length of a vortex centered on a nodal plane (or at the intersection of two nodal planes) of the condensate and one centered half way between neighboring nodal planes. Understanding this quantitatively requires constructing a vortex solution in the crystalline background, which is a challenging task. In the conventional neutron star crust, a vortex in a neutron superfluid is pinned on "impurities" embedded in the superfluid, namely the lattice of positively charged nuclei. In rotating crystalline color superconducting quark matter, the vortices are deformations of the phase and magnitude of the same condensate whose underlying magnitude modulation is the origin of the pinning. Unlike in the case of the shear modulus, which describes the response to a stress on length scales long compared to those characteristic of the crystal itself, the deformations introduced by a vortex will occur on length scales comparable to the lattice spacing of the underlying crystal. This means that constructing the vortices must be done self-consistently with analyzing the crystal

structure itself — the pinning sites are in no sense extraneous impurities. We can provide a crude estimate of the pinning force, but we defer a quantitative response to this challenge to future work.

To estimate the pinning force, let us suppose (contrafactually) that the core radius of a vortex $\xi \sim 1/\Delta$ is much smaller than the spacing between nodal planes of the crystalline condensate. If such a vortex is located where the underlying crystalline condensate is maximal, it will have to deform that condensate maximally since at the center of the vortex the condensate must vanish. Clearly, it will be energetically advantageous to locate the vortex at the intersection of nodal planes where the condensate already vanishes in the absence of a vortex. This argument translates into a pinning energy per unit length given at the level of dimensional analysis by

$$\frac{E_p}{\ell} = f\,|\Omega_{\text{crystalline}}|\,\xi^2 \tag{4.99}$$

where $|\Omega_{\text{crystalline}}|$ is the condensation energy of the crystalline phase and where f is some dimensionless factor. The corresponding pinning force per unit length is given by

$$\frac{F_p}{\ell} = \frac{f\,|\Omega_{\text{crystalline}}|\,\xi^2}{b}\,, \tag{4.100}$$

where the length scale b is half the spacing between neighboring nodal planes and hence one quarter of the lattice spacing. In both the CubeX and 2Cube45z crystals, $b = \pi\sqrt{3}/(4q) = 1.13/\delta\mu$. Recalling that $\delta\mu = M_s^2/(8\mu)$, we can get a sense of the scale of b by seeing that $b = 18, 12$ fm for $M_s^2/\mu = 100, 150$ MeV. Reading from plots in Ref. [46], we see that for $\Delta_0 = 25$ MeV this range of M_s^2/μ corresponds to a robust crystalline phase with $|\Omega_{\text{crystalline}}| \sim 2 \times 10^5$ MeV^4 and $\Delta \sim 5 - 10$ MeV if the crystal has the 2Cube45z structure or $\Delta \sim 10 - 15$ MeV if the crystal has the CubeX structure. We immediately see that $\xi = 1/\Delta$ and b are comparable length scales, which makes this analysis unreliable at a quantitative level. One way of saying this is that the dimensionless factor f must then be very much less than one, since the energy benefit by moving the vortex by a distance b is of order $|\Omega_{\text{crystalline}}|\xi^2$ only if making this move shifts the core from a place where the condensate was maximal

within the core area ξ^2 to a place where it is close to vanishing. A calculation of f in the case where $\xi \sim b$ as is relevant in our context requires a quantitative analysis, but it is clear that the energy benefit of moving the vortex by a distance b must then be $\ll |\Omega_{\rm crystalline}|\xi^2$. Putting the pieces together, we can write an estimate of the pinning force per unit length as

$$\frac{F_p}{\ell} = 0.7 \frac{\rm MeV}{(10{\rm fm})^2} \left(\frac{f}{0.01}\right) \left(\frac{|\Omega_{\rm crystalline}|}{2\times 10^5\ {\rm MeV}^4}\right) \left(\frac{\xi}{20\ {\rm fm}}\right)^2 \left(\frac{15\ {\rm fm}}{b}\right) , \qquad (4.101)$$

where our choice of $f \sim 0.01$ as a fiducial value is a pure guess and the dependence of the other quantities in the estimate (4.101) on Δ_0 and M_s^2/μ can be obtained from the results of Ref. [46], with the fiducial values we have used being reasonable for $\Delta_0 = 25$ MeV and $M_s^2/\mu = 100 - 150$ MeV.

We can compare our estimate (4.101) to the pinning force on neutron vortices in a conventional crust [123], in which neutron superfluid vortices are pinned on nuclei [109, 110, 111, 112, 113, 114, 115, 116, 117, 118, 119, 120, 121]. The pinning energy of a vortex per ion on which it is pinned is $E_p^{\rm NM} \sim 1 - 3$ MeV [110, 111, 112], the ions are spaced by a lattice spacing $b_{\rm NM} \sim 25 - 50$ fm [112], and the superfluid vortices have core radii $\xi_{\rm NM} \sim 4 - 20$ fm [112]. Hence, the pinning force per unit length is [111, 112]

$$\frac{E_p^{\rm NM}}{b_{\rm NM}\xi_{\rm NM}} = \frac{1 - 3\ {\rm MeV}}{(25 - 50\ {\rm fm})(4 - 20\ {\rm fm})}. \qquad (4.102)$$

Although our estimate (4.101) is quite uncertain, given that we have not constructed the vortex solutions for rotating crystalline color superconducting quark matter, it seems reasonable to estimate that the pinning force per unit length on vortices within a putative crystalline quark matter neutron star core is comparable to that on neutron superfluid vortices within a conventional neutron star crust.

Recent calculations of the profile of vortices in BCS-paired superfluid gases of ultracold fermionic atoms [137] may make it easier to estimate the pinning force on vortices in the crystalline quark matter phase. In the cold atom context, it turns out that the radius of the vortex core is much smaller than the correlation length $\xi \sim 1/\Delta$ which controls the long distance form of the vortex profile. Instead, the vortex core

radius is $\sim 1/k_F$, controlled by the Fermi momentum rather than by the correlation length. If this result were to be obtained in our context, it could mean replacing ξ in (4.101) by $(1/\mu) \sim 0.5$ fm, reducing our fiducial estimate (4.101) by a factor of 1600. However, if the vortex cores do turn out to be as narrow as this then the assumption with which we began our estimate, namely that the core size is much less than the lattice spacing, becomes factual rather than contrafactual. This would mean that there is no longer any reason to expect the dimensionless factor f to be much smaller than 1, and would considerably reduce the uncertainty in the estimate. Replacing f by 1 would increase the estimate (4.101) by a factor of 100, resulting in a pinning force which is only slightly smaller that on the superfluid neutron vortices within a conventional neutron star crust. We leave the determination of the profile of vortices in crystalline quark matter to future work, but it will clearly be very interesting to see whether they have narrow cores as in Ref. [137], and if so whether their pinning turns out to be controlled by their core radii or by the correlation length.

The third question which must be addressed is how, and how quickly, angular momentum can be transferred from a crystalline quark matter core to the outer crust. Some glitches are known to occur on timescales of minutes which means that if a glitch occurs within the core angular momentum must be transferred to the observed crust at least this fast. The core and crust are linked via being bathed in the same electron fluid and via magnetic fields. In the conventional glitch scenario, when the neutron superfluid in the crust suddenly slows down as its vortices come unpinned and the nonsuperfluid component of the crust, which includes the ions and the electrons, speeds up, the electron fluid couples the crust to the core well enough that the core also speeds up within seconds [124, 113]. We therefore expect that if a glitch occurs within a crystalline quark matter core, with this superfluid component slowing down, and if moving vortices can impart angular momentum to the electrons then the electron fluid will ensure that the entire rest of the star including the outer crust speeds up. In the conventional scenario, the mechanism by which moving vortices exert a torque on the ions, and hence the electrons, in the crust has been described in Refs. [115, 116, 117]. In our case, we have not demonstrated how moving vortices in

the crystalline phase can torque up the fluid of gapless charged quark quasiparticles, and hence the electrons.

So, tallying the status of the three questions that must be addressed: The first is settled, answered in the affirmative by our calculation of the shear modulus of the crystalline phase. The second remains to be addressed quantitatively but seems to be answered in the affirmative by our dimensional analysis estimate of the pinning force on vortices in the crystalline phase. The third remains open, not yet addressed in a satisfactory fashion but nevertheless with no reason to doubt that its answer is also affirmative. Addressing the third question and addressing the second question quantitatively both require constructing the rotational vortex solutions for rotating crystalline quark matter. This is therefore the crucial remaining step in completing the connection between the microphysics of crystalline color superconducting quark matter and the phenomenology of pulsar glitches, and hence determining whether the characteristics of observed glitches rule out, or are consistent with, the presence of crystalline color superconducting quark matter within neutron stars.

Finally, it is also worth asking whether a "core-quake" scenario could be a viable model of glitches [125, 126]. As a spinning neutron star slows down, it becomes less oblate. This will require macroscopic adjustments to the shape of a putative crystalline quark matter core. Given the enormous shear moduli of this rigid phase of matter, enormous amounts of elastic energy would be stored as the core is deformed and stressed, energy which would be released in core-quakes during which the crystalline core "breaks" and rearranges its structure so as to reduce its moment of inertia, consequently increasing its angular velocity. The original "crust-quake" model for pulsar glitches [127] failed because it failed to describe the magnitude and frequency of glitches in the Vela pulsar [112, 118, 119, 121]. Now that we know that crystalline quark matter has shear moduli which are 20 to 1000 times larger than those of the crust, core-quakes are worth re-investigating.

Appendix A

Neutrality of solutions with $\Delta_2 = \Delta_3$

In Section 2.7.1, we gave a general analysis of the free energy $\Omega(\Delta_2, \Delta_3)$. We showed that if we write (Δ_2, Δ_3) as $\sqrt{2}(\Delta_r \cos\theta, \Delta_r \sin\theta)$ the free energy takes the form (2.65), and therefore has extrema only at $\theta = \pi/4$ (namely $\Delta_2 = \Delta_3 = \Delta_r$) or $\theta = 0, \pi/2$ (namely a two flavor crystalline phase with only one Δ_I nonzero). As we have explained in Section 2.3.2, in the strict Ginzburg-Landau limit in which $\Delta_I/\delta\mu \to 0$ any solution (Δ_2, Δ_3) is neutral. (The argument is that choosing $\mu_e = M_s^2/(4\mu)$ as in neutral unpaired quark matter suffices since, unlike BCS superconductivity, crystalline color superconductivity does not require any modification of the unpaired Fermi momenta prior to pairing and since in the Ginzburg-Landau limit the modifications to number densities due to the pairing itself vanishes.) In this Appendix, we take a small step away from the strict Ginzburg-Landau limit. We assume that Δ_r is small, but do not work in the limit in which it vanishes. We then show that the only solutions with $\mu_e = M_s^2/(4\mu)$ and, consequently, $\delta\mu_2 = \delta\mu_3 = \delta\mu = M_s^2/(8\mu)$ which are electrically neutral are those with $\Delta_2 = \Delta_3 = \Delta_r$. The two-flavor crystalline phases with only one Δ_I nonzero are not neutral in three-flavor quark matter.

The result of this Appendix allows us to neglect solutions which have only one Δ_I nonzero. This is fortunate, because there are many two-flavor crystal structures for which the sextic coefficient $\bar{\gamma}$ is negative, meaning that to sextic order the

Ginzburg-Landau potential $\Omega(\Delta_2, \Delta_3)$ often has runaway directions along the Δ_2 and Δ_3 axes [39]. Furthermore, if the coefficient multiplying $\sin^2\theta$ in (2.65) is negative, for example if $\bar{\beta}$ and $\bar{\gamma}$ are both negative while $\bar{\beta}_{32}$ and $\bar{\gamma}_{322}$ are both positive as is the case for both the CubeX and the 2Cube45z crystal structures on which we focus, then the extremum of $\Omega(\Delta_2, \Delta_3)$ that we find with $\Delta_2 = \Delta_3$ appears to be a local maximum with respect to variation of θ away from $\pi/4$ while keeping μ_e fixed. We show in this Appendix that upon fixing $\mu_e = M_s^2/(4\mu)$ any solution with $\Delta_2 \neq \Delta_3$ is not neutral. For this reason, all these complications can be neglected, and we are correct to focus only on solutions with $\Delta_2 = \Delta_3$.

The more formal way to proceed would be to define an $\Omega_{\text{neutral}}(\Delta_2, \Delta_3)$, obtained by varying μ_e (and μ_3 and μ_8 too) at a given value of the Δ's in order to obtain neutrality, and then finding Δ_2 and Δ_3 that minimize $\Omega_{\text{neutral}}(\Delta_2, \Delta_3)$. We have done a partial version of this investigation in a few cases and have found that, as expected, Ω_{neutral} does have a minimum with μ_e very close to $M_s^2/(4\mu)$ and Δ_2 very close to Δ_3. A full exploration in this vein requires evaluating the Ginzburg-Landau coefficients without assuming $\delta\mu_2 \approx \delta\mu_3$ and, more challenging, requires reformulating our analysis to include nonzero μ_3 and μ_8. We have not attempted the latter, and it is in this sense that our preliminary investigation referred to above was "partial". We leave this to future work, and turn now to the promised derivation of the neutrality of solutions with $\Delta_2 = \Delta_3$ and $\mu_e = M_s^2/(4\mu)$.

We shall only consider crystal structures for which $\{\hat{\mathbf{q}}_2\}$ and $\{\hat{\mathbf{q}}_3\}$ are exchange symmetric, as this is the symmetry that allows the free energy to have extrema along the line $\Delta_2 = \Delta_3$. (Recall that by exchange symmetric we mean that there is a sequence of rigid rotations and reflections which when applied to all the vectors in $\{\mathbf{q}_2\}$ and $\{\mathbf{q}_3\}$ together has the effect of exchanging $\{\hat{\mathbf{q}}_2\}$ and $\{\hat{\mathbf{q}}_2\}$.) Because we wish to evaluate $\partial\Omega/\partial\mu_e$ at $\mu_e = M_s^2/(4\mu)$, we must restore μ_e to our expression for the free energy Ω, rather than setting it to $M_s^2/(4\mu)$ from the beginning. Recall from (2.20) that $\Omega_{\text{crystalline}}$ is the sum of the free energy for unpaired quark matter, which we know satisfies $\partial\Omega_{\text{unpaired}}/\partial\mu_e = 0$ at $\mu_e = M_s^2/(4\mu)$, and $\Omega(\Delta_2, \Delta_3)$. Upon

restoring the μ_e-dependence, the latter is given by

$$\begin{aligned}
&\Omega(\mu_e, \Delta_2, \Delta_3) = \\
&\frac{2\mu^2}{\pi^2}\Bigg[P\alpha(\delta\mu_2)\Delta_2^2 + P\alpha(\delta\mu_3)\Delta_3^2 \\
&\quad + \frac{1}{2}\left(\frac{1}{\delta\mu_2^2}\bar{\beta}_2\Delta_2^4 + \frac{1}{\delta\mu_3^2}\bar{\beta}_3\Delta_3^4 + \frac{1}{\delta\mu_3\delta\mu_2}\bar{\beta}_{32}\Delta_2^2\Delta_3^2\right) \\
&\quad + \frac{1}{3}\Bigg(\frac{1}{\delta\mu_2^4}\bar{\gamma}_2\Delta_2^6 + \frac{1}{\delta\mu_3^4}\bar{\gamma}_3\Delta_3^6 + \gamma_{233}(\delta\mu_2, \delta\mu_3)\Delta_2^2\Delta_3^4 \\
&\quad + \gamma_{322}(\delta\mu_2, \delta\mu_3)\Delta_3^2\Delta_2^4\Bigg)\Bigg] ,
\end{aligned} \tag{A.1}$$

where $\delta\mu_2$ and $\delta\mu_3$ can no longer be taken to be equal, as they are given by

$$\begin{aligned}
\delta\mu_3 &= \frac{\mu_e}{2} \\
\delta\mu_2 &= \frac{M_s^2}{4\mu} - \frac{\mu_e}{2} ,
\end{aligned} \tag{A.2}$$

which in particular means that

$$\frac{\partial\delta\mu_3}{\partial\mu_e} = -\frac{\partial\delta\mu_2}{\partial\mu_e} = \frac{1}{2} . \tag{A.3}$$

Because $\{\hat{\mathbf{q}}_2\}$ and $\{\hat{\mathbf{q}}_3\}$ are exchange symmetric, $\bar{\beta}_2 = \bar{\beta}_3 = \bar{\beta}$ and $\bar{\gamma}_2 = \bar{\gamma}_3 = \bar{\gamma}$. Because $\delta\mu_2 \neq \delta\mu_3$, however, the coefficients γ_{322} and γ_{233} are not equal and, furthermore, their $(\delta\mu_2, \delta\mu_3)$-dependence cannot be factored out as in (2.49) or (2.63). The coefficient γ_{322} depends on $\delta\mu_2$ and $\delta\mu_3$ through its dependence on $\mathcal{K}_{udusus}$: $\gamma_{322} = (3/2)\sum\mathcal{K}_{udusus}(\mathbf{q}_3^b, \mathbf{q}_3^b, \mathbf{q}_2^d, \mathbf{q}_2^e, \mathbf{q}_2^f, \mathbf{q}_2^a)$. $\mathcal{K}_{udusus}$ is given in (2.59). Note that its dependence on $\delta\mu_2$ and $\delta\mu_3$ comes via $\mathbf{q}_2 = \eta\,\delta\mu_2\,\hat{\mathbf{q}}_2$ and $\mathbf{q}_3 = \eta\,\delta\mu_3\,\hat{\mathbf{q}}_3$ in addition to the explicit dependence visible in (2.59). Similarly $\gamma_{233} = (3/2)\sum\mathcal{K}_{usudud}(\mathbf{q}_2^b, \mathbf{q}_2^b, \mathbf{q}_3^d, \mathbf{q}_3^e, \mathbf{q}_3^f, \mathbf{q}_3^a)$ where $\mathcal{K}_{usudud}$ has the same form as (2.59) except that $\delta\mu_2$ and $\delta\mu_3$ are interchanged. Using the definitions (2.49) and (2.63), one can confirm that (A.1) reduces to (2.64) if we take $\delta\mu_2 = \delta\mu_3$ and hence $\gamma_{322} = \gamma_{233}$.

We now differentiate Ω given in (A.1) with respect to μ_e, noting (A.3), obtaining

$$\begin{aligned}\frac{\partial\Omega}{\partial\mu_e} &= \frac{\partial\Omega}{\partial\Delta_2}\frac{d\Delta_2}{d\mu_e} + \frac{\partial\Omega}{\partial\Delta_3}\frac{d\Delta_3}{d\mu_e} + \frac{\mu^2}{\pi^2}\Bigg[P\frac{d\alpha(\delta\mu_3)}{d\mu_3}\Delta_3^2 - P\frac{d\alpha(\delta\mu_2)}{d\mu_2}\Delta_2^2 + \frac{\bar{\beta}}{\delta\mu_2^3}\Delta_2^4 - \frac{\bar{\beta}}{\delta\mu_3^3}\Delta_3^4 \\ &+ \left(\frac{1}{2\delta\mu_2^2\delta\mu_3} - \frac{1}{2\delta\mu_2\delta\mu_3^2}\right)\bar{\beta}_{32}\Delta_2^2\Delta_3^2 + \frac{4\bar{\gamma}}{3\delta\mu_2^5}\Delta_2^6 - \frac{4\bar{\gamma}}{3\delta\mu_3^5}\Delta_3^6 \\ &+ \frac{1}{3}\left(\frac{\partial\gamma_{233}(\delta\mu_2,\delta\mu_3)}{\partial\delta\mu_3} - \frac{\partial\gamma_{233}(\delta\mu_2,\delta\mu_3)}{\partial\delta\mu_2}\right)\Delta_2^2\Delta_3^4 \\ &+ \frac{1}{3}\left(\frac{\partial\gamma_{322}(\delta\mu_2,\delta\mu_3)}{\partial\delta\mu_3} - \frac{\partial\gamma_{322}(\delta\mu_2,\delta\mu_3)}{\partial\delta\mu_2}\right)\Delta_2^4\Delta_3^2\Bigg] .\end{aligned} \tag{A.4}$$

We shall only evaluate $\partial\Omega/\partial\mu_e$ at values of Δ_2 and Δ_3 which are solutions to the gap equations $\partial\Omega/\partial\Delta_2 = 0$ and $\partial\Omega/\partial\Delta_3 = 0$, meaning that the first two terms in (A.4) vanish. Furthermore, we shall only evaluate $\partial\Omega/\partial\mu_e$ at $\mu_e = M_s^2/(4\mu)$, where $\delta\mu_2 = \delta\mu_3 = \delta\mu$, and at solutions for which $\Delta_2 = \Delta_3$. Under these circumstances, the terms involving α, $\bar{\beta}_2$, $\bar{\beta}_{32}$ and $\bar{\gamma}_2$ vanish and (A.4) becomes

$$\left.\frac{\partial\Omega}{\partial\mu_e}\right|_{\mu_e=\frac{M_s^2}{4\mu},\ \Delta_2=\Delta_3=\Delta_{\rm min}} = \frac{\mu^2}{3\pi^2}\left[\frac{\partial\gamma_{233}}{\partial\delta\mu_3} - \frac{\partial\gamma_{233}}{\partial\delta\mu_2} + \frac{\partial\gamma_{322}}{\partial\delta\mu_3} - \frac{\partial\gamma_{322}}{\partial\delta\mu_2}\right]\Delta_{\rm min}^6\Bigg|_{\delta\mu_2=\delta\mu_3=\delta\mu} \tag{A.5}$$

We argue that this vanishes as follows. Consider a particular term that contributes to $\partial\gamma_{322}/\partial\delta\mu_2$, $\partial\mathcal{K}_{udusus}(\mathbf{q}_3^b,\mathbf{q}_3^b,\mathbf{q}_2^d,\mathbf{q}_2^e,\mathbf{q}_2^f,\mathbf{q}_2^a)/\partial\delta\mu_2$. This is a complicated integral of a function which depends on the unit momentum vectors $(\hat{\mathbf{q}}_3^b,\hat{\mathbf{q}}_2^d,\hat{\mathbf{q}}_2^e,\hat{\mathbf{q}}_2^f,\hat{\mathbf{q}}_2^a)$ and on $\delta\mu_2$ and $\delta\mu_3$. From rotational invariance, we know that the value of the integral can depend on the relative orientation of the unit momentum vectors and on $\delta\mu_2$ and $\delta\mu_3$ but must be independent of common rotations of all the unit vectors. Now, all the crystal structures that we consider are exchange symmetric, meaning that for every quintuple of unit momentum vectors, $(\hat{\mathbf{q}}_3^b,\hat{\mathbf{q}}_2^d,\hat{\mathbf{q}}_2^e,\hat{\mathbf{q}}_2^f,\hat{\mathbf{q}}_2^a)$ with the first chosen from $\{\mathbf{q}_3\}$ and the last four chosen from $\{\mathbf{q}_2\}$ there exists a quintuple $(\hat{\mathbf{q}}_2^b,\hat{\mathbf{q}}_3^d,\hat{\mathbf{q}}_3^e,\hat{\mathbf{q}}_3^f,\hat{\mathbf{q}}_3^a)$ with the first chosen from $\{\mathbf{q}_2\}$ and the last four chosen from $\{\mathbf{q}_3\}$ such that the unit vectors in each of these two quintuples have the same relative orientation among themselves. This means that for every term $\partial\mathcal{K}_{udusus}(\mathbf{q}_3^b,\mathbf{q}_3^b,\mathbf{q}_2^d,\mathbf{q}_2^e,\mathbf{q}_2^f,\mathbf{q}_2^a)/\partial\delta\mu_2$. occur-

ring in $\partial\gamma_{322}/\partial\delta\mu_2$, there is a corresponding term $\partial\mathcal{K}_{usudud}(\mathbf{q}_2^b,\mathbf{q}_2^b,\mathbf{q}_3^d,\mathbf{q}_3^e,\mathbf{q}_3^f,\mathbf{q}_3^a)/\partial\delta\mu_3$ occurring in $\partial\gamma_{233}/\partial\delta\mu_3$ such that $\partial\mathcal{K}_{usudud}(\mathbf{q}_2^b,\mathbf{q}_2^b,\mathbf{q}_3^d,\mathbf{q}_3^e,\mathbf{q}_3^f,\mathbf{q}_3^a)/\partial\delta\mu_3$ is related to $\partial\mathcal{K}_{udusus}(\mathbf{q}_3^b,\mathbf{q}_3^b,\mathbf{q}_2^d,\mathbf{q}_2^e,\mathbf{q}_2^f,\mathbf{q}_2^a)/\partial\delta\mu_2$ by the interchange of $\delta\mu_2$ and $\delta\mu_3$. Consequently, for $\delta\mu_2=\delta\mu_3$ the two contributions cancel pair by pair when we evaluate $\partial\gamma_{322}/\partial\delta\mu_2-\partial\gamma_{233}/\partial\delta\mu_3$ or $\partial\gamma_{322}/\partial\delta\mu_3-\partial\gamma_{233}/\partial\delta\mu_2$. In this way, the right hand side of (A.5) vanishes, as we set out to show. We conclude that solutions to the gap equations with $\Delta_2=\Delta_3$ and $\mu_e=M_s^2/(4\mu)$ meaning $\delta\mu_2=\delta\mu_3$ are neutral.

It is easy to see that the cancellations required in the proof of neutrality do not occur for solutions with $\Delta_2\neq\Delta_3$. For example, following a derivation analogous to that above, we find that a solution with $\Delta_2=0$ and only Δ_3 nonzero is neutral with $\mu_e=M_s^2/(4\mu)$ only if

$$P\frac{\partial\alpha(\delta\mu_3)}{\partial\delta\mu_3}\Delta_3^2-\frac{\bar{\beta}_3}{\delta\mu_3^3}\Delta_3^4-\frac{4\bar{\gamma}_3}{3\delta\mu_3^5}\Delta_3^6=0\ , \tag{A.6}$$

a condition which has no reason to be satisfied. The study of solutions with $\Delta_2\neq\Delta_3$ therefore requires that they be constructed from the beginning with $\delta\mu_2\neq\delta\mu_3$ and with μ_e fixed by the neutrality condition. We leave this to future work, focussing in Section 2.7 on solutions with $\Delta_2=\Delta_3$ which, we have proved here, are neutral.

Appendix B

Translating $\langle us \rangle$ relative to $\langle ud \rangle$ does not avoid repulsion

We have seen in Section 2.7 that crystal structures in which a vector from $\{\mathbf{q}_2\}$ and a vector from $\{\mathbf{q}_3\}$ make a 180° angle are strongly disfavored, with infinite quartic and sextic Ginzburg-Landau coefficients $\bar{\beta}_{32}$ and $\bar{\gamma}_{322}$. Suppose we consider a structure like that in which $\{\mathbf{q}_2\}$ and $\{\mathbf{q}_3\}$ are coincident cubes, a disastrous choice. The way that we have improved upon this disastrous choice in Section 2.7.4 is to rotate one cube relative to the other. Indeed, if we choose a 45° rotation about an axis perpendicular to a face of the cube, we obtain the 2Cube45z structure which is one of the two crystal structures that we find to be most favorable. In this Appendix, we ask whether we can instead avoid the infinite free energy cost of antipodal pairs by translating the $\langle ud \rangle$ condensate relative to the $\langle us \rangle$ condensate in position space, rather than rotating it. We find that the answer is no, and furthermore show that the Ginzburg-Landau free energy Ω that we have evaluated does not change if the $\langle ud \rangle$ condensate is translated relative to the $\langle us \rangle$ condensate.

Corresponding to each $\{\mathbf{q}_I\}$ in momentum space we get a function $\Delta_I(\mathbf{r})$ in position space which varies as $\Delta_I(\mathbf{r}) \sim \sum_{\mathbf{q}_I^a} e^{2i\mathbf{q}_I^a \cdot \mathbf{r}}$. To analyze the effects of translating $\Delta_2(\mathbf{r})$ relative to $\Delta_3(\mathbf{r})$, it is helpful to restore the notation of (2.32) with $\Delta(\mathbf{q}_I^a)$ representing the gap parameter corresponding to the momentum component $\mathbf{q}_I^a$. $\Delta_2(\mathbf{r})$

or $\Delta_3(\mathbf{r})$ can then be written as

$$\Delta_I(\mathbf{r}) = \sum_{\mathbf{q}_I^a} \Delta(\mathbf{q}_I^a) e^{2i\mathbf{q}_I^a \cdot \mathbf{r}} \,. \tag{B.1}$$

Translating $\Delta_2(\mathbf{r})$ in the $\hat{\mathbf{n}}$ direction by a distance s corresponds to the transformation $\Delta_2(\mathbf{r}) \to \Delta_2(\mathbf{r} - s\hat{\mathbf{n}})$ which multiplies each $\Delta(\mathbf{q}_2^a)$ in the sum in (B.1) by a different phase factor $\exp[-2is\mathbf{q}_2^a \cdot \hat{\mathbf{n}}]$. This is not just an (irrelevant) overall phase multiplying $\Delta_2(\mathbf{r})$ because it depends on the momentum component. The gap equation for the Δ_2 components, as in (2.32), is now given by

$$\begin{aligned}
\Delta^*(\mathbf{q}_2^a) e^{2is\mathbf{q}_2^a \cdot \hat{\mathbf{n}}} = -\frac{2\mu^2 \lambda}{\pi^2} \Bigg[& \Delta^*(\mathbf{q}_2^a) e^{2is\mathbf{q}_2^a \cdot \hat{\mathbf{n}}} \Pi_{31}(\mathbf{q}_2^a, \mathbf{q}_2^a) \\
& + \sum_{\mathbf{q}_2^b \mathbf{q}_2^c \mathbf{q}_2^d} \Delta^*(\mathbf{q}_2^b) \Delta(\mathbf{q}_2^c) \Delta^*(\mathbf{q}_2^d) e^{2is(\mathbf{q}_2^b - \mathbf{q}_2^c + \mathbf{q}_2^d) \cdot \hat{\mathbf{n}}} J_{3131}(\mathbf{q}_2^b, \mathbf{q}_2^c, \mathbf{q}_2^d, \mathbf{q}_2^a) \delta_{\mathbf{q}_2^b - \mathbf{q}_2^c + \mathbf{q}_2^d - \mathbf{q}_2^a} \\
& + \frac{1}{2} \sum_{\mathbf{q}_3^b \mathbf{q}_3^c \mathbf{q}_2^d} \Delta^*(\mathbf{q}_3^b) \Delta(\mathbf{q}_3^c) \Delta^*(\mathbf{q}_2^d) e^{2is\mathbf{q}_2^d \cdot \hat{\mathbf{n}}} J_{1213}(\mathbf{q}_3^b, \mathbf{q}_3^c, \mathbf{q}_2^d, \mathbf{q}_2^a) \delta_{\mathbf{q}_3^b - \mathbf{q}_3^c + \mathbf{q}_2^d - \mathbf{q}_2^a} \Bigg] \,.
\end{aligned} \tag{B.2}$$

where we have worked only to cubic order. Using $\mathbf{q}_2^b - \mathbf{q}_2^c + \mathbf{q}_2^d = \mathbf{q}_2^a$ we conclude that the phase factor in front of the $J_{3131}(\mathbf{q}_2^b, \mathbf{q}_2^c, \mathbf{q}_2^d, \mathbf{q}_2^a)$ term is simply $\exp[2is(\mathbf{q}_2^a) \cdot \hat{\mathbf{n}}]$. In addition, we saw that for $\mathbf{q}_3^b - \mathbf{q}_3^c + \mathbf{q}_2^d = \mathbf{q}_2^a$ to hold we need to have $\mathbf{q}_3^b = \mathbf{q}_3^c$ and $\mathbf{q}_2^d = \mathbf{q}_2^a$. This makes the phase factor in front of $J_{1213}(\mathbf{q}_3^b, \mathbf{q}_3^c, \mathbf{q}_2^d, \mathbf{q}_2^a)$ also $\exp[2is(\mathbf{q}_2^a) \cdot \hat{\mathbf{n}}]$. We conclude that (up to cubic order) the gap equation for each $\Delta(\mathbf{q}_2^a)$ simply picks up an overall phase. The same is true for the gap equation for each $\Delta(\mathbf{q}_3^a)$. We therefore conclude that the free energy is unchanged up to quartic order when $\Delta_2(\mathbf{r})$ is translated relative to $\Delta_3(\mathbf{r})$. This guarantees that such a translation cannot alleviate the large $\bar{\beta}_{32}$ arising from antipodal (or near antipodal) pairs of momenta occurring in $\{\mathbf{q}_2\}$ and $\{\mathbf{q}_3\}$. This argument can easily be extended to include the sextic terms in the free energy; they too are unchanged when $\Delta_2(\mathbf{r})$ is translated relative to $\Delta_3(\mathbf{r})$.

Appendix C

Phonon mass is zero to all orders in Δ

In this Appendix, we show explicitly that there cannot be any term in the phonon effective action at any order in Δ and at any order in $\mathbf{u}_I(x)$ which is nonzero if $\mathbf{u}_I(x)$ is constant over space and time, other than a trivial constant. Equivalently, we show that if we expand the Lagrangian density as a power series in $\mathbf{u}_I(x)$, every term has at least one derivative acting on each $\mathbf{u}_I(x)$, meaning that the mass of the phonons is zero. This is guaranteed by Goldstone's theorem, but the explicit demonstration of this "obvious" result is nontrivial and for this reason we give it here.

Before proceeding, we recall Eqs. (4.12) and (4.13), which imply that

$$\Delta_I^u(x) = \Delta_I \sum_{\mathbf{q}_I^a} \exp\bigl(2i\mathbf{q}_I^a \cdot (\mathbf{r} - \mathbf{u}_I(x))\bigr) \ . \tag{C.1}$$

Since we want to prove the result to arbitrary powers in the $\mathbf{u}$ fields, we do not make an expansion in small $\mathbf{u}$. In terms of Feynman diagrams, this means that in evaluating the effective action in Eq. (4.30) we resum the vertices with increasing powers of $\mathbf{u}_I$. Therefore any vertex for Δ_I comes with a factor $\epsilon_{I\alpha\beta}\epsilon_{Iij}\exp\bigl(-2i\mathbf{q}_I^a \cdot \mathbf{u}_I(x)\bigr)$ and a momentum insertion $2\mathbf{q}_I^a$. On the other hand, the vertex for Δ_I^* comes with a vertex factor $\epsilon_{I\alpha\beta}\epsilon_{Iij}\exp(2i\mathbf{q}_I^a \cdot \mathbf{u}_I(x))$ and a momentum insertion $-2\mathbf{q}_I^a$.

Integrating out the χ fields in Eq. (4.30) is equivalent to calculating all pos-

sible one-fermion-loop diagrams with arbitrarily many external phonon insertions. (Higher loop diagrams with internal phonon propagators are suppressed by powers of $\Lambda_{\rm IR}/\Delta$, with $\Lambda_{\rm IR}$ the typical energy of the phonon fields, and are therefore completely negligible.) A generic one-loop diagram will have n_I vertices proportional to $\Delta_I \exp\bigl(-2i\mathbf{q}_I^{a_\kappa}\cdot\mathbf{u}_I(x)\bigr)$ at which momenta $2\mathbf{q}_I^{a_\kappa}$ are inserted into the loop, and n_I vertices proportional to $\Delta_I^* \exp\bigl(2i\mathbf{q}_I^{a_\tau}\cdot\mathbf{u}_I(x)\bigr)$ at which momenta $-2\mathbf{q}_I^{a_\tau}$ are inserted into the loop. Here, $\kappa = 1,2,3...n_I$ and $\tau = 1,2,3..n_I$. The number of appearances of Δ_I has to be the same as that of Δ_I^* because the diagram can only depend on powers of $|\Delta_I|^2$. Different one-loop diagrams correspond to different choices of n_1, n_2 and n_3 and different choices of the $\mathbf{q}_I^{a_\kappa}$'s and the $\mathbf{q}_I^{a_\tau}$'s from among the sets $\{\mathbf{q}_I\}$. The color and flavor indices for the propagators in the diagram linking the vertices into a loop are chosen to be consistent with the color and flavor epsilon symbols associated to each vertex. The contribution from a generic one-loop diagram will be

$$\mathcal{I} \propto |\Delta_1|^{2n_1}|\Delta_2|^{2n_2}|\Delta_3|^{2n_3} \times \mathrm{Tr}\Bigg[\frac{1}{i\partial\!\!\!/ + \mu\!\!\!/_{j1}} e^{2\mathbf{q}_1^{a_1}\cdot(\mathbf{r}-\mathbf{u}_1(x))} \frac{1}{i\partial\!\!\!/ - \mu\!\!\!/_{j2}} e^{-2\mathbf{q}_2^{a_1}\cdot(\mathbf{r}-\mathbf{u}_2(x))} \frac{1}{i\partial\!\!\!/ + \mu\!\!\!/_{j3}} e^{2\mathbf{q}_1^{a_2}\cdot(\mathbf{r}-\mathbf{u}_1(x))}\ldots\Bigg] . \tag{C.2}$$

We are interested in evaluating only the contribution from such a diagram in which no derivatives act on any $\mathbf{u}_I$ fields. This contribution is given by

$$\mathcal{I} \propto |\Delta_1|^{2n_1}|\Delta_2|^{2n_2}|\Delta_3|^{2n_3} \times \mathrm{Tr}\Bigg[\exp\Bigl\{i\sum_I 2\mathbf{u}_I(x)\cdot\Bigl(\sum_{a=a_1}^{a_{n_I}}\mathbf{q}_I^a - \sum_{b=b_1}^{b_{n_I}}\mathbf{q}_I^b\Bigr)\Bigr\} \times \frac{1}{i\partial\!\!\!/ + \mu\!\!\!/_{j1}} e^{2\mathbf{q}_1^{a_1}\cdot\mathbf{r}} \frac{1}{i\partial\!\!\!/ - \mu\!\!\!/_{j2}} e^{-2\mathbf{q}_2^{a_1}\cdot\mathbf{r}} \frac{1}{i\partial\!\!\!/ + \mu\!\!\!/_{j3}} e^{2\mathbf{q}_1^{a_2}\cdot\mathbf{r}}\ldots\Bigg] . \tag{C.3}$$

Momentum conservation implies that the net momentum added to the loop is zero, i.e.

$$\sum_I \left(\sum_{a=a_1}^{a_{n_I}}\mathbf{q}_I^a - \sum_{b=b_1}^{b_{n_I}}\mathbf{q}_I^b\right) = 0 . \tag{C.4}$$

(As we argued after Eq. (4.41), the momenta contributed by ϕ is much smaller than

$|\mathbf{q}_I|$.)

We now recall from Section 4.3 that the magnitude of the $\mathbf{q}_I$ are different for different I. ($|\mathbf{q}_2| = \eta\delta\mu_2$ is close in value to $|\mathbf{q}_3| = \eta\delta\mu_3$, but they are not exactly equal because $\delta\mu_2$ and $\delta\mu_3$ differ by terms of order M_s^4/μ^3.) This means that the momentum conservation condition (C.4) can only be satisfied if

$$\sum_{a=a_1}^{a_{n_I}} \mathbf{q}_I^a - \sum_{b=b_1}^{b_{n_I}} \mathbf{q}_I^b = 0 \,, \tag{C.5}$$

separately for *each* I. This implies that in Eq. (C.3), the coefficients of each of the $\mathbf{u}_I$ cancel, and thus implies that Eq. (C.3), the contribution of a generic one-loop diagram in which no derivatives act on any $\mathbf{u}_I$'s, is independent of $\mathbf{u}_I$, making it a trivial constant in the phonon effective action. The phonons are therefore massless to all orders in Δ and $\mathbf{u}_I$.

As a special case, we can now demonstrate Eq. (4.38) explicitly. That is, we can show explicitly that $-\frac{1}{4G}\int d^4x\, \mathrm{tr}_{CF}\big((\Delta^u_{CF})^\dagger \Delta^u_{CF}\big)$ is independent of $\mathbf{u}_I$ as must be the case since it includes no derivatives acting on $\mathbf{u}_I$, and so would constitute a mass term for the $\mathbf{u}_I$ if it were to depend on the $\mathbf{u}_I$. Indeed,

$$\begin{aligned} -\frac{1}{4G}\int d^4x\, \mathrm{tr}_{CF}\big((\Delta^u_{CF})^\dagger \Delta^u_{CF}\big) &= -\frac{1}{G}\int d^4x \sum_I (\Delta_I \Delta_I^*) \sum_{\mathbf{q}_I^a} \sum_{\mathbf{q}_I^b} e^{2\mathbf{q}_I^a\cdot(\mathbf{r}-\mathbf{u}_I(x))} e^{-2\mathbf{q}_I^b\cdot(\mathbf{r}-\mathbf{u}_I(x))} \\ &= -(VT)\frac{1}{G}\sum_I (\Delta_I\Delta_I^*) P_I \,, \end{aligned} \tag{C.6}$$

as given in (4.38).

Appendix D

Single plane wave

In this Appendix, we investigate phonons in the presence of a condensate for which only one of the three Δ_I is nonzero, meaning that only quarks with two different colors and flavors form Cooper pairs. We take $\Delta_3 \neq 0$ and $\Delta_1 = \Delta_2 = 0$. This implies that there is pairing only between ur and dg quarks, and between ug and dr quarks, where r, g and b refer to the colors of the quarks. Furthermore, we assume that the set $\{\mathbf{q}_3\}$ contains only one vector, $\mathbf{q}$, so that $\Delta_3(x)$ varies in space as a single plane wave, $\Delta_3(\mathbf{r}) = \Delta_3 \exp(2i\mathbf{q}\cdot\mathbf{r})$. In this simple case it is possible to derive the phonon effective action and the shear moduli without employing the Ginzburg-Landau expansion, working to order ϕ^2.

The oscillation of the condensate is described by a single phonon field, $\mathbf{u}_3(x)$. In analogy with Eq. (4.13), we define

$$\begin{aligned} \Delta_3^u(x) &= \Delta_3 e^{2i\mathbf{q}\cdot(\mathbf{r}-\mathbf{u}_3(x))} \\ &\approx \Delta_3 e^{2i\mathbf{q}\cdot\mathbf{r}}\left(1 - i\phi(x) - \frac{1}{2}\phi(x)^2\right) \end{aligned} \tag{D.1}$$

where $\phi(x) = 2\mathbf{q}\cdot\mathbf{u}_3(x)$.

This condensate breaks translational symmetry in the $\hat{\mathbf{q}}$ direction, but leaves an $O(2)$ symmetry corresponding to rotations about the $\hat{\mathbf{q}}$-axis unbroken. Taking $\hat{\mathbf{q}}$ along the z axis, the potential energy $\mathcal{U}$ of Eqs. (4.69) and (4.71) must be symmetric

under rotations about the z-axis, taking the form

$$\begin{aligned}\mathcal{U} =& \frac{\lambda^{zzzz}}{2}(s^{zz})^2 \\ &+ \frac{\lambda^{xzxz}}{2}\left((s^{xz})^2 + (s^{zx})^2 + (s^{yz})^2 + (s^{zy})^2\right) ,\end{aligned} \tag{D.2}$$

where the strain tensors s^{mu} are defined in (4.70). λ^{zzzz} and $\lambda^{xzxz} = \lambda^{yzyz}$ are the two independent elastic moduli that we will now evaluate.

In writing the Lagrangian in terms of the Nambu-Gorkov fields, we ignore the quarks that do not participate in pairing. We also note that the inverse propagator can be written as a block diagonal matrix made up of four blocks that correspond to the ur particles and dg holes, dg particles and ur holes, ug particles and dr holes and dr particles and ug holes. Since only quarks that belong to the same block interact, the inverse Nambu-Gorkov propagator can be written as

$$S^{-1} = S^{-1}_{ur-dg} \oplus S^{-1}_{dg-ur} \oplus S^{-1}_{ug-dr} \oplus S^{-1}_{dr-ug} , \tag{D.3}$$

with

$$\begin{aligned} S^{-1}_{ur-dg} &= \begin{pmatrix} i\partial\!\!\!/ + \mu\!\!\!/_u & (C\gamma^5)\Delta_3^u(x) \\ -(C\gamma^5)\Delta_3^{u*}(x) & (i\partial\!\!\!/ - \mu\!\!\!/_d)^T \end{pmatrix} , \; S^{-1}_{dg-ur} = \begin{pmatrix} i\partial\!\!\!/ + \mu\!\!\!/_d & (C\gamma^5)\Delta_3^u(x) \\ -(C\gamma^5)\Delta_3^{u*}(x) & (i\partial\!\!\!/ - \mu\!\!\!/_u)^T \end{pmatrix} , \\ S^{-1}_{ug-dr} &= \begin{pmatrix} i\partial\!\!\!/ + \mu\!\!\!/_u & -(C\gamma^5)\Delta_3^u(x) \\ (C\gamma^5)\Delta_3^{u*}(x) & (i\partial\!\!\!/ - \mu\!\!\!/_d)^T \end{pmatrix} , \; S^{-1}_{dr-ug} = \begin{pmatrix} i\partial\!\!\!/ + \mu\!\!\!/_d & -(C\gamma^5)\Delta_3^u(x) \\ (C\gamma^5)\Delta_3^{u*}(x) & (i\partial\!\!\!/ - \mu\!\!\!/_u)^T \end{pmatrix} . \end{aligned} \tag{D.4}$$

The phonon effective action is obtained by integrating out the Nambu-Gorkov fields, yielding the result

$$\begin{aligned} i\mathcal{S}[\mathbf{u}] = \log(Z[\mathbf{u}]) =& -i\frac{1}{G}(VT)|\Delta_3|^2 \\ &+ 2\mathrm{Tr}_{\mathrm{ng}} \log\left(S^{-1}_{ur-dg}\right) , \end{aligned} \tag{D.5}$$

where we have used the property that the contributions from the four blocks, S^{-1}_{ur-dg}, S^{-1}_{ug-dr}, S^{-1}_{dr-ug} and S^{-1}_{dg-ur}, are equal. Since the trace of an operator does not change

upon making a unitary transformation, corresponding to a change of basis, we can simplify S^{-1} by choosing a basis which gets rid of the $\exp(2i\mathbf{q}\cdot\mathbf{r})$ and the $C\gamma^5$ appearing with Δ_3. In the new basis,

$$S^{-1}_{ur-dg} = \begin{pmatrix} e^{-i\mathbf{q}\cdot\mathbf{r}} & 0 \\ 0 & (C\gamma^5)e^{i\mathbf{q}\cdot\mathbf{r}} \end{pmatrix} \begin{pmatrix} i\partial\!\!\!/ + \mu\!\!\!/_u & (C\gamma^5)\Delta_3^u(x) \\ -(C\gamma^5)\Delta_3^{u*}(x) & (i\partial\!\!\!/ - \mu\!\!\!/_d)^T \end{pmatrix} \begin{pmatrix} e^{i\mathbf{q}\cdot\mathbf{r}} & 0 \\ 0 & (-C\gamma^5)e^{-i\mathbf{q}\cdot\mathbf{r}} \end{pmatrix}$$
$$= \begin{pmatrix} i\partial\!\!\!/ + \not{q} + \mu\!\!\!/_u & \Delta_3(1 - i\phi - \frac{1}{2}\phi^2) \\ \Delta_3^*(1 + i\phi - \frac{1}{2}\phi^2) & i\partial\!\!\!/ - \not{q} - \mu\!\!\!/_d \end{pmatrix}. \tag{D.6}$$

In this simple case, the inverse propagator in the absence of the phonons can be inverted. (This is why we do not need to resort to the Ginzburg Landau approximation.) Hence we separate S^{-1}_{ur-dg} into $S^{-1}_{ur-dg} = S^{-1}_{\Delta} + \Sigma$ with

$$S^{-1}_{\Delta} = \begin{pmatrix} i\partial\!\!\!/ + \not{q} + \mu\!\!\!/_u & \Delta_3 \\ \Delta_3^* & (i\partial\!\!\!/ - \not{q} - \mu\!\!\!/_d) \end{pmatrix} \tag{D.7}$$

and

$$\Sigma = \begin{pmatrix} 0 & \Delta_3(-i\phi - \frac{1}{2}\phi^2) \\ \Delta_3^*(+i\phi - \frac{1}{2}\phi^2) & 0 \end{pmatrix}. \tag{D.8}$$

Since we have rotated out the phase $\exp(2i\mathbf{q}\cdot\mathbf{r})$ from Δ_3, the off-diagonal components of S^{-1}_{Δ} do not depend on position anymore. Upon inverting S^{-1}_{Δ}, one gets the full propagator for the fermions in the absence of phonons, to all orders in Δ. This propagator is diagonal in momentum space and therefore can be written in a simple way employing the weak-coupling approximation and the HDET formalism (implemented as in Eqs. (4.46) and (4.47) or more formally as in Ref. [100]), yielding

$$S_{\Delta}(p) = \frac{1}{D_{\Delta}(p)} \begin{pmatrix} (\tilde{V}\cdot p - \hat{\mathbf{v}}\cdot\mathbf{q} - \delta\mu_3) & -\Delta_3 \\ -\Delta_3^* & (V\cdot p - \hat{\mathbf{v}}\cdot\mathbf{q} - \delta\mu_3) \end{pmatrix}, \tag{D.9}$$

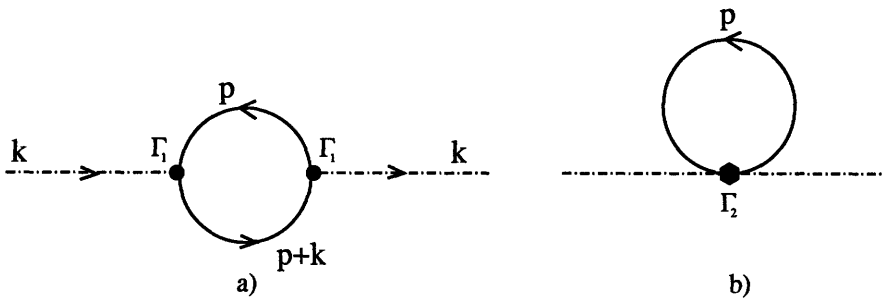

Figure D-1: Diagrams contributing to the phonon self-energy. The dot-dashed lines correspond to the propagator of the phonon fields. Full lines correspond to the full propagator of quark quasi-particles. The phonon-quark-quark vertices Γ_1 and the phonon-phonon-quark-quark vertex Γ_2 are also shown. Diagram b) contributes only to the zero momentum polarization tensor. Diagram a) is nonvanishing for any value of the external momentum k of the phonon.

where

$$\begin{aligned} D_\Delta(p) &= (\tilde{V}\cdot p - \hat{\mathbf{v}}\cdot\mathbf{q} - \delta\mu_3)(V\cdot p - \hat{\mathbf{v}}\cdot\mathbf{q} - \delta\mu_3) \\ &\quad -|\Delta_3|^2 \,. \end{aligned} \tag{D.10}$$

We now consider the interaction with the phonon field. To second order in ϕ, there are two interaction vertices, $i\phi(x)\Gamma_1$ and $-\frac{1}{2}\phi(x)^2\Gamma_2$, where

$$\Gamma_1 = \begin{pmatrix} 0 & -\Delta_3 \\ \Delta_3^* & 0 \end{pmatrix} \text{ and } \Gamma_2 = \begin{pmatrix} 0 & \Delta_3 \\ \Delta_3^* & 0 \end{pmatrix} . \tag{D.11}$$

The phonon effective action to order ϕ^2 is given by the diagrams in Fig. D-1, namely

$$\mathcal{S}^{\phi^2} = \mathrm{Tr}(S_\Delta\,\phi\,\Gamma_1 S_\Delta\,\phi\,\Gamma_1) - \mathrm{Tr}(S_\Delta\,\phi^2\,\Gamma_2)\,, \tag{D.12}$$

where the trace is over Nambu-Gorkov indices and space-time. Evaluating the action along the same lines as in Section 4.4.5, we find

$$\mathcal{S}^{\phi^2} = \frac{\mu^2}{\pi^2}\Delta_3^2 \int \frac{d^4k}{(2\pi)^4}\phi(k)\phi(-k)\int\frac{dp^0}{2\pi i}\int_{-\Lambda}^{\Lambda} ds \int \frac{d\hat{\mathbf{v}}}{4\pi}\frac{(V\cdot k)(\tilde{V}\cdot k)}{D_\Delta(p+k)D_\Delta(p)}\,, \tag{D.13}$$

where the k-independent second diagram in Fig. D-1 has cancelled the k-independent contribution from the first diagram. We then integrate over p_0 and $\hat{\mathbf{v}}$ analytically and do the s-integral numerically. Upon returning to position space, the action takes the form (4.77) which, in this simple case, reduces to

$$\mathcal{S}^{\phi^2} = \frac{1}{2}\int d^4x \left[\frac{\rho}{4q^2}(\partial_0\phi(x))^2 - \frac{\kappa_\perp}{4q^2}(\partial_\perp\phi(x))^2 - \frac{\kappa_{||}}{4q^2}(\partial_{||}\phi(x))^2\right] , \tag{D.14}$$

where $\partial_{||} \equiv \hat{\mathbf{q}}(\hat{\mathbf{q}}\cdot\vec{\partial})$ and $\partial_\perp \equiv \vec{\partial} - \partial_{||}$. We have written the factors of $4q^2 = 4\eta^2\delta\mu^2$ in the denominators in (D.14) in order to facilitate comparison to (D.2). The potential energy $\mathcal{U}$ in (D.14) can easily be written in the form given in Eq. (D.2) by substituting $\phi = 2\mathbf{q}\cdot\mathbf{u}_3$ and keeping only the term symmetric in $\partial_i\mathbf{u}_j$. Taking $\hat{\mathbf{q}}$ in the z direction, one can easily see that $\lambda^{zzzz} = \lambda_{||}$ and $\lambda^{xzxz} = \lambda^{yzyz} = \lambda_\perp$.

The coefficients ρ, $\lambda_\perp$ and $\lambda_{||}$ are each proportional to μ^2 and have nontrivial Δ_3- and $\delta\mu_3$-dependence. We have obtained them numerically for arbitrary values of Δ_3, and by plotting them versus Δ_3^2 at small Δ_3 we have checked that ρ and $\lambda_{||}$ are proportional to Δ_3^2 and $\lambda_\perp$ is consistent with being proportional to Δ_3^4. Within the accuracy of our numerical analysis, we find $\rho = \lambda_{||} = \kappa$ to order Δ_3^2, where κ is given by (4.82). This is in agreement with what we obtain from the phonon effective action (4.80) evaluated to order Δ_3^2 in the Ginzburg-Landau approximation, upon specializing (4.80) to the single plane wave case. It therefore provides a useful check on our calculations. Whether via the Ginzburg-Landau analysis of the main Sections of this paper or via the numerical all-order-in-Δ_3 evaluation of this Appendix, we learn that $\lambda^{zzzz} = \kappa$ and $\lambda^{yzyz} = 0$ to order Δ_3^2, from which we conclude that the shear modulus of this single-plane-wave "crystal" is zero, to this order, and is presumably proportional to $\mu^2\Delta_3^4/\delta\mu^2$.

References

[1] D. J. Gross and F. Wilczek, Phys. Rev. Lett. **30**, 1343 (1973); H. Politzer, Phys. Rev. Lett. **30**, 1346 (1973).

[2] M. A. Stephanov, [arXiv:hep-lat/0701002]; K. Rajagopal, Acta. Phys. Polon., **B31**, 3021 (2000), [arXiv:hep-ph/0009058].

[3] H. Hamber and G. Parisi, Phys. Rev. Lett., **47**, **25**, 1792–1795, 1981;

[4] A. Ukawa, Int. J. Mod. Phys. A **21**, 726 (2006) [arXiv:hep-lat/0510009].

[5] J. C. Collins and M. J. Perry, Phys. Rev. Lett. **34**, 1353 (1975).

[6] D. J. Gross, R. D. Pisarski, and L. G. Yaffe, Rev. Mod. Phys. **53**, 43 (1981); L. McLerran, Rev. Mod. Phys. **58**, 1021 (1986); E. V. Shuryak, *The QCD Vacuum, Hadrons, and the Superdense Matter*, World Scientific, Singapore, 1988.

[7] F. Karsch, Nucl. Phys. B **83-84**(2000), 14-23, *Lattic QCD at Finite Temperature and Density*; R. V. Gavai and S. Gupta, Phys. Rev. **D71**, 114014, (2005) [arXiv:hep-lat/0412035]

[8] K. Rajagopal and F. Wilczek, [arXiv:hep-ph/0011333];

[9] For reviews, see K. Rajagopal and F. Wilczek, [arXiv:hep-ph/0011333]; M. G. Alford, Ann. Rev. Nucl. Part. Sci. **51**, 131 (2001) [arXiv:hep-ph/0102047]; G. Nardulli, Riv. Nuovo Cim. **25N3**, 1 (2002) [arXiv:hep-ph/0202037]; S. Reddy, Acta Phys. Polon. B **33**, 4101 (2002) [arXiv:nucl-th/0211045]; T. Schäfer, arXiv:hep-ph/0304281; D. H. Rischke, Prog. Part. Nucl. Phys. **52**, 197 (2004) [arXiv:nucl-

th/0305030]; M. Alford, Prog. Theor. Phys. Suppl. **153**, 1 (2004) [arXiv:nucl-th/0312007]; M. Buballa, Phys. Rept. **407**, 205 (2005) [arXiv:hep-ph/0402234]; H. c. Ren, [arXiv:hep-ph/0404074]; I. Shovkovy, [arXiv:nucl-th/0410091]; T. Schäfer, [arXiv:hep-ph/0509068]; T. Schäfer, [arXiv:hep-ph/0602067].

[10] P. Jacobs and X.-N. Wang, Prog. Part. Nucl. Phys., **54**, 443-534, (2005), [arXiv:hep-ph/0405125]; PHOBOS Collaboration, Nucl. Phys., **A757**, Vol. 1-2, 28-101 (2005)

[11] P. deForcrand and O. Philipsen, [arXiv:hep-lat/0611027]

[12] J. Pochodzalla, Prog. Part. Nucl. Phys. **39**, 443 (1997)

[13] J. Berges and K. Rajagopal, Nucl. Phys. **B538**, 215 (1999) [hep-ph/9804233].

[14] M. G. Alford, K. Rajagopal and F. Wilczek, Phys. Lett. B **422**, 247 (1998) [arXiv:hep-ph/9711395].

[15] M. A. Halasz, A. D. Jackson, R. E. Shrock, M. A. Stephanov, and J. J. Verbaarschot, Phys. Rev. **D58**, 096007 (1998).

[16] M. Stephanov, Phys. Rev. Lett. **76** 4472 (1996).

[17] M. Buballa and M. Oertel, hep-ph/0202098; Nucl. Phys. A **703** (2002) 770 [hep-ph/0109095].

[18] A. Barducci, R. Casalbuoni, S. DeCurtis, R. Gatto, G. Pettini, Phys. Lett. **B231**, 463 (1989), Phys. Rev. **D41**, 1610 (1990); S. P. Klevansky, Rev. Mod. Phys. **64**, 649 (1992); A. Barducci, R. Casalbuoni, G. Pettini, R. Gatto, Phys. Rev. **D49**, 426 (1994).

[19] R. Rapp, T. Schäfer, E. V. Shuryak and M. Velkovsky, Phys. Rev. Lett. **81**, 53 (1998) [arXiv:hep-ph/9711396].

[20] J. Bardeen, L.N. Cooper, and J.R. Schrieffer, Phys. Rev. **108**, 1175 (1957).

[21] M. G. Alford, K. Rajagopal and F. Wilczek, Nucl. Phys. B **537**, 443 (1999) [arXiv:hep-ph/9804403].

[22] R. Rapp, T. Schäfer, E. V. Shuryak and M. Velkovsky, Annals Phys. **280**, 35 (2000) [arXiv:hep-ph/9904353].

[23] I. A. Shovkovy and L. C. Wijewardhana, Phys. Lett. **B470**, 189 (1999) [arXiv:hep-ph/9910225].

[24] N. Evans, J. Hormuzdiar, S. D. Hsu and M. Schwetz, Nucl. Phys. **B581**, 391 (2000) [hep-ph/9910313].

[25] T. Schäfer and F. Wilczek, Phys. Rev. **D60**, 074014 (1999) [hep-ph/9903503].

[26] K. Rajagopal and F. Wilczek, Phys. Rev. Lett. **86**, 3492 (2001) [hep-ph/0012039].

[27] K. Rajagopal and F. Wilczek, Phys. Rev. Lett. **86**, 3492 (2001) [arXiv:hep-ph/0012039].

[28] S. Alexander and J. McTague, Phys. Rev. Lett. **41**, 705 (1978); for a textbook treatment, see P. M. Chaikin and T. C. Lubensky, *Principles of Condensed Matter Physics*, (Cambridge University Press, 1995).

[29] Stable bulk matter must be neutral under all gauged charges, whether they are spontaneously broken or not. In the case of the electromagnetic gauge symmetry, this simply requires zero charge density. In the case of the color gauge symmetry, bulk matter must in fact be a color singlet, which is a more restrictive condition than mere color neutrality. However, the free energy cost of projecting a color neutral state onto a color singlet state falls rapidly with volume, as long as we are considering volumes larger than the size of a Cooper pair. Given that if quark matter occurs within the core of a neutron star the relevant volumes will be of order cubic kilometers, whereas Cooper pairs have sizes of order fm, it is more than sufficient to consider only the consequences of enforcing color neutrality. See P. Amore, M. C. Birse, J. A. McGovern and N. R. Walet, Phys. Rev. D **65**, 074005 (2002) [arXiv:hep-ph/0110267].

[30] M. Alford, J. Berges and K. Rajagopal, Nucl. Phys. **B558**, 219 (1999) [hep-ph/9903502].

[31] P. Bedaque, Nucl. Phys. **A697**, 569 (2002) [hep-ph/9910247].

[32] M. G. Alford, K. Rajagopal, S. Reddy and F. Wilczek, Phys. Rev. **D64**, 074017 (2001) [hep-ph/0105009].

[33] M. Alford and K. Rajagopal, JHEP **0206**, 031 (2002) [arXiv:hep-ph/0204001].

[34] M. G. Alford, J. A. Bowers and K. Rajagopal, Phys. Rev. D **63**, 074016 (2001) [arXiv:hep-ph/0008208].

[35] J. A. Bowers, J. Kundu, K. Rajagopal and E. Shuster, Phys. Rev. D **64**, 014024 (2001) [arXiv:hep-ph/0101067].

[36] R. Casalbuoni, R. Gatto, M. Mannarelli and G. Nardulli, Phys. Lett. B **511**, 218 (2001) [arXiv:hep-ph/0101326].

[37] A. K. Leibovich, K. Rajagopal and E. Shuster, Phys. Rev. D **64**, 094005 (2001) [arXiv:hep-ph/0104073].

[38] J. Kundu and K. Rajagopal, Phys. Rev. D **65**, 094022 (2002) [arXiv:hep-ph/0112206].

[39] J. A. Bowers and K. Rajagopal, Phys. Rev. D **66**, 065002 (2002) [arXiv:hep-ph/0204079].

[40] R. Casalbuoni and G. Nardulli, Rev. Mod. Phys. **263**, 320 (2004) [arXiv:hep-ph/0305069].

[41] R. Casalbuoni, R. Gatto, M. Mannarelli, G. Nardulli, M. Ruggieri and S. Stramaglia, Phys. Lett. B **575**, 181 (2003) [Erratum-ibid. B **582**, 279 (2004)] [arXiv:hep-ph/0307335].

[42] J. A. Bowers, [arXiv:hep-ph/0305301].

[43] R. Casalbuoni, M. Ciminale, M. Mannarelli, G. Nardulli, M. Ruggieri and R. Gatto, Phys. Rev. D **70**, 054004 (2004) [arXiv:hep-ph/0404090].

[44] R. Casalbuoni, R. Gatto, N. Ippolito, G. Nardulli and M. Ruggieri, Phys. Lett. B **627**, 89 (2005) [arXiv:hep-ph/0507247].

[45] M. Mannarelli, K. Rajagopal and R. Sharma, arXiv:hep-ph/0603076.

[46] K. Rajagopal and R. Sharma, Phys. Rev. D **74**, 094019 (2006) [arXiv:hep-ph/0605316]; K. Rajagopal and R. Sharma, J. Phys. G **32**, S483 (2006) [arXiv:hep-ph/0606066].

[47] R. D. Pisarski and D. H. Rischke, Phys. Rev. Lett. **83**, 37 (1999) [nucl-th/9811104]; Phys. Rev. **D60**, 094013 (1999) [nucl-th/9903023]; Phys. Rev. **D61**, 051501 (2000) [nucl-th/9907041]; R. D. Pisarski and D. H. Rischke, Phys. Rev. **D61**, 074017 (2000) [nucl-th/9910056].

[48] A. Schmitt, Q. Wang and D. H. Rischke, Phys. Rev. **D66**, 114010 (2002) [arXiv:nucl-th/0209050].

[49] M. Alford, J. A. Bowers, and K. Rajagopal, Lect. Notes Phys. **578**, 235 (2001) [arXiv:hep-ph/0101067].

[50] M. Alford, M. Braby, M. W. Paris and S. Reddy, Astrophys. J. **629**, 969 (2005) [arXiv:nucl-th/0411016].

[51] D. Page and S. Reddy, Annual Review of Nuclear and Particle science, **56**, 327-374, (2006)

[52] N. K. Glendening, "*Compact stars*", Springer-Verlag, New York, Berlin, Heidelberg (2000).

[53] M. Alford and S. Reddy, [arXiv:nucl-th/0211046].

[54] T. Schafer, Nucl. Phys. B **575**, 269 (2000) [arXiv:hep-ph/9909574].

[55] B. Barrois, Nucl. Phys. **B129** (1977) 390. S. Frautschi, Proceedings of workshop on hadronic matter at extreme density, Erice 1978. B. Barrois, "Nonperturbative effects in dense quark matter", Cal Tech PhD thesis, UMI 79-04847-mc (1979).

[56] D. T. Son, Phys. Rev. D **59**, 094019 (1999)

[57] K. Rajagopal and E. Shuster, Phys. Rev. **D62**, 085007 (2000) [hep-ph/0004074].

[58] G. W. Carter and D. Diakonov, Phys. Rev. **D60**, 016004 (1999) [hep-ph/9812445]; Nucl. Phys. **B582**, 571 (2000) [hep-ph/0001318].

[59] N. Evans, S. D. Hsu and M. Schwetz, Nucl. Phys. **B551**, 275 (1999) [hep-ph/9808444]; Phys. Lett. **B449**, 281 (1999) [hep-ph/9810514].

[60] T. Schäfer and F. Wilczek, Phys. Lett. **B450**, 325 (1999) [hep-ph/9810509].

[61] M. Iwasaki and T. Iwado, Phys. Lett. B **350**, 163 (1995).

[62] M. Alford, C. Kouvaris and K. Rajagopal, Phys. Rev. Lett. **92**, 222001 (2004) [arXiv:hep-ph/0311286].

[63] M. Alford, C. Kouvaris and K. Rajagopal, Phys. Rev. D **71**, 054009 (2005) [arXiv:hep-ph/0406137].

[64] D. Bailin and A. Love, Phys. Rept. **107**, 325 (1984).

[65] A. W. Steiner, S. Reddy and M. Prakash, Phys. Rev. D **66**, 094007 (2002) [arXiv:hep-ph/0205201].

[66] M. Huang, P. f. Zhuang and W. q. Chao, Phys. Rev. D **67**, 065015 (2003) [arXiv:hep-ph/0207008];

[67] K. Rajagopal and A. Schmitt, Phys. Rev. D **73**, 045003 (2006) [arXiv:hep-ph/0512043].

[68] I. Shovkovy and M. Huang, Phys. Lett. B **564**, 205 (2003) [arXiv:hep-ph/0302142]; M. Huang and I. Shovkovy, Nucl. Phys. A **729**, 835 (2003) [arXiv:hep-ph/0307273].

[69] E. Gubankova, W. V. Liu and F. Wilczek, Phys. Rev. Lett. **91**, 032001 (2003) [arXiv:hep-ph/0304016].

[70] M. Huang and I. A. Shovkovy, Phys. Rev. D **70**, 051501 (2004) [arXiv:hep-ph/0407049]; M. Huang and I. A. Shovkovy, Phys. Rev. D **70**, 094030 (2004) [arXiv:hep-ph/0408268]; I. Giannakis and H. C. Ren, Phys. Lett. B **611**, 137 (2005) [arXiv:hep-ph/0412015]; M. Alford and Q. h. Wang, J. Phys. G **31**, 719 (2005) [arXiv:hep-ph/0501078]; M. Huang, Phys. Rev. D **73**, 045007 (2006) [arXiv:hep-ph/0504235]; E. V. Gorbar, M. Hashimoto and V. A. Miransky, Phys. Lett. B **632**, 305 (2006) [arXiv:hep-ph/0507303]; E. V. Gorbar, M. Hashimoto, V. A. Miransky and I. A. Shovkovy, arXiv:hep-ph/0602251; K. Iida and K. Fukushima, arXiv:hep-ph/0603179.

[71] R. Casalbuoni, R. Gatto, M. Mannarelli, G. Nardulli and M. Ruggieri, Phys. Lett. B **605**, 362 (2005) [Erratum-ibid. B **615**, 297 (2005)] [arXiv:hep-ph/0410401]; K. Fukushima, Phys. Rev. D **72**, 074002 (2005) [arXiv:hep-ph/0506080].

[72] K. Fukushima, arXiv:hep-ph/0603216.

[73] P. F. Bedaque, H. Caldas and G. Rupak, Phys. Rev. Lett. **91**, 247002 (2003) [arXiv:cond-mat/0306694]; M. M. Forbes, E. Gubankova, W. V. Liu and F. Wilczek, Phys. Rev. Lett. **94**, 017001 (2005) [arXiv:hep-ph/0405059]; S. Reddy and G. Rupak, Phys. Rev. C **71**, 025201 (2005) [arXiv:nucl-th/0405054]; J. Carlson and S. Reddy, Phys. Rev. Lett. **95**, 060401 (2005) [arXiv:cond-mat/0503256].

[74] S. Jochim, M. Bartenstein, A. Altmeyer, G. Hendl, C. Chin, J. Hecker Denschlag, R. Grimm, Phys. Rev. Lett. 91, 240402 (2003) : C. H. Schunck, M. W. Zwierlein, C. A. Stan, S. M. F. Raupach, W. Ketterle, A. Simoni, E. Tiesinga, C. J. Williams, P. S. Julienne, *"Feshbach Resonances in Fermionic Lithium-6"*, [arXiv:cond-mat/0407373].

[75] M. W. Zwierlein, A. Schirotzek, C. H. Schunck, and W. Ketterle, Science **311**, 492 (2006) [arXiv:cond-mat/0511197].

[76] G. B. Partridge, W. Li, R. I. Kamar, Y.-a. Liao, and R.G. Hulet, Science **311**, 503 (2006) [arXiv:cond-mat/0511752].

[77] R. Combescot and T. Mora, Europhysics Letters, **68**, 79,(2004), [arXiv:cond-mat/0311042].

[78] R. Combescot and T. Mora, *Transitions to the Fulde-Ferrell-Larkin-Ovchinnikov phases at low temperature in two dimensions*, [arXiv:cond-mat/0405028].

[79] R. Combescot and T. Mora, *Transition to the Fulde-Ferrel-Larkin-Ovchinnikov planar phase : a quasiclassical investigation with Fourier expansion*, [arXiv:cond-mat/0410672].

[80] R. Combescot and T. Mora, *Transition to the Fulde-Ferrel-Larkin-Ovchinnikov phases in three dimensions : a quasiclassical investigation at low temperature with Fourier expansion*, [arXiv:cond-mat/0412449].

[81] K. Iida and G. Baym, Phys. Rev. D **63**, 074018 (2001) [Erratum-ibid. D **66**, 059903 (2002)] [arXiv:hep-ph/0011229].

[82] F. Neumann, M. Buballa and M. Oertel, Nucl. Phys. A **714**, 481 (2003) [arXiv:hep-ph/0210078].

[83] M. Alford, C. Kouvaris and K. Rajagopal, arXiv:hep-ph/0407257.

[84] P. F. Bedaque and T. Schäfer, Nucl. Phys. A **697**, 802 (2002) [arXiv:hep-ph/0105150]; D. B. Kaplan and S. Reddy, Phys. Rev. D **65**, 054042 (2002) [arXiv:hep-ph/0107265]; A. Kryjevski, D. B. Kaplan and T. Schäfer, Phys. Rev. D **71**, 034004 (2005) [arXiv:hep-ph/0404290];

[85] A. Kryjevski and T. Schäfer, Phys. Lett. B **606**, 52 (2005) [arXiv:hep-ph/0407329]; A. Kryjevski and D. Yamada, Phys. Rev. D **71**, 014011 (2005) [arXiv:hep-ph/0407350]; M. Buballa, Phys. Lett. B **609**, 57 (2005) [arXiv:hep-ph/0410397]; M. M. Forbes, Phys. Rev. D **72**, 094032 (2005) [arXiv:hep-ph/0411001].

[86] A. Kryjevski, arXiv:hep-ph/0508180; T. Schafer, Phys. Rev. Lett. **96**, 012305 (2006) [arXiv:hep-ph/0508190].

[87] A. Gerhold and T. Schafer, arXiv:hep-ph/0603257.

[88] A. Gerhold and A. Rebhan, Phys. Rev. D **68**, 011502 (2003) [arXiv:hep-ph/0305108]; A. Kryjevski, Phys. Rev. D **68**, 074008 (2003) [arXiv:hep-ph/0305173]; A. Gerhold, Phys. Rev. D **71**, 014039 (2005) [arXiv:hep-ph/0411086]; D. D. Dietrich and D. H. Rischke, Prog. Part. Nucl. Phys. **53**, 305 (2004) [arXiv:nucl-th/0312044];

[89] T. Schäfer, Phys. Rev. D **62**, 094007 (2000) [arXiv:hep-ph/0006034]; A. Schmitt, Q. Wang and D. H. Rischke, Phys. Rev. D **66**, 114010 (2002) [arXiv:nucl-th/0209050]; M. G. Alford, J. A. Bowers, J. M. Cheyne and G. A. Cowan, Phys. Rev. D **67**, 054018 (2003) [arXiv:hep-ph/0210106]; A. Schmitt, [arXiv:nucl-th/0405076]; A. Schmitt, Phys. Rev. D **71**, 054016 (2005) [arXiv:nucl-th/0412033]; M. G. Alford and G. A. Cowan, J. Phys. G **32**, 511 (2006) [arXiv:hep-ph/0512104]; M. Buballa, J. Hosek and M. Oertel, Phys. Rev. Lett. **90**, 182002 (2003) [arXiv:hep-ph/0204275]

[90] A. I. Larkin and Yu. N. Ovchinnikov, Zh. Eksp. Teor. Fiz. **47**, 1136 (1964)[Sov. Phys. JETP **20**, 762 (1965)]; P. Fulde and R. A. Ferrell, Phys. Rev. **135**, A550 (1964); S. Takada and T. Izuyama, Prog. Theor. Phys. **41**, 635 (1969).

[91] K. Gloos *et al.*, Phys. Rev. Lett. **70**, 501 (1993).

[92] G. Yin and K. Maki, Phys. Rev. B **48**, 650 (1993); M. R. Norman, Phys. Rev. Lett. **71**, 3391 (1993); H. Schimanski *et al.* Physica B **199**, 125 (1994).

[93] Y. Matsuda and H. Shimahara [cond-mat/0702481].

[94] R. Movshovich, M. Jaime, J. D. Thompson, C. Petrovic, Z. Fisk, P. G. Pagliuso and J. L. Sarrao, PRL, **86**, 5152 (2001).

[95] H. Shimahara, J. Phys. Soc. Jpn. **67**, 736 (1998) [cond-mat/9711017].

[96] L. N. Bulaevskii, Zh. Eksp. Teor. Fiz. **65**, 1278 (1973), translation: Sov. Phys. JETP **38**, 634 (1974); H. Shimahara, Phys. Rev. B **50**, 12760 (1994); H. Burkhardt and D. Rainer, Ann. Physik **3**, 181 (1994); G. Murthy and R. Shankar, J. Phys. Cond. Matt. **7**, 9155 (1995); H. Shimahara and D. Raine, J. Phys. Soc. Jpn. **66**, 3591 (1997); K. Yang and S. L. Sondhi, Phys. Rev. B **57**, 8566 (1998); U. Klein, D. Rainer and H. Shimahara, J. Low. Temp. Phys. **118**, 91 (2000) [cond-mat/9909124]; D. G. Agterberg and K. Yang, J. Phys.: Condens. Matter **13**, 9259 (2001) [cond-mat/0006344].

[97] A. I. Buzdin and V. V. Tugushev Zh. Eksp. Teor. Fiz. **85**, 735 (1983), translation: Sov. Phys. JETP **58**, 428 (1983); A. I. Buzdin and S. V. Polonskii, Zh. Eksp. Teor. Fiz. **93**, 747 (1987), translation: Sov. Phys. JETP **66**, 422 (1987); N. Dupuis, Phys. Rev. B **51**, 9074 (1995).

[98] M. S. Nam *et al.*, J. Phys. Cond. Matt. **11**, L477 (1999); S. Manalo and U. Klein, J. Phys. Cond. Matt. **28**, L471 (2000) [cond-mat/0006327].

[99] M. Ciminale, G. Nardulli, M. Ruggieri and R. Gatto, Phys. Lett. B **636**, 317 (2006) [arXiv:hep-ph/0602180].

[100] G. Nardulli, Riv. Nuovo Cim. **25N3**, 1 (2002) [arXiv:hep-ph/0202037].

[101] R. Casalbuoni, R. Gatto, M. Mannarelli and G. Nardulli, Phys. Rev. D **66**, 014006 (2002) [arXiv:hep-ph/0201059].

[102] R. Casalbuoni, E. Fabiano, R. Gatto, M. Mannarelli and G. Nardulli, Phys. Rev. D **66**, 094006 (2002) [arXiv:hep-ph/0208121].

[103] L. D. Landau and E. M. Lifschitz, *Theory of Elasticity*, 3rd edition, Oxford, Pergamon (1981).

[104] R. Anglani, G. Nardulli, M. Ruggieri and M. Mannarelli, Phys. Rev. D **74**, 074005 (2006) [arXiv:hep-ph/0607341].

[105] N. Iwamoto, Phys. Rev. Lett. **44**, 1637 (1980).

[106] For a recent analysis with references, see D. Page, J. M. Lattimer, M. Prakash and A. W. Steiner, Astrophys. J. Suppl. **155**, 623 (2004) [arXiv:astro-ph/0403657].

[107] Unlikely, but not resolved definitively. The calculation of Ref. [104] is a first step in the sense that it treats a very simple "crystal" structure in which the $\langle ud \rangle$ and $\langle us \rangle$ condensates are each single plane waves. The neutrino emissivity of the CubeX and 2Cube45z crystal structures remain to be calculated, meaning that it remains to be determined by how much the phase space for direct URCA reactions like $u + e \to d + \nu$ is reduced in these crystalline phases with pairing with many different wave vectors.

[108] M. Alford, P. Jotwani, C. Kouvaris, J. Kundu and K. Rajagopal, Phys. Rev. D **71**, 114011 (2005) [arXiv:astro-ph/0411560].

[109] P. W. Anderson and N. Itoh, Nature **256**, 25 (1975).

[110] M. A. Alpar, Astrophys. J. **213**, 527 (1977); M. A. Alpar, P. W. Anderson, D. Pines, and J. Shaham, Astrophys. J. **249**, L29 (1981); P. W. Anderson, M. A. Alpar, D. Pines and J. Shaham, Phil. Mag. A, **45**, 227 (1982).

[111] M. A. Alpar, P. W. Anderson, D. Pines, and J. Shaham, Astrophys. J. **276**, 325 (1984).

[112] M.A. Alpar, P.W. Anderson, D. Pines and J. Shaham, Astrophys. J. **278**, 791 (1984).

[113] M. A. Alpar, S. A. Langer and J. A. Sauls, Astrophys. J. **282**, 533 (1988); M. A. Alpar and J. A. Sauls, Astrophys. J. **327**, 723.

[114] M. A. Alpar, R. Nandkumar and D. Pines, Astrophys. J. **288**, 191 (1985). M. A. Alpar, R. Nandkumar and D. Pines, Astrophys. J. **311**, 197 (1986).

[115] R. I. Epstein and G. Baym, Astrophys. J. **387**, 276 (1992).

[116] B. Link, R. I. Epstein and G. Baym, Astrophys. J. **403**, 285 (1993).

[117] P. B. Jones, Mon. Not. R. Astron. Soc. **263**, 619 (1993); P. B. Jones, Phys. Rev. Lett. **79**, 792 (1997).

[118] M. A. Alpar, H. F. Chau, K. S. Cheng and D. Pines, Astrophys. J. **409**, 345 (1993); M. A. Alpar, H. F. Chau, K. S. Cheng and D. Pines, Astrophys. J. **427**, L29 (1994).

[119] M. A. Alpar and A. Baykal, Mon. Not. R. Astron. Soc., **269**, 849 (1994).

[120] M. A. Alpar, H. F. Chau, K. S. Cheng and D. Pines, Astrophys. J. **459**, 706 (1996).

[121] For reviews see D. Pines and M. A. Alpar, Nature **316**, 27 (1985); D. Pines in *Neutron Stars: Theory and Observation*, J. Ventura and D. Pines, eds., 57 (Kluwer, 1991); M. A. Alpar, in *The Lives of Neutron Stars*, M. A. Alpar *et al.*, eds., 185 (Kluwer, 1995).

[122] T. Strohmayer, H. M. van Horn, S. Ogata, H. Iyetomi and S. Ichimaru, Astrophys. J. **375**, 679 (1991).

[123] J. W. Negele and D. Vautherin, Nucl. Phys. A **207**, 298 (1973).

[124] I. Easson, Astrophys. J. **228**, 257 (1979).

[125] D. Pines, J. Shaham and M. Ruderman, Nature **237**, 83 (1972); G. Baym, D. Q. Lamb and F. K. Lamb, Astrophys. J. **208**, 829 (1976).

[126] B. Link, private communication.

[127] M. Ruderman, Nature **223**, 597 (1969); G. Baym, and D. Pines, Ann. Phys. **66**, 861 (1971).

[128] H. Abuki, M. Kitazawa and T. Kunihiro, Phys. Lett. B **615**, 102 (2005) [arXiv:hep-ph/0412382].

[129] S. B. Rüster, V. Werth, M. Buballa, I. A. Shovkovy and D. H. Rischke, Phys. Rev. D **72**, 034004 (2005) [arXiv:hep-ph/0503184].

[130] R. Casalbuoni, M. Ciminale, R. Gatto, G. Nardulli and M. Ruggieri, Phys. Lett. B **642**, 350 (2006) [arXiv:hep-ph/0606242].

[131] N. D. Ippolito, G. Nardulli and M. Ruggieri, arXiv:hep-ph/0701113.

[132] S. B. Rüster, I. A. Shovkovy and D. H. Rischke, Nucl. Phys. A **743**, 127 (2004) [arXiv:hep-ph/0405170].

[133] K. Fukushima, C. Kouvaris and K. Rajagopal, Phys. Rev. D **71**, 034002 (2005) [arXiv:hep-ph/0408322].

[134] R. X. Xu, Astrophys. J. **596**, L59 (2003) [arXiv:astro-ph/0302165]; A. Z. Zhou, R. X. Xu, X. J. Wu, N. Wang and X. Y. Hong, Astropart. Phys. **22**, 73 (2004) [arXiv:astro-ph/0404554]; R. X. Xu, D. J. Tao and Y. Yang, Mon. Not. Roy. Astron. Soc. Lett. **373**, L85 (2006) [arXiv:astro-ph/0607106].

[135] B. J. Owen, Phys. Rev. Lett. **95**, 211101 (2005) [arXiv:astro-ph/0503399].

[136] B. Abbott *et al.* [LIGO Scientific Collaboration], arXiv:gr-qc/0702039.

[137] R. Sensarma, M. Randeria and T.-L. Ho, Phys. Rev. Lett. **96**, 090403 (2006) [arXiv:cond-mat/0510761].